

**Exploration of neurological tumour derivation
across the Blood-Brain Barrier and development
of Artemisinin and its derivatives as metastatic
breast cancer therapies**

WenXiao Ji

Cardiff China Medical Research Collaborative

School of Medicine, Cardiff University

Cardiff

June 2025

Supervisors: Tracey A Martin, Wen G. Jiang

*Thesis submitted to Cardiff University for the degree of Doctor of
Philosophy (Medicine)*

Acknowledgements

Firstly, I would like to express my deepest gratitude to my primary supervisor, Dr. Tracey Martin, for her invaluable guidance, constant encouragement, and profound expertise throughout my doctoral journey. Her unwavering support and insightful feedback have significantly shaped this research and my growth as a scientist.

My heartfelt thanks also go to my co-supervisor, Prof. Wenguo Jiang, whose profound knowledge, meticulous guidance, and inspirational mentorship have greatly enriched my academic experience and contributed immensely to the success of my studies.

I am also sincerely thankful to Fiona Rouge, our dedicated laboratory manager, for her patience, outstanding management skills, and constant support. Fiona's attentive guidance has been instrumental in smoothly navigating laboratory procedures and experiments.

Special appreciation goes to Dr. Lin Ye from the neighbouring research group, whose patient and valuable guidance, expertise, and insightful suggestions have significantly supported my experimental techniques and overall research progress.

My deep appreciation extends to my fellow colleagues at CCMRC, including Shiqi Dong, Jia tong, Rhiannon Yannan Yu, Yali Xu, Yufei Lou, Cai Wang, Xiangyi Liu, Amber Li, Milad Eshmela, Manal Almri, Edward Xu, Jenny Zhang, and Richard Tian, for their camaraderie, constructive discussions, and unwavering support throughout my doctoral studies. I am especially grateful for their dedication and kindness in caring for my cell cultures during holidays, generously sharing their time and knowledge in jointly exploring and mastering new experimental techniques, offering continuous assistance in performing and

troubleshooting experiments, and engaging in insightful and inspiring discussions whenever challenges arose. Their constant encouragement, friendship, and collaborative spirit have significantly enriched my academic journey, making my doctoral experience truly memorable and rewarding.

I would also like to extend my heartfelt appreciation to my seniors Amy Liu, Jimmy Zeng, Han Gao and Ziqian Fang, whose guidance, practical advice, and warm encouragement have greatly helped me throughout my PhD journey.

Lastly, I owe special thanks to my parents and my young sister, whose emotional support and encouragement have sustained me through every challenge encountered during this journey.

Summary

This doctoral research thoroughly investigates the mechanisms underlying breast cancer metastasis to the brain, particularly focusing on the role and modulation of the blood-brain barrier (BBB) and the potential therapeutic application of Artemisinin and its derivatives. Brain metastasis remains a significant obstacle in breast cancer treatment due to the impermeable nature of the BBB, which substantially restricts the efficacy of existing therapeutic strategies.

The study comprehensively explores the function of tight junction proteins, specifically claudin-8 (CLDN8), in regulating BBB permeability and the metastatic progression of breast cancer cells. To address this, extensive experimental methodologies were employed, including advanced molecular biology techniques such as quantitative real-time PCR, RNA sequencing for global gene expression profiling, Western blotting for protein expression validation, and immunofluorescence microscopy to assess protein localisation changes. Functional cellular assays, including invasion, migration, and adhesion assays, were rigorously performed to evaluate the biological impacts of CLDN8 expression changes. Additionally, BBB integrity assays involving transendothelial electrical resistance (TEER) measurements and paracellular permeability assays were utilized to precisely quantify barrier function.

Key findings demonstrated that Artemisinin treatment markedly influences the expression levels and subcellular localization of tight junction proteins, especially causing a significant reduction in CLDN8 expression. This downregulation was associated with increased permeability of the BBB, facilitating improved penetration of therapeutic agents into the brain tissues. Further mechanistic investigations revealed critical interactions between CLDN8 and pivotal signalling pathways, notably the β -catenin pathway, providing insights into the molecular mechanisms driving Artemisinin's effects.

Incorporation of clinical samples enhanced the translational value of this study, where analyses confirmed that decreased CLDN8 expression correlated with enhanced metastatic capability and poorer clinical outcomes in breast cancer patients. Complementary bioinformatic analyses utilizing patient data from The Cancer Genome Atlas (TCGA) provided additional validation, underscoring the prognostic significance of CLDN8 and other tight junction components in breast cancer metastasis to the brain.

Ultimately, this comprehensive study significantly advances our understanding of the BBB's regulatory mechanisms in metastatic breast cancer and identifies Artemisinin and its derivatives as promising candidates for improving therapeutic outcomes. These results present a robust foundation for future clinical exploration, aiming to overcome current treatment barriers associated with breast cancer brain metastasis, thereby contributing valuable knowledge towards the development of more effective clinical strategies.

List of abbreviations

AMPK: AMP-activated protein kinase;

APC: Adenomatosis Polyposis Coli Tumour Suppressor;

AR: androgen receptor;

AUC: area under the curve ;

BBB: Blood-Brain Barrier;

BC: Breast cancer

BCBM: breast cancer brain metastasis;

BCRP: breast cancer resistant protein;

BMD: Brain metastasis disease;

BNC1: Basonuclin 1;

BTB: blood-tumour barrier;

CCDC8: Coiled-Coil Domain Containing 8;

CDK: Cyclin-Dependent Kinase;

CLDN: Claudin;

CNS: central nervous system;

CTNNB1: Catenin (Cadherin-Associated Protein), Beta 1;

DAB: 3,3' -Diaminobenzidine;

DFS: disease-free survival;

DHA: dihydroartemisinin ;

ER: oestrogen receptor;

ERBB2: Erb-B2 Receptor Tyrosine Kinase 2, also known as HER2;

ERBB3: Erb-B2 Receptor Tyrosine Kinase 3, also known as HER3;

ERBB4: Erb-B2 Receptor Tyrosine Kinase 4, also known as HER4;

EGFR: Epidermal growth factor receptor. Also known as HER1

EMT: Epithelial-mesenchymal transition;

FBPS: Fructose-1,6-bisphosphatase ;

FBS: foetal bovine serum;

FITC: Fluorescein isothiocyanate ;

GALNT9: Polypeptide N-acetylglucosaminyltransferase 9 ;

GNMT: glycine N-methyltransferase ;

GAPDH : Glyceraldehyde-3-Phosphate Dehydrogenase;

GSK3B: Glycogen Synthase Kinase 3 Beta;

IF: immunofluorescence;

IHC: immunohistochemistry;

JAM: junctional adhesion molecule;

KLHL3: Kelch Like Family Member 3;

MAguk: membrane-associated guanylate kinase;

MLCK: myosin light chain kinase;

MMP: matrix metalloproteinases;

mTOR: mammalian target of rapamycin ;

MTT: 3-(4,5-dimethylthiazol-2-yl)-2,5-diphenyltetrazolium bromide;

OCLN: Occludin;

ORR: Objective Response Rate;

OS: Overall survival;

OSCC: Oral squamous cell carcinoma ;

PARP: Poly ADP-ribose polymerase;

PCP: paracellular permeability;

PCR: Polymerase chain reaction;

PD-1: Programmed Cell Death 1 Protein;

PD-L1: Programmed Death Ligand 1;

PFS: Progression free survival;

Pgp: P-glycoprotein;

PI3K: phosphatidylinositol-3-kinase;

PIPOX: peroxidase sarcosine oxidase;

PKC: Protein kinase C;

PR: progesterone receptor;

RHO: Rhodopsin;

ROC: receiver operating characteristic;

ROS: Reactive oxygen species ;

SARDH: sarcosine, dehydrogenase ;

SGK1: Serum/Glucocorticoid Regulated Kinase 1;

SRS: stereotactic radiosurgery ;

STAT3: Signal Transducer and Activator of Transcription;

STC2: Stanniocalcin-2;

TCGA: The Cancer Genome Atlas;

TEER: transendothelial electrical resistance;

TJ: tight junctions;

TJP: Tight junctional proteins, also known as ZO

TKI: Tyrosine kinase inhibitor;

T-DM1: Trastuzumab-emtansine;

TNBC: triple-negative breast cancer;

TNF: Tumour necrosis factor;

TOP2A: DNA Topoisomerase II Alpha;

TUBB3; β III-tubulin;

VEGF: Vascular Endothelial Growth Factor;

WB: Western blot;

WBRT: whole-brain radiotherapy;

WNK: (With-No-Lysine [K]) kinase, e.g., WNK1/WNK4 as needed;

WNT: Wiggless-Type MMTV Integration Site Family;

ZO: Zonula Occludens, also known as TJP (tight junctional proteins);

Category	Title	Publication / Report Information
Published Articles	Knockdown of Claudin-8 (CLDN8) Indicates a Link Between Breast Cancer Cell Sensitivity to Chemotherapeutics and Reveals a Potential Use of CLDN8 as a Molecular Diagnostic and Target for Therapy(1)	<i>Int J Mol Sci</i> (2025)
	Tight Junctional Protein Family, Claudin in Cancer and Cancer Metastasis(2)	<i>Front Oncol</i> (2025)
	Claudin-10 in the Blood–Brain Barrier Function of Cerebral Endothelial Cells and Transendothelial Invasion of Breast Cancer Cells(3)	<i>Anticancer Res</i> (2023)
Completed, Pending Publication	Evaluating the Prognostic and Therapeutic Implications of DUSP7 Expression in Breast Cancer: Insights from Clinical and Cellular Analyses	—
	Artemisinin Modulates the Blood–Brain Barrier and Suppresses Brain Metastatic Breast Cancer via CLDN8 and β -Catenin Pathways	—
Published Conference Reports	<i>Expression of Dual Specific Phosphatase-7 (DUSP7/PYST2) and Its Connection with Salt Inducible Kinases (SIKs) and Downstream MKKs in Breast Cancer</i>	<i>Cancer Res</i> (2023) 83: P4-08-22

Category	Title	Publication / Report Information
	<i>Marvel D3 and Its Associated Junctional Proteins in Breast Cancer</i>	<i>Cancer Res</i> (2023) 83: P2-26-20
	<i>Dual Specific Phosphatase-7 (DUSP7/PYST2) and Its Role in Regulating Vascular Endothelial Functions</i>	<i>Cancer Res</i> (2023) P2-16-09

Table of Contents

Character I: Metastatic Brain Tumour	
1.1 Incidence of Brain metastasis	20
1.2 Tumour type	21
1.3 Clinical manifestation of Breast Cancer Brain Metastasis	21
1.3.1 Wntless/Integrated (Wnt) and Notch pathways	23
1.3.2 Epidermal Growth Factor Receptor (EGFR) and Phosphatase and Tenzin Homolog (PTEN) pathways	24
1.3.3 Vascular Endothelial Growth Factor (VEGF) and Signal Transducer and Activator of Transcription 3(STAT3)	25
1.3.4 β II micro tubulin and DNA Topoisomerase II Alpha (TOP2A)	26
1.3.5 Basonuclin 1(BNC1), Polypeptide N-acetylglucosaminyltransferase 9 (GALNT9), Coiled-Coil Domain Containing 8 (CCDC8)	26
1.3.6 Human Epidermal Growth Factor Receptor (HER2) and Human Epidermal Growth Factor Receptor 3 (HER3)	27
1.3.7 Receptors on astrocytes associated with Brain Metastasis	27
1.3.8 Sarcosine metabolism-related proteins	28
1.3.9 Fructose-1,6-bisphosphatase (FBPS)	28
1.3.10 Reactive oxygen-related proteins	29
1.3.11 Clinical symptoms and sites of Brain Metastasis	29
1.3.12 Comparison of symptomatic and asymptomatic brain metastases	30
1.4 Treatments	31
1.4.1 Systemic treatment for HER2-positive Breast Cancer Brain Metastasis	31
1.4.2 Targeted therapies	32
1.4.2.1 Monoclonal antibodies	33
1.4.2.2 Trastuzumab Emtansine (TDM1)	34
1.4.2.3 [vic-]trastuzumab duocarmazine (SYD985)	34
1.4.2.4 [Fam-]trastuzumab deruxtecan (DS-8201)	35
1.4.2.5 First-generation of tyrosine kinase inhibitors (TKIs)	35
1.4.2.6 New-generation TKIs	36
1.4.3 Endocrine therapy	37
1.4.3.1 Cyclin-Dependent Kinase 4 and 6 (CDK4/6) inhibitors	37
1.4.3.2 Phosphatidylinositol 3-Kinase / Protein Kinase B / Mammalian Target of Rapamycin inhibitors (PI3K/Akt/mTOR) inhibitors	38
1.4.4 Triple-negative breast cancer (TNBC) patients with BM treatment	39
1.4.4.1 Chemotherapies for Triple-negative breast cancer	39

1.4.4.2 Vascular endothelial growth factor (VEGF) pathway	41
1.4.4.3 Immunotherapies	42
1.4.4.4 Poly ADP-ribose polymerase (PARP)	43
1.4.4.5 Paclitaxel Treva tide (ANG1005).....	43
1.4.5 Local treatment for Breast Cancer Brain Metastasis.....	44
1.4.5.1 Whole Brain Radiotherapy (WBRT) and Stereotactic Radiosurgery (SRS)	44
1.4.5.2 Combining surgery with Stereotactic Radiosurgery	45
1.4.6 Proton therapy.....	46
1.5 Limitations of Current Treatments	48
1.6 Structure and function of the Tight Junction	49
1.7 Tight junction proteins	51
1.7.1 Occludin (OCLDN).....	53
1.7.2 Claudin (CLDNs).....	54
1.7.3 Junctional Adhesion Molecule (JAM)	57
1.7.4 ZO-1,2,3.....	60
1.7.5 Cingulin.....	60
1.8 The function of Claudin-8	61
1.9 Artemisinin	66
1.9.1 Discovery and Antimalarial Use	66
1.9.2 Artemisinin as a model Compound for Blood–Brain Barrier (BBB) Penetration	71
1.9.3 Anticancer Effects of Artemisinin in Breast Cancer	75
1.10 Study Hypothesis	76
1.11 Aims and Objectives of the Study	76
Chapter II: Materials and Methods	
2.1 Cell Culture and Cell Lines	78
2.2 Molecular Biology Techniques	79
2.2.1 RNA Extraction and cDNA Synthesis	79
2.2.2 Quantitative Real-Time PCR (qPCR)	79
2.2.3 Western Blotting (Protein Extraction and Analysis).....	80
2.3 Functional Cell Assays	82
2.3.1 Cell Adhesion Assay	83
2.3.2 Cell Invasion Assay	83
2.3.3 Cell Migration Assay (Scratch Wound Assay).....	84
2.4 Blood-Brain Barrier and Endothelial Assays	85
2.4.1 Permeability Coefficient (PC) Assay	86
2.4.2 Transendothelial Electrical Resistance (TEER) Assay.....	87
2.5 Protein Interaction and Localization Studies	88
2.5.1 Immunofluorescence (IF) Microscopy	88
2.5.2 Co-Immunoprecipitation (Co-IP)	89
2.5.3 Subcellular Fractionation	91

2.6 In Vitro Pharmacology and Drug Treatment Assays	92
2.6.1 CLDN8 Gene Knockdown in Cell Lines	92
2.6.2 Drug Sensitivity (IC ₅₀) Assays	93
2.6.3 MTT Cell Proliferation Assay	94
2.7 Artemisinin Treatment	96
2.8 Tissue Specimens and Histological Analysis	97
2.8.1 Clinical Specimens and Ethical Approval	97
2.8.2 RNA Extraction and qPCR for Tissue Samples	98
2.8.3 Immunohistochemistry and Histological Scoring	99
2.9 Transcriptomic and Bioinformatic Data Analysis	100
2.9.1 RNA Sequencing and Pathway Enrichment	100
2.9.2 Public Genomic Data (TCGA Cohort Analysis)	102
2.10 Statistical Analysis	103
2.11 qPCR Primers	105
2.12 Antibodies	107
Chapter III : A Preliminary Exploration of Artemisinin’s Regulation of the Blood-Brain Barrier in Breast Cancer Brain Metastasis	
3.1 Introduction	112
3.2 Materials and methods	113
3.2.1 Cell Lines	113
3.2.2 RNA Sequencing and Enrichment Analysis	113
3.2.3 Quantitative analysis of TJ proteins in endothelial cells using real time polymerase chain reaction (QPCR)	114
3.2.4 RNA isolation, cDNA synthesis and reverse transcript polymerase chain reaction (PCR).	114
3.3 Results	115
3.3.1 RNA Sequencing and Identification of Key Pathways	115
3.3.2 CLDN8 as a Key Target in Tight Junction Regulation	119
3.3.3 CLDN-8 Transcription levels in cells	121
3.4 Discussion	121
Chapter IV: Investigation of CLDN8 Expression and It’s Potential Role in Breast Cancer Based on TCGA and Cardiff Clinical Cohort Analysis	
4.1 Introduction	126
4.2 Materials and Methods	127
4.2.1 Tissue cohort	127
4.2.2 Immunohistochemistry (IHC) Analysis	128
4.2.3 Statistical Analysis	129
4.3 Results	129
4.3.1 CLDN8 mRNA Expression in Breast Cancer (TCGA Database)	129
4.3.2 Correlation of CLDN8 Expression with Clinicopathological Factors	131
4.3.3 CLDN8 Expression and Patient Prognosis	134
4.3.4 CLDN8 and Hormone Receptor Status	136

4.3.5 CLDN8 Protein Expression in Different Breast Cancer Subtypes (IHC Analysis)	137
4.3.6 Expression of CLDN8 in Brain Metastatic Tissues from Tumours with Different Pathological Grades (IHC Analysis)	142
4.4 Discussion	145
Chapter V: Role of CLDN8 in Response to Different Breast Cancer Treatment Modalities	
5.1 Introduction	150
5.2 Materials and Methods	151
5.2.1 Cell Lines and Culture Conditions	151
5.2.2 Drugs and Antibodies	151
5.2.3 Patients' response to chemotherapies and evaluation	151
5.2.4 RNA Extraction and qPCR Analysis	152
5.2.5 Protein Extraction and Western Blotting	153
5.2.6 In Vitro Drug Sensitivity Assays	154
5.2.7 MTT-Based Cellular Growth Assay	154
5.2.8 Statistical Analysis	155
5.3 Results	155
5.3.1 CLDN8 Expression with Breast Cancer Treatment Modalities	155
5.3.2 CLDN8 Expression and Response to Breast Cancer Treatments	159
5.3.3 Validation of CLDN8 Knockdown in Breast Cancer Cell Lines	160
5.3.4 CLDN8 Expression and Endocrine Therapy Response in Breast Cancer Subgroups	163
5.3.5 CLDN8 Expression and Anti-HER2 Therapy Response in Breast Cancer Subgroups	169
5.3.6 CLDN8 Expression and Chemotherapy Response in Breast Cancer Subgroups	176
5.4 Discussion	185
Chapter VI: Functional Analysis of CLDN8 in a Breast Cancer Brain Metastasis Model	
6.1 Introduction	189
6.2 Materials and Methods	191
6.2.1 Cell Lines and Culture Conditions	191
6.2.2 Knockdown of CLDN8	191
6.2.3 Artemisinin Treatment Protocol	192
6.2.4 Cell Adhesion Assay	192
6.2.5 Cell Invasion Assay	192
6.2.6 Cell Migration Assay (Scratch Assay)	192
6.2.7 Permeability Coefficient (PCP) Assay	193
6.2.8 Transendothelial Electrical Resistance (TEER) Assay	193
6.3 Results	193
6.3.1 CLDN8 Knockdown Efficiency and Validation	193
6.3.2 Impact of CLDN8 Knockdown and Artemisinin on Breast Cancer Cell Adhesion	196
6.3.3 Scratch Wound Healing Assay Results for Breast Cancer Cell Lines	198
6.3.4 Invasion Assay Results for Breast Cancer Cells Across the Blood-Brain Barrier (BBB)	199

6.3.5 Impact of Artemisinin Treatment on TEER and Paracellular Permeability of Breast Cancer Cell Lines.....	202
6.3.6 CLDN8 Knockdown Efficiency in TY10 and hCMEC/D3 Endothelial Cells	205
6.3.7 Adhesion of Endothelial Cells.....	206
6.3.8 Scratch Wound Healing Assay Results for Endothelial Cells.....	207
6.3.9 TNBC Cell Invasion Assay Across Endothelial Cell Monolayers	210
6.3.10 Impact of Artemisinin Treatment on TEER and Paracellular Permeability of Endothelial Cells	211
6.3.11 Combined Treatment of Brain Metastatic Breast Cancer with Artemisinin	215
6.4 Discussion	217
Chapter VII: Protein-Level Effects of Artemisinin on Tight Junctions and the Wnt/ β-Catenin Pathway: Potential Role in Breast Cancer Metastasis	
7.1 Introduction	222
7.2 Materials and Methods	225
7.2.1 Cell Culture.....	225
7.2.2 Treatments	225
7.2.3 Western Blot (WB) Analysis	226
7.2.4 Protein Array	226
7.2.5 Subcellular Fractionation	227
7.2.6 Immunofluorescence (IFC)	227
7.2.7 Co-Immunoprecipitation (Co-IP)	228
7.2.8 Kinexus Phosphoprotein Array	228
7.3 Results	229
7.3.1 Artemisinin Reduces CLDN8 Expression in CMEC/D3 Cells	229
7.3.2 Artemisinin and CLDN8 Knockdown Affect β -catenin Expression.....	231
7.3.3 Artemisinin and CLDN8 Knockdown Differentially Regulate β -catenin Expression in Brain Endothelial and Breast Cancer Cells	236
7.3.4 Subcellular Localisation of β -catenin in CMEC/D3 and MDA-231 Cells	239
7.3.5 Localization and Colocalization of ZO1 and CLDN8	241
7.3.6 Co-Immunoprecipitation (Co-IP) of CLDN8 and β -catenin	244
7.3.7 Structural Changes of CLDN8 and β -catenin Following Artemisinin Treatment	245
7.3.8 Impact of Artemisinin on AKT, GSK3 β , and β -catenin Phosphorylation in hCMEC/D3 Cells	247
7.4 Discussion	249
Chapter VIII: General Discussion	
8.1 Key findings from the current study	255
8.1.1 CLDN8 Downregulation in Breast Cancer	255
8.1.2 CLDN8 as a Prognostic Biomarker.....	255
8.1.3 Functional Role of CLDN8 in Cell Adhesion and Invasiveness.....	256
8.1.4 Artemisinin's Impact on Cancer and Endothelial Cells	257

8.1.5 Effects of Artemisinin on Tight Junction Integrity	258
8.1.6 Relationship between CLDN8 expression and breast cancer treatment sensitivity and implications for Artemisinin therapy	259
8.1.7 Artemisinin-Induced Changes in Protein Localization and Interaction between CLDN8 and β -catenin.....	260
8.1.8 Molecular Mechanisms – CLDN8, β -Catenin, and Artemisinin	261
8.2 Clinical Relevance and Therapeutic Implications	266
8.3 Limitations of the Study and Future Directions	270
8.3.1 Sample Size and Cohort Composition	270
8.3.2 In Vitro Model Limitations	270
8.3.3 Mechanistic Depth	271
8.3.4 Artemisinin Pharmacology.....	272
8.3.5 Breadth of Efficacy.....	273
8.4 Conclusion	273

Character I: Metastatic Brain Tumour

1.1 Incidence of Brain metastasis

Cancer arises when mutations occur in somatic or germ cells, leading to unchecked cell growth and division. For solid tumours, the deadliest aspect is the ability of tumour cells to spread from their primary site to distant organs through mechanisms such as direct invasion, lymphatic or vascular routes, or implantation. Prior to determining a treatment plan, assessing the extent and specific locations of metastases is essential, as this information often influences therapeutic choices and prognosis. (4) Brain metastases have a particularly poor prognosis and poor survival outcomes, which brings a grand clinical challenge. (5) More than 50% of adult intracranial tumours diagnosed worldwide are metastases derived from primary extracerebral malignancies (6). Largely incurable, brain metastatic disease (BMD) is responsible for 90% of mortality attributed to cerebral malignancy (7). The aetiology of brain metastatic disease (BMD) is complex and influenced by multiple factors, primarily the characteristics of the primary tumour and the interval between initial diagnosis and treatment of the primary malignancy (8). Primary malignancies of lung, breast, colon, renal or melanoma origin most commonly metastasise to the brain in adults (9). The increased sensitivity of radiological imaging modalities has improved detection and surveillance of BMD, which may not have been previously diagnosed. Consequently, the incidence of BMD remains difficult to quantify. This is compounded by improved primary malignancy systemic therapy increasing overall survival and likelihood of BMD development (10). General conclusions drawn from the literature imply the incidence of BMD, particularly in developed nations is increasing (11-13). Thus, management regimes require enhancement and modification in order to satisfactorily abate the projected boom in BMD. Historically, post-mortem data and population-based studies have underestimated BMD morbidity and mortality (13).

1.2 Tumour type

The classification of breast cancer into molecular subtypes has become essential for guiding personalized treatment and prognosis. The 2011 St. Gallen International Expert Consensus proposed four primary molecular subtypes based on the expression of oestrogen receptor (ER), progesterone receptor (PR), human epidermal growth factor receptor 2 (HER2), and Ki-67, a proliferation marker(14). These subtypes include Luminal A, Luminal B, HER2-positive (HER2+), and triple-negative breast cancer (TNBC). Luminal A tumours, characterized by high ER and PR expression, low HER2 expression, and a low Ki-67 index, generally have the most favourable prognosis and are often managed with hormone therapy due to their hormone receptor positivity. Luminal B tumours, while also ER-positive, show a higher Ki-67 index and may have variable HER2 expression, indicating a more aggressive profile that may require chemotherapy in addition to hormone therapy.

HER2-positive breast cancers, marked by elevated HER2 expression, are associated with rapid growth and aggressive behaviour. While these cancers historically had poor prognoses, the development of HER2-targeted therapies has significantly improved patient outcomes. In contrast, triple-negative breast cancer (TNBC), which lacks ER, PR, and HER2 expression, is notably aggressive and has fewer treatment options. Due to its lack of hormonal or HER2 targets, TNBC is primarily treated with chemotherapy, though it generally carries a poorer prognosis. These subtypes exhibit distinct clinical and pathological features, underscoring the importance of molecular classification for effective treatment planning and prognosis. Accurate staging and subtyping are therefore critical in predicting outcomes and tailoring therapeutic approaches for breast cancer patients.

1.3 Clinical manifestation of Breast Cancer Brain Metastasis

Breast cancer is the second leading cause of death among malignant tumours in women, with 90% of fatalities attributed to metastases. Common metastatic sites include the lung, bone, liver, and central nervous system (CNS). The incidence of CNS metastases is approximately 15%, but this rate significantly increases to about 30%-50% in HER2-positive and triple-negative breast cancers(15). For breast cancer cells to metastasize to the brain, they must first cross the blood-brain barrier (BBB)(16). Breast cancer cells utilize surface ligands to bind to receptors on endothelial cells, activating various signalling pathways that alter BBB permeability, thus allowing successful invasion into brain tissue, as illustrated in Figure 1.3.

Figure 1.3 clearly depicts the entire process of breast cancer cell metastasis from the primary tumour site to the brain: Initially, cancer cells breach the basement membrane of breast ducts, invade surrounding tissues, and enter the bloodstream (intravasation). Subsequently, these circulating cancer cells travel to the brain microvasculature, interacting via specific surface ligands with receptors on brain endothelial cells, crossing the tight junction-based BBB, and infiltrating brain parenchyma. Finally, the cancer cells colonize, proliferate, and form metastatic tumours within the brain microenvironment.

Studies have indicated that after traversing the BBB, ligands on the surface of breast cancer cells bind to receptors on endothelial cells, thereby activating various signalling pathways that subsequently stimulate brain tissue cells, facilitating the selective metastasis of breast cancer cells to the brain(17).

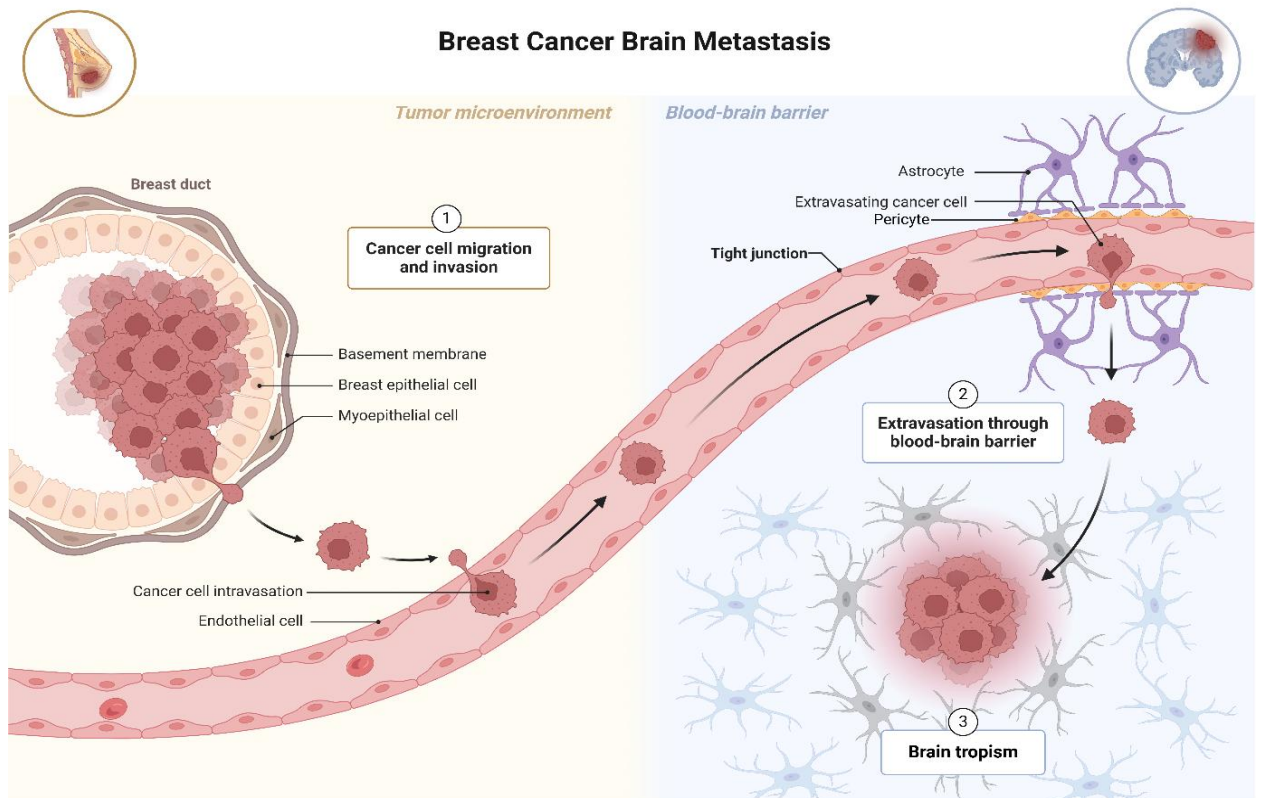


Figure 1.3 Schematic of breast cancer brain metastasis. (1) Cancer cells migrate from breast ducts, invade surrounding tissues, and enter the bloodstream (intravasation). (2) Circulating cancer cells extravasate through the BBB into brain tissue. (3) Cancer cells adapt and proliferate, establishing metastatic tumours within the brain (16). (Created by Chiara C. (18)).

1.3.1 Wingless/Integrated (Wnt) and Notch pathways

The Wingless/Integrated (Wnt) and Notch signalling pathways play crucial roles in the maintenance of normal stem cells and are also implicated in tumour stem cell regulation(19). Nam et al(20) developed a model of breast cancer brain metastasis using the MDA-MB-435 cell line, which was historically classified as a breast cancer line but later identified as being of melanoma (M14) origin(21). They discovered that high levels of interleukin-1 β (IL-1 β) in these brain-metastatic cells could stimulate the expression of JAG2 in nearby astrocytes. This crosstalk initiates

the Notch signalling pathway in both astrocytes and cancer stem cells, where Notch receptors engage with ligands on adjacent cells, forming complexes that undergo proteolytic cleavage. This cleavage releases the Notch intracellular domain (NICD), which translocates to the nucleus, where it acts as a transcriptional activator for numerous genes associated with tumour growth and survival. Consequently, the upregulated Notch signalling enhances BCBM cell proliferation and tumour progression, highlighting its potential as a therapeutic target in metastatic brain tumours. Additionally, the interplay between IL-1 β , JAG2, and Notch signalling reflects the dynamic interaction between the tumour microenvironment and metastasizing cancer cells, underlining the complex regulatory mechanisms driving metastasis.

1.3.2 Epidermal Growth Factor Receptor (EGFR) and Phosphatase and Tenzin Homolog (PTEN) pathways

Takagi et al. (22) highlighted the pivotal role of the epidermal growth factor receptor (EGFR) pathway and its downstream effectors in promoting breast cancer brain metastasis (BCBM). The signalling pathways involved include PTEN, mammalian target of rapamycin (mTOR), and phosphatidylinositol-3-kinase (PI3K), all of which regulate key cellular processes like proliferation, survival, and migration, contributing to metastasis progression. The study identified critical proteins, such as EGFR (HER1), HER2, HER3, PIK3CA, and Akt, that are regulated by these pathways. EGFR, HER2, and HER3 are members of the ErbB receptor family and activate signalling cascades that support tumour growth and resistance to apoptosis. Specifically, HER2 overexpression is linked to more aggressive tumour traits and increased metastatic potential, while HER3 enhances HER2 signalling via dimerization. Downstream, the PI3K/AKT/mTOR axis is activated, promoting cell survival and proliferation. PIK3CA mutations often lead to hyperactivation of the PI3K pathway, driving tumour aggressiveness. The Akt

kinase supports cellular growth and survival, both crucial for metastasis. PTEN acts as a tumour suppressor by negatively regulating the PI3K pathway; its loss, common in metastatic breast cancers, leads to unchecked PI3K/AKT activity, enhancing survival and mobility of cancer cells. Moreover, mTOR influences metabolism, protein synthesis, and autophagy, and its dysregulation is linked to increased metastatic potential. Therefore, targeting the mTOR pathway represents a promising therapeutic strategy for managing brain metastasis in breast cancer.

1.3.3 Vascular Endothelial Growth Factor (VEGF) and Signal Transducer and Activator of Transcription 3(STAT3)

The formation of breast cancer brain metastasis (BCBM) is influenced by both breast cancer cell characteristics and host factors, with vascular endothelial growth factor (VEGF) and signal transducer and activator of transcription 3 (STAT3) playing pivotal roles (22). VEGF and STAT3 play an important role in the development of BCBM. BC cells can release VEGF to induce neovascularization in brain metastases and then VEGF binds to receptors on the surface of endothelial cells to activate the VEGF receptor VEGFR2, which in turn activates downstream signalling STAT3, PI3K and MEK-ERK(23). These signalling pathways promote tumour cell survival, proliferation, and angiogenesis, crucial for metastasis development. STAT3 not only acts downstream of VEGF signalling but also influences the tumour microenvironment, modulating VEGF receptors on cerebrovascular endothelial cells and enhancing BBB permeability. This upregulation of VEGFR2 facilitates the migration of breast cancer cells across the BBB, promoting invasion. Furthermore, factors like hypoxia-inducible factor 1-alpha (HIF-1 α) contribute to BCBM by inducing VEGF expression under hypoxic conditions, enhancing angiogenesis. This complex interplay establishes a positive feedback loop that supports tumour growth in the brain. Thus, targeting the VEGF-VEGFR2 and STAT3 pathways presents a promising therapeutic strategy to

inhibit BCBM development by reducing neovascularization, BBB permeability, and metastatic cell invasion.(24)

1.3.4 β III micro tubulin and DNA Topoisomerase II Alpha (TOP2A)

Kanojia et al(25) identified that the neuronal marker β III-tubulin (TUBB3) is overexpressed in breast cancer (BC) cell lines with brain metastases, with its expression significantly linked to distant metastasis. Knockdown of TUBB3 in BC cell models (MDA-Br, GLIM2, and MDA-MB-468) resulted in reduced invasive capacity and a decreased proliferation rate, indicating TUBB3's role in enhancing metastatic potential. In MCF-7 cells, decreased TUBB3 and TOP2A expression reduced cell proliferation and promoted apoptosis. Clinically, TUBB3-positive breast cancer patients exhibited a lower proliferation rate and better disease-free survival (DFS) and overall survival (OS) compared to TUBB3-negative patients, suggesting TUBB3's prognostic value. However, the relationship between TUBB3 expression and breast cancer brain metastasis remains *in vitro*, and further research is needed to confirm its role in clinical settings and its potential as a therapeutic target.

1.3.5 Basonuclin 1(BNC1), Polypeptide N-acetylglucosaminyltransferase 9 (GALNT9), Coiled-Coil Domain Containing 8 (CCDC8)

Pangeni *et al* (26) identified aberrant expression of GALNT9 (an O-glycosylation initiator), CCDC8 (a microtubule dynamics regulator), and BNC1 (a transcription factor) in primary breast cancer brain metastases (BCBM). Their study revealed distinct methylation patterns, with these genes highly methylated in brain metastases but poorly methylated in primary breast cancer. Specifically, methylation of BNC1 and GALNT9 occurred in the late stages of BCBM, while CCDC8 underwent methylation at earlier stages, indicating its role in the initial events of brain metastasis. These differential methylation patterns suggest that

epigenetic modifications significantly influence breast cancer progression and metastasis. The late stage hypermethylation of BNC1 and GALNT9 may contribute to tumour cell adaptability within the brain microenvironment, whereas early methylation of CCDC8 could be essential for initial invasion and metastasis. Targeting these methylation events offers a potential therapeutic strategy for managing BCBM, while understanding their dynamics could aid in developing early detection biomarkers.

1.3.6 Human Epidermal Growth Factor Receptor (HER2) and Human Epidermal Growth Factor Receptor 3 (HER3)

HER3 is closely associated with HER2, forming a dimer that plays a critical role in the progression of breast cancer brain metastasis. The HER2-HER3 dimer facilitates the ability of breast cancer cells to cross the tight junctions (TJ) of the BBB, thereby promoting metastasis to the brain. This process is highly dependent on the signalling activity of both HER2 and HER3. The interaction between HER2 and HER3 activates downstream pathways, such as PI3K/AKT and MAPK, which are crucial for cell survival, proliferation, and migration. The dimerization of HER2 and HER3 not only enhances signalling potency but also helps breast cancer cells adapt to the brain microenvironment, supporting their invasion and establishment within the brain. Consequently, targeting the HER2-HER3 interaction or its downstream signalling pathways could be an effective therapeutic strategy to prevent or reduce brain metastasis, especially in HER2-positive breast cancer patients. This underscores the importance of HER3 in the metastatic cascade and highlights the potential of anti-HER3 therapies as an adjunct to current HER2-targeted treatments.

1.3.7 Receptors on astrocytes associated with Brain Metastasis

Astrocytes secrete matrix metalloproteinases (MMP), including MMP-1, MMP-2 and MMP-9(27). In CNS leukemia, MMP-2 and MMP-9 secreted by leukemic cells promote the disruption of TJ proteins, thus increasing intercellular permeability and leukemic cells crossing the BBB(28). It was found that that by co-culturing metastatic breast cancer cells with astrocytes, the invasive capacity of breast cancer cells was increased, leading to a significant increase in the incidence of BM(17). Although astrocytes can upregulate fibrinolytic enzymes to defend against invasive metastasis and promote FasL death signal paracrine, this response may lead to high expression of serine protease inhibitor and serine protease inhibitor B2 in BCBM cells, which promotes tumour invasion in brain tissue, leading to the progression of BCBM(17).

1.3.8 Sarcosine metabolism-related proteins

Sarcosine is a sensitive tumour marker in prostate cancer and is associated with tumour metastasis (29, 30). Previous studies have shown that sarcosine metabolism-related proteins are highly expressed in HER2 molecular subtypes of breast cancer and that the inhibition of sarcosine synthesis inhibits the growth of breast cancer(31, 32). The expression levels of sarcosine, glycine N-methyltransferase (GNMT), sarcosine, dehydrogenase (SARDH) and peroxidase sarcosine oxidase (PIPOX) were evaluated in metastatic breast cancer tissues. The expression levels of GNMT and sarcosine were usually high in brain and lung metastases of breast cancer, while PIPOX was low. This suggests that these proteins are significantly associated with brain metastases and lung metastases of breast cancer, but the exact mechanism needs to be further investigated(33).

1.3.9 Fructose-1,6-bisphosphatase (FBPS)

Malignant tumour cells consume more nutrients and energy than benign tumour cells(34). This is known as the 'Warburg effect', which compensates for the normal

glycolytic pathway to produce energy and nutrients. A study has shown that gluconeogenesis is enhanced in BCBM, while the ability of oxidise glutamine and branched-chain amino acids increased. After the silencing of FBPS genes resulted in a decrease in the activity of BCBM cells(35). In clinical practice, compared with primary BC cells, the activity of FBPS in BCBM decreased. However, FBPS and glycogen are indispensable for normal metabolism in humans, making it difficult to develop targeted drugs to treat BCBM.

1.3.10 Reactive oxygen-related proteins

Previous studies have shown that in ovarian cancer tissues, redox buffering systems such as thioredoxin, glutathione and antioxidant systems (catalase and superoxide dismutase) are differentially overexpressed or under-expressed in ovarian cancer tissues(36). Reactive oxygen species (ROS) can oxidize and reduce sensitive proteins in various tumour metastasis signalling pathways. The expression of ROS-related proteins was found to be significantly increased in metastases of breast cancer, including brain metastases(37). The site specificity of peroxidase in BCBM was shown by Kim et al(38) The expression of peroxidase was higher in brain metastases compared to bone metastases. In addition, the expression of ROS-related proteins correlated with the prognosis of patients.

1.3.11 Clinical symptoms and sites of Brain Metastasis

Breast cancer patients with brain metastases will survive only 1 month if they are not given any treatment in time(39). According to different treatment options, there are different improvements in survival benefit, see chapter 1.1.4 for details. The majority of brain metastases were multiple foci (54.2%), with the cerebellum and frontal lobe of the brain being the most common sites of brain metastases, accounting for 33% and 16%, respectively. Clinical symptoms associated with

brain metastases included headache (35%), vomiting (26%), nausea (23%), hemiparesis (22%), visual changes (13%), seizures (12%), and altered state of consciousness (7%)(40).

1.3.12 Comparison of symptomatic and asymptomatic brain metastases

Brain metastases usually occur in advanced BC, they rarely occur in early breast cancer patients and are usually detected by cranial imaging after the onset of neurological clinical symptoms. Of all patients with brain metastases from breast cancer, 16% to 19% exhibit clinical symptoms(41). There is also a clinical group of patients with occult brain metastases, this group of patients does not have any clinical symptoms and is only detected during routine examination.

Studies by Miller et al, Niwińska et al(42) showed that this group of patients accounted for 14.8% to 36%, although biopsies showed that 18% to 30% may be more realistic(41). This may be because the lesions are too small or too few; in the vast majority of patients, metastases do not result in brain tissue enema, and only a few larger lesions can be found with brain tissue oedema around them(42). In contrast, in single brain metastases metastatic lesions, only 19% exhibited clinical symptoms(41).

1.4 Treatments

Late diagnosis increases not only mortality rate but also the high cost of medical care(43). Unfortunately, the main form of treatment is palliative, which means that the survival rate of most patients cannot be improved. Nevertheless, as research has progressed, several treatment modalities have shaken the fatal status of BM in some spine BM subgroups.

Currently, local treatment remains the mainstay of BCBM treatment, including surgery, stereotactic radio surgery (SRS) and whole-brain radiotherapy (WBRT). The choice of treatment is determined by the patient's prognosis, the presence of neurological symptoms, and the number of metastases(44). Local treatment is more specific and effective for BM, though it has more serious adverse effects. Systemic therapy for BCBM is a systemic approach to cancer that includes chemotherapy, endocrine therapy, immunotherapy and targeted therapy. The systemic treatment of BCBM depends mainly on the molecular subtypes of breast cancer, the expression status of the oestrogen receptor, progesterone receptor and HER2. Many drugs targeting the primary site of breast cancer cannot cross the BBB, and some lipophilic drugs are easily excreted by the efflux pump of the BBB. This poses a challenge for the treatment of BCBM. Blood-tumour barrier (BTB) is more permeable than the BBB, but drugs still do not reach effective therapeutic concentrations. In addition, the BTB is more heterogeneous, resulting in higher drug concentrations in different parts of the tumour. How to overcome BBB, BTB and efflux pumps is an urgent issue in BCBM treatment. In this paper, we summarize the effects of traditional and new systemic therapies on the treatment of BCBM in HER2+, hormonal receptor (HR+), TNBC. In addition, discuss the local treatment and prognosis of BM briefly, with a view to providing a reference for the treatment of BCBM.

1.4.1 Systemic treatment for HER2-positive Breast Cancer Brain Metastasis

The HER2 receptor is a member of the tyrosine kinase receptor and epidermal growth factor receptor family. Approximately 20% of breast cancer belong to this subtype. HER2+ can contribute to the aggressive growth of breast cancer cells(45). Compared to other types of breast cancer, HER2+ tumours are more likely to be BCBM. The HER2 pathway is one of the most studied pathways for the treatment of breast cancer. According to statistics, 50% of HER2+ breast cancer patients deteriorated into intracranial metastases(46). A preclinical solid model study found a high number of metastatic HER2+ BC in the ventricles of the brain, which confirms that HER2+ breast cancer cells have a tendency to metastasize to CNS(47). HER2 upregulation enhances the role of growth signals in the extracellular environment, promoting cell survival and proliferation through a variety of downstream effects. Drugs targeting HER2 can block this downstream effect and improve the prognosis of patients with HER2+ breast cancer, but at the same time, central nervous system (CNS) metastases are increasing. Numerous studies have demonstrated a significant increase in survival time for patients treated with anti-HER2.

The main HER2-targeting drugs currently available include monoclonal antibodies, antibody-drug conjugates (ADCs) and tyrosine kinase inhibitors (TKI). TKI block the intracellular segment of HER2 molecules to exert anti-tumour effects, while ADCs target HER2 monoclonal antibodies coupled with cytotoxic drugs to further kill tumour cells.

1.4.2 Targeted therapies

Surgical resection is only suitable for limited BM, and the high recurrence rate after surgery requires adjuvant postoperative radiotherapy (48) and radiotherapy leads to significant late adverse effects such as cognitive impairment. In addition,

most of the existing chemotherapy or large molecule targeted drugs cannot effectively cross the BBB. For these reasons, it is especially important to develop targeted drugs and related therapies that can overcome the BBB effectively. One study demonstrated a greater disruption of the BBB during BCBM in triple-negative breast cancer patients compared to HER2+ patients(49). It can be inferred that once brain metastasis occurs, the BBB is disrupted. Unexpectedly, drugs that could not pass through the BBB were able to pass through the BBB and became useful for treatment. The application of new targeted drugs in BCBM patients is reviewed as follows(50).

1.4.2.1 Monoclonal antibodies

To date, evidence for the efficacy of trastuzumab, a class of drugs, in BMBC is based on retrospective studies. Like most other monoclonal antibodies, trastuzumab cannot cross the intact BBB. As a result, trastuzumab has a gradient in concentration in various body fluids. Prior to any local treatment, the ratio of trastuzumab in cerebrospinal fluid and plasma was 1:420 and will be substantially increased to 1:79 after radiotherapy. One study demonstrated that the median time to BCBM was significantly longer in BC patients treated with trastuzumab (15 months vs 10 months, $p = 0.035$) (51). The median of survival time (14.9 vs 4.0 months, $p = 0.0005$) was longer than in patients not treated with trastuzumab. However, much of this prolonged survival time was due to the control of extracranial disease. Pertuzumab, another monoclonal antibody against a different antigenic epitope of the HER2 receptor, has been approved in combination with trastuzumab and doxorubicin for patients with metastatic HER2 overexpressed breast cancer(51). In a clinical trial evaluating Pertuzumab and trastuzumab (CLEOPATRA trial), in which the median time to progression of CNS BM was used as the study endpoint. The median time was 15.0 months in the Pertuzumab-

treated group and 11.9 months in the placebo group(52). These studies suggest an association between the use of trastuzumab and the development of less aggressive BM. However, it is not possible to conclude from these results whether trastuzumab is a direct or indirect effect on BM. Because it cannot be excluded that it is the probability of developing secondary BM decreases after the new systemic lesions. Given that both trastuzumab and patuximab provide a survival benefit for patients with BCBM, further research is needed.

1.4.2.2 Trastuzumab Emtansine (TDM1)

Trastuzumab-emtansine (T-DM1) composed of trastuzumab and the microtubule inhibitor DM1 is an antibody-drug conjugate, has been approved for second-line treatment of HER2+ MBC after failure of trastuzumab and pertuzumab therapy. Following the results of the randomized phase 3 EMILIA trial(53). T-DM1 was associated with a statistically significant improvement in PFS and OS compared with sodium tyrosine combination therapy (HR for OS = 0.68, $p < 0.001$). Those improvements may be due to better control of systemic disease. The same conclusion was obtained in several studies using T-DM1 in combination with other systemic therapies(54, 55).

However, a study found that T-DM1 combined with SRS may increase the incidence of radio necrosis(56). Given that the small number of patients in this study, a larger prospective study is needed to assess the safety of T-DM1 in combination with SRS and the maximum tolerated dose and duration of administration.

1.4.2.3 [vic]-trastuzumab duocarmazine (SYD985)

The ADC [vic]-trastuzumab duocarmazine (SYD985) is comprised of the monoclonal antibody trastuzumab and a cleavable linker - the drug is called valine-citrulline-seco-DUocarmycin-hydroxyBenzamide-Azaindoleand has been

granted Fast Track designation by the US Food and Drug Administration (FDA). The Phase I NCT02277717 trial(57), a dose-expansion cohort of 146 patients with metastatic breast cancer, including 8 with BCBM, showed that SYD985 was safe and effective. However, there are no published data on SYD985 in the treatment of BM, so the role of SYD985 in BCBM needs to be further investigated.

1.4.2.4 [Fam-]trastuzumab deruxtecan (DS-8201)

DS-8201 consists of trastuzumab and deruxtecan, a topoisomerase I inhibitor. The Phase II DESTINY-Breast01 trial explored its effectiveness as a posterior line of treatment(58). In 184 patients with metastatic breast cancer who had previously received T-DM1 treated with DS-8201, the median PFS was 16.4 months, with an objective response rate (ORR) of 60.9% as assessed by an independent review committee; 24 of these patients had previously received treatment without brain metastasis-related disease. The median PFS was 18.1 months for 24 previously treated BCBM patients without symptoms related to BM. Of note, the incidence of lung disease increased after DS-8201 treatment and care should be taken to monitor pulmonary symptoms during treatment.

1.4.2.5 First-generation of tyrosine kinase inhibitors (TKIs)

An increasing number of small-molecule inhibitors are under clinical investigation. The first generation of full-molecule tyrosine kinase inhibitors (TKIs) for HER2+ are promising agents for HER2+ BCBM because they can cross the BBB. Lapatinib is one of them, which can target and inhibit both EGFR and HER2 receptor tyrosine kinases. It is worth mentioning that lapatinib is a substrate for transport carriers [such as P-glycoprotein (Pgp) and BCRP] located at the BBB. Lapatinib has different concentrations in different settings of the CNS, and the concentration of lapatinib transferred to the CNS in plasma has been reported to be about 26% by nucleotide tracers, while the concentration in normal brain

parenchyma is relatively low at 1.3% to 2.8%(59). The intracranial response rate of single-agent lapatinib is too low, and the results of a phase II clinical study suggest that the intracranial response rate of lapatinib with capecitabine in the treatment of patients with HER2 overexpression BCBM was 66%, with a median time to intracranial lesion progression of 5.5 months(60). However, the benefit remains modest in terms of clinical. Notably, half of the patients in this trial were asymptomatic, so the intracranial response may have been overestimated. Fortunately, these results suggest a better treatment effect with lapatinib for patients with early diagnosis. Despite these important results, there is no direct evidence that the lapatinib-capecitabine combination is superior to trastuzumab-based therapy in controlling BM or as a preventive treatment.

1.4.2.6 New-generation TKIs

Neratinib and Tucatinib, with specific BM endpoints, has been developed as new-generation TKIs(61). Forty patients with HER2 overexpressing BCBM experienced disease worsening despite the use of one or more first-line drugs for CNS-directed therapy. Switching to single agent treatment with neratinib showed a low intracranial response rate of approximately 8% and progression-free survival of 1.9 months(62). Tucatinib activity on BM was a prespecified secondary endpoint of the large pivotal HER2CLIMB trial(63), which was the largest randomized trial to date with a specific BM endpoint trial. It analysed the results of adding tucatinib to trastuzumab and capecitabine in patients with pre-disposed HER2+ MBC. There was a 68% reduction in the risk of progression or death. (HR 0.32, $p < 0.00001$). The main toxic effect was diarrhoea. Notably, the efficacy of tucatinib on BM was identical to that of the entire population. It again suggests that the effect of drug treatment on brain disease progression is mostly equivalent to the effect observed in extracerebral disease. The results of these 2 studies suggest that the combination of drugs that pass through BBB in patients with

BCBM can be used to treat both intracranial and extracranial lesions with relatively good results.

1.4.3 Endocrine therapy

Endocrine therapy remains a cornerstone for hormone receptor-positive (HR+) breast cancer treatment, but its effectiveness in managing brain metastases (BM) is not well established. In recent years, cyclin-dependent kinase 4/6 (CDK4/6) inhibitors have revolutionized HR+ breast cancer treatment by delaying disease progression and overcoming resistance to traditional endocrine therapies, although their role in brain metastasis remains challenging due to the difficulty of reaching effective concentrations within the brain. Additionally, targeting the phosphatidylinositol-3-kinase/protein kinase B/mammalian target of rapamycin (PI3K/Akt/mTOR) pathway has expanded treatment options for patients with breast cancer brain metastasis (BCBM), as this pathway plays a key role in cell growth and survival. The combination of CDK4/6 inhibitors, PI3K/Akt/mTOR inhibitors, and endocrine therapy offers a promising approach for managing HR+ BCBM by addressing resistance mechanisms and improving treatment efficacy. However, the BBB remains a significant obstacle, prompting ongoing research into novel agents and drug delivery methods that can effectively penetrate the BBB. These advancements underscore the importance of an integrated therapeutic approach to enhance disease control and improve the quality of life for HR+ breast cancer patients with brain metastases.

1.4.3.1 Cyclin-Dependent Kinase 4 and 6 (CDK4/6) inhibitors

The CDK-4/6 pathway regulates the cell transition from G1 to S-phase division. The intact pRb gene leads to the release of various transcription factors during this transition(64). This step is crucial for controlling cell proliferation, which is dysregulated in a wide range of cancer cells(65).

About 50% of HR+ breast cancer patients develop drug resistance during endocrine therapy. Blocking downstream signalling pathways by inhibiting CDK4/6 is a therapeutic strategy to counteract resistance. Since 2015, CDK4/6 inhibitors such as Palbociclib, Ribociclib and Abemaciclib have been invented, and these drugs are showing increasing effects in the treatment of patients with advanced HR+ BC. Recent trials have explored their potential role in patients with HR+ BCBM. A report of Abemaciclib in patients with BCBM showed good CNS penetration, with drug concentrations in plasma comparable to those in cerebrospinal fluid(66). The phase II NCT02308020 trial included patients with BCBM who had previously received multiple lines of therapy and showed that after monotherapy with Abemaciclib, CNS patients were treated with a single dose of Abemaciclib. The results showed an ORR of 6%, a clinical benefit rate of 25% and a median PFS of 4.4 months for CNS after monotherapy with Abemaciclib(67). A meeting abstract has evaluated the safety of Abemaciclib in the treatment of HR+ BCBM. The conclusion demonstrated, compared to pre-treatment, treatment with CDK4/6 inhibitors resulted in a significant increase not only in loss-of-function mutations in retinoblastoma gene 1 ,but also in PI3K/Akt, cell cycle and Hippo signalling pathways(68). These genomic alterations may be associated with CDK4/6 inhibitor resistance.

1.4.3.2 Phosphatidylinositol 3-Kinase / Protein Kinase B / Mammalian Target of Rapamycin inhibitors (PI3K/Akt/mTOR) inhibitors

The recurrence of HR+ breast cancer is often associated with activation of the PI3K/Akt/mTOR pathway. PI3K/Akt/mTOR inhibitors have shown promising efficacy in metastatic breast cancer, but clinical data on their use in the treatment of BCBM are scarce. The two most common aberrations in this important pathway are PIK3CA mutations and PTEN deletion(69, 70). PIK3CA mutations are found in 28-47% of HR+ tumours and 23-33% of HER2+ BC, whereas PTEN deletion is seen

in 29-44% of HR+ tumours and 22% of HER2+ BC(71). In contrast, PIK3CA mutations and PTEN gene deletions occur in triple-negative BC patients are 7% and 35% separately(72). The mTOR inhibitor Enviroximes and PI3K inhibitor Buparlisib are currently being studied clinically in patients with BCBM. These clinical trials will provide more evidence of the role of the mTOR pathway in BCBM.

1.4.4 Triple-negative breast cancer (TNBC) patients with BM treatment

Triple-negative breast cancer (TNBC) is a highly aggressive subtype, predominantly affecting younger women and characterized by a high propensity for metastasis, recurrence, and brain metastasis (BM). Despite chemotherapy being the mainstay of treatment for TNBC, the prognosis remains poor due to the absence of specific actionable targets, highlighting the urgent need for novel therapeutic strategies. Recent studies have shown that anti-angiogenic agents and immune checkpoint inhibitors hold significant promise in improving outcomes for TNBC patients. Anti-angiogenic therapies, by inhibiting tumour vasculature development, can effectively limit tumour growth and metastasis. Meanwhile, immune checkpoint inhibitors have emerged as a potential treatment option by reactivating the immune system to target TNBC cells, demonstrating encouraging results in clinical trials. Combination therapies, integrating these targeted approaches with chemotherapy, are also being explored to enhance treatment efficacy and overcome resistance. Ongoing research aims to identify more precise molecular targets, improve patient selection for immunotherapy, and ultimately develop more effective and personalized treatment strategies for TNBC, particularly for those at risk of or suffering from brain metastasis.

1.4.4.1 Chemotherapies for Triple-negative breast cancer

Traditional chemotherapy has a limited role in the treatment of BCBM because the BBB restricts the passage of large molecule drugs. In addition, there are various ATP-conjugated efflux transport proteins, including P-glycoprotein and breast cancer resistant protein (BCRP) bind to structurally different to structurally different drugs and render them ineffective

Objective remission rate (ORR) is the proportion of patients whose tumour volume shrinks to a pre-specified value and can maintain the minimum time requirement and is a direct measure of the anti-tumour activity of a drug. None of the older chemotherapeutic agents such as capecitabine, cisplatin, cyclophosphamide, etoposide, 5-fluorouracil, gemcitabine, methotrexate, vinorelbine, and vincristine have been approved for the treatment of BM from breast cancer for this indication. Although they have received good response rates in the treatment of BM. (ORR up to 40%) . (73, 74)Some studies from two decades ago showed that patients with these older chemotherapy drugs had only 2.9 months of progression-free survival (PFS) and only 5.5 months of overall survival (OS). These discouraging values shatter the illusion that BCBM can be cured with chemotherapy alone, but they also showed that some chemotherapeutic agents can partially penetrate BTB to obtain the effects of systemic therapy.

As technology evolves, combining nanotechnology and polymerization chemistry to deliver larger amounts of drugs directly to cancer cells in a controlled manner has become a popular area of cancer research. A number of new anti-cancer chemotherapeutic agents have emerged(75). For example, paclitaxel-albumin conjugated type is a combination of hydrophobic paclitaxel and human serum albumin carrier by nanotechnology, which is more easily decomposed *in vivo* than solvent-based paclitaxel and can transport paclitaxel to tumour tissues through cytokinesis with relative targeting. The main drug metabolism characteristics are

linear pharmacokinetics, with a biphasic decrease in concentration after intravenous injection, and renal excretion is not the main metabolic route, but 20% excretion in the faeces. The clinical dose range is larger (80~375mg/m²) than that of conventional solvent-based paclitaxel. Moreover, allergic reactions are rare, glucocorticoid pretreatment is not required before clinical administration, and the infusion time is short, which is convenient for clinical administration(76). Using nanotechnology, irinotecan pegol has been investigated as the first long-acting topoisomerase 1 inhibitor that provides sustained exposure(77). It both prolongs the exposure time of SN-38 (the active metabolite of irinotecan) and reduces its toxicity at the same time. For similar drug improvement purposes, MM-398 (nano liposomal irinotecan) is also being investigated as a new drug that can penetrate the BBB(78).

1.4.4.2 Vascular endothelial growth factor (VEGF) pathway

The VEGF pathway plays a crucial role in the development of various malignant tumours. In TNBC breast cancer, it is hoped that VEGF inhibitors such as bevacizumab will play a key role in improving efficacy against metastatic disease. However, multiple phase III clinical trials and meta-analyses showed that the addition of bevacizumab failed to provide any survival benefit in metastatic breast cancer(79). Most of these studies did not include patients with BM, because the investigators feared that bevacizumab would cause intracranial haemorrhage. For such improvement, we have a more rigorous and optimistic attitude. On the one hand, bevacizumab is used safely in primary brain tumours like glioblastoma without significant bleeding risk. On the other hand, bevacizumab acts on the vasculature in meningiomas, causing changes that are difficult to detect by ordinary scans, this phenomenon is often seen in primary CNS tumours.

Hu *et al* reported a case of TNBC patients who had previously received fifth-line therapy. After receiving sixth-line therapy with apatinib combined with irinotecan and S-1, partial remission of intracranial lesions was achieved(80). This also sheds light on the therapeutic potential of antiangiogenic drugs in TNBC patients with BM.

1.4.4.3 Immunotherapies

In recent years, breakthroughs in breast cancer immunotherapy have been achieved with the advancement of related research. With the presentation of the results of the phase III IMpassion130 study at the European Society of Medical Oncology (ESMO) annual meeting at the end of 2018, breast cancer has officially entered the era of immunotherapy(81). However, in the field of BM, the exploration of immunotherapy in the brain has been particularly late. This is because researchers used to think that the brain was an "immune privileged" area, meaning that the presence of antigens in the brain did not elicit an inflammatory immune response.

The turning point came from recent studies where immune checkpoint inhibitors achieved better efficacy in both non-small cell lung cancer and melanoma BM (82, 83). Thus, immunity therapy may be effective for BM in TNBC patients as it is for BM from other tumours. Atezolizumab (an antibody targeting the programmed death receptor 1 / PD-L1) has been approved in combination with nab-paclitaxel for the treatment of TNBC patients with BM. In the phase III clinical trial of IMpassion130 for TNBC(84), a total of 902 patients, 61 of whom had BM, were enrolled and randomized to atezolizumab /placebo combined with albumin-bound paclitaxel; the results showed that the PD-L1-positive patients in the

atezolizumab group had a 7-month longer OS compared with the placebo group (25.0 months vs. 18.0 months). However, L1-negative patients had almost no survival benefit (19.7 months vs. 19.6 months). The lack of statistical significance can be explained by the small size of the BM population, as only 6.3% of the study population.

1.4.4.4 Poly ADP-ribose polymerase (PARP)

Poly ADP-ribose polymerase (PARP) inhibitors can hinder the repair of DNA single-strand damage and are found in breast cancer susceptibility gene 1/2 (breast cancer susceptibility gene 1/2). A clinical study of the PARP inhibitor OLYMPIAD did not enrol patients with BM. In contrast, the EMBRACA study included 63 BCBM patients, and the results showed that the PARP inhibitor talazoparib was more effective than the choice of therapy (capecitabine, eribulin, gemcitabine or vinorelbine monotherapy)(85). The median PFS was significantly prolonged (8.6 months vs 5.6 months, HR = 0.54), and the ORR was improved (62.6% vs 27.2%) in the Nitrogen group. In addition, the PFS benefit achieved with talazoparib was consistent across prespecified subgroups, including patients with a history of BM. It may be a new hope for TNBC patients BM, but more prospective studies are needed.

1.4.4.5 Paclitaxel Treva tide (ANG1005)

ANG1005 is composed of three paclitaxel molecules linked to the brain-targeting peptide angioprep-2, which induces transcytosis across the BBB by recognizing low-density lipoprotein receptor-related protein 1. A phase II study(86) included 72 patients with recurrent BCBM, and the results showed that ANG1005 could effectively control intracranial and extracranial lesions, improve symptoms of BM, and prolong survival, especially for patients with leptomeningeal metastases. This

drug is very inspiring for our project to develop Artemisinin to carry targeted drugs to penetrate the BBB.

1.4.5 Local treatment for Breast Cancer Brain Metastasis

Local treatment is still the cornerstone of BCBM treatment. The question of how to integrate local and systemic therapy remains a pressing one. Local therapy can disrupt the BBB, thereby increasing the concentration of drugs in brain tissue and providing better control of intracranial lesions.

The guidelines for the treatment of HER2+ BCBM published by ASCO in 2018 also recommend that systemic therapy with drugs that are readily transmissible through the BBB be used for BCBM that progresses after local treatment(44).

For patients with rapidly progressing extracranial lesions, systemic therapy should be administered first, and local treatment of intracranial lesions should be considered after the extracranial lesions have stabilized; while for patients with severe BM, local treatment can be administered first to reduce intracranial pressure and then maintained with systemic therapy after the symptoms have subsided. For patients with stable extracranial lesions and progressive intracranial lesions during treatment, the systemic treatment regimen can be considered unchanged with enhanced local therapeutic interventions.

1.4.5.1 Whole Brain Radiotherapy (WBRT) and Stereotactic Radiosurgery (SRS)

SRS treatment is superior to WBRT in that it provides local control of the lesion by delivering photon radiation with high precision. SRS is widely used in the treatment of BM because of its high accuracy and minimally invasive nature. SRS is suitable for patients with one to three intracranial metastases, tumour diameter <3 cm, controlled disease and good health. In patients aged <50 years, SRS alone

did not affect the recurrence of BM and may benefit specific patients(87). When BM recur, WBRT or reintroduction of SRS can be salvage therapy. The results of a meta-analysis compared the efficacy of SRS alone with WBRT combined with SRS for BM showed that SRS combined with WBRT did not prolong OS in patients with multiple BM. However, the use of SRS in combination with WBRT for breast cancer BM reduces the rate of local tumour recurrence and distant metastases compared to SRS only. In addition, the use of both HER2-targeted therapy and SRS can also delay local recurrence, although the potential for serious adverse effects should be noted(88).

1.4.5.2 Combining surgery with Stereotactic Radiosurgery

A prospective randomised controlled trial found no significant difference in local control rates or overall survival between SRS and surgery(89). However, SRS prolongs the duration of cognitive decline(90). This finding is particularly important for clinicians when making treatment decisions, as it highlights the trade-offs between different therapeutic approaches. While both SRS and surgery are effective in terms of controlling tumour growth and maintaining overall survival, the impact on cognitive function becomes a critical consideration for patient quality of life. The prolonged cognitive decline observed with SRS suggests that, for certain patients—especially those for whom preserving neurocognitive function is a priority—surgery might be a preferable option, potentially followed by other forms of postoperative radiotherapy to minimize cognitive side effects. This provides an evidence-based rationale for tailoring postoperative radiotherapy strategies based on individual patient needs, aiming to balance effective tumour control with quality-of-life considerations. Furthermore, it underscores the necessity of involving patients in shared decision-making, providing them with comprehensive information about the risks and

benefits of each treatment modality to ensure that their personal preferences and priorities are reflected in the chosen therapeutic approach.

1.4.6 Proton therapy

The use of proton therapy in cancer treatment is increasing and the number of registered proton centres worldwide is growing. According to the latest data published by the Particle Therapy Collaborative Group (PTCG) in September 2020, a total of 110 operational particle facilities are registered. In addition, there are at least 64 particle beam centres currently under construction or in the planning stage(91).

A proton beam interacting with matter can release little energy and little variation at the beginning of the range, called plateau region and a large amount of energy near the end of the range, forming a spike called the Bragg Peak, after which the energy deposition falls rapidly to 0. The energy deposition curve is shown in Figure 1.4.6 Using this property, the Bragg Peak can be placed at the location of the tumour by selecting the right proton energy, effectively reducing the dose to the normal tissue in front of and behind the tumour, thus better protecting the normal tissue. Protons have a larger mass relative to the extranuclear electrons and are less susceptible to scattering, which can effectively reduce the irradiation penumbra. Proton-based radiotherapy has the advantage of minimising the radiation dose to normal structures adjacent to the tumour compared to standard photon therapy.

Proton therapy has the potential to reduce long-term adverse brain effects for patients with BM, such as radiation necrosis(92). There is currently no precise definition of the extent of the reduction in radiation dose to the brain and how much benefit it can provide to the patient. Therefore, the search for predictive biomarkers of late toxicity may shed light on the potential of proton-SRS treatment in reducing the incidence of radionecrosis. On the other hand, it is not well understood whether protons influence normal cells of the nervous system. Taking all this into account, well-designed trials are necessary to assess the clinical efficacy of proton-SRS in patients suffering from BMs.

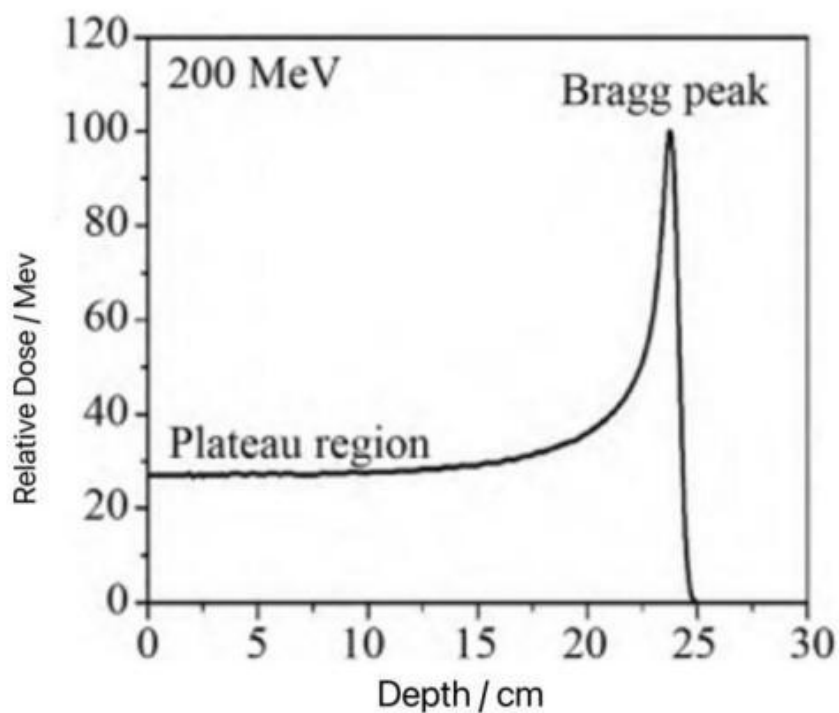


Figure: 1.4.6 Proton dose death distribution curve. A proton beam deposits little energy in the initial part of its range (plateau region) and releases most of its energy near the end of its path, forming a sharp Bragg Peak, after which the dose rapidly drops to zero. By adjusting the proton energy, the Bragg Peak can be precisely placed at the tumour site, maximising tumour dose while sparing surrounding normal tissue.

1.5 Limitations of Current Treatments

Despite the advances in managing brain metastases from breast cancer (BCBM), significant limitations still impede effective treatment. Local treatment approaches, such as surgery and radiotherapy, though effective in controlling localized brain metastases, carry substantial adverse effects, including neurocognitive impairments and the risk of radionecrosis. Whole-brain radiotherapy (WBRT) and stereotactic radiosurgery (SRS) often lead to cognitive decline, impacting the patient's quality of life. Systemic therapies, including chemotherapy, endocrine therapy, immunotherapy, and targeted therapies, face significant challenges due to the BBB. Many chemotherapeutic and large-molecule targeted drugs cannot effectively penetrate the BBB, leading to insufficient therapeutic concentrations within the brain. Moreover, the blood-tumour barrier (BTB) is heterogeneous, resulting in variable drug concentrations within the tumour and complicating consistent treatment efficacy.

Even the newer targeted therapies, such as monoclonal antibodies, tyrosine kinase inhibitors, and antibody-drug conjugates, face barriers related to limited penetration through the BBB and the development of drug resistance. Additionally, the efficacy of endocrine therapy in managing hormone receptor-positive BCBM is limited, with the BBB preventing effective drug concentrations in the brain. Chemotherapies, while useful in some cases, generally show poor outcomes due to rapid excretion and resistance mechanisms.

Proton therapy, while promising in minimizing radiation exposure to normal tissues and reducing long-term adverse effects, also has notable limitations. The high cost of proton therapy limits its accessibility for many patients, and its availability is restricted due to the limited number of treatment centres worldwide. Additionally, there is still a lack of sufficient clinical data to determine its efficacy compared to conventional radiotherapy in terms of overall survival

and quality of life. Moreover, uncertainties remain regarding the potential effects of proton therapy on normal brain cells and the optimal criteria for patient selection.

Given these challenges, the need for novel approaches that can effectively overcome these barriers is critical. Artemisinin, a compound originally used as an antimalarial, shows promise in penetrating the BBB and potentially delivering anti-cancer effects. This motivates the exploration of Artemisinin as an innovative treatment modality for BCBM, aiming to address the limitations of current therapies by providing an effective means to target both intracranial and extracranial lesions while minimizing adverse effects.

1.6 Structure and function of the Tight Junction

A series of junctional complexes exist in the lateral membranes between adjacent epithelial or endothelial cells, including tight junctions, adherens junctions, gap junctions, and desmosomes. Among these, tight junctions are located at the top of the junctional complex and serve multiple functions, including acting as a barrier, a fence, and a signal transducer. Tight junctions form an impermeable fluid barrier between adjacent cell membranes, characterized by discrete fusion sites between neighbouring cytoplasmic membranes, continuous intramembrane particles on the protoplasmic surface, and corresponding extramembrane grooves. These protein complexes create mesh-like fibres that link adjacent cells and seal intercellular spaces, as shown in Figure 1.6 As can be seen in the diagram, TJs are present between adjacent endothelial cells, forming closed cords. Sealing off the spaces between the lateral sides of the cells. Prevents the diffusion of substances within the gaps between cells. Since the mid-1980s, the molecular components of tight junctions have been extensively studied to better understand their structure and function.(93, 94). The tight junctions between the epithelium and endothelium perform four main physiological functions: I) sealing the epithelium and

endothelium; II) acting as a sensor of cell signalling, influencing cell polarity, differentiation and proliferation; III) mediating intercellular adhesion; and IV) acting as a barrier to cell migration and movement. Cell adhesion is essential for gene expression, differentiation, motility and growth (95). The regulation of cell adhesion is mediated by a multimolecular complex of cell adhesion molecules, transmembrane receptors and cytoskeletal proteins. Although the barrier function of tight junctions is well understood, their role as multiprotein complexes in cell polarity, proliferation and differentiation has only recently been recognized(96). In addition, tumour development is often associated with altered or absent tight junctional structures in epithelial and endothelial cells. As shown in the diagram 1.6., there are many membrane proteins present in the cell membrane. They are mobile. However, because of the presence of TJ, protein A at the top is unable to flow to the sides and base of the cell. Protein B on the sides is also unable to flow to the top and base. This means that one of the functions of the TJ is to maintain cell polarity (1); external substances have to be transported across the membrane to reach the stroma, which demonstrates the TJ acts as a selective permeability barrier (2); the TJ forms the lamellar structure of the epithelial tissue and helps to maintain a certain mechanical strength of the epithelium.

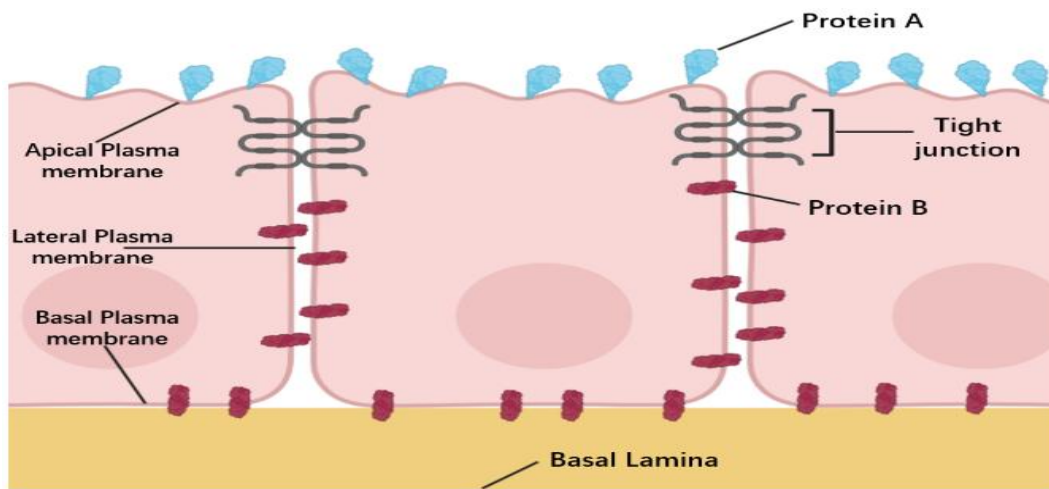


Figure 1.6 Tight junctions maintain cell polarity and barrier function. Tight junctions (TJs) seal the intercellular space between adjacent epithelial/endothelial cells, preventing paracellular diffusion. By restricting membrane protein movement (Protein A at the apical side and Protein B at the lateral side), TJs maintain cell polarity, act as a selective permeability barrier, and help preserve epithelial integrity. (Created by the author using BioRender).

1.7 Tight junction proteins

The tight junction consists of three main structural regions: (I) Transmembrane proteins, including members of the CLDN (claudin) and OCLDN (occludin) families, as well as junctional adhesion molecule (JAM) family members. These transmembrane proteins form the backbone of the tight junction and are crucial for cell-cell adhesion(97). Claudin, for instance, determine the specific ion permeability properties of the tight junction, effectively contributing to the selective paracellular transport of ions and solutes. Although occludin is not strictly necessary for the formation of tight junctions, it plays an important role in regulating the permeability and stability of these structures and also participates

in signal transduction pathways that influence cell behaviour(98). JAM proteins further contribute to the formation of tight junctions by promoting homotypic or heterotypic adhesion between adjacent cells, thereby strengthening the integrity of the barrier.

(II) Sub-membrane or plaque proteins, including the Zonula Occludens ZO-1, ZO-2, ZO-3 and catenins, are located on the cytoplasmic side of the cell membrane and act as scaffolding proteins. ZO proteins are crucial for linking transmembrane proteins, such as claudin, occludins and JAMs, to the actin cytoskeleton, thereby providing mechanical support and ensuring the stability of the tight junction. ZO-1, ZO-2, and ZO-3 interact not only with tight junction proteins but also with signalling molecules, playing a dual role in maintaining the structure of tight junctions and mediating signal transduction. ZO proteins facilitate the clustering of transmembrane proteins into functional complexes, which is critical for maintaining the barrier function of tight junctions. Although catenin's are more commonly associated with adherent's junctions, they also play a supportive role in tight junctions by interacting with cadherins and integrating different cell adhesion systems, thereby enhancing intercellular cohesion(97).

(III) Tight junction-related regulatory proteins include kinases, phosphatases, small GTPases, and other signalling proteins that regulate the assembly, disassembly, and permeability of tight junctions. The regulation of tight junctions is a highly dynamic process, responding to various physiological and pathological stimuli, such as inflammation, oxidative stress, and mechanical forces. Kinases such as protein kinase C (PKC) and myosin light chain kinase (MLCK) phosphorylate tight junction components like occludin and ZO proteins, modulating their interactions and thus influencing tight junction permeability. Small GTPases, including RhoA, Rac1, and Cdc42, regulate the organization of the actin cytoskeleton, which directly impacts the tightness and resilience of the

junction(97). These regulatory proteins ensure that tight junctions can adapt to changing cellular environments, maintaining tissue homeostasis while allowing appropriate responses to external signals(97).

Among these structural regions, the integration of transmembrane proteins is essential for the correct assembly and function of tight junction structures through homotypic or heterotypic interactions. Furthermore, peripheral or plaque-anchored proteins, such as ZO-1, perform a scaffold-like function to assemble tight junction molecules and link them to the actin cytoskeleton and associated regulatory proteins. This anchoring to the cytoskeleton is crucial not only for the mechanical stability of tight junctions but also for facilitating dynamic remodelling in response to physiological changes. By linking the transmembrane components to the cytoskeleton, ZO-1 and other plaque proteins enable tight junctions to maintain their barrier function while adapting to mechanical and chemical stimuli, thereby ensuring the proper function of epithelial and endothelial barriers.

Recent research has also highlighted the dynamic nature of tight junctions, demonstrating that their permeability can be regulated in response to various physiological and pathological stimuli(99). For example, inflammatory cytokines, growth factors, and changes in cellular stress can modulate the expression and function of tight junction proteins, leading to alterations in barrier integrity. Dysregulation of tight junctions has been implicated in a variety of diseases, including inflammatory bowel disease, cancer metastasis, and neurodegenerative disorders, where compromised barrier function can contribute to disease progression. Understanding the molecular mechanisms underlying tight junction regulation and dysfunction is therefore critical for developing therapeutic strategies aimed at restoring barrier integrity in disease states.

1.7.1 Occludin (OCLDN)

Occludin was the first transmembrane protein to be identified(100). Occludin has a molecular weight of about 65 kD, consisting of four hydrophobic transmembrane domains, both N-terminal and C-terminal in the cytoplasm, with one intracellular loop and two extracellular loops. The extracellular loop of Occludin has many conserved glycine and tyrosine. There are many serine and threonine residues in the N- and C-terminal domains. The expression of Occludin is associated with various tissue and organ(101). Evidence suggests that Occludin protein is not a necessary component of TJ integrity. For example, embryonic stem cells, which do not express Occludin, are also capable of forming TJs(102). Saitou et al(103) knocked out Occludin in mice (*Mus musculus*), their results showed normal electrophysiology of the intestinal epithelium despite many histomorphology abnormalities.

1.7.2 *Claudin (CLDNs)*

Claudin have a molecular weight of 22-25 kDa and 27 members of the claudin family of proteins have been identified to date(104). Claudin 1-10, -14, -15, -17 and -19 share sequence homology and functional similarity and are often referred to as classical claudin(105). The simple structure diagram as 1.7.2A. Its transmembrane or cytoplasmic part determines the construction of tightly attached filaments, independent of the extracellular structural domain. This is why TJ chains are observed as lines or stripes under electron microscopy (Figure 1.7.2). The extracellular loops of Claudin in adjacent cell membranes can interact and thus close the cell gap, which is one of the reasons for the formation of TJs and ion permeation selectivity. Among the proteins that make up tight junctions, Claudin proteins play the most important role(106). Abnormal expression of Claudin proteins can lead to structural damage and functional impairment of epithelial and endothelial cells. Their abnormal expression has been observed in various epithelial-derived tumours, indicating that Claudin proteins may play an

important role in the invasion and metastasis of tumours (97). The loss and rearrangement of Claudin proteins or epithelial cadherin are important triggers for the mechanism of malignant tumour metastasis because the infiltration and metastasis of tumour cells are closely related to the destruction of intercellular connections. This destruction is caused by the loss or weakening of cell-cell adhesion, which is an important component of the tight junctions, where Claudin proteins play a critical role. Therefore, the relationship between Claudin proteins and intercellular connections is interdependent and inseparable (97). On the other hand, abnormal expression of Claudin proteins can disrupt the structure and impair the cellular function of epithelial and endothelial cells. The expression of tight junction proteins is also tissue-specific in malignant tumours, with different types of Claudin proteins expressed in cervical, colorectal, pancreatic, and renal cancers. Upregulation or downregulation of Claudin protein expression leads to the formation of abnormal tight junctions, ultimately contributing to the reduction of cell differentiation and polarity(98). Therefore, the abnormal expression of Claudin proteins often affects the biological behaviour of tumour cells in human malignancies. Abnormal expression of Claudin proteins is closely related to cancer cell invasion. When epithelial cells transform from a non-invasive phenotype to an interstitial cell that can freely move in the extracellular matrix, their invasive properties are enhanced(107). During the process of epithelial-mesenchymal transition, some transcription factors such as Slug, Snail, Twist, Zeb1, and Zeb2 play a crucial role(108). Regulating these transcription factors may lead to abnormal loss of cell adhesion and intercellular connections, causing primary tumour cells to spread to distant sites(108). The mechanism inducing epithelial-mesenchymal transition involves the participation of cell adhesion molecules such as epithelial cadherin, but the involvement of Claudin has not been confirmed(109).

Existing studies have demonstrated that Stanniocalcin-2 (STC2) can regulate the protein kinase C/CLDN1 pathway to inhibit breast cancer invasion and metastasis. Hou et al.(110)confirmed this by knocking out the gene STC2, which resulted in the inhibition of breast cancer invasion and metastasis. Moreover, a correlation analysis conducted by MA et al.(111) between CLDN1 and prognosis revealed that lack of CLDN1 expression was only correlated with lymph node metastasis. Negative CLDN1 expression was significantly associated with poorer recurrence-free outcomes, regardless of whether the lymph nodes were negative or positive. Multifactorial analysis also demonstrated that CLDN1 negative expression is an independent risk factor for recurrence and death. Therefore, CLDN1 expression is a predictive indicator of poor prognosis for breast cancer.

Studies have shown a close relationship between CLDN2 and breast cancer liver metastasis, and Tabariès et al (112) demonstrated that CLDN2 promotes breast cancer liver metastasis through tumour cell-hepatocyte interaction. In contrast to the CLDN2 levels in the primary tumour of breast cancer patients, Claudia was found to be more active in breast cancer liver metastases than in the primary tumour of breast cancer patients. CLDN2 levels were elevated in liver metastases but not in skin metastases; Tabariès et al further showed that lymphocytes regulate CLDN2 expression and can be a therapeutic target for breast cancer liver metastases(113). PDZ motif is essential for the anchorless growth and survival of cancer cells. It is essential for the survival of cancer cells and is thought to play a role in metastasis. It also promotes the adhesion of malignant cells to extracellular fibronectin and type IV collagen and type IV collagen on the extracellular matrix composed of type IV collagen. Adhesion of malignant cells to fibronectin and type IV collagen of the extracellular matrix was promoted by increasing the surface expression of the integrin receptor on breast cancer cells. Surface expression of the receptor on breast cancer cells.

It is worth mentioning that claudin 3, 4 and 6 also control the motility of MCF-7 and MDA-MB-415 breast cancer cell lines(114). A study demonstrated that CLDN4 expression has a relationship with nodal metastasis. Increased expression of CLDN4 enhances maintenance of the cancer microenvironment and stemness.(115) Osanai et al(116) showed increased resistance to apoptosis after CLDN6 knockdown in breast cancer MCF-7 cells, supporting the hypothesis that CLDN6 downregulation could lead to breast cancer tumour formation, and suggesting that the CLDN6 methylation phenotype may contribute to tumour formation and invasion. The results of Wu et al(117) showed that CLDN6 may act through the p38 mitogen-activated protein kinase pathway and that its inhibition may reverse CLDN6-induced apoptosis, invasion and metastasis, and that CLDN6 expression was negatively correlated with breast cancer invasion and metastasis. One experiment demonstrated that the inhibitory effect of ER β on breast cancer cell migration and invasion was mediated by CLDN6, which induced a beclin1-dependent autophagic cascade(118). There is a study suggesting that CLDN6 is transcriptionally upregulated by HIF-1 α under hypoxic conditions(119). Loss of CLDN6 may lead to increased HIF-1 α -driven breast cancer metastasis in a Small Ubiquitin-like Modifier conjugation-dependent manner.(119)

CLDN8 is downregulated in breast cancer(120).Low expression of CLDN8 is associated with lymph node metastasis. Low expression of both CLDN8 and AR indicates poor prognosis, while their expression is positively correlated. (120) Martin et al demonstrated that overexpression of claudin 20 in breast cancer cells decreases TER and thus increases their motility. and reduced trans-epithelial resistance.(121)

1.7.3 Junctional Adhesion Molecule (JAM)

JAM is a member of the immunoglobulin family, It consists of five members, JAM A/B/C/4/L, with a molecular weight of about 40 kD, all of them are all single transmembrane glycoproteins(122). Based on sequence similarity, JAM was divided into two subclasses. JAM A/B/C are the first subclass with a class II PDZ domain module at its C-terminus, which interacts directly with ZO-1 and Par-3. JAM 4/L belongs to a second subclass with a class I PDZ domain-containing module at its C-terminus (123). JAM forms a complex with Occludin, ZO-1 and other TJ proteins. They are widely expressed in lymphoid tissue, brain endothelial cells and various epithelial cells. In addition, they play a role in the migration of endothelial cells, maintenance of vascular function and regulation of cell permeability(97).

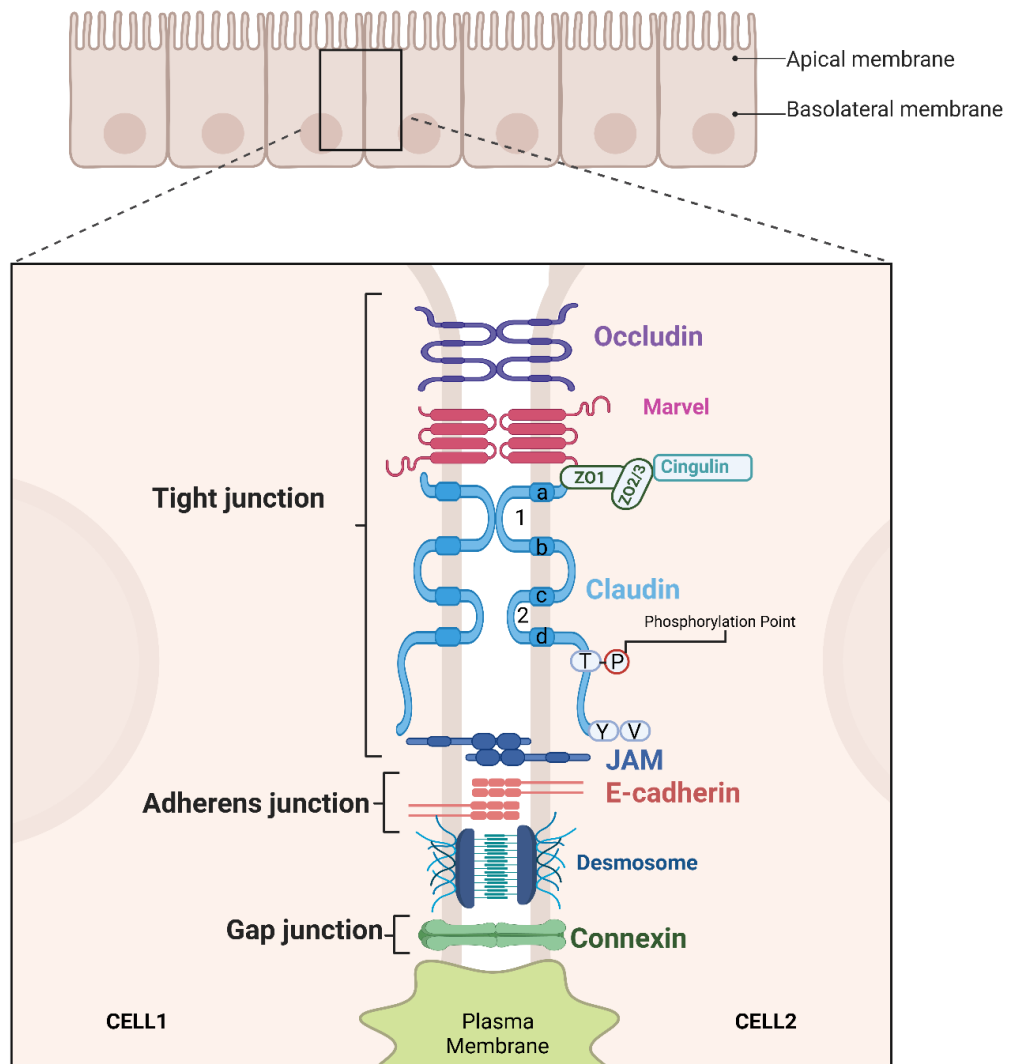


Figure 1.7.2 1,2: illustrates the structural components of cell junctions in endothelial cells, with a focus on tight junctions, which are formed by key proteins such as Claudin, Occludin, and Junctional Adhesion Molecule (JAM). Claudin proteins are shown with their extracellular loop domains and four transmembrane regions (labelled as a, b, c, d), which are critical for their function. The amino acids in the transmembrane regions a and d, as well as in the extracellular loop, are highly conserved, ensuring structural integrity and functional consistency. The first extracellular loop plays a pivotal role in determining the transmembrane resistance of tight junctions and the selectivity of paracellular pathways, directly influencing barrier function. Meanwhile, the tight junction structure is stabilized through interactions involving the transmembrane domains and cytoplasmic regions. These regions also contain phosphorylation points and PDZ-binding motifs, which are essential for interactions with scaffold proteins, further enhancing the stability and functionality of tight junctions. (Created by the author using BioRender) .

1.7.4 ZO-1,2,3

The ZO proteins belong to the membrane-associated guanylate kinase (MAGUK) family, which is the bridge to the TJ meshwork and is involved in maintaining and regulating the barrier function of polar cells. The ZO family consists of ZO-1 to 3, with molecular weights of 220, 160 and 130 kD, respectively, and ZO-1 was the first cytoplasmic protein identified in the TJ. The ZO family is characterized by three N-terminal PDZ domains (PDZ-1 to 3), a central SH3 and GUK domain, and a proline-rich region. PDZ1 binds to the C-terminus of the transmembrane protein Claudin and is important for the assembly of TJ. PDZ2 mediates the interaction between ZO proteins, forming heterodimers, and is also important for the regulation of TJ structure and function. PDZ3 is able to bind to the transmembrane protein JAM. The SH3 domain is a small protein domain containing about 60 amino acid residues, with homology to the viral junction protein c-Crk, phosphodiesterase and many non-catalytic parts of cytoplasmic tyrosine kinases, and facilitates the binding of JAM to the PDZ-3 domain, which binds proline-rich ligands and mediates the assembly of large multiprotein complexes (124, 125). The GUK domain has sequence similarity to guanylate kinase and mediates protein interactions (126).

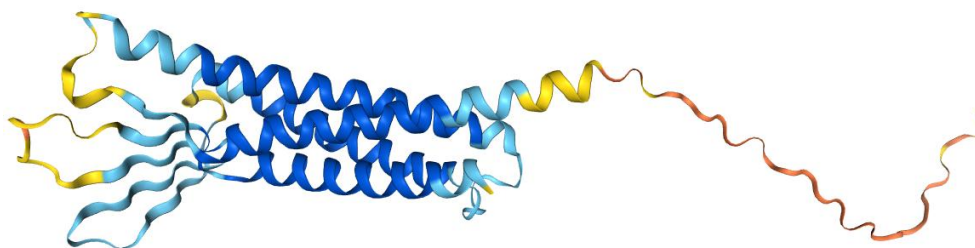
1.7.5 Cingulin

Cingulin has a molecular weight of 140 kD and its N-terminus is bound to ZO-1 and cytoskeletal proteins (mainly F-actin), acting as a link between the cytoskeleton and cytoplasmic proteins in the TJ. The structure is an elongated helix-helix dimer, like the myosin tail, containing both a head and a tail structural domain. The sequence analysis shows that it has partial homology with myosin, suggesting a possible interaction between Cingulin and myosin. Some studies showed that the epithelial tissue of Cingulin knockout mice had a normal TJ, suggesting that the deletion of Cingulin had no effect on the formation of the TJ

complex. However, it is worth mentioning that the gene expression levels of Claudin-2, -6 and -7 were increased. Furthermore, Cingulin could be phosphorylated by AMP-activated protein kinase (AMPK), which could enhance the TJ and cytoskeletal microtubule systems(127).

1.8 The function of Claudin-8

As shown in Figure 1.8, the structure is color-coded from blue (N-terminus) to red (C-terminus), indicating the predicted Local Distance Difference Test (pLDDT) scores, which reflect the confidence level of the structural prediction. Blue regions represent high-confidence structured domains, while red regions indicate flexible or disordered areas with lower prediction confidence. CLDN8 is a member of the claudin family, typically forming four transmembrane helices. The left portion of the image shows the transmembrane domain, while the extended C-terminal tail on the right may be involved in signalling or protein-protein interactions.



Confidence for predicted structure:

- Very high (pLDDT > 90)
- Confident (90 > pLDDT > 70)
- Low (70 > pLDDT > 50)
- Very low (pLDDT < 50)

Figure 1.8. Predicted 3D structure of Claudin-8 (CLDN8) protein (Image source: AlphaFold Protein Structure Database)

In addition to being involved in the construction of cell junctions alone, CLDN8 can also induce CLDN4 to move to the cell membrane region and participate in the construction of tight junctions together. After knockdown of Claudin-8 expression, CLDN4 is stalled in the endoplasmic reticulum and Golgi structure and cannot participate in the barrier composition of the cytosolic membrane(128). Unlike other proteins in the family, CLDN8 has the dual function of participating in the construction of junctions alone and assisting other connexins. CLDN8 form selectively permeable pores at the cell membrane level that are molecule size or charge specific, coordinating intercellular small molecule transfer while maintaining the epithelial barrier to macromolecules and effectively maintaining the proper functioning of the cellular bypass transport channels. CLDN8 was found to be highly expressed in the distal colon epithelium, increasing Na⁺ uptake by affecting ENaC, participating in the maintenance of Na⁺ ion gradients, and forming a barrier that simultaneously prevents reverse Na⁺ leakage(129). The paracellular pathway formed by CLDN8 plays an important role in substance metabolism and acid-base homeostasis by regulating charge polarity and influencing the passage of ions.

It is important to note that the barrier isolation of claudin proteins and molecular transmission coexist, resulting in contrasting expression levels in various epithelial tissues levels in various epithelial tissues. This can explain the difference in the barrier or transport function of CLDN8 in different cells.

The kidney is involved in maintaining the stability of the body's internal environment through the production and excretion of urine. Abnormal expression of CLDN8 results in dysregulation of electrolyte delivery and dysfunctional reabsorption and secretion in renal tubular epithelial cells. Hou J et al (128) showed that inhibition of CLDN8 expression decreased the permeability of the

renal collecting tubular paracellular pathway to Cl⁻ and had no effect on the permeability to Na⁺. Gordon's syndrome is an autosomal dominant disorder with clinical manifestations of hypertension, hyperchloremia, and hyperkalaemia, for which there is no effective prevention method. KLHL3, an E3 ligase ubiquitin ion channel protein, is one of the causative proteins in Gordon's syndrome, and a study(130) have found that Claudin-8 can be directly bound by KLHL3, leading to ubiquitination and degradation of CLDN8 and altered Cl-permeability, further causing elevated blood pressure and electrolyte disturbances.

Eduardo Molina-Jijon et al(131) found that in the renal unit of mice with type I diabetes, aldosterone promotes the transcription and expression of CLDN8 through SGK1 and WNK4 pathways promote CLDN8 transcription and expression, abnormally constrict tightened tight junction structures and reduced ion permeability of paracellular pathways, leading to diabetic kidney damage.

Guan M et al (132) found that in an African American population, CLDN8 expression was associated with end-stage renal failure due to type 2 diabetes. The progression of diabetic nephropathy is expected to be mitigated by targeted interference with Claudin-8 expression.

Most prostate cancers are androgen dependent. shikari D et al (133) found that CLDN8 is a downstream site of androgen action. The effect of androgens on CLDN8 is time-dependent and activates androgen receptor binding sites in the promoter region of CLDN8, which is involved in the transcriptional translation of CLDN8 and promotes the proliferation and migration of androgen-dependent prostate cancer cells. Androgens affect the progression of prostate cancer by regulating the expression of nodal CLDN8. Targeted interference with the transcriptional translation of CLDN8 is expected to block the chain of action of androgens and inhibit the development of tumour cells, which has potential research value.

Infectious diarrhoea is caused by pathogenic flora in the intestine, and the emergence of new pathogens and increased drug resistance increase the difficulty of treatment and prognostic assessment. Residues of tetracycline in intestinal cells can downregulate CLDN8 expression, disrupting the tight junction barrier and developing dysbiosis(134).

Inflammatory bowel disease (IBD), which includes ulcerative colitis (UC) and Crohn's disease (CD), is a group of chronic, nonspecific inflammatory diseases of the intestine. Its aetiology is not yet clear and no effective and precise treatment has been found. Zeissig S et al [26] found reduced expression of Claudin-8 along with redistribution and altered permeability of cytosolic cations in colonic epithelial cells in pathological tissues of Crohn's disease patients. Clark PM et al(135) found that in the pathological tissues of Crohn's disease, the expression of the gene encoding CLDN8 was downregulated. Whereas in pathological tissues of ulcerative colitis, the expression of CLDN8 was found to be downregulated in Crohn's disease pathology, but not in ulcerative colitis pathology. The effect of miR-223 on Claudin-8 was found to inhibit Claudin-8 activity, which in turn stimulated the IL-23 signalling pathway and contributed to inflammation(136). IL-23 signalling pathway, contributing to inflammatory bowel disease. Tight junctions' changes in structure allow for disruption of barrier function, over proliferation of epithelial cells, and inflammatory intestinal lesions occur. Targeted adjustment of miR-223 and Claudin-8 expression is expected to provide new therapeutic tools for patients with inflammatory bowel disease.

Microarray prediction analysis showed that CLDN8 is a valid indicator for prognostic risk assessment of colon cancer (137), and CLDN8 expression is downregulated in colon cancer tissues (138).

Nearly 90% of malignant tumours originate from epithelial cells. Tumours of epithelial cell origin are characterized by loss of cell polarization and altered

intercellular adhesion capacity as key factors in tumour invasion and metastasis, which are directly related to the role of Claudin proteins. Ki67 is a nuclear antigen that reflects cell proliferation activity. Zhang X et al(139) demonstrated that CLDN8 expression was elevated in nasopharyngeal carcinoma cells compared with normal nasal mucosa and positively correlated with lymphatic metastasis. Whereas with no significant correlation between age, Ki67 index, pathological grade and clinical stage, and that claudin-8 may contribute to the development and progression of nasopharyngeal carcinoma. Zhao XY et al(140) found that CLDN8 was down-regulated in Oral squamous cell carcinoma (OSCC) compared with normal oral mucosa cells. However, the overall survival rate of OSCC patients with relatively high CLDN8 expression was reduced, suggesting that Claudin-8 may play distinct roles in different stages of OSCC progression, which needs to be further explored.

Lu SL et al(141) found that Claudin-8 was highly expressed in high-grade invasive ductal carcinoma tissues of the breast, and the luminal epithelial subtype was predominant.

CLDN8 also has great potential application in the field of molecularly targeted therapies. Osteosarcoma is the most common primary sarcoma of the human long bone epiphysis. Xu et al(142) found that interference with CLDN8 expression blocked the transition from G1 to S phase of the U2OS cell cycle in osteosarcoma and induced apoptosis of cancer cells, which providing a direction for finding new therapeutic means for osteosarcoma.

A further study demonstrated that in the respiratory system, CLDN8 was shown to be expressed only in the resorption epithelium of the conductive airways and not in the alveolar epithelium expression. Knockdown of CLDN8 results in the inability of occludin to participate in the construction of tight junction structures. Glucocorticoids can upregulate CLDN8 through glucocorticoid receptors,

resulting in increased permeability of the paracellular pathway(143). It has implications for the targeting of impaired lung epithelial barrier function in respiratory diseases.

In general, few studies have been reported on CLDN8, but it has been found to play a role not only in the maintenance of normal physiological functions, but also to be expressed abnormally in a variety of diseases, especially in relation to the development of reproductive and digestive diseases and epithelial-derived malignancies. For CLDN8 expression and the mechanism of action of its regulatory factors, and to find or design target factors that specifically bind to them to interfere with the cell phenotype for therapeutic purposes, need to be further investigated and explored.

1.9 Artemisinin

1.9.1 Discovery and Antimalarial Use

In 1971, Artemisinin or Qinghao was derived from the sweet wormwood plant (*Artemisia annua*) by Chinese scientists as part of the collaborative 'Project 523' (144). In 1971, Tu and colleagues obtained a potent antimalarial extract from *A. annua*, eventually identifying the active compound Artemisinin, which showed 100% effectiveness against malaria parasites in animal tests. This breakthrough provided a novel therapy for chloroquine-resistant malaria and has since saved millions of lives(145). Tu Youyou's discovery remained anonymous for years (the research was initially published without author names), but it later earned her a Lasker Award in 2011 and the 2015 Nobel Prize in Medicine, highlighting Artemisinin as "arguably the most important pharmaceutical intervention in the last half-century".

Artemisinin and its family of drugs rapidly became central to malaria treatment worldwide. Unlike earlier antimalarials, Artemisinin is fast-acting and effective

against all blood stages of *Plasmodium*, including young parasite forms that quinine and other drugs might miss(146). Crucially, Artemisinin-based therapies remain effective against multi-drug-resistant strains of *P. falciparum*. To prolong efficacy and prevent resistance, the World Health Organization (WHO) has recommended Artemisinin-based combination therapies (ACTs) as the first-line treatment for uncomplicated falciparum malaria since the mid-2000s(146). These combinations pair a rapid-acting Artemisinin derivative with a longer-acting partner drug. Notably, Artemisinin-based drugs are credited with dramatically reducing malaria mortality over the past decades, including treatment of severe cerebral malaria, where intravenous artesunate has become the gold standard therapy (replacing quinine) due to its superior efficacy and safety.

After the discovery of Artemisinin, researchers in China and elsewhere quickly recognized that the parent compound had suboptimal pharmaceutical properties (poor solubility and a very short half-life). By the mid-1980s, several semi-synthetic derivatives were developed by modifying Artemisinin's structure. The first step was the production of dihydroartemisinin (DHA) via reduction of the lactone to a lactol, which yielded a molecule with an active hydroxyl at C-10 that could be further derivatized. From DHA, ethers and esters were synthesized: artesunate (a sodium hemi succinate ester) and artemether (a methyl ether) were among the earliest and most successful derivatives. These compounds exhibited even greater antimalarial potency than Artemisinin itself. DHA is the key active metabolite to which artesunate and artemether are converted in the body; it is the most biologically active form, though it is not used as a monotherapy due to its instability and short lifespan in vivo. In addition to artemether and artesunate, other derivatives include artemether (ethyl ether at C-10, like artemether in lipophilicity), and newer investigational analogues. For instance, Artemisinin is a 10-alkylamino derivative (containing a bulky amino substituent at C-10) designed to improve drug stability and efficacy against malaria. These derivatives

collectively demonstrate how different ligands (substituents) at the C-10 position influence the drug's properties.

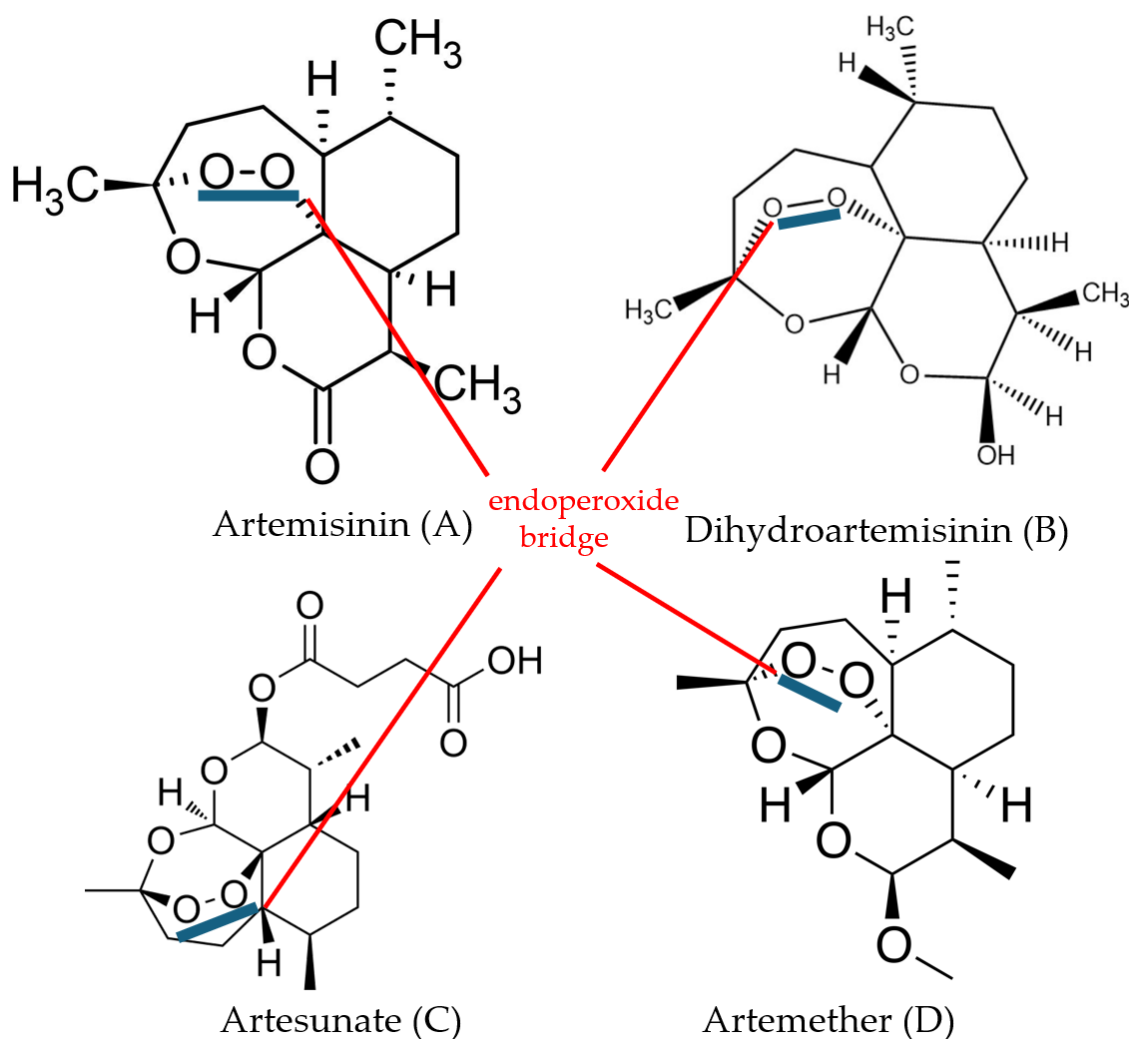


Figure 1.9: Chemical structures of Artemisinin (A) and its principal semi-synthetic derivatives: dihydroartemisinin (B), artesunate (C), and artemether (D). Artemisinin's core structure is a sesquiterpene lactone with an unusual 1,2,4-trioxane ring containing an endoperoxide bridge (peroxide linkage) – this endoperoxide is highlighted in the figure as the pharmacophore essential for antimalarial activity. Dihydroartemisinin (DHA) (B) is the hydrogenated lactone form of Artemisinin (produced by reduction of the lactone), and it retains the peroxide moiety. Artesunate (AS) (C) is the hemisuccinate ester of DHA (attachment of a succinic acid group at the C10 position), making it far more water-soluble than Artemisinin. Artemether (AM) (D) is the methyl ether derivative of DHA, which increases lipophilicity. (Created by the author using BioRender)

Artemisinin itself is a neutral molecule with multiple oxygen heterocycles but limited polarity. It has an unusual solubility profile – it is sparingly soluble in water (approximately 0.04 mg/mL at 25 °C) and only moderately soluble in nonpolar oils(146, 147). In fact, Artemisinin is soluble in many aprotic organic solvents (like ethanol, acetone, chloroform) but not in hydrophilic or lipophilic solvents extremes(147). This makes formulation challenging. By contrast, its derivatives span a range of polarities: artesunate's disodium salt is water-soluble (for injection), whereas artemether/artemether are highly lipophilic (oil-soluble). Artemisinin and its analogues are relatively small molecules (molecular weight ~ 282 for Artemisinin, ~ 300–350 for derivatives) with multiple chiral centers (Artemisinin has seven stereo genic centers)(148). The drug's stereochemistry is important for activity – the natural configuration is required for potency (though interestingly, some simplified peroxide analogues show activity irrespective of stereochemistry)(146). All Artemisinin are characterized by the endoperoxide bridge, which is chemically fragile. This peroxide is responsible for the thermal instability and short shelf-life of some derivatives (DHA is especially prone to decomposition if not formulated carefully(148)).

Pharmacologically, Artemisinin has extremely rapid action against parasites but also a rapid clearance from the body. Plasma half-lives of Artemisinin and its derivatives are on the order of 30 minutes to a few hours(146). They are primarily metabolized in the liver (CYP450 enzymes, especially CYP2B6, play a major role in Artemisinin metabolism)(146). Because of this quick elimination and the potential for parasites to survive if a single agent is used, monotherapy can lead to high recrudescence (relapse) rates(146). This is why combination therapy is essential – the partner drug clears remaining parasites while the Artemisinin quickly reduces parasite biomass by orders of magnitude. In terms of safety, Artemisinin drugs are generally well-tolerated; they can cause transient neurotoxicity at very high doses

in animal studies, but in clinical use the main concern has been rare, delayed hemolysis after IV artesunate therapy (a manageable side effect).

Despite the extensive use of Artemisinin, its precise mechanism of action is not fully elucidated and remains a subject of research. What is established is that the endoperoxide bridge in Artemisinin is critical – when this peroxide bond is cleaved (for example, by reaction with ferrous iron), it produces highly reactive radicals. The leading hypothesis is that Artemisinin is activated by heme or intracellular ferrous iron (Fe^{2+}) within the malaria parasite. The iron-mediated cleavage of the endoperoxide yields oxygen-centered and carbon-centered free radicals(149). These radicals then alkylate and damage vital biomolecules in the parasite. Artemisinin can form adducts with heme and covalently modify parasite proteins, wreaking widespread damage on parasite membranes and metabolic processes. This oxidative burst mechanism explains the rapid parasitocidal effect of Artemisinin.

Several molecular targets have been proposed for Artemisinin's action. One prominent theory posited that Artemisinin might directly inhibit a parasite enzyme, PfATP6, a SERCA-type calcium pump, when activated by iron, leading to disrupted calcium homeostasis(150). Some studies in yeast and Plasmodium suggested Artemisinin could bind PfATP6 (with reduced binding if mutations are present)(150). However, this remains controversial, and Artemisinin likely has multiple targets. Proteomic studies show Artemisinin can alkylate a range of parasite proteins once its radical is formed – these include proteins involved in metabolism, hemoglobin digestion, and stress responses (151). Another recent identified target is PfDdi1, a Plasmodium protease; computational and experimental data indicate Artemisinin might bind to its active site motif, inhibiting its function(151). It's also known that Artemisinin can disrupt parasite mitochondrial function and redox balance(146). In essence, Artemisinin's mode of

action is pleiotropic, but all pathways originate from the unique peroxide-triggered radical generation.

Notably, Artemisinin's ability to generate radicals is also being leveraged beyond malaria parasites. For example, rapidly dividing cancer cells with high iron uptake are hypothesized to be vulnerable to Artemisinin's radical damage. Artemisinin has been shown to induce oxidative stress and trigger apoptosis in certain cancer cell lines by similar mechanisms (involving iron-catalyzed radical formation that damages cancer cell components)(149). It may also interfere with cellular pathways such as angiogenesis and NF- κ B signaling in tumour cells. Nonetheless, much of this anticancer mechanism overlaps with the radical generation concept that first emerged from antimalarial action.

1.9.2 Artemisinin as a model Compound for Blood–Brain Barrier (BBB)

Penetration

One particularly intriguing aspect of Artemisinin research is its interaction with the BBB. The BBB is a tightly regulated interface that prevents most drugs and pathogens from entering the brain. Artemisinin's role in treating cerebral malaria hinted that it could reach the brain compartments; indeed, its efficacy in that condition implies that adequate concentrations of the drug (or its active metabolites) cross the BBB to affect parasites sequestered in cerebral microvasculature. The ability of Artemisinin derivatives to penetrate the BBB relates partly to their lipophilicity. Artesunate, for instance, though administered in a water-soluble form, is converted to DHA which is relatively lipophilic; DHA and artemether can diffuse across endothelial cell membranes of the BBB(152). One study noted that artesunate fulfils the lipophilicity requirement for transcellular diffusion into brain tissue(152), suggesting that therapeutically meaningful levels can cross into the brain parenchyma (especially when the

barrier is already compromised by infection or inflammation, as in cerebral malaria).

In blood–brain barrier (BBB) research, Artemisinin serves as a valuable model compound, distinct from its derivatives. As the parent molecule, Artemisinin provides a stable and structurally intact scaffold to probe fundamental transport mechanisms across the BBB, without the confounding issue of instantaneous metabolic activation. Its relatively neutral and moderately lipophilic profile is representative of many small-molecule drugs, making it insightful for studying passive diffusion and carrier-independent penetration routes. In contrast, certain derivatives (artesunate or artemether) are either highly polar or rapidly metabolized, which can obscure the analysis of how the molecule itself traverses the BBB. Artemisinin's chemical stability ensures that the compound reaching the brain is the same as the one administered, thus any observed effects on BBB crossing can be attributed to Artemisinin itself rather than a downstream metabolite. Indeed, there has been a noted knowledge gap regarding Artemisinin's direct effects on BBB physiology and using Artemisinin as a starting point allows researchers to explore these effects in a controlled way. By avoiding the rapid biotransformation's seen with derivatives(153), one can clearly delineate the penetration pathway and interactions of the parent compound. In summary, Artemisinin's representativeness and simplicity (as a single active entity) make it an ideal probe to unravel BBB transport mechanisms, whereas its derivatives, with their swift conversion and multi-step actions, are less suited for such mechanistic clarity.

Beyond simply crossing into the brain, Artemisinin compounds appear to modulate the integrity and permeability of the BBB. Recent research indicates that Artemisinin could be used deliberately to transiently open the BBB, which is of great interest for enhancing drug delivery to the brain. In an *in vitro* BBB model

using human brain endothelial cells, Artemisinin was found to influence tight junction (TJ) proteins that normally seal the paracellular spaces between endothelial cells. Claudin-5, a key tight junction protein in brain vessels, was significantly down-regulated in brain endothelial cells after Artemisinin exposure (at non-cytotoxic concentrations), and immunofluorescence showed disruptions in TJ protein localization(154). Functionally, low-dose Artemisinin treatment led to a decrease in transendothelial electrical resistance (TEER) and an increase in paracellular permeability in brain endothelial monolayers, indicating a loosening of the barrier(154). Interestingly, this effect was selective for brain endothelium: the same low dose caused a significant drop in resistance in brain-derived endothelial cell lines, but not in non-brain endothelial cells (human umbilical vein endothelial cells)(154). Higher concentrations of Artemisinin (> 1 mM in that study) caused a more drastic loss of barrier function (and were possibly cytotoxic)(154), whereas a mild concentration (~0.01 mM) produced a moderate and reversible increase in permeability(154). These findings suggest Artemisinin exhibits a biphasic effect on the BBB: at safe concentrations it can transiently open the tight junctions, whereas at excessive concentrations it may damage the endothelium. The ability to transiently open the BBB is potentially very useful – it could allow co-administered drugs (for example, chemotherapeutics or antibiotics that normally struggle to penetrate the CNS) to better reach brain tissue. Indeed, the researchers concluded that Artemisinin may have the capacity to transiently increase the permeability of the BBB and could serve as an adjuvant to facilitate drug delivery to the brain(154). This concept is being explored especially in the context of treating brain metastases of cancer, where delivering drugs across the intact BBB is a major hurdle(154).

Mechanistically, how does Artemisinin open the BBB? The *in vitro* study noted changes in tight junction protein expression and localization, as mentioned.

Artemisinin likely affects signalling pathways in endothelial cells. One possibility

is through its anti-inflammatory action: Artemisinin can reduce levels of pro-inflammatory cytokines like TNF- α and IL-1 β that are known to tighten or loosen the BBB depending on context(155, 156). By reducing an ongoing inflammation in the CNS or at the barrier, Artemisinin might stabilize certain aspects of BBB function while loosening paracellular TJs to allow passage of drugs. There is some evidence from neurological disease models supporting a protective role: for example, dihydroartemisinin (DHA) was reported to protect BBB integrity in a sepsis model, counteracting the usually deleterious effects of inflammation. In a 2022 study, DHA inhibited the transcription factor Snail1 (SNAIL1) in brain endothelial cells, which in turn upregulated occludin, a tight junction protein—this preserved BBB tightness during endotoxemia (sepsis) and reduced permeability(155). Here, Artemisinin's derivative helped maintain the BBB against inflammatory disruption, highlighting a context-dependent effect. Another study found Artemisinin could inhibit microglial activation via TLR4 pathways, preventing inflammation-induced BBB leakage in a model of neuroinflammation(156, 157). These findings seem at first glance contradictory to the idea of Artemisinin increasing permeability. The reconciliation is that Artemisinin's BBB modulation is dynamic: in healthy or mildly inflamed conditions, it can transiently loosen tight junctions (useful for drug delivery), but in severely inflamed conditions that dangerously compromise the BBB, it can exert anti-inflammatory effects that overall preserve or restore barrier integrity. Essentially, Artemisinin tends to normalize the BBB function – if the BBB is overly tight (blocking needed therapeutics), Artemisinin might open it; if the BBB is excessively leaky due to inflammation, Artemisinin's calming of inflammation results in a net protective effect.

From a clinical standpoint, exploiting Artemisinin to enhance BBB permeability is an exciting avenue. For diseases like brain tumours, Alzheimer's, and central nervous system (CNS) infections, delivering drugs across the BBB is a key challenge. Traditional methods to disrupt the BBB (such as osmotic opening with

mannitol or focused ultrasound) carry risks. A pharmacological approach using a well-tolerated drug like Artemisinin or artesunate could be a gentler alternative.

In metastatic breast cancer research, Artemisinin is being investigated as an adjunct to help anti-cancer drugs penetrate brain metastases(154). Its inherent anti-cancer and anti-inflammatory properties could provide a two-pronged benefit: directly affecting tumour cells and microenvironment and improving drug delivery. However, this strategy is nascent and requires careful dosing strategies to avoid excessive BBB disruption or toxicity.

In summary, Artemisinin and its derivatives not only cross the blood–brain barrier but can modulate its permeability. Low, controlled doses of Artemisinin might transiently relax the tight junction “gatekeepers” of the BBB to allow therapeutic agents into the brain, which is a significant finding for future neurological therapies(154). Concurrently, Artemisinin can mitigate inflammatory damage at the BBB, which is valuable in conditions like cerebral malaria, viral encephalitis, or sepsis-associated encephalopathy. These dual actions underscore Artemisinin’s versatility: it is a potent antimalarial and a promising modulator of the BBB, warranting further research into its mechanism and optimal use in neurology and oncology.

1.9.3 Anticancer Effects of Artemisinin in Breast Cancer

Numerous studies have demonstrated that Artemisinin and its derivatives, such as dihydroartemisinin (DHA) and artesunate, exert selective cytotoxicity against various breast cancer cell lines while sparing normal cells(158, 159). The underlying mechanisms include the induction of apoptosis through caspase activation, cell cycle arrest at the G1 or G2/M phase, and inhibition of angiogenesis and metastasis-related signaling pathways(158).

For instance, Guan et al. (2020) reported that Artemisinin induced apoptosis, autophagy, and G2/M cell cycle arrest in cisplatin-resistant MDA-MB-231 breast cancer cells, highlighting its potential against drug-resistant phenotypes. Similarly, Efferth and colleagues demonstrated that artesunate triggers apoptosis in MCF-7 cells via caspase-8, -9, and -3 activation. Moreover, Artemisinin derivatives, including ARS and DHA can inactivate cancer-associated fibroblasts by suppressing TGF- β signaling, thereby inhibiting breast cancer growth and

metastasis both *in vitro* and *in vivo*(160). Collectively, these findings suggest that Artemisinin possesses promising anticancer activity in breast cancer by targeting multiple molecular pathways; however, its efficacy in brain metastasis and interaction with the blood–brain barrier (BBB) remain poorly understood.

1.10 Study Hypothesis

Artemisinin and its derivatives can enhance the permeability of the BBB while exhibiting anti-tumour effects, allowing drugs to effectively cross the BBB and reach the brain for treatment without increasing the risk of cancer metastasis. Specifically, these compounds may regulate tight junction (TJ) proteins to maintain or improve the barrier function of endothelial cells and exert anti-tumour activity against breast cancer cells. This hypothesis provides a scientific foundation for the application of Artemisinin in treating brain metastatic cancer.

1.11 Aims and Objectives of the Study

This study will integrate both clinical and *in vitro* experiments to elucidate the mechanisms by which Artemisinin modulates tight junction structures and its efficacy as an anti-cancer agent. The goal is to explore whether Artemisinin can effectively enhance BBB permeability while providing therapeutic benefits against cancer without promoting metastasis.

Chapter II: Materials and Methods

2.1 Cell Culture and Cell Lines

A panel of human breast cancer cell lines and brain endothelial cell lines was used to model the experimental systems. The breast cancer cell lines represented major subtypes of breast cancer: MCF-7 (luminal A, oestrogen receptor-positive), BT-474 and MDA-MB-361 (luminal B, HER2-positive/ER-positive), HCC1419 and SK-BR-3 (HER2-overexpressing), and MDA-MB-231 (triple-negative). All cancer cell lines were originally obtained from the American Type Culture Collection (ATCC, Manassas, VA, USA). In addition, human brain microvascular endothelial cells hCMEC/D3 and TY10 were used to model the BBB environment. These endothelial cell lines provide an *in vitro* model of the tight junction-bearing brain endothelium.

To investigate the functional role of CLDN8 in breast cancer and endothelial cells, CLDN8 knockdown was performed using small interfering RNA (siRNA) transfection mediated by Lipofectamine RNAiMAX (Invitrogen, USA). Approximately 70,000 cells were seeded per well for transfection. Following 48 hours of incubation, knockdown efficiency was verified by quantitative PCR (qPCR) and Western blot analysis.

Cells were grown under standard culture conditions at 37 ° C in a humidified atmosphere with 5% CO₂. Breast cancer cell lines were cultured in either Dulbecco's Modified Eagle Medium (DMEM) or RPMI-1640 medium, depending on the line: for example, MCF-7 and MDA-MB-231 were maintained in DMEM, whereas BT-474, MDA-MB-361, SK-BR-3, and HCC1419 were maintained in RPMI-1640. All media were supplemented with 10% (v/v) *foetal* bovine serum (FBS) and 1% penicillin–streptomycin antibiotic mix. The brain endothelial cell lines (hCMEC/D3 and TY10) required specialized growth conditions: they were cultured in Endothelial cell culture medium was purchased from Merck KGaA, Darmstadt, Germany (formerly Sigma-Aldrich). supplemented with 5% FBS,

endothelial cell growth supplements, and 1% penicillin–streptomycin. Culture flasks and plates were monitored regularly, and cells were sub-cultured at ~80% confluence using 0.25% trypsin-EDTA for detachment. All cell lines were confirmed to be mycoplasma-free and were used at low passage numbers to ensure consistent behaviour.

2.2 Molecular Biology Techniques

2.2.1 RNA Extraction and cDNA Synthesis

Total RNA was isolated from cultured cells (and where applicable, from tissue samples) using TRIzol® Reagent (Merck KGaA, formerly trading in Poole as Sigma-Aldrich Co. Ltd.) according to the manufacturer's instructions. After lysis in TRIzol, chloroform was added to separate phases, and RNA was precipitated from the aqueous phase with isopropanol. The resulting RNA pellets were washed in 75% ethanol, air-dried, and resuspended in RNase-free water. RNA yield and purity were evaluated spectrophotometrically (absorbance at 260/280 nm), and integrity was verified by gel electrophoresis. Typically, 1 µg of high-quality RNA was used for complementary DNA (cDNA) synthesis. Reverse transcription was performed using the iScript™ cDNA Synthesis Kit (Bio-Rad Laboratories, Hercules, CA, USA). RNA samples were combined with kit reagents (including random primers and reverse transcriptase) and incubated according to the recommended thermal cycling program (25 °C for 5 min, 42 °C for 30 min, 85 °C for 5 min) to generate cDNA. The cDNA products were either used immediately for PCR or stored at –20 °C for later analysis.

2.2.2 Quantitative Real-Time PCR (qPCR)

Quantitative PCR (qPCR) was employed to measure gene expression levels (in particular, *CLDN8* mRNA) in both cell line samples and patient tissue samples. PCR amplification was performed on generated cDNA using sequence-specific primers and a fluorescent detection chemistry. Depending on the experiment, either a SYBR Green dye-based detection method (Applied Biosystems, Warrington, UK) or a probe-based system was used. In some assays, the Amplifluor™ Uniprimer Universal qPCR system (Intergern, New York, USA) was utilized, which employs a universal FAM-tagged probe in combination with gene-specific primers containing a Z-sequence. Each 20 µL qPCR reaction typically contained cDNA corresponding to ~50 ng RNA input, 300 nM of forward and reverse primers (designed specifically for the target gene and spanning exon–exon junctions when possible), and a master mix with DNA polymerase and dNTPs. Reactions were run in triplicate for each sample on a real-time PCR thermocycler (ABI Prism or Bio-Rad CFX system), under cycling conditions of initial denaturation (95 °C, 2 min) followed by 40 cycles of 95 °C for 10 s and 60 °C for 30 s (annealing/extension). GAPDH was used as the housekeeping reference gene for normalization in all qPCR analyses. No-template controls were included to ensure absence of contamination. Fluorescence data were collected in real time, and threshold cycle (Ct) values were obtained using instrument software. Relative gene expression was calculated using the $2^{-\Delta\Delta Ct}$ method, comparing each sample's target gene Ct to its GAPDH Ct and then to a calibrator (such as an untreated control sample). Primer sequences for *CLDN8*, *GAPDH*, and other genes of interest were designed in-house and are documented in Table 2.2 of this thesis. Quantitative data from qPCR experiments were used to assess differences in mRNA expression (for example, comparing *CLDN8* expression in knockdown vs. control cells, or in tumour vs. normal tissues).

2.2.3 Western Blotting (Protein Extraction and Analysis)

Protein expression and knockdown efficiency were evaluated by Western blotting. Cells were lysed in ice-cold RIPA buffer (50 mM Tris-HCl pH 7.5, 150 mM NaCl, 1% NP-40, 0.5% sodium deoxycholate, 0.1% SDS) supplemented with protease and phosphatase inhibitor cocktails (Sigma-Aldrich) to prevent protein degradation and dephosphorylation. Lysates were incubated on ice for ~30 minutes and clarified by centrifugation ($14,000 \times g$, 15 min, 4 °C) to remove cell debris. The supernatant containing total protein was collected, and protein concentration was determined using a BCA protein assay (Pierce/Thermo Fisher Scientific, Loughborough, UK) with bovine serum albumin standards. For each sample, an equal amount of protein (typically 20–30 μg) was mixed with 2 \times Laemmli SDS sample buffer and boiled for 5 minutes to denature proteins.

Proteins were separated by size via SDS-PAGE, using an appropriate percentage polyacrylamide gel (10% resolving gel for 10–250 kDa range). Following electrophoresis, proteins were transferred to a polyvinylidene difluoride (PVDF) membrane using a wet transfer apparatus (100 V for 1–2 hours at 4 °C). After transfer, membranes were blocked in 5% non-fat milk (or 5% bovine serum albumin for phospho-proteins) prepared in Tris-buffered saline with 0.1% Tween-20 (TBST) for 1 hour at room temperature to block non-specific binding sites. The blots were then incubated overnight at 4 °C with primary antibodies specific to the proteins of interest. The following primary antibodies were used (at 1:1000 dilution unless stated otherwise): anti-CLDN8 (Claudin-8, Abcam, Cambridge, UK), anti- β -catenin (Sigma-Aldrich, UK), anti-GSK3 β (glycogen synthase kinase-3 β , Cell Signalling Technology, Danvers, MA, USA), anti-ZO-1 (zonula occludens-1 tight junction protein, Sigma-Aldrich), and anti-GAPDH (Sigma-Aldrich). GAPDH served as a loading control in all blots. After primary antibody incubation, membranes were washed three times in TBST, then incubated with the appropriate horseradish peroxidase (HRP)-conjugated secondary antibody (anti-mouse or anti-rabbit IgG, as appropriate; Dako/Agilent, UK) for 1 hour at room

temperature. Excess secondary antibody was removed by washing in TBST (3 × 10 min). Protein bands were then visualized using an enhanced chemiluminescence (ECL) detection reagent (Amersham ECL Select, GE Healthcare) and captured on an imaging system. Where required, band intensities were quantified by densitometry (ImageJ software, NIH, Bethesda, Maryland, USA), and target protein levels were normalized to GAPDH. Western blotting was employed both to confirm CLDN8 knockdown at the protein level and to investigate the expression of signalling proteins (such as β -catenin, GSK3 β , ZO-1) under different treatment conditions.

Additionally, a high-throughput phosphoprotein array was used for broad protein analysis. A Kinexus[®] Phospho-Proteome Array (Kinexus Bioinformatics Corporation, Vancouver, Canada) was performed to profile changes in protein phosphorylation signalling networks in selected conditions. Protein lysates from key experimental groups (control untreated cells, Artemisinin-treated cells, and CLDN8-knockdown cells) were fluorescently labelled and hybridized to the Kinexus antibody microarray, which contains antibodies against hundreds of signalling proteins and phospho-epitopes. After incubation and washing, the arrays were scanned for fluorescence intensity. Differential signals between conditions were analysed to identify significant changes in protein expression or phosphorylation status. This unbiased proteomic approach complemented the targeted Western blot analyses by highlighting potential signalling pathways modulated by Artemisinin treatment or CLDN8 loss.

2.3 Functional Cell Assays

To assess the effects of treatments on cellular behaviour, a series of functional *in vitro* assays was conducted on breast cancer cells, examining cell adhesion, invasion, and migration capabilities. Unless otherwise stated, these assays were performed using untreated control cells versus Artemisinin-treated cells (to

evaluate the drug's effect on cell behaviour) or using CLDN8-knockdown cells versus control cells (to evaluate the role of CLDN8).

2.3.1 Cell Adhesion Assay

Cell adhesion was evaluated using a Matrigel-based adhesion assay. Breast cancer cell lines (MCF-7, MDA-MB-231, SK-BR-3, and MDA-MB-361) were pre-treated with artemisinin at a final concentration of 10 μ M for 24 hours, or with an equivalent volume of DMSO as vehicle control. After treatment, cells were trypsinized and resuspended in serum-free DMEM at a density of 2×10^5 cells/mL.

Ninety-six-well plates were coated with Matrigel diluted 1:200 in serum-free medium (50 μ L per well) and air-dried in a biosafety cabinet to form a uniform basement membrane layer. The coated wells were then rehydrated with PBS for 1 hour at 37 °C before seeding cells. Subsequently, 2×10^4 cells in 100 μ L of serum-free medium were added to each well and allowed to adhere for 1 hour at 37 °C in a humidified incubator (5% CO₂).

After incubation, non-adherent cells were gently removed by washing three times with warm PBS. The adherent cells were fixed with 4% paraformaldehyde for 15 minutes, stained with DAPI (1 μ g/mL in PBS) for 10 minutes at room temperature, and washed again with PBS. Images were captured using a fluorescence microscope ($\times 10$ objective), and the number of adherent cells (DAPI-positive nuclei) was counted in 4 random fields per well using ImageJ software.

Each condition was tested in three replicate wells ($n = 3$), and the mean number of adherent cells was used for statistical analysis. This assay quantitatively assessed the adhesive capacity of breast cancer cells under different treatment conditions.

2.3.2 Cell Invasion Assay

Cell invasive capacity was measured using a Transwell invasion assay. We utilized Boyden chamber inserts with 8 μ m pore membranes fitted in 24-well plates. Uniquely, to model tumour cell passage across an endothelial barrier (such as the BBB), the invasion assay was set up as a co-culture system. Brain endothelial cells (hCMEC/D3 or TY10) were first cultured to confluence on the underside of the Transwell membrane or in the bottom of the well, forming a monolayer representing the BBB. Separately, breast cancer cells (MDA-MB-361,

SK-BR-3, MDA-MB-231, MCF-7) were serum-starved overnight to enhance invasive behaviour, then treated with Artemisinin or control as required. For the invasion assay, a small aliquot of Matrigel (diluted in serum-free medium) was applied to the upper side of the insert membrane and allowed to form a thin gel layer, providing an extracellular matrix barrier. Cancer cells were then seeded into the upper chamber of the insert (typically 3×10^3 cells per insert for highly invasive MDA-MB-231 or SK-BR-3, and up to 7×10^3 for less invasive MCF-7, to account for differences in baseline invasiveness). The insert was placed into a well where the bottom compartment contained a confluent layer of endothelial cells and medium with chemoattractant (10% FBS). Cells in the insert were thus separated from the bottom well by both the porous membrane and the endothelial monolayer. The co-culture was incubated for 24 hours, allowing cancer cells to invade through the Matrigel, traverse the porous membrane, and pass the endothelial barrier into the lower chamber. After 24 hours, non-invading cells on the top side of the membrane were carefully removed with a cotton swab. The cells that had invaded to the underside of the insert membrane were fixed in 4% paraformaldehyde and stained (with crystal violet or DAPI). The number of invaded cells was then quantified by counting under a microscope. Five random fields per insert were counted for cell nuclei at 20 \times magnification, and the average was taken. Where available, an automated imaging system (EVOS™ FL Cell Imaging System (Thermo Fisher Scientific, Waltham, MA, USA).) was used to capture images and assist in counting. The invasion index was expressed as the average number of cells per field for each condition. This assay thus assessed the ability of breast cancer cells to penetrate an endothelial barrier and extracellular matrix, mimicking the process of metastasis across the BBB.

2.3.3 Cell Migration Assay (Scratch Wound Assay)

Cell migratory ability was examined using a scratch wound assay. Breast cancer cells (SK-BR-3, MDA-MB-231, MCF-7) were grown in 6-well culture plates until they formed a confluent monolayer. Using a sterile 200 μ L pipette tip, a straight scratch (wound) was made through the monolayer in each well, creating a cell-free gap \sim 1 mm in width. The wells were gently washed with PBS to remove detached cells and debris. Cells were then incubated in medium with a low serum concentration (1–2% FBS, to minimize proliferation) and treated with Artemisinin (10 μ M) or DMSO control. Immediately after scratching (time 0 h), each wound was photographed under a phase-contrast microscope to record the initial wound width. The cultures were returned to the incubator, and further images of the same wound area were captured at regular intervals (such as 24 hours and 48 hours post-scratch). Care was taken to mark reference points or use an automated stage to image the same region of each well over time. The extent of cell migration was quantified by measuring the remaining wound area or the distance migrated by the wound edges at each time point. This was typically done using image analysis software: the area of the cell-free region at each time was measured and normalized to the 0 h area. The wound closure percentage was calculated as: $(Area_{0h} - Area_t) / Area_{0h} \times 100$. Alternatively, the migration rate could be expressed in μ m/hour of gap closure. Each condition was tested in triplicate wells, and the results were averaged. A faster decrease in the wound area (greater closure) indicates higher migratory capacity. By comparing treated vs. control cells, the effect of Artemisinin on cell migration could be determined, while comparisons of CLDN8-knockdown vs. control cells revealed the contribution of CLDN8 to migratory behaviour.

2.4 Blood-Brain Barrier and Endothelial Assays

To specifically evaluate the function and integrity of the endothelial monolayer (BBB model) under different conditions, two complementary assays were

performed: a permeability assay to measure molecular flux across the barrier and a transendothelial electrical resistance assay to measure barrier tightness.

hCMEC/D3 and TY10 brain endothelial cells were used for these BBB integrity assays. Prior to each assay, endothelial cells were seeded on permeable supports and allowed to form tight junctions.

2.4.1 Permeability Coefficient (PC) Assay

Endothelial monolayer permeability was quantified using a FITC-dextran tracer flux method. Brain endothelial cells (hCMEC/D3 or TY10) were seeded onto collagen-coated Transwell inserts (0.4 μm pore size polyester membranes) at a density of approximately $5\text{--}7 \times 10^4$ cells per insert. Cells were cultured in EGM-2 medium and grown for 2–3 days until a confluent, electrically resistant monolayer formed on the insert (as verified by visual inspection and TEER measurements). For the permeability assay, the culture medium in each insert was replaced with serum-free medium. Fluorescein isothiocyanate (FITC)-conjugated dextran (average molecular weight ~ 40 kDa; Sigma-Aldrich) was used as a fluorescent tracer molecule. FITC-dextran was added to the upper chamber of the Transwell insert (the “luminal” side of the endothelial monolayer) at a final concentration of 100 $\mu\text{g}/\text{mL}$. The lower chamber (abluminal side) was filled with an equal volume of serum-free medium. Endothelial cells were then exposed to the condition of interest – for example, treatment with Artemisinin (10 μM added to the upper chamber media) or control treatment – and incubated at 37 $^\circ\text{C}$. At specified time points (0.5, 1, 2, 4, and 6 hours after adding the tracer), a 100 μL sample of medium was collected from the lower chamber of each well. Each time a sample was taken, an equal volume of fresh medium was added back to the lower chamber to maintain volume. The concentration of FITC-dextran that diffused into the lower chamber was determined by measuring fluorescence (excitation ~ 490 nm, emission ~ 520 nm) using a fluorescence plate reader. A standard curve

of known FITC-dextran concentrations was used to convert fluorescence readings to dextran quantities. The flux rate was calculated and the permeability coefficient (P_e) of the monolayer was determined using the formula: $P_e = \frac{1}{A \times C_0} \frac{dQ}{dt}$, where A is the surface area of the membrane, C_0 is the initial concentration in the donor (upper) chamber, and dQ/dt is the rate of appearance of tracer in the receiver (lower) chamber. Lower permeability (i.e. lower dextran flux) indicates a tighter endothelial barrier. Each experimental condition was tested in triplicate inserts, and an acellular insert (no cells) served as a positive control for maximum diffusion. This assay allowed us to assess how treatments like Artemisinin impacted the leakiness of the BBB model.

2.4.2 Transendothelial Electrical Resistance (TEER) Assay

Barrier integrity was also measured in real-time by transendothelial electrical resistance (TEER), which gauges the electrical resistance across the cell monolayer and correlates with tight junction integrity. Brain endothelial cells (hCMEC/D3 or TY10) were seeded onto Transwell inserts as described above and grown to confluence. TEER was measured using an EVOM2 voltammeter with STX chopstick electrodes (World Precision Instruments, Sarasota, FL, USA). The electrodes were sterilized and then placed so that one probe was in the upper chamber and the other in the lower chamber of each Transwell, forming a circuit across the endothelial layer. Baseline TEER values (in ohms) were recorded for each insert once the monolayer matured (typically 3–4 days after seeding). Inserts were then assigned to treatment or control groups. For treated groups, Artemisinin (10 μ M) was added to the culture medium on the cells (both apical and basal sides to avoid concentration gradients) and TEER was monitored at regular intervals (every 2–4 hours) over a 24-hour period. Control inserts received an equivalent volume of DMSO (the solvent for Artemisinin) to ensure changes were not due to solvent effects. All measurements were performed at 37 °C. A

blank insert without cells was used to measure background (media-only) resistance, and this value was subtracted from each sample reading. TEER readings were converted to the standard unit of resistance area product ($\Omega\cdot\text{cm}^2$) by multiplying by the membrane area (for 24-well inserts, area $\approx 0.33\text{ cm}^2$). An increase in TEER indicates enhanced tight junction function (less permeability), whereas a decrease in TEER indicates barrier compromise. Each condition was measured in at least triplicate, and the mean TEER \pm SEM was plotted over time. The TEER assay provided a dynamic assessment of BBB integrity in response to Artemisinin, complementing the endpoint dextran permeability measurements.

2.5 Protein Interaction and Localization Studies

A series of techniques was employed to investigate protein–protein interactions and the subcellular localization of key proteins (notably CLDN8 and its associated signalling partners) under different experimental conditions. These techniques included immunofluorescence microscopy, co-immunoprecipitation, and subcellular fractionation.

2.5.1 Immunofluorescence (IF) Microscopy

Immunofluorescence was used to visualize the cellular localization of CLDN8 and other proteins (such as β -catenin and ZO-1) in both breast cancer and endothelial cells, and to observe any changes upon Artemisinin treatment or CLDN8 knockdown. Cells grown on sterile glass coverslips (placed in 24-well plates) were treated as required (incubated with 5 μM Artemisinin for 24 h or transfected with CLDN8 siRNA as described below). After treatment, cells were fixed in 4% paraformaldehyde (PFA) in PBS for 15 minutes at room temperature, which preserves cellular structures. Following fixation, cells were rinsed with PBS and then permeabilized with 0.1% Triton X-100 (in PBS) for 5 minutes to allow antibody access to intracellular epitopes. Non-specific binding was blocked by

incubating the samples with 5% bovine serum albumin (BSA) or normal goat serum in PBS for 30 minutes. Primary antibodies were then applied to the coverslips and incubated overnight at 4 °C in a humidified chamber. The primary antibodies used for IF staining included the same targets as for Western blot (anti-CLDN8, anti- β -catenin, anti-ZO-1, etc.), at optimized concentrations (typically 1:100 to 1:200 for IF). After overnight incubation, coverslips were washed thoroughly in PBS (3 \times 5 min) to remove unbound primary antibodies. Next, appropriate fluorophore-conjugated secondary antibodies (Alexa Fluor 488 goat anti-rabbit IgG, Alexa Fluor 594 goat anti-mouse IgG; Thermo Fisher Scientific) were applied at 1:500 dilution for 1 hour at room temperature in the dark. These secondary antibodies bind to the primaries and emit fluorescence at specific wavelengths. Unbound secondary was removed by PBS washes (as above). Finally, coverslips were mounted onto glass slides using a mounting medium containing DAPI (4',6-diamidino-2-phenylindole) to counterstain cell nuclei. Edges of coverslips were sealed with clear nail varnish to prevent drying. Slides were examined under a fluorescence microscope (Nikon or Olympus epifluorescence microscope) or a confocal laser scanning microscope. Appropriate filter sets were used to visualize DAPI (blue), Alexa488 (green), and Alexa594 (red) signals. Images were captured using imaging software with identical exposure settings between treatment groups for comparability. Immunofluorescence images allowed the determination of protein localization (for example, membrane junctional localization of CLDN8 and ZO-1, or nuclear versus cytoplasmic distribution of β -catenin) and provided qualitative insight into changes such as CLDN8 loss or β -catenin redistribution upon Artemisinin treatment. Co-localization of proteins could also be assessed in merged channels.

2.5.2 Co-Immunoprecipitation (Co-IP)

Co-immunoprecipitation experiments were carried out to probe physical interactions between CLDN8, β -catenin (β -catenin), and other proteins in the cellular signalling complexes. Cells grown in 10 cm dishes were treated (with Artemisinin or transfected with siRNA) as needed, then lysed in IP lysis buffer (like RIPA but milder, 50 mM Tris pH 7.4, 150 mM NaCl, 1% NP-40, 0.1% SDS, plus protease inhibitors). Lysates were pre-cleared by centrifugation and by incubating with protein A/G agarose beads alone (to reduce non-specific binding). For each Co-IP, equal amounts of protein from the cleared lysate (typically 500 μ g–1 mg total protein) were incubated with 2–4 μ g of a specific primary antibody or control IgG. In our case, to investigate interactions involving β -catenin, lysates were incubated with an anti- β -catenin antibody (Sigma-Aldrich) overnight at 4 °C with gentle rotation. In parallel, a control sample was incubated with a non-specific IgG of the same isotype to serve as a negative control for non-specific binding. The following day, protein A/G agarose beads (Santa Cruz Biotechnology, sc-2003) were added to the lysate + antibody mixtures and incubated for an additional 2 hours at 4 °C. These beads bind to the Fc region of antibodies, thus pulling down the antibody–antigen complexes. After incubation, the bead–antibody–protein complexes were pelleted by gentle centrifugation (3000 \times g for 1 min) and washed thoroughly with ice-cold lysis buffer (3–5 washes) to remove non-bound proteins. Finally, bound proteins were eluted by adding 2 \times SDS loading buffer and heating at 95 °C for 5 minutes, which dissociates the immune complexes. The samples (immunoprecipitated) were then analysed by SDS-PAGE and Western blotting. For example, to test if CLDN8 and β -catenin interact, the Co-IP with anti- β -catenin was probed on a Western blot with anti-CLDN8 antibody. Conversely, a Co-IP with anti-CLDN8 (if performed) could be probed for β -catenin. As a control, blots were also probed for β -catenin to confirm successful pull-down. The presence of a target protein band in the specific IP lane but not in the IgG control IP lane was taken as evidence of a protein–protein interaction. Through Co-IP, we examined whether Artemisinin treatment

or CLDN8 knockdown affected the association of β -catenin with tight junction proteins (like ZO-1) or other partners, indicating potential mechanisms by which CLDN8 influences signalling pathways.

2.5.3 Subcellular Fractionation

To determine the distribution of proteins across cellular compartments, subcellular fractionation was performed on cells under different conditions. A Subcellular Protein Fractionation Kit (Thermo Fisher Scientific) was used to sequentially extract proteins from distinct cellular fractions: cytosolic, membrane, cytoskeletal, and nuclear. Briefly, cells from a confluent 10 cm dish were harvested and pelleted by gentle scraping and centrifugation. The pellet was first treated with a cytoplasm isolation buffer (containing digitonin to selectively permeabilize the plasma membrane) to release the cytosolic contents. After centrifugation, the supernatant was saved as the cytosolic fraction. The remaining pellet was then incubated with a membrane extraction buffer (containing a mild detergent) to solubilize membrane-bound proteins; centrifugation yielded a membrane fraction (supernatant) and a pellet containing nuclei and cytoskeleton. Next, a cytoskeletal buffer was applied to extract cytoskeletal-associated proteins, producing a cytoskeletal fraction. Finally, the pellet was treated with nuclear extraction buffer (high salt) to break up chromatin and release nuclear proteins. Each step was carried out on ice or 4 °C, and all buffers included protease and phosphatase inhibitors to preserve protein states. The success of fractionation was verified by probing for known marker proteins in each fraction via Western blot: for instance, GAPDH for cytosol, Na⁺/K⁺-ATPase or pan-cadherin for membrane, β -actin or vimentin for cytoskeleton, and Lamin A/C or histone H3 for nucleus. After validation, the fractions were analysed for the proteins of interest (CLDN8, β -catenin, ZO-1, etc.). By comparing the presence of these proteins in membrane vs. cytosolic/nuclear fractions with and without Artemisinin treatment or CLDN8

knockdown, we could observe shifts in localization. For example, a reduction of β -catenin in the membrane fraction coupled with an increase in the nuclear fraction would suggest translocation to the nucleus (potentially indicative of Wnt/ β -catenin pathway activation). Subcellular fractionation thus provided insight into how Artemisinin or loss of CLDN8 might alter the compartmental distribution of signalling molecules, thereby affecting cell function.

2.6 In Vitro Pharmacology and Drug Treatment Assays

To examine the effects of various therapeutics on breast cancer cells and to evaluate how CLDN8 expression influences drug responses, a series of in-vitro drug treatment assays were performed. Exponentially growing cells (60–70% confluence) were seeded and allowed to adhere for 24 h before drug exposure. Cells were then treated with a panel of standard breast cancer drugs, as well as artemisinin—the focal compound of this study—for 24, 48, or 72 h depending on the assay type. For migration and adhesion assays, drugs were added directly to the assay system, and cells were exposed to the indicated compounds during the experimental period; and for molecular analyses (Western blot and qRT-PCR), cells were harvested after 24 treatments. All treatments were performed in appropriate culture medium with solvent-only (DMSO \leq 0.1%) controls included in parallel to account for vehicle effects.

2.6.1 CLDN8 Gene Knockdown in Cell Lines

To investigate the functional role of CLDN8, we silenced the CLDN8 gene in breast cancer and endothelial cells using a small interfering RNA approach. A specific siRNA targeting human *CLDN8* (Santa Cruz Biotechnology, sc-44865) was used for knockdown. Cells were seeded at an appropriate density (~50–70% confluence) one day prior to transfection. Transient transfection of the siRNA was performed using Lipofectamine® RNAiMAX (Invitrogen, Paisley, UK) or Lipofectamine 2000 reagent, following the manufacturer's protocol. In a typical transfection, siRNA (at 50 nM final concentration) was diluted in Opti-MEM® reduced-serum medium and combined with the Lipofectamine reagent (diluted separately in Opti-MEM). The lipid–siRNA complexes were allowed to form for

20 minutes at room temperature, then added to cells in antibiotic-free growth medium. After 6 hours, the medium was refreshed with complete growth medium. Knockdown cells were incubated for 48–72 hours post-transfection to allow for protein depletion. In parallel, a scrambled (non-targeting) siRNA or mock transfection (Lipofectamine only) was used to generate control cells. The efficiency of CLDN8 knockdown was confirmed at the mRNA level by qPCR and at the protein level by Western blotting, as described earlier. Typically, CLDN8 mRNA expression was reduced by >80%, and CLDN8 protein became nearly undetectable in knockdown cells compared to controls. These CLDN8-deficient cells (CLDN8_KD) and their corresponding controls were then used in subsequent drug sensitivity and functional assays to determine how loss of CLDN8 affects cellular responses.

2.6.2 Drug Sensitivity (IC_{50}) Assays

A panel of nine anticancer drugs, representing major treatment classes for breast cancer, was tested on breast cancer cell lines to determine their efficacy and to see if CLDN8 knockdown alters drug sensitivity. The drugs included chemotherapeutic agents (paclitaxel, docetaxel, cisplatin, and methotrexate), HER2-targeted therapies (neratinib and lapatinib, small-molecule HER2 tyrosine kinase inhibitors), and endocrine therapies (tamoxifen, fluvastatin, and anastrozole). All drugs were obtained from Sigma-Aldrich (St. Louis, MO, USA) and prepared as concentrated stock solutions in the recommended solvents (DMSO for most agents, ethanol for fluvastatin) before dilution into culture media. For each drug, *in vitro* cytotoxicity was assessed using a 3-day cell viability assay to estimate the half-maximal inhibitory concentration (IC_{50}).

Cells (either wild-type or CLDN8-knockdown) were plated in 96-well flat-bottom plates at a density of $3-5 \times 10^3$ cells per well in 100 μ L of growth medium and allowed to attach overnight. The next day, drugs were added in a range of

concentrations (typically a 7-point or 8-point dilution series for each drug). For example, concentrations might span from 0.1 nM to 10 μ M for potent drugs or up to 100 μ M for less potent compounds, adjusted based on preliminary experiments. Each concentration was tested in at least 4 replicate wells. Control wells received no drug (0 μ M) but the same final solvent concentration (maximally 0.1% DMSO). Cells were then incubated with the drugs for 72 hours at 37 °C. After the treatment period, cell viability was measured via a crystal violet staining method. The culture medium was aspirated, and wells were gently washed with PBS. Cells were then fixed with 4% formaldehyde (50 μ L per well, 15 min), rinsed, and stained with 0.1% crystal violet solution (in 10% ethanol) for 20 minutes. Excess dye was removed by thorough washing with water, and the plates were air-dried. Stained cells (representing surviving cells) were solubilized by adding 100 μ L of 10% acetic acid to each well and agitating for 5 minutes. The absorbance of each well was read at 590 nm using a spectrophotometric plate reader, with higher absorbance indicating more viable cells. The raw absorbance values were normalized to the no-drug control (100% viability). Dose–response curves were plotted for each drug by fitting the data to a sigmoidal curve (variable-slope four-parameter logistic model) using GraphPad Prism software. The IC₅₀ was defined as the drug concentration that reduced cell viability by 50% relative to untreated controls and was determined from the fitted curves. For each cell line, IC₅₀ values in CLDN8-knockdown cells were compared to those in control cells. A shift in the IC₅₀ (either higher, indicating drug resistance, or lower, indicating increased sensitivity) in the knockdown cells would suggest that CLDN8 influences the response to that drug. All experiments were performed at least in triplicate, and mean IC₅₀ values \pm standard error were reported.

2.6.3 MTT Cell Proliferation Assay

Cell proliferation rates under different conditions were measured using an MTT assay (a colorimetric assay based on the conversion of MTT dye to formazan by mitochondrial enzymes in metabolically active cells). This assay was utilized to evaluate the impact of CLDN8 knockdown on baseline cell growth over several days. Cells with CLDN8 knockdown and their control counterparts were seeded in 96-well plates at an initial density of $\sim 1 \times 10^3$ cells per well in 100 μ L of medium (day 0). For each cell line, multiple identical plates were prepared so that cell growth could be assessed on consecutive days. Starting 24 hours after seeding (day 1) and on each subsequent day (up to day 5), an MTT reagent (Thiazolyl Blue Tetrazolium Bromide, Sigma-Aldrich) was added to a set of wells (final concentration 0.5 mg/mL) and incubated for 3–4 hours at 37 °C. Viable cells convert the yellow MTT into insoluble purple formazan crystals. After incubation, the supernatant was carefully removed, and 100 μ L of DMSO was added to each well to dissolve the formazan. The plate was shaken gently for 10 minutes, and the absorbance was measured at 540 nm (with a reference wavelength of 630 nm) on a microplate reader. Absorbance values are directly proportional to the number of viable cells. For each cell line, an initial reading on day 1 served as a baseline, and subsequent readings showed the increase in cell number. Growth curves were plotted as absorbance (or normalized viability) versus time. The doubling time of each cell line under each condition was estimated from the exponential portion of the curve. The assay was conducted with at least five replicate wells per time point for each condition, and the results were expressed as mean \pm SEM. By comparing growth curves of CLDN8-knockdown cells to controls, we determined whether loss of CLDN8 affected proliferation (slower growth if CLDN8 is pro-proliferative, or faster if CLDN8 normally restrains growth). This proliferation assay also provided context for interpreting drug sensitivity results, ensuring that any differences in drug response were not simply due to baseline growth rate differences.

2.7 Artemisinin Treatment

Artemisinin, the sesquiterpene lactone derived from *Artemisia annua*, was a central compound of interest in this study and was tested in various experimental contexts (effects on endothelial cells, on cancer cell behaviour, etc.). Artemisinin (Sigma-Aldrich) was prepared as a 100 mM stock solution in dimethyl sulfoxide (DMSO) and stored at $-20\text{ }^{\circ}\text{C}$. Working concentrations of Artemisinin was freshly prepared by diluting the stock in culture medium immediately before use. Cells were exposed to Artemisinin at concentrations ranging from $1\text{ }\mu\text{M}$ up to $25\text{ }\mu\text{M}$, depending on the assay. This range has been widely used in previous studies investigating the anticancer or endothelial regulatory effects of artemisinin and its derivatives and is considered pharmacologically relevant and non-cytotoxic within this range(161). In most experiments examining cellular behaviour (adhesion, invasion, migration) or molecular changes, a concentration of $5\text{--}10\text{ }\mu\text{M}$ for 24 hours was employed as a representative pharmacological dose that elicits biological effects without causing gross cytotoxicity. In specific mechanistic assays on endothelial barrier function, a higher dose ($10\text{ }\mu\text{M}$ for 24 hours) was used to ensure robust modulation of tight junctions. For the investigation of β -catenin signalling pathway alterations, cells were treated with artemisinin at concentrations of 5, 10, 15, and $20\text{ }\mu\text{M}$ for 24 hours to assess dose-dependent effects on pathway regulation. In all cases, control cells received an equivalent volume of DMSO (vehicle), which did not exceed 0.1% (v/v) in the final culture medium. After the specified treatment duration (24 hours, or shorter for time-course experiments like 30 min vs. 0 hour in qPCR studies), cells were either harvested for molecular analyses or processed for functional assays as described in the relevant sections above. The Artemisinin treatment protocol was consistently applied across experiments to allow comparison of results. For example, when studying gene expression changes, endothelial and cancer cells were treated with $10\text{ }\mu\text{M}$ Artemisinin for 0.5 hour or 24 hours and then RNA was

extracted for qPCR or RNA-seq. In functional assays, cells were pre-treated with Artemisinin for 24 hours before being subjected to adhesion/invasion tests. This standardized approach enabled us to dissect the effects of Artemisinin on both the brain endothelial barrier and breast cancer cells in a controlled manner.

2.8 Tissue Specimens and Histological Analysis

To complement the cell-based experiments, clinical breast cancer tissue samples were analysed for CLDN8 expression at both the mRNA and protein levels. This involved collecting patient specimens with appropriate ethical approval, extracting RNA for qPCR, and performing immunohistochemical staining for CLDN8 on tissue sections. The relationships between CLDN8 expression and clinicopathological features were then evaluated.

2.8.1 Clinical Specimens and Ethical Approval

Patient tissue samples were obtained from the Cardiff Cancer Hospital Biobank under approved protocols. A total of 127 breast tissue specimens were included, comprising primary breast tumour tissues from patients with various breast cancer subtypes (luminal A, luminal B, HER2-positive, and triple-negative breast cancers) as well as a set of adjacent normal breast tissues (from mastectomy specimens) used as non-tumour controls. Tumour and normal breast tissue (n = 33) specimens were obtained from different patients, and the normal tissues served as non-tumour controls. All samples were collected with informed patient consent in accordance with the Declaration of Helsinki. Ethical approval for use of these human tissues was granted by the Cardiff University School of Medicine Research Ethics Committee, and the study was conducted in compliance with institutional guidelines for human research. Clinical data such as tumour grade, stage, hormone receptor status, HER2 status, and patient outcomes (follow-up

duration, survival status) were retrieved from medical records and de-identified. Each tissue sample was coded and processed anonymously.

Fresh tumour specimens intended for RNA analysis were preserved in RNAlater solution (Thermo Fisher Scientific, Waltham, MA, USA) and stored at -80°C until extraction. Samples intended for histology were fixed in 10% neutral-buffered formalin and embedded in paraffin. The use of these clinical specimens enabled correlation of our experimental findings with real-world patient data, thereby strengthening the translational relevance of the study.

2.8.2 RNA Extraction and qPCR for Tissue Samples

For mRNA analysis of clinical samples, total RNA was extracted from ~ 20 mg of each frozen tissue using TRIzol® Reagent (as described for cell lines, with additional homogenization using a rotor-stator tissue homogenizer). The isolated RNA was treated with DNase I (Thermo Fisher Scientific) to remove any genomic DNA contamination, then purified. cDNA was synthesized from 1 μg of tissue RNA using the iScript™ cDNA Synthesis Kit. Quantitative PCR was performed to measure *CLDN8* transcript levels in each tissue, following the same qPCR protocol outlined earlier. A SYBR Green-based detection method was used for tissue qPCR analyses, with primers specific to *CLDN8* and the reference gene GAPDH. Each tissue cDNA was run in triplicate qPCR reactions. The relative expression of *CLDN8* in tumour vs. normal samples was determined by the $2^{-\Delta\Delta\text{Ct}}$ method (using a pooled normal breast sample as the calibrator). Melt curve analysis confirmed the specificity of amplification. The qPCR results were then correlated with clinicopathological data: for instance, comparisons were made between *CLDN8* levels in different breast cancer subtypes, and any association with tumour grade or patient outcome was noted. These data provided insight into whether *CLDN8* is dysregulated in breast cancer and if its expression has clinical significance.

2.8.3 Immunohistochemistry and Histological Scoring

Immunohistochemistry (IHC) was performed to assess CLDN8 protein expression in formalin-fixed, paraffin-embedded (FFPE) tissue sections. Paraffin blocks were cut into 4 μm thick sections using a microtome and mounted on charged glass slides. Slides were baked at 60 °C for 1 hour to improve tissue adherence. To begin the IHC staining, slides were de-paraffinized by immersion in xylene (2 \times 5 min) and rehydrated through a graded ethanol series (100%, 90%, 70% ethanol, 5 min each) ending in distilled water. Antigen retrieval was carried out to unmask epitopes: sections were heated in a citrate buffer (10 mM citric acid, pH 6.0) at 95–100 °C for 15–20 minutes (using a microwave oven or water bath), then allowed to cool slowly to room temperature. After retrieval, slides were rinsed in TBS (Tris-buffered saline). Endogenous peroxidase activity was quenched by treating sections with 3% H_2O_2 in methanol for 10 minutes. Non-specific binding was blocked by incubating slides in 5% normal goat serum (in TBS with 0.1% Tween-20) for 30 minutes.

Sections were then incubated with the primary antibody against CLDN8. A rabbit polyclonal anti-CLDN8 antibody (the same as used for Western blot, Abcam) was applied at an optimized concentration (\approx 1:100 dilution) and incubated overnight at 4 °C in a humidified chamber. Negative control sections were incubated with rabbit IgG isotype control or with primary antibody omitted, to ensure specificity. The following day, slides were washed in TBST (3 \times 5 min). An HRP-linked secondary antibody (such as Envision+ Dual Link system-HRP, Dako) was then applied for 30 minutes at room temperature. This HRP-conjugated polymer detects bound primary antibodies. After another series of TBST washes, the antigen–antibody complex was visualized using 3,3'-diaminobenzidine (DAB) chromogen. DAB working solution was prepared according to kit instructions and applied to each section for \sim 5 minutes, resulting in a brown precipitate at sites of

CLDN8 expression. The reaction was stopped by rinsing in water once the desired stain intensity was achieved. Sections were then counterstained with haematoxylin for 20–30 seconds to stain nuclei light blue. Slides were "blued" under running tap water (to develop the haematoxylin to blue) and then dehydrated through graded alcohols, cleared in xylene, and mounted with a coverslip using DPX mounting medium.

Staining evaluation was performed using a 40× objective, based on the percentage of CLDN8-positive cells and staining intensity in 2 randomly selected fields. The proportion of positive tumour cells was categorised as follows: no positive cells (0); <25% positive cells (1); 25–50% (2); 50–75% (3); and >75% (4). The staining intensity was graded as follows: unstained (0), light brown (1), brown (2), and dark brown (3). The staining index (SI) was calculated using the formula: SI = staining intensity × proportion of positively stained cells. CLDN8 expression was evaluated using the SI-scored method, with cutoff points of ≤ 3 and > 3 . As previously reported, the staining score for CLDN8 was determined by considering the extent of tumour coverage and the proportion of positive staining.

2.9 Transcriptomic and Bioinformatic Data Analysis

Large-scale gene expression data were utilized to gain additional insights into CLDN8 and related pathway alterations. This included both RNA sequencing of selected cell samples within this study and analysis of public transcriptomic datasets from breast cancer cohorts.

2.9.1 RNA Sequencing and Pathway Enrichment

Whole transcriptome RNA sequencing (RNA-seq) was performed on representative breast cancer and brain endothelial samples to identify gene expression changes induced by Artemisinin treatment. Specifically, MDA-MB-231 triple-negative breast cancer cells and hCMEC/D3 endothelial cells were treated

with Artemisinin (10 μ M, 24 h) or DMSO (control). Total RNA from these samples was submitted to BMG Gene (a genomic services provider) for RNA-seq library preparation and sequencing. Poly-A+ mRNA was enriched, fragmented, and converted into cDNA libraries, which were then sequenced on an Illumina platform to generate paired-end reads (approximately 20 million read pairs per sample). The raw sequencing reads were quality-checked (FastQC) and aligned to the human reference genome (hg38) using STAR or HISAT2 aligner. Gene-level read counts were obtained and normalized (FPKM or TPM values calculated). Differential expression analysis between Artemisinin-treated and control groups for each cell type was carried out using DESeq2, yielding a list of genes significantly up- or down-regulated by Artemisinin (using a false discovery rate < 0.05 as the significance threshold).

To interpret the biological significance of these changes, pathway enrichment analysis was conducted. The set of differentially expressed genes in each cell type was analysed using Metascape and KEGG pathway analysis. Metascape (an online tool that integrates Gene Ontology and multiple pathway databases) was used to identify pathways and processes over-represented in the gene list. Notably, both hCMEC/D3 and MDA-MB-231 cells showed enrichment of genes in the tight junction signalling pathway and related processes after Artemisinin exposure. Key pathways such as “Tight Junction assembly,” “cell–cell adhesion,” and “Wnt/ β -catenin signalling” were highlighted by this analysis. The KEGG (Kyoto Encyclopaedia of Genes and Genomes) pathway mapper further confirmed that many Artemisinin-responsive genes fell within the canonical tight junction pathway and adherens junction interactions. Networks of differentially expressed genes were visualized to illustrate connections between CLDN8 and other junctional proteins or signalling mediators. These transcriptomic results guided the focus of subsequent experiments (for example, identifying CLDN8 as a candidate of interest and examining β -catenin signalling changes). All raw

sequence data and processed results are documented in Supplementary Data. The RNA-seq and enrichment analysis thus provided an unbiased, global view of how Artemisinin perturbs cellular gene expression, supporting the hypothesis that it modulates BBB integrity at the molecular level.

2.9.2 Public Genomic Data (TCGA Cohort Analysis)

To place our findings in a broader clinical context, we analysed breast cancer patient data from The Cancer Genome Atlas (TCGA) and an internal Cardiff clinical cohort. Level 3 mRNA expression data for CLDN8 were obtained from the TCGA Breast Invasive Carcinoma (BRCA) dataset using the Genomic Data Commons portal (All TCGA data were downloaded in August 2023). This included RNA-seq expression (in TPM or RSEM values) for hundreds of breast tumours across different subtypes, as well as a smaller set of normal breast tissue samples. Data were filtered to exclude low-quality samples (those not meeting TCGA quality control metrics or with low read counts). In total, expression data from approximately 1100 breast tumours and 100 normal breast samples were available. CLDN8 expression in tumours were compared to normal breast tissue using an unpaired *t*-test to determine if CLDN8 is significantly dysregulated in cancer. Further, the TCGA cases were stratified by clinical and molecular features: subtype (PAM50 classification or hormone receptor/HER2 status), tumour stage (I–IV), and histologic grade. ANOVA or non-parametric Kruskal Wallis tests were used to assess differences in CLDN8 mRNA levels across these groups.

In addition to expression correlations, survival analysis was performed using the TCGA cohort. Patients were divided into CLDN8-high vs. CLDN8-low groups (for example, using the upper vs. lower tertile of CLDN8 expression, or an optimal cutoff determined by ROC analysis). Kaplan–Meier survival curves were generated for outcomes such as overall survival (OS) and disease-free survival (DFS). The log-rank test was used to compare survival distributions between

groups. A trend was observed where higher CLDN8 expression was associated with slightly improved DFS in some subgroups, though this did not reach statistical significance in all cases. This trend was consistent with our experimental data suggesting CLDN8 might have a protective role.

For the Cardiff clinical cohort (160 patients described above), we similarly examined associations. CLDN8 mRNA levels (from qPCR) and CLDN8 IHC H-scores were each correlated with clinical data. For categorical comparisons (CLDN8 high vs low in ER-positive vs ER-negative tumours), Chi-square tests or Fisher's exact tests were used. For continuous correlations (CLDN8 vs. percentage of Ki-67 proliferation index), Pearson or Spearman correlation coefficients were calculated as appropriate. The small sample size limited statistical power, but the trends supported the larger TCGA findings.

All bioinformatic and statistical analyses were conducted using SPSS (v27, IBM Corp.) and R software. Public data usage was in accordance with TCGA publication guidelines. By leveraging these public and internal datasets, we were able to validate whether patterns observed in our laboratory models (such as CLDN8 downregulation in aggressive cancer and its link to patient outcomes) are evident in clinical populations, thereby reinforcing the relevance of CLDN8 and Artemisinin-related pathways in breast cancer brain metastasis.

2.10 Statistical Analysis

All quantitative data generated in this study were subjected to rigorous statistical analysis to determine significance and reliability. Statistical calculations were performed using IBM SPSS Statistics 27 (IBM Corp., Armonk, NY, USA) and cross-verified with GraphPad Prism 9 (GraphPad Software, San Diego, CA, USA) for graphing and additional tests. Data is generally presented as the mean \pm standard error of the mean (SEM) from at least three independent experiments (or

independent biological samples, in the case of patient tissues), unless stated otherwise.

Before hypothesis testing, data distributions were examined. The Shapiro–Wilk test (and visual inspection of histograms) was used to assess normality of continuous data. For comparisons between two groups, an independent Student's *t*-test was employed if data were normally distributed (comparing mean CLDN8 mRNA levels in tumour vs. normal tissue, or mean IC₅₀ values in CLDN8-knockdown vs. control cells). If the assumption of normality (or homogeneity of variances by Levene's test) was violated, the non-parametric Mann–Whitney U test was used instead. For comparisons among multiple groups (CLDN8 expression across more than two subtypes or treatments), a one-way ANOVA was performed when parametric conditions were met, followed by post-hoc tests (Tukey's HSD or Bonferroni) for pairwise comparisons. In cases of non-normal data or ordinal scoring (such as H-scores, which range 0–300, or when sample sizes were small), a Kruskal Wallis test was applied, followed by Dunn's multiple comparison test if needed.

Categorical data (proportion of CLDN8-high vs. low cases by subtype) were analysed using Chi-square tests or Fisher's exact tests (if expected counts were low). Correlations between continuous variables (for instance, CLDN8 mRNA level vs. patient age, or between CLDN8 H-score and Ki-67 index) were evaluated using Pearson's correlation coefficient (*r*) for linear correlations, or Spearman's rho for non-parametric ranking correlation.

For survival analyses, Kaplan–Meier curves were generated to illustrate differences in patient outcomes based on CLDN8 expression categories. The log-rank (Mantel–Cox) test was used to compare survival distributions between groups (CLDN8-high vs. CLDN8-low). Hazard ratios (HR) with 95% confidence intervals were calculated using Cox proportional hazards regression to estimate

the effect of CLDN8 on survival while adjusting for potential confounders (such as subtype or treatment status) in multivariate models.

In all tests, a p -value of < 0.05 was considered statistically significant. Degrees of significance are reported in the text or figure legends where appropriate ($p < 0.01$, $p < 0.001$). All experiments were designed with appropriate controls and replicates to ensure statistical robustness. Data analysis was conducted in consultation with a biostatistician to confirm the validity of the chosen tests. The comprehensive statistical approach ensured that conclusions drawn from the data (such as the effect of Artemisinin on barrier function, or the association of CLDN8 with drug response and outcomes) are supported by objective evidence and not due to random chance.

2.11 qPCR Primers

As shown in table 2.11 *Forward (F)* and *Reverse (R)* primer sequences (5' → 3') for quantitative PCR targets used in the thesis. Primer design for many targets incorporates a 5' tail (in reverse primers denoted "Z") compatible with a universal Amplifluor probe system. Amplicon sizes are provided.

Table 2.11 qPCR Primers

Gene (Target)	Forward Primer (5'–3')	Reverse Primer (5'–3')	Amplicon Size
GAPDH (housekeeping)	CTGAGTACGTCGTGGAGTC	ACTGAACCTGACCGTACACAGAGAT GATGACCCTTTTG	93 bp
Claudin 1 (CLDN1)	GAAGTGTATGAAGTGCTTGG	ACTGAACCTGACCGTACACAGACCT GCAAGAAGAAATA	88 bp
Claudin 2 (CLDN2)	TATAGCACCTTCTGGGCCT	CCTTGGAGAGCTCCTTGTGG	432 bp
Claudin 3 (CLDN3)	ATGCAGTGCAAGGTGTACGA	TGGTGGCCGTGTACTTCTTC	403 bp
Claudin 4 (CLDN4)	TGGGAGGGCCTATGGATGAA	GGTGGACAGTTGCAGCAAAG	422 bp
Claudin 5 (CLDN5)	TTCCTGGACCACAACATC	ACAGACGGGTCTGAAAACCT	353 bp

Gene (Target)	Forward Primer (5'-3')	Reverse Primer (5'-3')	Amplicon Size
Claudin 6 (CLDN6)	CCGTCATCCGGGACTTCTAT	TGGTAGGGTACTCAGAGGGC	225 bp
Claudin 7 (CLDN7)	ATAACCCTTTGATCCCTACC	ACTGAACCTGACCGTACAACAGGAA CAGGAGAGCAGT	113 bp
Claudin 8 (CLDN8)	GCTTGAGAGAAGCTCTCTACTT	ACTGAACCTGACCGTACAAGCTACT GCTCTTTTCGTTG	104 bp
Claudin 9 (CLDN9)	CTTCATCGGCAACAGCATCG	AAGTCCTGGATGATGGCGTG	339 bp
Claudin 10 (CLDN10)	GTCTCCAAGTCAAGGACT	ACTGAACCTGACCGTACAGCAAATA TGGAACCAAAG	114 bp (qPCR)
Claudin 11 (CLDN11)	CCGGTGTGGCTAAGTACA	ACTGAACCTGACCGTACACACACAG GGAACCAGATG	97 bp
Claudin 12 (CLDN12)	CTCTGCCTGATTGGAATG	ACTGAACCTGACCGTACAACCTGCA CTATTGACCAGAC	87 bp
Claudin 14 (CLDN14)	CACCCTACAGGCCCTACC	ACTGAACCTGACCGTACAGTCTTTGT AGGCAGCTGGT	92 bp
Claudin 17 (CLDN17)	CTGCTTATTGGCATCTGTG	ACTGAACCTGACCGTACATGAAGTT CCCAGAAGGTATG	84 bp
Claudin 18 (CLDN18)	GGATCATGTTTATTGTCTCA	ACTGAACCTGACCGTACACATCCAG AAGTTAGTCACCAG	83 bp
Claudin 20 (CLDN20)	AGCAAACCTTTCTGGATCTGA	ACTGAACCTGACCGTACACAGAAAA TCATGCCAGAGAT	114 bp
Claudin 23 (CLDN23)	CCGCCATCAAGTACTACAG	ACTGAACCTGACCGTACACCACCGA GTTGGTGTAGG	129 bp
Claudin 24 (CLDN24)	AATGGGCTGGGATTTCTGGG	CTGGGGACAAAGTCTGGGAC	215 bp
JAM-A (F11R)	AACAAGATCACAGCTTCTA	CTTACTCGAAGTCCCTTCT	600 bp
JAM-B (JAM2)	ATATCCGGATCAAAAATGTG	CATTTTC ACTCATTGTCGTG	588 bp
JAM-C (JAM3)	TTGATGAGATTGTGATCGAG	ACTGAACCTGACCGTACAATCTTGCC TACTGGTACAGC	88 bp
JAM4 (IGSF5)	GCAATGGATCTGCTTACCTTA	ACTGAACCTGACCGTACAGGTTTCATT CTCAGCGACTAC	84 bp
JAM-C2 (JAM-C)	CTGCTGTTTACAAGGACGAC	CAGATGCCCAACGTGATCAG	172 bp
JAM-D (CXADR-like)	CCGGATCTGGAGGAATGGAA	GCTTAGCACCACCATGTCAC	204 bp
Occludin (OCLN)	ATGTCATCCAGGCCTC	ATAGACAATTGTGGCA	579 bp

Gene (Target)	Forward Primer (5'–3')	Reverse Primer (5'–3')	Amplicon Size
β -Catenin (β -catenin)	AAAGGCTACTGTTGGATTGA	TCCACCAGAGTGAAAAGAAC	525 bp
ZO-1 (TJP1)	CCACATACAGATACGAGTCCT C	TGGCTTATGCTGAGATGAAGG	533 bp
ZO-2 (TJP2)	CAAAAGAGGATTTGGAATTG	GAGACCATACTCTTCGTTTCG	844 bp
β -Actin (ACTB)	GGACCTGACTGACTACCTCA	ACTGAACCTGACCGTACAAGCTTCTC CTTAATGTCACG	187 bp
MAGI1 (BAIAP1)	CTGACCAATGCAGAGAAGAT	ACTGAACCTGACCGTACATTGGTGGT ATTCTTGTCTC	86 bp
MAGI2 (ARIP2)	CTGGAGGAAGACGAGTGAG	ACTGAACCTGACCGTACACCTACTTC CGGCAGACCT	118 bp
MAGI3 (BAIAP3)	CCTGACACCGCAGTAATTT	ACTGAACCTGACCGTACAGCCTCTCT CCAGCTCTACTG	81 bp

Note: Primer sequences marked with a 5' tail (the Z sequence “ACTGAACCTGACCGTACA”) were used in conjunction with a universal fluorescent probe in a two-component qPCR detection system. Unmarked primers are conventional oligonucleotides. All primers were typically used at 100–300 nM final concentration in qPCR reactions, and amplicon sizes were verified by gel electrophoresis.

2.12 Antibodies

As shown in table 2.12, the list of antibodies utilized for Western blot (WB), immunofluorescence (IF), immunohistochemistry (IHC), and co-immunoprecipitation (Co-IP) experiments, including their targets, clonality, source, and working applications/dilutions.

Table 2.12 Antibodies

Target Protein	Antibody Type & Clone	Supplier & Clone number	Applications (Dilution)	Notes
Claudin-8 (CLDN8)	Rabbit Polyclonal A	Abcam (ab211439) Polyclonal	IHC (1:100), WB (1:1000); IF (1:100)	Recognizes tight junction protein CLDN8.
GAPDH (housekeeping)	Mouse Monoclonal	Santa Cruz (Sc32233) 6C5	WB (1:2000–1:5000)	Loading control for protein normalization in WB; ~36 kDa band.
β -Catenin (β -catenin)	Mouse Monoclonal Antibody	Santa Cruz (sc393501) A-5	WB (1:1000), IF (1:200), Co-IP (2 μ g per 500 μ g lysate) file-euefy8b71ahyntpg6omfy	Detects total β -catenin (~92 kDa). Used in WB for pathway analysis and as IP antibody to pull down β -catenin protein complexes
ZO-1 (TJP1)	Mouse Monoclonal &1A12	Thermo Fisher #33-9100 (Invitrogen) ZO1-1A12	IF (1:200), WB (1:1000)	Tight junction scaffold protein ZO-1 (~220 kDa). To examine junction integrity (co-stained with CLDN8). WB to assess expression changes.
Phospho-GSK3 β (Ser ⁹)	Goat Polyclonal	Santa Cruz (Sc11757)	WB (1:1000)	Detects GSK3 β when inactivated by Ser ⁹ phosphorylation. Used to monitor pathway activity under Artemisinin treatment.

Target Protein	Antibody Type & Clone	Supplier & Clone number	Applications (Dilution)	Notes
Phospho- β -Catenin (Thr ⁴¹ /Ser ⁴⁵)	Rabbit Monoclonal & 23H16L13	Thermo Fisher #703638	WB (1:1000)	Marks β -catenin phosphorylated by GSK3 β (degradation-associated). Used to confirm Artemisinin-induced β -catenin regulation.
Secondary (WB) – HRP		Bio-Rad #1706515 (Polyclonal)	WB (1:3000)	Binds rabbit primary Abs; ECL detection. Also, Goat Anti-Mouse IgG HRP
Secondary (IF) – Fluor	Anti-mouse; Anti-Rabbit	SIGMA F5262; T5393; F1262	IF (1:500)	FITC fluorescence for CLDN8 and ZO-1 proteins (green fluorescence). TRIC fluorescence used for β -catenin (red fluorescence).

Notes: All primary antibodies were validated for human specificity and used according to manufacturers' protocols. CLDN8 antibody was critical for confirming successful CLDN8 knockdown in cells (loss of the ~23 kDa band on WB) and for detecting membranous CLDN8 in tissue sections (IHC scoring). β -Catenin antibody was used both to analyse downstream signalling changes by Western blot (cytoplasmic and nuclear levels) and as a capture antibody in Co-IP experiments to probe protein interactions with CLDN8. ZO-1 antibody helped visualize tight junction continuity by IF, often co-localizing with CLDN8 at cell borders. The phospho-specific antibodies (p-GSK3 β , p- β -Catenin) were used to monitor pathway modulation: for instance, a decrease in Ser⁹-phosphorylated GSK3 β and an increase in Thr⁴¹/Ser⁴⁵-phosphorylated β -catenin indicated activation of GSK3 β and enhanced β -catenin degradation in Artemisinin-treated cells. Secondary antibodies for immunofluorescence were chosen to match the host species of primaries and were highly cross adsorbed to minimize non-specific staining; all IF images included DAPI nuclear counterstain. Dilutions were optimized by titration (, GAPDH 1:5000 yielded a strong single band with minimal background). Each antibody was stored at 4°C (short-term) or -20°C (long-term) as recommended, and working solutions were prepared in the appropriate blocking buffers (5% milk for WB, 1% BSA or serum for IF/IHC). To ensure that protein-level findings are corroborated by transcript-level evidence, we provide the following overview of the RNA-seq and TCGA pipelines. MDA-MB-231 and hCMEC/D3 cells were treated with artemisinin (10 μ M, 24 h) or DMSO control. Libraries were prepared after poly-A enrichment (BMG Gene) and sequenced on an Illumina platform with paired-end reads (~20 million read pairs per sample). Raw reads underwent quality control with FastQC and were aligned to hg38 using STAR/HISAT2 to obtain gene-level counts and

FPKM/TPM quantification. Differential expression was analyzed with DESeq2 (FDR < 0.05). Enrichment analyses were performed with Metascape and KEGG, focusing on Tight Junction, cell adhesion, and Wnt/ β -catenin pathways to guide downstream WB/IF and functional experiments. Raw and processed data are provided in Supplementary Data. To place the findings in a clinical context, Level-3 mRNA expression data for TCGA-BRCA were downloaded from the Level 3gust 2023) in TPM/RSEM units. After quality filtering, ~1,100 tumour and ~100 normal breast tissue samples were included. Differences in CLDN8 expression between tumour and normal tissues were assessed by unpaired t-test. Stratified analyses by molecular subtype/receptor status, stage, and grade used ANOVA or Kruskal Wallis tests. Survival analyses divided patients into high/low expression groups using tertiles or ROC-optimized cut-offs; Kaplan–Meier curves for OS/DFS were compared with log-rank tests. Statistics were performed in R and SPSS. Trends in this public cohort were cross-validated against our IHC scores and protein-level readouts.

**Chapter III : A Preliminary Exploration of
Artemisinin's Regulation of the Blood-Brain Barrier
in Breast Cancer Brain Metastasis**

3.1 Introduction

The BBB serves as a critical defence mechanism, protecting the central nervous system (CNS) from harmful substances. However, its highly selective nature also prevents many therapeutic agents from effectively reaching intracranial lesions, thus limiting the efficacy of treatments for brain metastases. Artemisinin and its derivatives, widely used for the treatment of cerebral malaria, are well-known for their high efficacy, safety, and broad pharmacological activities, including anti-parasitic, anti-tumour, anti-inflammatory, and anti-microbial properties.

The development of neurological disorders, including brain metastases, is complex, involving multiple etiologist and pathophysiological processes. Recent research indicates that drugs with single mechanisms of action and severe side effects are unlikely to be ideal for treating these conditions. Effective treatment of brain tumours requires drugs capable of penetrating the BBB, exhibiting a strong anti-tumour effect, and having minimal toxicity. Unfortunately, no current drug meets all these criteria. Artemisinin, due to its multifaceted pharmacological properties and ability to maintain high concentrations in brain tissue, may present a promising therapeutic approach for breast cancer brain metastasis.

The mechanism by which Artemisinin penetrates the BBB is still under investigation, though its small molecular weight (less than 500 Daltons) is believed to facilitate this process. Given the importance of Tight junctions (TJs) in maintaining BBB integrity, we hypothesized that Artemisinin could exert its effects by modulating TJ proteins in endothelial cells, thereby altering BBB permeability.

To explore this hypothesis, we conducted RNA sequencing on breast cancer cells (MDA-MB-231) and brain endothelial cells (hCMEC/D3), both treated and untreated with Artemisinin. The sequencing results revealed significant

enrichment in genes associated with TJ pathways, suggesting that Artemisinin may affect TJ-related mechanisms. Based on these findings, we performed further experiments, including quantitative PCR (qPCR) and functional assays, to evaluate the impact of Artemisinin on TJ protein expression in both peripheral and cerebral blood vessel endothelial cells (HECV and hCMEC/D3, respectively).

This initial research identified CLDN8 as a critical TJ protein affected by Artemisinin, which could serve as a potential marker for TJs and warrant further investigation. The results from this study provide insights into the potential mechanism of Artemisinin in altering BBB permeability and its implications for treating breast cancer brain metastasis.

3.2 Materials and methods

3.2.1 Cell Lines

The cell lines used in this study included hCMEC/D3 and HECV, purchased from the American Type Culture Collection (ATCC), USA. To cover the main breast cancer subtypes, we utilized luminal A (MCF-7), luminal B (BT-474, MDA-MB-361), HER2-positive (HCC-1419), and triple-negative (MDA-MB-231) cell lines. Endothelial cell lines, including HUVEC, HMVEC, TY9, and TY10, as well as complementary cell lines MRC5 and MET5A, were also included for broader observations. The culture conditions were optimized with DMEM supplemented with 10% fetal bovine serum (FBS) and antibiotics for most cell lines, while BT-474 and MDA-MB-361 were maintained in RPMI medium with similar supplements.

3.2.2 RNA Sequencing and Enrichment Analysis

RNA sequencing was conducted by BMG Gene on MDA-MB-231 and hCMEC/D3 cells, divided into control (untreated) and experimental (Artemisinin-treated) groups. Differential expression analysis highlighted significant changes in the

expression of genes involved in Tight Junction (TJ) pathways. To better understand the biological significance, we used Metascape for pathway enrichment analysis, which confirmed that Artemisinin treatment predominantly affected TJ-related pathways, indicating a potential mechanism involving BBB modulation.

3.2.3 Quantitative analysis of TJ proteins in endothelial cells using real time polymerase chain reaction (QPCR)

HCMEC/D3 cells were treated with Artemisinin and divided into 2 timed groups: 0H, 30 mins. Total RNA was extracted using TRIzol and tested for purity and integrity. Reverse transcription for complementary DNA, amplified and detected by QPCR using Amplifluor Uniprimer Universal system (Intergern Company, New York, USA), details could be seen in Chapter 2 (Section 2.7.8). Primer applied in QPCR was listed in Table 2.2. Every sample was repeated for three groups.

3.2.4 RNA isolation, cDNA synthesis and reverse transcript polymerase chain reaction (PCR).

Based on the results of QPCR, CLN8 was analysed as a potential marker. Tri reagent kit (Sigma-Aldrich, Inc., Poole, Dorset, England, UK) was applied to isolate the RNA. Followed by reverse transcription procedure, RNA was translated into the complement DNA using the iScript™ cDNA Synthesis Kit (Bio-Rad Laboratories, California, USA). Conventional PCR reaction was performed according to the protocol in chapter 2 (section 2.7.5). GAPDH was used as the house-keeping gene, Primer sequences for GAPDH and CLDN8 were listed in Table 2.2.

3.3 Results

3.3.1 RNA Sequencing and Identification of Key Pathways

RNA sequencing analysis identified significant gene expression changes associated with TJ pathways following Artemisinin treatment in breast cancer and brain endothelial cells. As shown in Figure 3.3.1, distinct gene expression patterns were observed, highlighting genes specifically related to TJ regulation.

Anchored to the two differential profiles in Figure 3.3.1, the KEGG Tight Junction map in Figure 3.3.2A indicates that Artemisinin drives a two-compartment remodeling spanning the endothelium (hCMEC/D3) and the tumour compartment (MDA-MB-231).

In hCMEC/D3, several junctional scaffold and signalling nodes are downregulated, including MAGI1 (a MAGUK adaptor that tethers claudins/occludin to actin), CTNNBIP1 (β -catenin–interacting inhibitor linking TJ to transcriptional outputs) (162), and PIK3CB (PI3K catalytic subunit that couples junctions to cytoskeletal dynamics) (163). Concomitantly, COL4A1 (basement-membrane type IV collagen) and CADM4 (cell-adhesion molecule) decrease, pointing to a weakened endothelial barrier matrix and cell–cell adhesion platform(164).

In MDA-MB-231, Artemisinin induces a complementary shift favouring junction remodelling and motility: cytoskeleton/adhesion regulators such as ACTN1, FLNA, and MYO9A are upregulated(165), whereas guidance/adhesion cues including SEMA3C and PIEZO2 are downregulated, a pattern consistent with higher contractility and altered cell–cell contacts(166, 167).

When these gene-level changes are overlaid onto the KEGG Tight Junction schema (Fig. 3.3.2A), a mechanistic picture emerges in which Artemisinin (i) suppresses

endothelial TJ stabilizers (MAGI1–CTNNBIP1–PIK3CB axis with basement-membrane support via COL4A1/CADM4), thereby loosening the BBB paracellular seal, and (ii) reprograms tumour cytoskeleton/adhesion (ACTN1/FLNA/MYO9A↑ with SEMA3C/PIEZO2↓), favouring junction turnover(168). This systems view is mirrored by the Metascape network (Figure 3.3.2B), where endothelial TJ/scaffold genes and tumour cytoskeletal modules cluster into functionally connected communities that jointly impinge on cell–cell adhesion and BBB integrity, aligning with our TEER/PCP readouts elsewhere in other chapter.

Overall, these results suggest that Artemisinin exerts its therapeutic effects by modulating critical pathways related to TJ regulation, potentially influencing the integrity of the BBB and offering insights for developing novel treatments for breast cancer brain metastasis.

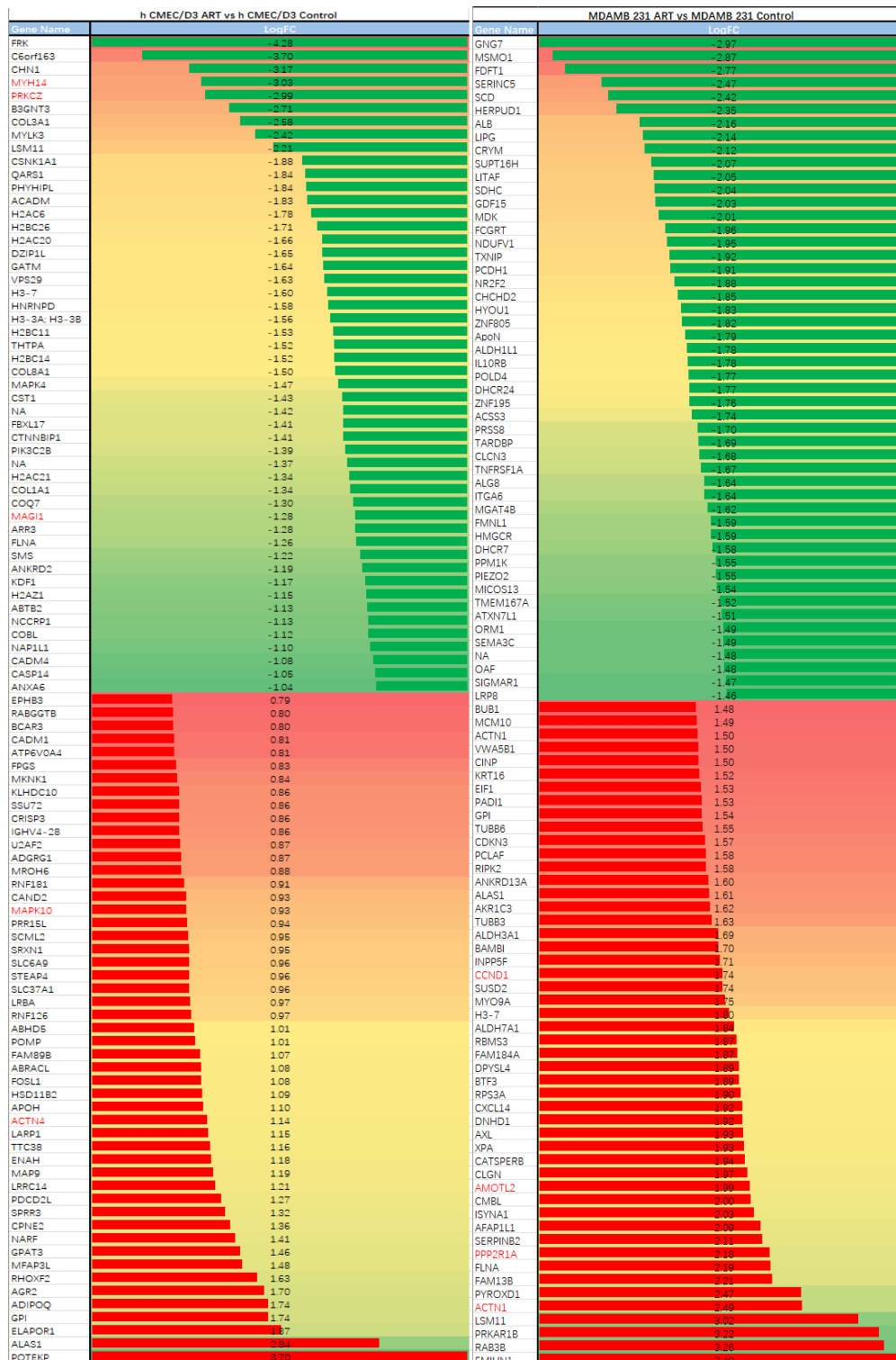
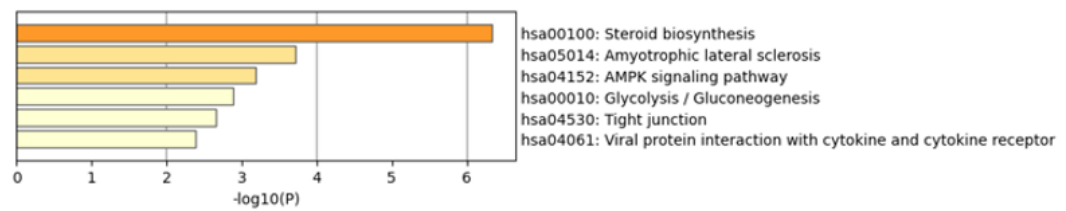
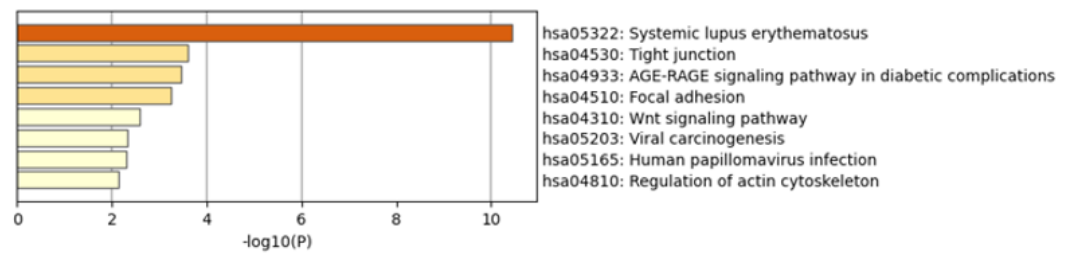


Figure 3.3.1 The gene expression changes in hCMEC/D3 and MDA-MB-231 cells after treatment with Artemisinin compared to the control group. Green and red bars represent significant downregulation and upregulation of genes, indicating a decrease or increase in gene expression, respectively. Genes marked in red are those involved in the TJ pathway.

A MDA-MB-231



hCMEC/D3



B

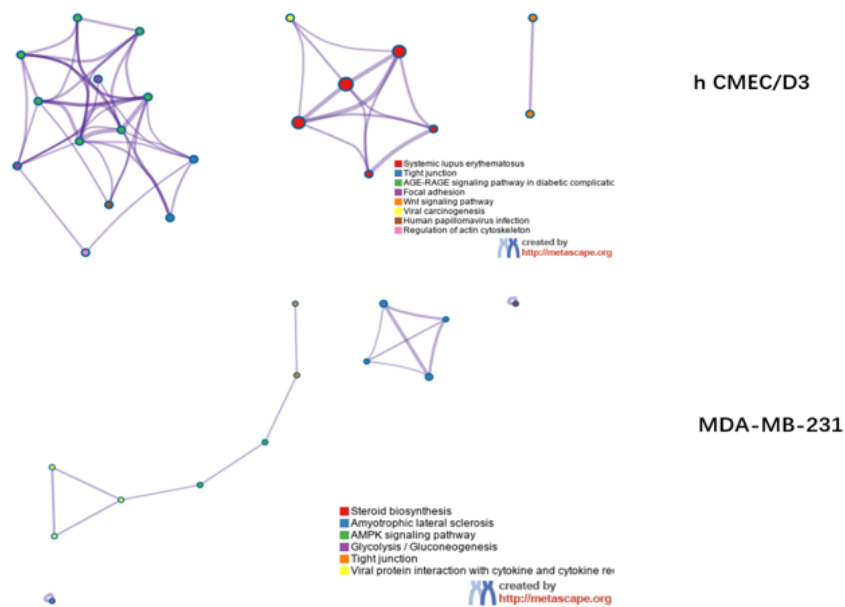


Figure 3.3.2 (A) Enrichment analysis results of differentially expressed genes (KEGG pathways) in hCMEC/D3 and MDA-MB-231 cells. The TJ pathway is a common pathway shared by both cell types. (B) Network map of differentially expressed genes in MDA-MB-231 and hCMEC/D3 cells (Metascape analysis). The network illustrates the interactions among differentially expressed genes and their functional clustering.

3.3.2 CLDN8 as a Key Target in Tight Junction Regulation

Following the identification of significant changes within TJ pathways from RNA sequencing analysis, quantitative PCR (qPCR) was performed to validate the expression levels of key TJ-related genes. The results highlighted CLDN8 as notably downregulated in hCMEC/D3 cells treated with Artemisinin, as clearly demonstrated in Figure 3.3.3. Given the established role of CLDN8 in maintaining tight junction integrity and cellular adhesion, this pronounced decrease suggests its potential involvement as a critical mediator in the regulation of the BBB function. Consequently, the downregulation of CLDN8 following Artemisinin exposure underscores its possible significance in modulating BBB permeability and emphasizes its relevance as a target for therapeutic strategies aimed at breast cancer brain metastasis.

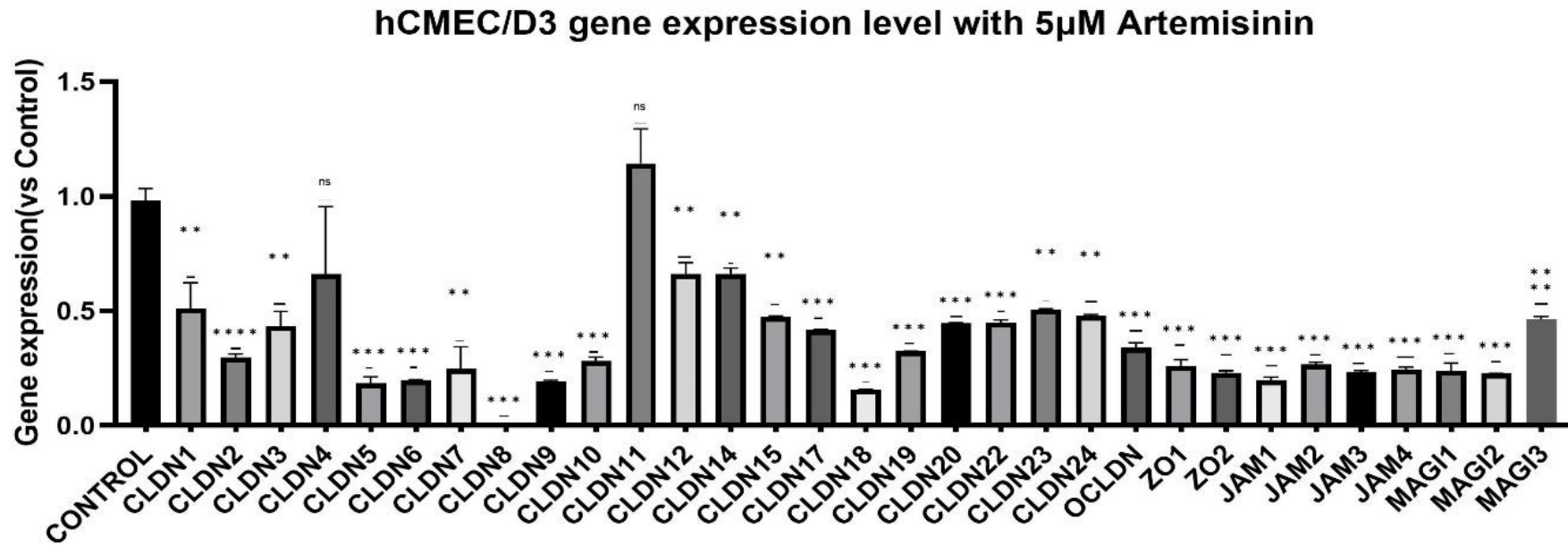


Figure 3.3.3 The gene expression levels in hCMEC/D3 cells after treatment with 5 μ M Artemisinin is displayed. Following Artemisinin treatment, the expression of CLDN8 significantly decreased, along with other tight junction proteins.

3.3.3 CLDN-8 Transcription levels in cells

To assess the broader relevance of CLDN8, we extended the qPCR analysis across major breast-cancer subtypes—luminal A (MCF-7), luminal B (BT-474, MDA-MB-361), HER2-positive (HCC-1419) and triple-negative (MDA-MB-231)—as well as endothelial models relevant to the BBB (hCMEC/D3, HUVEC, HECV, TY10). Primer sets yielded single, specific amplicons of the expected lengths (CLDN8, 104 bp; reference GAPDH, 93 bp), migrating between the 50 bp and 150 bp markers on a 50 bp DNA ladder. Melt-curve analysis showed single peaks without primer-dimers. CLDN8 transcripts were detected in nearly all tested breast-cancer subtypes and endothelial cell lines (Figure 3.3.4), supporting a broadly shared role in junctional regulation within tumour epithelium and tight-junction maintenance in BBB-relevant endothelium.

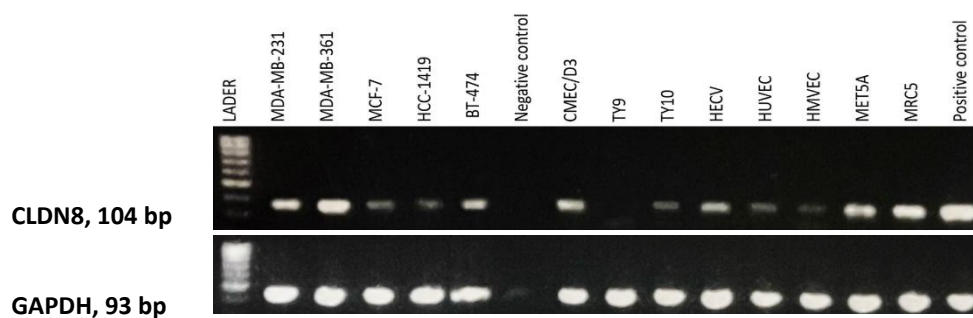


Figure 3.3.4 qPCR detection of CLDN8 across breast-cancer subtypes and endothelial cell lines. Representative 2% agarose gel shows single amplicons at the expected sizes (CLDN8, 104 bp; GAPDH, 93 bp) run alongside a 50 bp DNA ladder (bands at 50/100/150/200/250/300 bp; enhanced 100/200 bp markers). Melt curves display single peaks for each primer pair. CLDN8 expression was detected in nearly all models examined.

3.4 Discussion

In this study, we investigated the effects of Artemisinin on TJ protein regulation in breast cancer and endothelial cells. RNA sequencing of hCMEC/D3 and MDA-MB-231 cells treated with Artemisinin revealed significant changes in the expression of genes associated with TJ pathways, suggesting that Artemisinin may modulate the BBB and influence breast cancer metastasis. Given that the BBB is a major obstacle to effective drug delivery for brain metastases, these findings provide important insights into how Artemisinin might facilitate drug delivery to the brain by modulating TJ integrity.

The TJs between brain capillary endothelial cells are 50-100 times tighter than those in surrounding capillaries, with major components including claudin, occludins, the adhesion molecule JAM, and the cytoplasmic auxiliary protein ZO-1. These components, along with endothelial cells, form the basis of the BBB. The hCMEC/D3 cell line, derived from human temporal lobe microvessels, represents a model of the human BBB suitable for studying CNS-related drug transport mechanisms(169). We applied Artemisinin to both HECV cells and hCMEC/D3 cells to simulate the effects of Artemisinin on TJ proteins in endothelial cells of peripheral and cerebral vasculature.

Among the TJ-related genes identified, CLDN8 emerged as a significant target. qPCR analysis confirmed that CLDN8 was significantly downregulated in hCMEC/D3 cells after Artemisinin treatment, while no significant change was observed in HECV cells. This differential effect suggests that Artemisinin has a more targeted impact on intracranial endothelial cells compared to peripheral endothelial cells. The consistent downregulation of CLDN8 in hCMEC/D3 cells suggests that Artemisinin may increase BBB permeability by altering TJ integrity, potentially enhancing drug

delivery to the brain, especially for treating brain metastases from breast cancer.

The consistent expression of CLDN8 across multiple breast cancer subtypes and endothelial cell lines further supports its potential as a marker for TJ integrity. In breast cancer cells, CLDN8 was expressed regardless of the subtype, indicating that it may play a fundamental role in maintaining cell polarity and adhesion. In endothelial cells, CLDN8's role in maintaining TJ integrity suggests that its downregulation could lead to increased vascular permeability, which may facilitate the movement of tumour cells or therapeutic agents across the endothelial barrier.

In addition to CLDN8, other TJ proteins such as CLDN9 and JAM2 were also affected by Artemisinin treatment, albeit to a lesser extent. This broader modulation of the TJ complex by Artemisinin indicates that its effect on the BBB may involve multiple proteins, ultimately leading to alterations in BBB integrity that affect drug permeability. Notably, CLDN8 showed the most specificity among these targets, highlighting its central role in regulating TJs.

The time-dependent changes in gene expression observed in our study highlight the dynamic nature of Artemisinin's effects. Within the first two hours of treatment, there was a rapid alteration in TJ-related genes, including CLDN8, indicating that Artemisinin acts early to modify BBB permeability. This aligns with previous research suggesting that Artemisinin and its derivatives can rapidly affect cellular pathways, likely by modulating signalling cascades involved in TJ regulation.

Nearly 90% of malignant tumours originate from epithelial cells, which are characterized by a loss of cell polarization and altered intercellular adhesion—key factors in tumour invasion and metastasis that are directly

linked to the role of claudin proteins(170). Claudin-8 has been reported to exhibit varying expression patterns depending on the cancer type. For example, its expression is elevated in nasopharyngeal carcinoma and correlated with lymphatic metastasis, while in oral squamous cell carcinoma (OSCC), its expression is often downregulated, with high levels correlating with reduced overall survival(171). These contrasting roles suggest that Claudin-8 may play distinct roles depending on the stage and type of cancer.

To validate whether Artemisinin-induced changes in CLDN8 were consistent across different breast cancer subtypes, we cultured all breast cancer subgroups of cell lines and found that CLDN8 was expressed in all subtypes without exception. This consistency further underscores the potential of CLDN8 as a target in treating breast cancer metastasis.

Claudin-8 also shows great promise in molecularly targeted therapies. Previous research has demonstrated that Claudin-8 expression is critical for maintaining epithelial barrier function in multiple systems (143). In the respiratory system, for instance, the knockdown of Claudin-8 impaired the tight junctions, affecting the structural integrity of the epithelial barrier. These insights suggest that targeting Claudin-8 may be useful not only for modulating BBB permeability but also for restoring barrier function in conditions where epithelial integrity is compromised.

In summary, this study demonstrates that Artemisinin can modulate the expression of TJ proteins, particularly CLDN8, in endothelial cells, leading to increased BBB permeability. This modulation offers a potential mechanism for enhancing drug delivery to the brain, which is particularly relevant for treating breast cancer brain metastasis. However, further studies are needed to elucidate the precise molecular pathways involved and to validate these findings in *in vivo* models.

**Chapter IV: Investigation of CLDN8 Expression
and It's Potential Role in Breast Cancer Based on
TCGA and Cardiff Clinical Cohort Analysis**

4.1 Introduction

Tight Junctions (TJs) are structures composed of transmembrane proteins (such as claudin and occludins) and connecting proteins (such as ZO-1), which regulate selective permeability between cells and play an important role in maintaining cell polarity. The disruption of TJs is a key step in tumour cell invasion and metastasis during the progression of malignant tumours such as breast cancer. Therefore, studying the expression of TJ proteins in breast cancer and their relationship with tumour characteristics is of great significance for understanding the biological properties of breast cancer.

CLDN8, a member of the claudin family, is involved in the formation and maintenance of TJs and has attracted increasing attention in recent years. In certain types of cancer, the expression of CLDN8 is associated with cell adhesion, polarity maintenance, and tumour metastasis. However, the role of CLDN8 in breast cancer remains unclear, and systematic studies on its expression differences across various breast cancer subtypes and its relationship with clinical characteristics are lacking. This study aims to explore the expression of CLDN8 in breast cancer using data from the TCGA database and the Cardiff clinical cohort, in order to provide theoretical support for CLDN8 as a prognostic marker and potential therapeutic target for breast cancer.

In Chapter 3, we explored the regulatory effect of Artemisinin on TJ proteins, particularly CLDN8, in breast cancer and endothelial cells. RNA sequencing results showed that Artemisinin treatment significantly altered the expression of several genes related to TJs, suggesting that Artemisinin may affect breast cancer metastasis by modulating the BBB. CLDN8 was identified as one of the key targets of Artemisinin, and qPCR analysis further confirmed that CLDN8 was significantly downregulated in hCMEC/D3 cells after Artemisinin

treatment, indicating that Artemisinin may increase BBB permeability by affecting TJ structures, thereby aiding drug delivery. The consistent expression of CLDN8 across multiple breast cancer subtypes and endothelial cell lines further supports its potential as a marker for TJ integrity. In breast cancer cells, the expression of CLDN8 is not affected by subtype, indicating that it may have a fundamental role in maintaining cell polarity and adhesion.

Through large-scale transcriptome data from the TCGA database, we systematically analysed the mRNA expression of CLDN8 in breast cancer and normal breast tissue and compared its expression among different breast cancer subtypes. In addition, through the analysis of samples from the Cardiff clinical cohort, we further examined the protein expression levels of CLDN8 in breast cancer patients and its relationship with tumour grade, TNM stage, and patient prognosis. By combining data from these two sources, this study attempts to comprehensively reveal the role of CLDN8 in the clinical expression of breast cancer, particularly its specific expression characteristics in different breast cancer subtypes and its potential impact on treatment response.

4.2 Materials and Methods

4.2.1 Tissue cohort.

As previously documented (172), we used a freshly frozen cohort of breast cancer tissues, comprising both tumour and adjacent normal mammary tissues. Written informed consent was obtained from all patients before participation, and the study received ethical approval from the Bro Taf Health Authority (ethics approval No. 01/4303 and 01/4046). Following surgical procedures, patients were monitored in a follow-up study with a median follow-up duration of 120 months.

4.2.2 Immunohistochemistry (IHC) Analysis

The breast cancer tissue microarray slides BR1503f (<https://tissuearray.com>) was used in this project. Immunohistochemistry (IHC) was performed as previously described. The TMA slide was dewaxed in xylene and rehydrated in a graded series of ethanol/distilled water. Heat-induced antigen retrieval was performed in citrate buffer (pH 6.0) for 20 min in a microwave. After cooling, the slides were blocked in PBS containing 5% horse serum for 2 h at RT.

The sections were then incubated overnight at 4 °C with a primary antibody against CLDN8 (1:200; Abcam, ab211439). After washing thoroughly in PBS, the staining protocol proceeded using the Vectastain Universal Elite ABC Kit (cat no. PK-6200; Vectastain Universal Elite ABC kit, Vector Laboratories, Inc, Newark, USA.) following the manufacturer's protocol. Briefly, using the reagent from the kit, sections were incubated for 30 min with biotinylated secondary antibody, washed with PBS, and then incubated at room temperature for 30 min with ABC tertiary reagent. The staining was then developed using 3,3'-Diaminobenzidine (DAB) substrate for 10 minutes. Following a brief wash in tap water, the slide was counterstained with Gill's haematoxylin, then washed in tap water, dehydrated in a graded series of ethanol, cleared in xylene and finally mounted with DPX (Dibutyl phthalate Polystyrene Xylene).

Under a 40× objective, staining evaluation was performed based on the percentage of CLDN8-positive cells and staining intensity in 2 randomly selected fields. The proportion of positive tumour cells was categorised as follows: no positive cells (0); <25% positive cells (1); 25–50% (2); 50–75% (3); and >75% (4). The staining intensity was graded as follows: unstained (0), light brown (1), brown (2), and dark brown (3). The staining index (SI) was

calculated using the formula: $SI = \text{staining intensity} \times \text{proportion of positively stained cells}$. CLDN8 expression was evaluated using the SI-scored method, with cutoff points of ≤ 3 and > 3 . As previously reported, the staining score for CLDN8 was determined by considering the extent of tumour coverage and the proportion of positive staining.

4.2.3 Statistical Analysis

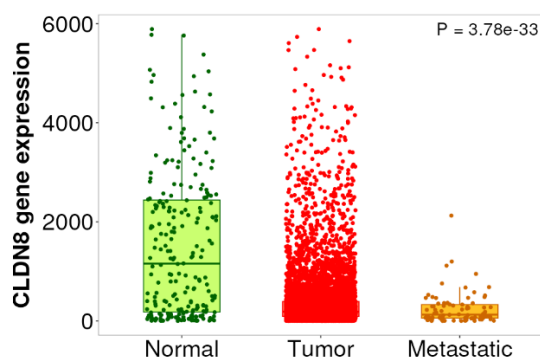
Statistical analysis was performed using SPSS software. Descriptive statistics were conducted on CLDN8 mRNA and protein expression levels, and independent t-tests were used to compare differences in expression between tumour and normal tissues. Kaplan–Meier survival analysis was used to assess the relationship between CLDN8 expression and disease-free survival (DFS) and overall survival (OS) of patients, and the log-rank test was used to compare survival curves. All tests were two-sided, with a significance level set at $p < 0.05$.

4.3 Results

4.3.1 CLDN8 mRNA Expression in Breast Cancer (TCGA Database)

The expression of CLDN8 was compared between normal breast tissues, primary tumour tissues, and metastatic tissues to assess its potential role in tumour progression. The results indicate that CLDN8 expression is significantly reduced in both tumour and metastatic tissues compared to normal tissues (Figure 4.3.1). Specifically, CLDN8 expression in normal tissues is significantly higher compared to tumour tissues ($p = 2.96e-33$) and metastatic tissues ($p = 2.61e-16$). Furthermore, metastatic tissues exhibit significantly lower CLDN8 expression compared to primary tumour tissues ($p = 1.08e-02$).

These findings suggest that the downregulation of CLDN8 is associated with the progression of breast cancer, from primary tumour development to metastatic spread. The significant decrease in CLDN8 expression in metastatic tissues compared to primary tumours further implies that CLDN8 may play a crucial role in maintaining cellular adhesion and preventing metastasis. The marked reduction in CLDN8 expression from normal to metastatic tissues highlights its potential as a biomarker for breast cancer progression and metastatic risk.



	Normal-Tumor	Normal-Metastatic	Tumor-Metastatic
Dunn.test.P	2.96e-33	2.61e-16	1.08e-02

Figure 4.3.1 CLDN8 expression in normal, tumour, and metastatic breast tissues (TCGA database). CLDN8 is highest in normal tissues, with significant reductions in tumour and metastatic tissues ($p = 3.78e-33$). (Figure from [TNMplot](#))

4.3.2 Correlation of CLDN8 Expression with Clinicopathological Factors

CLDN8 expression quantified by qPCR and normalised to ACTB (CLDN8/ACTB) was evaluated against key clinicopathological variables (Table 4.3.2). The overall tumour cohort comprised 127 patients, with 33 normal tissues included as a non-tumour reference. Analyses were performed per patient: where upstream sampling had multiple TMA cores, values were averaged to a single per-patient measure; non-evaluable samples (loss/damage/no tumour) were excluded. Because data completeness differed across variables, denominators vary by section and are reported explicitly below—this explains why the TNM analyses include 121 patients, whereas prognosis analyses include 122 patients.

Across Nottingham Prognostic Index (NPI; total N = 122) strata, CLDN8/ACTB showed distributional differences (NPI 1, n = 68: 1,711,548 ± 787,236; NPI 2, n = 38: 595,577 ± 365,831; NPI 3, n = 16: 3,789,543 ± 3,783,313). Although lower CLDN8 tended to align with poorer NPI, the Good vs Poor contrast did not reach significance (p = 0.60). In the histological grade analysis (total N = 125), CLDN8 decreased with increasing grade (G1, n = 24: 2,384,515 ± 1,565,553; G2, n = 43: 2,024,130 ± 1,075,842; G3, n = 58: 1,236,049 ± 1,112,698), but pairwise G3 vs G1 was not significant (p = 0.55). For TNM stage (total N = 121), lower CLDN8 was associated with advanced disease: Stage 2 (n = 40: 147,915 ± 79,628) and Stage 4 (n = 4: 1,528 ± 865) were both significantly lower than Stage 1 (n = 70: 1,847,370 ± 745,199) (p = 0.028 and p = 0.017, respectively). A binary

summary likewise showed Early (TNM1) n = 70: $1,847,370 \pm 745,199$ versus Late (TNM2/3/4) n = 51: $1,527,451 \pm 1,417,314$. With respect to clinical outcomes (total with follow-up N = 122), patients who developed metastasis (n = 7) had markedly lower CLDN8 (69.9 ± 69.7) than disease-free patients (n = 90: $1,362,493 \pm 555,523$; p = 0.017), whereas differences were not significant for local recurrence (n = 5: $480,948 \pm 480,824$) or breast-cancer-specific death (n = 16: $3,888,853 \pm 3,776,552$). Figure 4.3.1 visualises subgroup distributions as mean \pm SEM with individual patient points, and Table 4.3.2 reports exact n/N denominators alongside mean \pm SD to ensure internal consistency.

Suggested table footnote: "Overall qPCR tumour cohort N = 127; normal tissues N = 33. TNM analyses: N = 121 (complete TNM available). Prognosis analyses: N = 122 (follow-up/outcome available). Denominator differences reflect variable-specific missingness. CLDN8 values are qPCR CLDN8/ACTB; multiple cores per patient were averaged; non-evaluable samples were excluded."

Table 4.3.2.

Clinical samples	N	Actin (mean \pm SD)	P-value*
NPI			
Good	68	1711548 \pm 787236	-
Moderate	38	595577 \pm 365831	0.2 ^a
Poor	16	3789543 \pm 3783313	0.6 ^a
Grade			
1	24	2384515 \pm 1565553	-
2	43	2024130 \pm 1075842	0.85 ^b
3	58	1236049 \pm 1112698	0.55 ^b
TNM			
1	70	1847370 \pm 745199	-
2	40	147915 \pm 79628	0.028 ^c
3	7	8114627 \pm 8106883	-
4	4	1528 \pm 865	0.017 ^c
Clinical outcome			
Disease free	90	1362493 \pm 555523	-
Metastasis	7	69.9 \pm 69.7	0.017 ^d
Local recurrence	5	480948 \pm 480824	0.25 ^d
Died of BrCa	16	3888853 \pm 3776552	0.52 ^d
All BrCa Incidence	28	2410280 \pm 2265834	0.66 ^d

Note: p-values are compared as follows — (a) NPI group: to the Good group, (b) GRADE group: to Grade 1, (c) TNM group: to TNM 1, and (d) Clinical outcome group: to Disease free.

4.3.3 CLDN8 Expression and Patient Prognosis

Data from the Cardiff cohort were used to investigate the prognostic significance of CLDN8 expression in breast cancer. As shown in Figure 4.3.3, a total of 102 cases were included in the analysis. CLDN8 expression levels were categorized into high and low groups based on the median expression value within the cohort. Samples with expression levels above the median were classified as the high-expression group (n = 67), while those below the median were classified as the low-expression group (n = 35).

Higher expression levels of CLDN8 were significantly correlated with improved disease-free survival (DFS), as indicated by a hazard ratio of 0.443 and a p-value of 0.027 (Figure 4.3.3A). This association was notably pronounced in oestrogen receptor negative (ER (-)) patients, where high CLDN8 expression was markedly linked to better DFS outcomes (p = 0.007) (Figure 4.3.3B). Conversely, in the context of human epidermal growth factor receptor 2 (HER2) status, CLDN8 expression did not demonstrate a significant prognostic value for DFS among HER2(-) patients (p = 0.316) (Figure 4.3.3C), suggesting its predictive capacity may not extend to this subgroup. Furthermore, our analysis did not reveal a significant association between CLDN8 levels and overall survival (OS) in the studied cohort (p = 0.274) (Figure 4.3.3D), nor did it substantiate the role of CLDN8 as a determinant of DFS in either ER (+) (p = 0.432) (Figure 4.3.3E) or HER2(+) (p = 0.349) (Figure 4.3.3F) breast cancer patients. These patterns persisted upon further stratification, with CLDN8 expression not serving as a significant predictor of DFS in patients with triple-negative breast cancer (p = 0.55) (Figure 4.3.3G), ER(-)/HER2(+) (p = 0.719) (Figure 4.3.3H), or ER(+)/HER2(-) (p = 0.463) (Figure 4.3.3I). Collectively, these findings underscore the potential of CLDN8 as a marker of favourable prognosis in ER (-) breast cancer, while also

highlighting the complexity of its role across various breast cancer subtypes, thus necessitating additional research to elucidate its clinical utility.

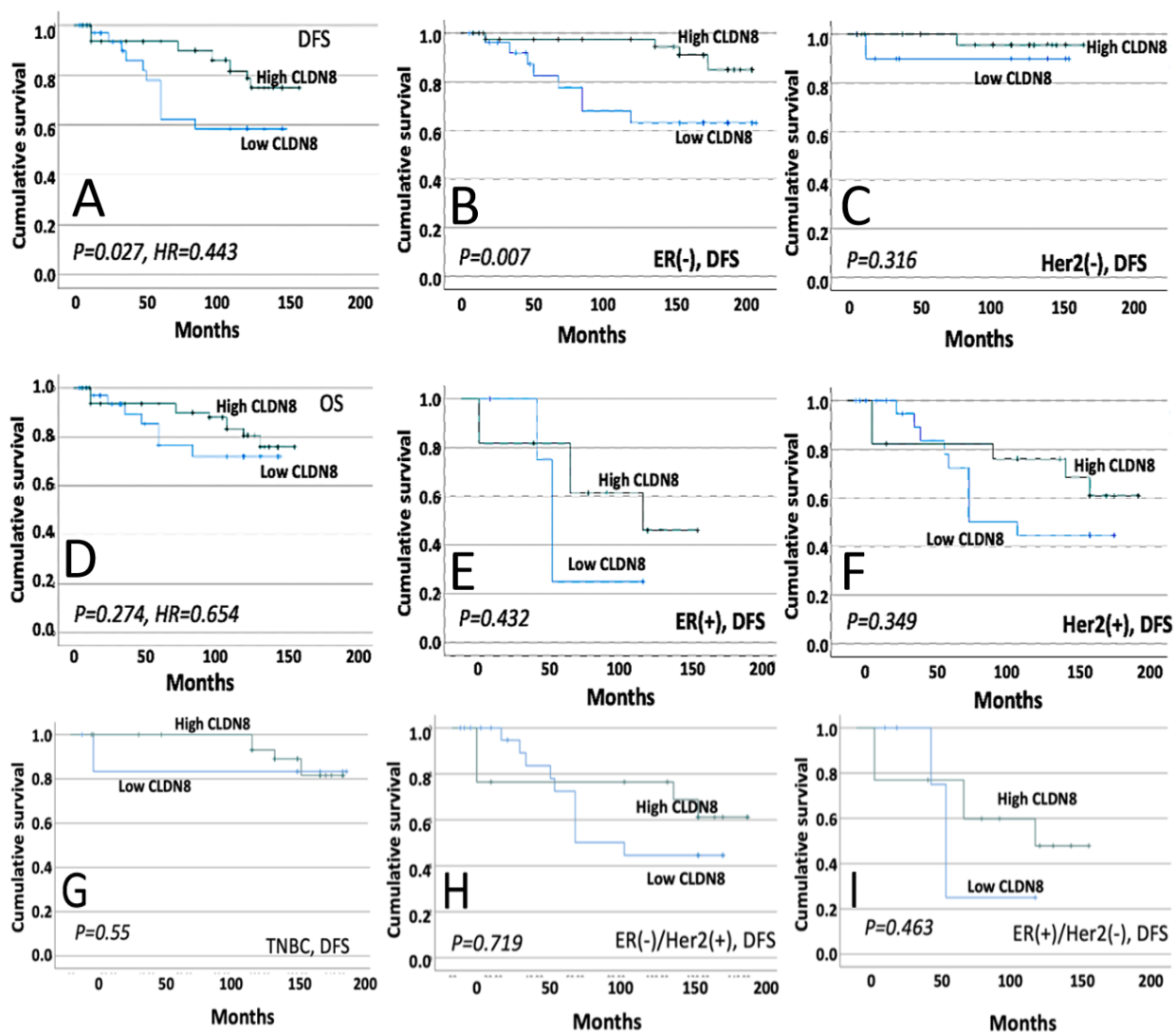


Figure 4.3.3: Survival analyses of CLDN8 (median cut-off), DFS in High vs. Low CLDN8 Levels (A); ER(-) Patient DFS with CLDN8 Levels (B); HER2(-) Patient DFS with CLDN8 Levels (C); OS in High vs. Low CLDN8 Levels (D); ER(+) Patient DFS with CLDN8 Levels (E); HER2(+) Patient DFS with CLDN8 Levels (F); TNBC Patient DFS with CLDN8 Levels (G); ER(-)/HER2(+) Patient DFS with CLDN8 Levels (H); ER(+)/HER2(-) Patient DFS with CLDN8 Levels (I). "DFS" stands for Disease-Free Survival, "OS" stands for Overall Survival, "ER" refers to Estrogenic Receptor status, "HER2" refers to Human Epidermal growth factor Receptor 2 status, and "TNBC" stands for Triple-Negative Breast Cancer.

4.3.4 CLDN8 and Hormone Receptor Status

The correlation between CLDN8 expression levels and hormone receptor status, specifically oestrogen receptor (ER) and HER2, was further examined using data from the TCGA database. As illustrated in Figure 4.3.4, significant differences in CLDN8 expression were observed between ER-positive and ER-negative breast cancer samples. Notably, ER-negative tumours displayed significantly higher CLDN8 expression compared to ER-positive tumours ($p < 0.0001$, Figure 4.3.4B). Conversely, no significant difference in CLDN8 expression was identified when comparing HER2-positive and HER2-negative tumour samples ($p = 0.6955$, Figure 4.3.4A).

These findings indicate that CLDN8 expression is particularly relevant in the context of ER status, suggesting its potential as an informative marker predominantly associated with ER-negative breast cancer subtypes, whereas its relevance appears limited regarding HER2 status.

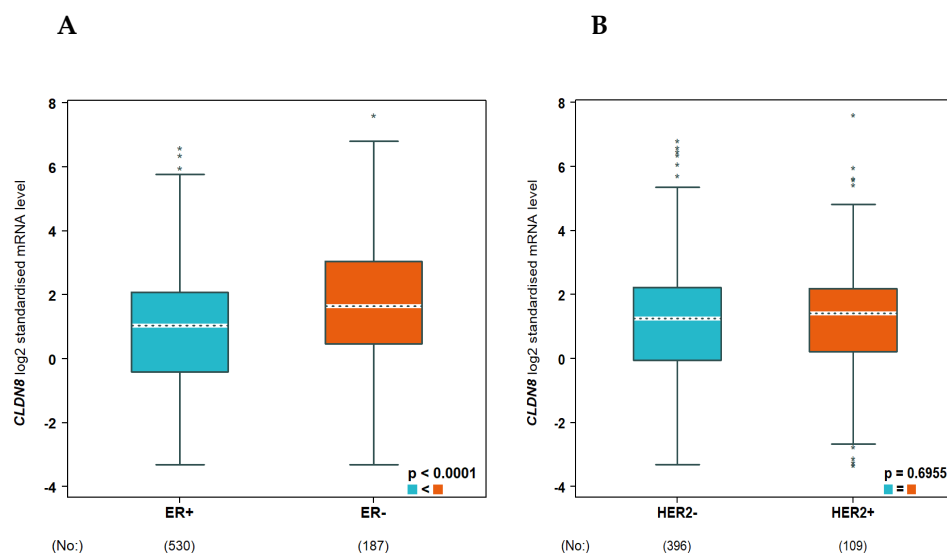


Figure 4.3.4 (A) CLDN8 expression in HER2-negative vs. HER2-positive breast cancer samples. (B) ER-positive vs. ER-negative breast cancer samples.

4.3.5 CLDN8 Protein Expression in Different Breast Cancer Subtypes (IHC Analysis)

IHC analysis demonstrated distinct alterations in CLDN8 expression across different histological grades of breast cancer (Figure 4.3.5A). In normal breast tissue, CLDN8 was primarily localised to the cell membrane of ductal epithelial cells, with mild cytoplasmic staining. In Grade 1 tumours, CLDN8 expression was enhanced, predominantly membrane-localised, but with increased cytoplasmic staining, indicating partial disruption of normal tight junction functionality. As the tumour grade progressed, CLDN8 expression became more diffuse. In Grade 2 tumours, there was a noticeable shift towards cytoplasmic staining with reduced membrane localisation, suggesting a loss of cell-cell adhesion integrity. In Grade 3 tumours, CLDN8 expression was significantly reduced, exhibiting a homogeneous staining pattern with minimal membrane localisation, further indicating the loss of barrier function in high-grade breast cancer. These findings suggest that CLDN8 undergoes a marked transition from membrane localisation in normal ducts to diffuse cytoplasmic expression in high-grade tumours, with substantial reduction in Grade 3 cancers.

To further investigate the role of CLDN8 in tumour progression, IHC staining was analysed across different TNM stages (Figure 4.3.5B). In early-stage tumours (T1), CLDN8 was primarily localised to the cell membrane with observable cytoplasmic staining, maintaining high expression levels and indicating partial preservation of tight junction function. As the tumour advanced to T2, membrane localisation weakened, and cytoplasmic staining became more prominent, suggesting a decline in cell-cell junction integrity. In T3 tumours, CLDN8 expression intensity decreased further, with heterogeneous staining patterns and a shift towards cytoplasmic expression,

indicating progressive functional loss. By T4, CLDN8 expression was significantly diminished, with almost no membrane localisation and only faint cytoplasmic staining in a few cells. These results suggest that as tumours progress to higher TNM stages, CLDN8 expression declines, potentially contributing to increased invasiveness and tumour aggressiveness.

CLDN8 expression was also assessed in different molecular sub-types of breast cancer, including ER-positive (ER+), HER2-positive (HER2+), ER+/HER2+ double-positive, and triple-negative breast cancer (TNBC) (Figure 4.3.5C). In ER+ breast cancer, CLDN8 was primarily membrane-localised with moderate cytoplasmic staining, indicating retained tight junction function. In ER+/HER2+ tumours, membrane localisation was preserved, but cytoplasmic staining increased, suggesting a potential influence of HER2-related signalling on CLDN8 distribution. In HER2+ tumours, CLDN8 expression was reduced, exhibiting a more diffuse staining pattern with diminished membrane localisation, implying that HER2 signalling may promote CLDN8 downregulation or functional alteration. TNBC showed the lowest CLDN8 expression levels, with almost no membrane staining and weak or absent cytoplasmic staining, indicating a further loss of function. The stark contrast in CLDN8 expression.

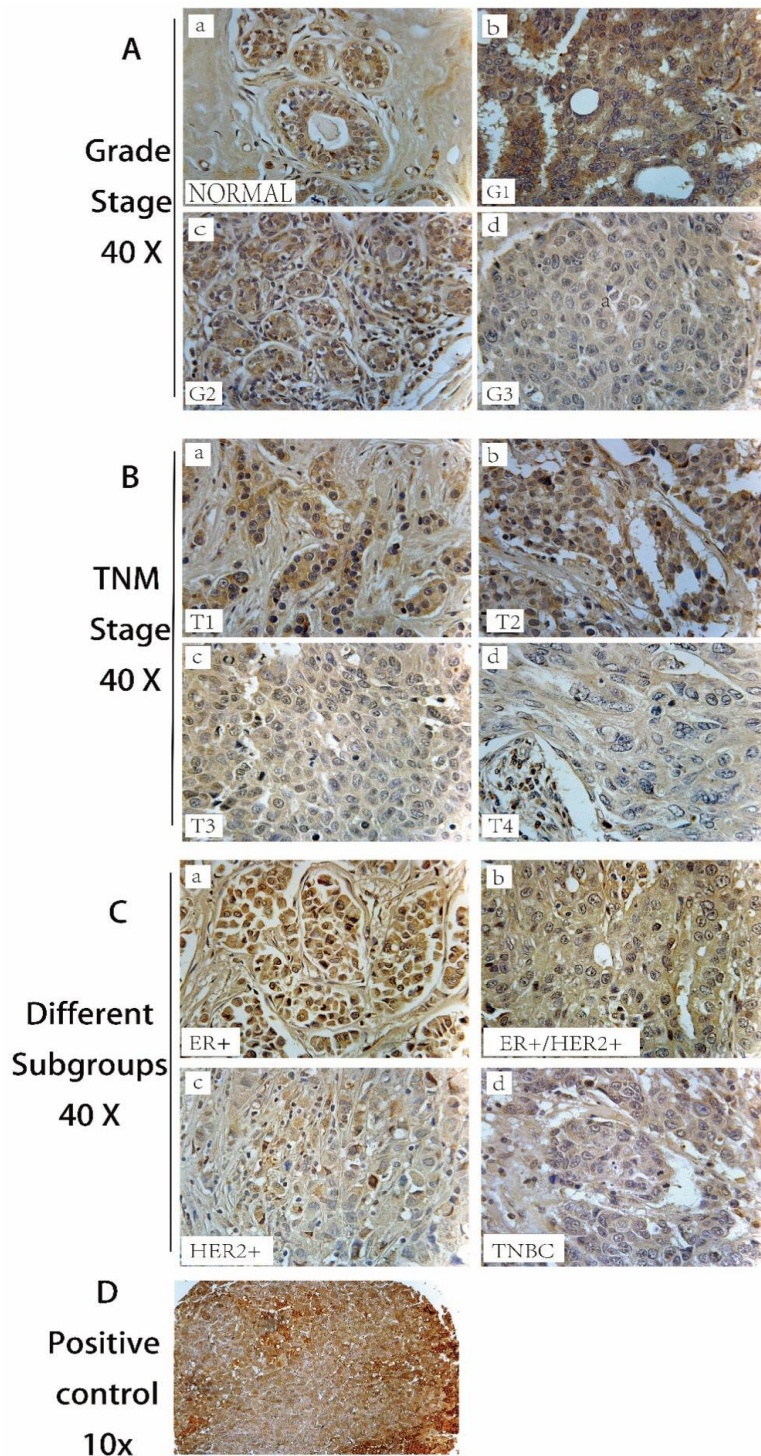


Figure 4.3.5 Immunohistochemical (IHC) staining of CLDN8 expression in breast cancer tissues. (A) CLDN8 expression in normal breast tissue and different histological grades of breast cancer. (a) Normal breast tissue, (b) Grade 1 (G1), (c) Grade 2 (G2), (d) Grade 3 (G3). (B) CLDN8 expression in different TNM stages of breast cancer. (a) T1, (b) T2, (c) T3, (d) T4. (C) CLDN8 expression in different breast cancer subtypes. (a) ER+ (oestrogen receptor-positive), (b) ER+/HER2+ (double positive), (c) HER2+ (HER2-positive), (d) TNBC (triple-negative breast cancer). (D) Positive control image at 10× magnification.

Table 4.3.5. Statistical Analysis of CLDN8 Expression Across Breast Cancer Grades, TNM Stages, and Molecular Subtypes

	Total Cases	Intensity				Statistical significance	
		0	1	2	3	Chi-square	p value
Entire cohort							
Adjacent normal breast tissue	6	0 (0%)	1 (16.67%)	3(50%)	2 (33.33%)		
Tumour	144	33 (22.9%)	65 (44.8%)	30 (20.8%)	10 (7%)		
Pathology type							
Invasive ductal carcinoma	116	28 (24%)	49 (42%)	29 (25%)	10 (9%)		
Intraductal carcinoma	14	5 (42%)	7 (58%)	0 (0%)	0 (0%)		
Fibroadenoma	6	0 (0%)	5 (83%)	1 (17%)	0 (0%)		
Grade							
Grade1	8	0 (0%)	2 (25%)	5 (62.5%)	1 (12.5%)		
Grade2	80	11 (13.8%)	48 (60%)	18 (22.5%)	5 (6.3%)	7.69	0.053 ^a
Grade3	28	11 (39.3%)	10 (35.7%)	4 (14.3%)	1 (4%)	9.61	0.022 ^a
T stage							
T1	6	2 (33%)	2 (33%)	2 (33%)	0 (0%)		
T2	72	6 (8.3%)	44 (61.1%)	19(26.4%)	5 (6.9%)		

T3	26	16 (61.5%)	5 (19.2%)	4 (15.3%)	1 (3.8%)	32.48	4.15E-07 ^b
T4	16	0 (0%)	11 (68.8%)	4 (25%)	1 (6.2%)		
Subtypes							
ER+	46	10(21.7%)	12(26.1%)	17(36.7%)	7(15.2%)	2.73	0.43
HER2+	29	9(31.0%)	12(41.4%)	7(24.1%)	1(3.4%)	9.02	0.03 ^c
TN	25	6(24%)	11(44%)	8(32%)	0(0%)	11.15	0.01 ^c
ER+/HER2+	13	2(15.4%)	3(23%)	6(46.1%)	2(15.4%)	1.64	0.65 ^c

Note: ^a Compared with Grade1 group; ^b Compared with T2 group; ^c Compared with Adjacent normal group

4.3.6 Expression of CLDN8 in Brain Metastatic Tissues from Tumours with Different Pathological Grades (IHC Analysis)

To investigate changes in CLDN8 protein expression in brain metastatic tissues derived from tumours of varying pathological grades, immunohistochemistry (IHC) was performed on a tissue microarray consisting of 86 brain metastasis samples, including cerebral cortex (n = 80) and cerebellum (n = 6) tissues.

As illustrated in Figure 4.3.6, CLDN8 expression was clearly related to the pathological grade of the primary tumour. Grade 1 metastatic tumour tissues displayed relatively high levels of CLDN8 expression, with 50% showing moderate (intensity level 2) to strong (intensity level 3) staining (Figure 4.3.6A). In Grade 2 tumours, there was an increase in the proportion of moderate staining (66.7%), accompanied by distinct membrane staining (Figure 4.3.6B). However, Grade 3 tumours showed a marked decrease in CLDN8 expression; 40% exhibited no detectable staining (intensity level 0), and only 23.3% retained moderate-to-strong expression (Figure 4.3.6C). Statistical analysis confirmed a significant reduction in CLDN8 expression between Grade 3 tumours and Grade 1 or Grade 2 tumours (Chi-square = 16.15, P = 0.00106), reinforcing the observation that higher tumour grade is associated with diminished CLDN8 expression in cerebral metastases.

Although limited by sample size (n = 6), cerebellar metastatic tumours exhibited consistent moderate CLDN8 staining, with most samples (66.7%) demonstrating uniform expression without strong staining or complete absence. Overall, these findings suggest a negative correlation between CLDN8 expression and primary tumour grade in brain metastatic tissues, supporting CLDN8's potential as a marker for evaluating tumour aggressiveness and invasiveness.

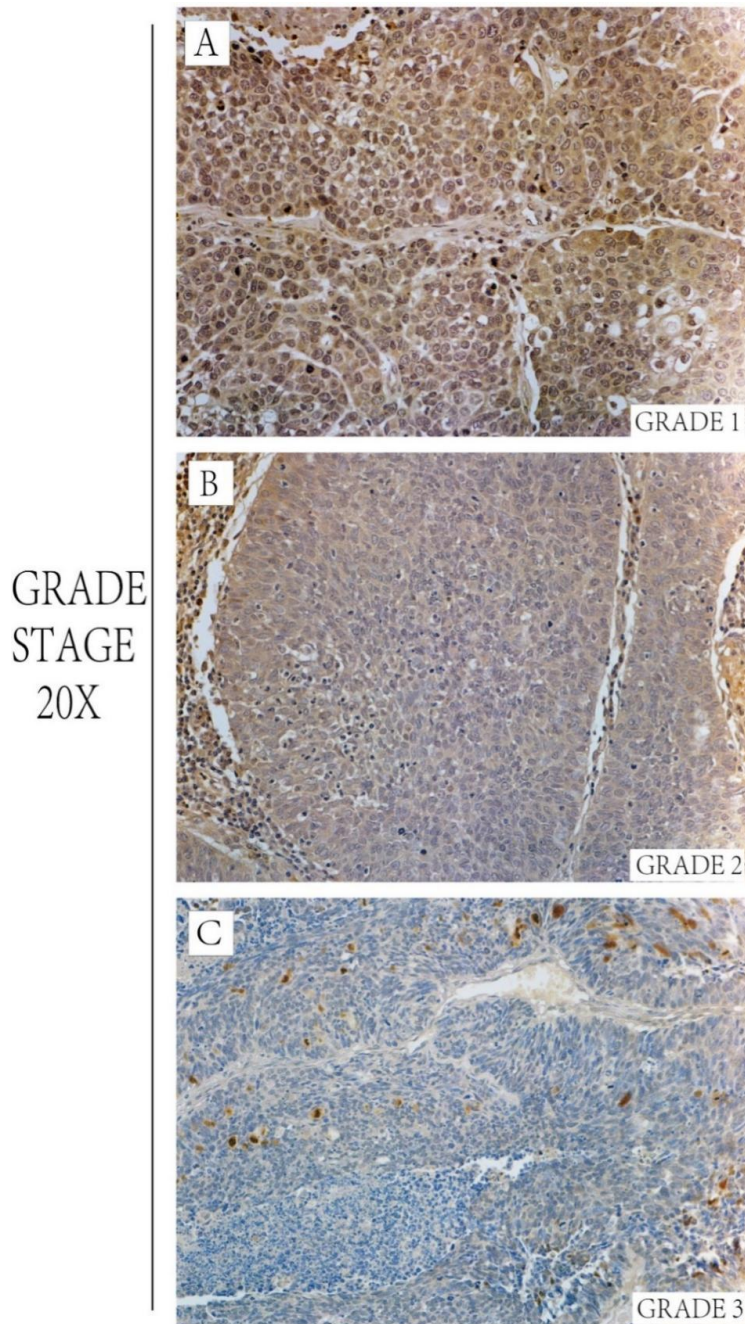


Figure 4.3.6 Immunohistochemical (IHC) staining illustrating CLDN8 protein expression in brain metastatic tissues originating from tumours of different pathological grades. (A) Grade 1 tumours exhibit relatively high CLDN8 expression, with noticeable moderate-to-strong staining intensity. (B) Grade 2 tumours demonstrate primarily moderate CLDN8 staining, with evident membrane localization. (C) Grade 3 tumours show significantly reduced CLDN8 expression, with weaker or absent staining. Magnification: 20X.

Table 4.3.6. Statistical Analysis of CLDN8 Expression in Brain Across Cancer Grades

	Total Cases	Intensity				Statistical significance	
		0	1	2	3	Chi-square	p value
Entire cohort							
Cerebrum	80	17 (21.25%)	28 (35.0%)	27 (33.75%)	8 (10.0%)		
Cerebellum	6	0 (0.0%)	2 (33.3%)	4 (66.7%)	0 (0.0%)		
Grade							
Grade1	2	0 (0.0%)	0 (0.0%)	1 (50.0%)	1 (50.0%)		
Grade2	12	0 (0.0%)	2 (16.7%)	8 (66.7%)	2 (16.7%)		
Grade3	30	12 (40.0%)	11 (36.7%)	6 (20.0%)	1 (3.3%)	16.15	0.00106

Note: Compared with Grade1+ Grade2 group.

4.4 Discussion

In this chapter, we systematically profiled Claudin-8 (CLDN8) in primary breast tumours and matched brain metastases using TCGA data, the Cardiff clinical cohort (qPCR), and IHC. Across these datasets, we found that CLDN8 carries clear clinical relevance—tracking with tumour grade, TNM stage and prognosis—and pointing to mechanistic links between CLDN8 loss in breast cancer and its brain metastatic counterparts. IHC analysis showed a stepwise decrease of CLDN8 from early to advanced TNM stages and from low- to high-grade tumours, consistent with reports that tight-junction claudins decline with EMT features and metastatic potential as epithelial polarity/adhesion is lost. In keeping with this biology, brain metastases displayed lower CLDN8 than their primaries, suggesting that weakened tight-junction architecture may facilitate dissemination and colonisation at distant sites. We also noted subtype-related differences—particularly lower CLDN8 in TNBC—compatible with the “claudin-low/mesenchymal-like” phenotype described for this subtype. Within the brain, cerebrum metastases showed greater heterogeneity than cerebellar lesions (which tended toward more uniform moderate staining), hinting at region-specific selective pressures during metastatic outgrowth.

These patterns broadly agree with prior IHC literature. In a 142-case primary-tumour series, Zhang et al. reported down-regulation of CLDN8 versus adjacent normal tissue and higher CLDN8 in tumours with favourable clinicopathology (N0, ER/PR positivity, low Ki-67), which mirrors the direction

of effect in our cohort (lower CLDN8 accompanying more aggressive features and poorer outcomes)(173). Two differences are noteworthy. First, scope: our analysis extends into the metastatic brain setting, documenting a further decline and site-specific variability, aspects not addressed in the primary-only comparator. Second, biomarker pairing: Zhang demonstrated a positive correlation between CLDN8 and AR and showed that CLDN8/AR co-expression associated with better OS/DFS; we did not systematically assess AR in our IHC panel, which may explain why prognostic contrasts appear stronger in their study.

Clinically, CLDN8 associated with prognostic composites such as the Nottingham Prognostic Index (NPI), supporting its use in risk stratification. Lower CLDN8 aligned with poorer outcomes, while differential expression across intrinsic subtypes adds biological context (notably lower levels in TNBC). In exploratory treatment-response analyses within our cohort, higher CLDN8 tended to accompany better outcomes in hormone-responsive disease, whereas lower CLDN8 coincided with greater sensitivity to chemotherapy and anti-HER2 regimens (hypothesis-generating and warranting validation).

We acknowledge two partial deviations from published patterns: (i) a subset of high-grade primaries retained moderate, patchy membranous CLDN8, and (ii) within-stage variability was wider than anticipated. variation: non-exclusive explanations include biological heterogeneity (intratumoural regional variation; subtype mix within stages), technical factors (antibody clone/lot,

epitope-retrieval pH/time, fixation and cold-ischaemia intervals) that modulate claudin antigenicity, scoring framework differences (our H-score cut-offs and emphasis on membranous staining while recording cytoplasmic signal) and cohort composition (TNBC proportion, prior therapy exposure, distribution of metastatic sites).

In both breast cancer tissues and brain endothelial cell samples derived from patients with brain metastases, Claudin-8 (CLDN8) staining was not strictly confined to the plasma membrane but also appeared within the cytoplasm. Although CLDN8 is a membrane-associated tight junction protein, this altered localization pattern is likely biologically relevant rather than a technical artefact. In metastatic breast cancer tissues, loss of epithelial polarity and tight junction disassembly during tumour progression can lead to the redistribution of CLDN8 from the membrane to the cytoplasm. Similarly, brain endothelial cells from patients with brain metastases often exhibit compromised barrier integrity and tight junction remodeling, reflecting a pathophysiological state of the blood–brain barrier (BBB). Therefore, the observed cytoplasmic or diffuse CLDN8 staining likely represents a functional disturbance of tight junctions associated with metastatic progression and BBB disruption.

In summary, convergent evidence from qPCR and IHC indicates that CLDN8 down-regulation accompanies tumour progression and metastasis, reinforces the mechanistic link between tight-junction integrity and metastatic behaviour,

and supports CLDN8 as a clinically relevant biomarker of breast cancer progression. Our data align with prior IHC studies in primaries and extend them to brain metastases. Incorporating CLDN8–AR co-expression and harmonised IHC workflows in future metastatic cohorts should refine its prognostic and potentially predictive utility.

Chapter V: Role of CLDN8 in Response to Different Breast Cancer Treatment Modalities

5.1 Introduction

In the treatment of breast cancer, the concept of personalized therapy has become increasingly important, as different breast cancer subtypes exhibit significant variability in their response to various treatment modalities. Therefore, identifying reliable biomarkers to predict treatment response and guide individualized treatment is of great clinical significance. Claudin-8 (CLDN8), a tight junction protein, plays an essential role in maintaining cell adhesion and polarity, and its expression in breast cancer has been closely linked to tumour progression and aggressiveness.

In previous chapters, we found that CLDN8 expression significantly decreases with increasing tumour stage and grade, suggesting that CLDN8 may play an important role in inhibiting tumour progression and maintaining cell differentiation. However, the specific role of CLDN8 in different breast cancer subtypes and its impact on treatment response remain poorly understood. Given the importance of CLDN8 in regulating tight junctions, cell adhesion, and barrier function, we hypothesize that CLDN8 may play a key role in determining breast cancer treatment responses, and its expression levels may influence the efficacy of different treatments, such as endocrine therapy, chemotherapy, and targeted therapy.

This chapter aims to explore the role of CLDN8 in breast cancer treatment, particularly how CLDN8 expression levels affect the response to endocrine therapy, chemotherapy, and targeted therapy in different breast cancer subtypes. By integrating clinical data and *in vitro* experiments, we aim to determine whether CLDN8 can serve as a biomarker for predicting treatment response and whether targeting CLDN8 can improve treatment outcomes for breast cancer patients. This study not only provides theoretical support for CLDN8 as a potential therapeutic target but also helps develop more effective

personalized treatment strategies to improve the prognosis of breast cancer patients.

5.2 Materials and Methods

5.2.1 Cell Lines and Culture Conditions

The cell lines utilised in this study were obtained from the American Type Culture Collection (ATCC) (LGC standard, England), comprising four human breast cancer cell lines: MDA-MB--231, MDA-MB--361, MCF-7, and SKBR-3. MDA-MB--231 and MCF-7 were cultured in Dulbecco's Modified Eagle Medium (DMEM), while MDA-MB--361 and SKBR-3 were cultured in RPMI-1640 Medium. The culturing medium was supplemented with 10% foetal calf serum (FCS) (Sigma Aldrich, Dorset, UK) and 1× antimicrobial solution (Sigma-Aldrich, Dorset, UK). Cells were maintained in a controlled environment with a pH level of 7.3, 95% humidity, 5% CO₂, and a temperature of 37 °C within an incubator.

5.2.2 Drugs and Antibodies

Four chemotherapy agents—paclitaxel, docetaxel, cisplatin, and methotrexate (MTX)—along with two anti-HER2 inhibitors (Neratinib and Lapatinib) and three endocrine therapies (Tamoxifen, Fulvestrant, and Anastrozole) were obtained from Sigma-Aldrich (Dorset, UK). These compounds were initially dissolved in DMSO and subsequently diluted to the required concentrations. For protein blotting, the following antibodies were used: mouse anti-human GAPDH (SC-32233) from Santa Cruz Biotechnologies Inc. (CA, USA) and rabbit anti-human CLDN8 (710222) from Thermo Fisher (Oxford, UK).

5.2.3 Patients' response to chemotherapies and evaluation

In this study, we utilised an extensive public database containing records of breast cancer patients along with their corresponding therapeutic interventions (ROC Plotter - Online ROC analysis (accessed on 1 December 2023)). The database utilised receiver operating characteristic (ROC) curve analysis to classify patients based on their responsiveness to specific therapies. As a result, area under the curve (AUC) values, along with statistical measures of treatment sensitivity, were recorded. Additionally, gene expression levels for the selected targets were analysed, with statistical significance assessed using the Mann-Whitney U test.

5.2.4 RNA Extraction and qPCR Analysis

Total RNA was extracted from tissue samples and colorectal cancer cell lines using the TRI Reagent Kit (Merck KGaA, Darmstadt, Germany) according to the manufacturer's protocol. After isolation, RNA concentrations were adjusted to 500 ng/ μ L and reverse transcription was performed using the GoScript™ Reverse Transcription System Kit (Promega Corporation, Madison, WI, USA) in a SimpliAmp thermocycler (Fisher Scientific UK, Leicestershire, UK). The resulting cDNA was stored at -20°C until further analysis.

CLDN8 transcript expression was quantified in tissue cohorts using the Amplifluor Uniprimer™ Universal qPCR system (Intergen Inc., Oxford, UK). Forward and reverse primers were designed with a Z sequence (5' - ACTGAACCTGACCGTACA-3') to enable incorporation of the FAM-tagged Uniprimer™ probe for fluorescent detection. The primer sequences were as follows: CLDN8 forward primer - ACTGAACCTGACCGTACAAGCTACTGCTCTTTTCGTTG and Z-tagged reverse primer - ACTGAACCTGACCGTACAAGCTACTGCTCTTTTCGTTG. Internal standard GAPDH forward primer sequences used was 5'-

CTGAGTACGTCGTGGAGTCC-3' and the GAPDH ZR primer sequence was 5'-ACTGA ACCTGACCGTACAGAGATGATGACCCTTTTG-3'. Each qPCR reaction included the forward and reverse primers, cDNA from tissue samples, Uniprimer™, and 2× Precision FAST qPCR master mix (Primer Design, Eastleigh, UK). Real-time PCR was performed using a Step OnePlus™ Real-Time PCR System (Thermo Fisher Scientific, Leicestershire, UK) under the following cycling conditions: an initial denaturation step at 95 °C for 10 minutes, followed by 100 cycles of 95 °C for 10 seconds, 55 °C for 35 seconds, and 72 °C for 10 seconds. Transcript levels were quantified relative to an internal reference gene with known transcript copy numbers. A series of standard samples, ranging from 10⁸ to 10¹ copies, were included on the same qPCR plates as the test samples under identical conditions. A standard curve generated from these standards was used to determine the relative transcript copy numbers in the unknown samples.

5.2.5 Protein Extraction and Western Blotting

Sodium dodecyl sulphate-polyacrylamide gel electrophoresis (SDS-PAGE) and Western blotting were performed as follows. Proteins were extracted from cultured cells using RIPA buffer and quantified with the Bio-Rad protein quantification kit (Bio-Rad Laboratories, Hertfordshire, UK). The extracted protein samples were then mixed with 2× Laemmli sample buffer, heated at 100°C for 5 minutes, and loaded onto a 10% SDS-PAGE gel for separation. Following electrophoresis, proteins were transferred onto a pre-activated PVDF membrane using a semi-dry transfer system, with methanol treatment applied beforehand. The membrane was blocked with 10% milk to prevent non-specific binding, followed by incubation with primary antibodies targeting CLDN8 (1:500; Abcam, ab211439) and GAPDH (1:5000; SANTA CRUZ; sc-32233). After primary antibody incubation, the membrane was

treated with a horseradish peroxidase (HRP)-conjugated secondary antibody. Protein detection was carried out using EZ-ECL chemiluminescent reagent (Geneflow Ltd., Litchfield, UK).

5.2.6 *In Vitro Drug Sensitivity Assays*

Cells were seeded into 96-well plates and treated with a series of drug dilutions at a 1:10 ratio. The selected drug concentrations were based on established IC₅₀ values and prior experimental data. After a 72-hour incubation, cells were fixed with 4% formalin, stained with 0.5% crystal violet, and washed before being solubilised in 10% acetic acid. Absorbance was measured at 595 nm using a spectrophotometer to assess cell density. Drug toxicity was calculated using the formula: Percentage drug toxicity = $[(\text{Absorbance of untreated control} - \text{Absorbance of drug-treated sample}) / \text{Absorbance of untreated control}] \times 100$. Scatter plots were generated to visualise the relationship between drug concentration and toxicity, and IC₅₀ values were determined using the best-fit curve method.

5.2.7 *MTT-Based Cellular Growth Assay*

MTT-based assays were conducted to assess the impact of CLDN8 on cell proliferation. In brief, 2×10^4 cells from each cell model were plated in triplicate onto three separate 96-well plates and incubated at 37°C with 5% CO₂. On Days 1, 3, and 5, 22 µL of 5 mg/mL MTT solution (Sigma-Aldrich Co., Poole, Dorset, UK) was added to each well, followed by a 4-hour incubation at 37°C with 5% CO₂. After incubation, the medium was removed, and 100 µL of dimethyl sulfoxide (DMSO) (Sigma-Aldrich Co., Poole, Dorset, UK) was added to each well to dissolve the formazan crystals. The plates were then incubated for an additional 10 minutes at 37°C with 5% CO₂, and

absorbance was measured at 540 nm using an LT4500 plate reader (Wolf Laboratories, York, UK).

5.2.8 Statistical Analysis

Statistical analyses were conducted using SPSS software (Version 27.0; IBM Corp., New York, USA). Group comparisons were evaluated using the Kruskal Wallis test and analysis of variance (ANOVA) where applicable. The Mann-Whitney U test was used for pairwise comparisons as detailed in the text. Survival analysis was performed using the Kaplan–Meier method with log-rank testing. Cox regression modelling was applied for both univariate and multivariate analyses. Classification assessments were carried out using the Receiver Operating Characteristic (ROC) analysis. A p value of <0.05 was considered statistically significant.

5.3 Results

5.3.1 CLDN8 Expression with Breast Cancer Treatment Modalities

The analysis of Claudin-8 (CLDN8) expression across different breast cancer treatment modalities provides compelling insights into its prognostic value. In Figure 5.3.1A, we observe that in the absence of systemic treatment, higher expression of CLDN8 is associated with improved disease-free survival (DFS), with a hazard ratio (HR) of 0.73 and a statistically significant log-rank P-value. This suggests that elevated CLDN8 levels could naturally indicate a more favourable prognosis for patients not undergoing systemic therapies.

When endocrine therapies were introduced, as shown in Figure 5.3.1B, there was a positive correlation between high CLDN8 expression and increased DFS, indicating that patients with elevated CLDN8 levels are more likely to

benefit from hormone-based treatments. The HR of 0.6 and the significant p value lend strong statistical support to this association.

Figure 5.3.1C illustrates the effects of comprehensive chemotherapy treatments, where no significant difference in DFS was observed between groups with high and low CLDN8 expression, as indicated by an HR close to 1. Figure 5.3.1D, however, suggests that high CLDN8 expression may confer resistance to neoadjuvant chemotherapy, reflected by a higher HR of 1.5.

In terms of overall survival (OS), Figure 5.3.1E demonstrates that high CLDN8 expression correlates with improved outcomes in patients without systemic treatment (HR = 0.62). Figure 5.3.1F further supports this pattern in patients receiving endocrine therapy, where high CLDN8 expression is linked to better survival (HR = 0.48). On the other hand, Figure 5.1G reveals that high CLDN8 expression predicts worse OS outcomes for patients undergoing chemotherapy, with an HR of 1.55 and marginal p value significance. Lastly, Figure 5.3.1H shows no significant survival difference between high and low CLDN8 expression groups in the context of neoadjuvant chemotherapy.

Synthesizing these findings, it becomes apparent that high CLDN8 expression is predictive of favourable responses to endocrine therapies, particularly in oestrogen receptor-positive breast cancer. Patients with high CLDN8 levels tend to experience better outcomes with hormone-based treatments compared to conventional chemotherapy. Notably, while high CLDN8 expression is linked to better survival outcomes without systemic treatment or with endocrine therapies, it inversely correlates with poorer outcomes under broader chemotherapeutic strategies. However, in the context of neoadjuvant chemotherapy, the predictive value of CLDN8 is not significant, suggesting a complex interplay of CLDN8 expression with various treatment types. This analysis underscores that high CLDN8 expression signifies endocrine

sensitivity but may indicate resistance to chemotherapy, especially in pre-surgical settings. As such, CLDN8 expression could serve as a key factor in tailoring personalized treatment strategies and improving therapeutic outcomes for breast cancer patients.

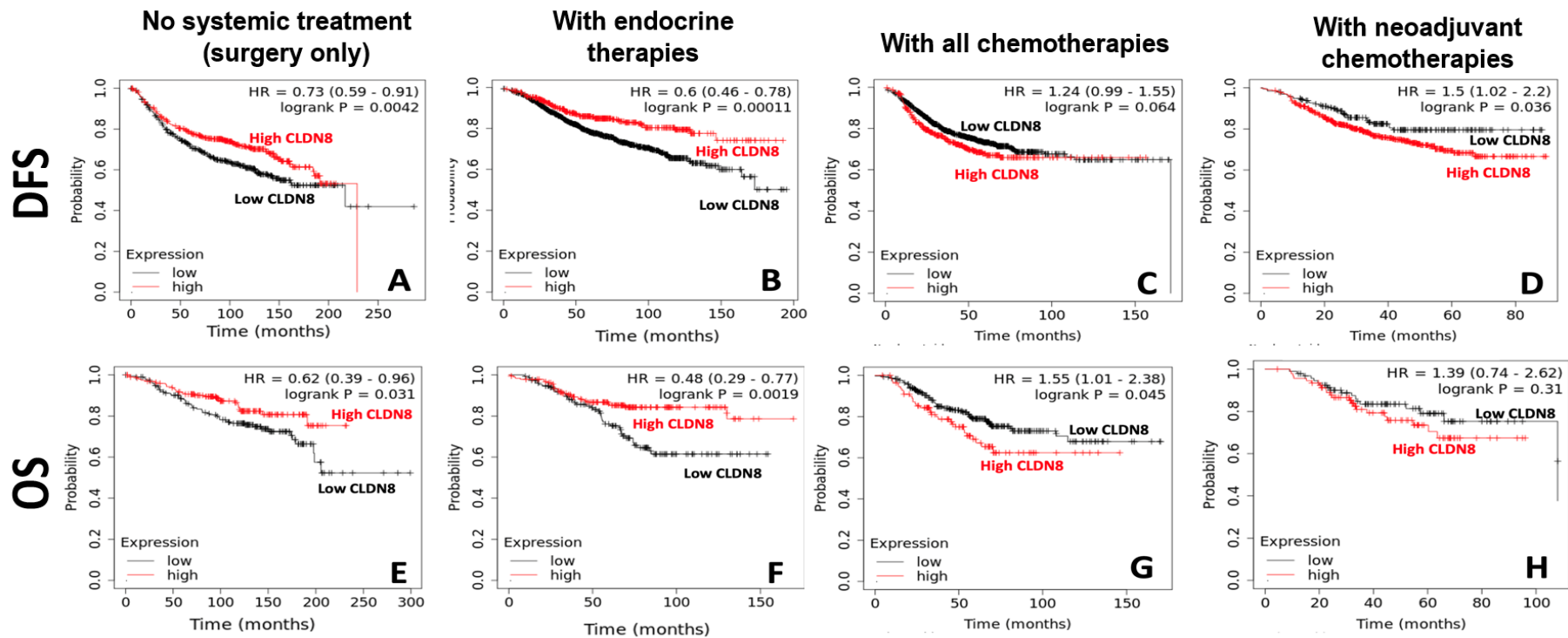
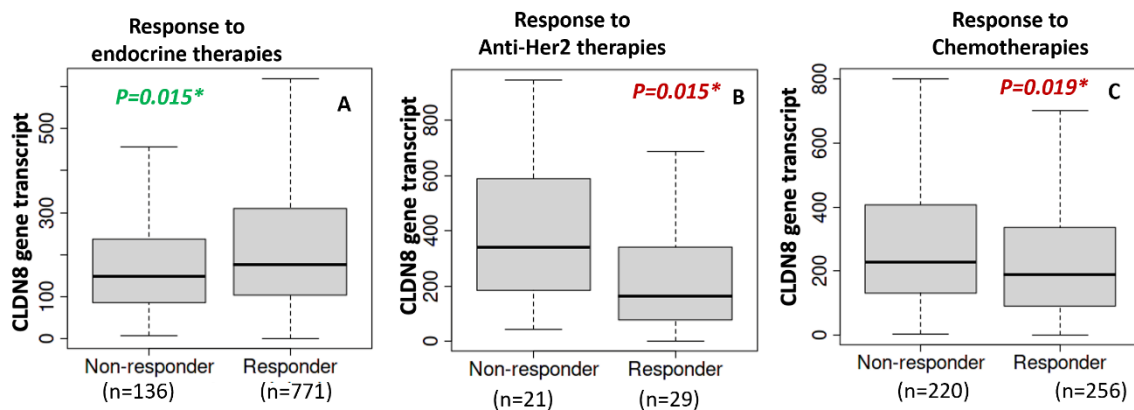


Figure 5.3.1: DFS with Surgery Only: CLDN8 Expression Impact (A); DFS with Endocrine Therapy: CLDN8 Expression Levels (B); DFS with All Chemotherapies: CLDN8 Expression Contrast (C); DFS with Neoadjuvant Chemotherapies: CLDN8 High vs. Low (D); OS with Surgery Only: High vs. Low CLDN8 Expression (E); OS with Endocrine Therapy: Impact of CLDN8 Expression (F); OS with All Chemotherapies: Comparing CLDN8 Levels (G); OS with Neoadjuvant Chemotherapies (H).

5.3.2 CLDN8 Expression and Response to Breast Cancer Treatments

The analysis of Claudin-8 (CLDN8) expression reveals a nuanced role in predicting breast cancer treatment responses. High CLDN8 expression is significantly associated with increased sensitivity to endocrine therapies, as evidenced by higher CLDN8 levels in responders ($p = 0.015$). In contrast, elevated CLDN8 levels are correlated with resistance to Anti-HER2 and chemotherapy treatments, with non-responders showing higher expression ($p = 0.015$ and $p = 0.019$, respectively). These findings suggest that patients with lower CLDN8 expression may be more responsive to Anti-HER2 and chemotherapy treatments. Therefore, CLDN8 could serve as a differential biomarker to guide personalized breast cancer therapy, helping to identify which patients may derive greater benefit from specific treatment modalities.



* By Mann-Whitney U test; based on 5-year RFS

Figure 5.3.2: (A) CLDN8 Expression in Endocrine Therapy Response; (B) CLDN8 Levels in Anti-HER2 Therapy Response; (C) CLDN8 Expression and Chemotherapy Response.

5.3.3 Validation of CLDN8 Knockdown in Breast Cancer Cell Lines

In preparation for the drug response experiments, it was essential to confirm that CLDN8 was effectively knocked down in the selected breast cancer cell lines. To this end, we utilized quantitative real-time PCR (qPCR) and Western blotting (WB) analyses to validate the efficiency of CLDN8 knockdown in four distinct breast cancer cell lines: MDA-MB-231, MDA-MB-361, SKBR3, and MCF7.

qPCR was conducted to measure CLDN8 expression at the mRNA level post-knockdown (KD). *ACTB* served as the internal control, and the $2^{-\Delta\Delta C_t}$ method was employed to determine relative gene expression changes between the wild type (WT) and KD cell lines. As shown in Figure 5.3.3A, there was a significant reduction in CLDN8 mRNA levels across all four cell lines after knockdown. Statistical analysis via an unpaired t-test confirmed the efficiency of knockdown, with * $P < 0.05$, ** $P < 0.01$, and *** $P < 0.001$ indicating varying levels of significance.

To confirm the knockdown at the protein level, Western blot analysis was performed. Protein lysates from both WT and KD variants of MDA-MB-231, MDA-MB-361, SKBR3, and MCF7 were collected. The levels of CLDN8 protein expression were assessed, with β -Actin used as a loading control to ensure accurate comparison across samples. As illustrated in Figure 5.3.3B, a marked reduction in CLDN8 protein levels was observed in the KD groups compared to the WT groups, which validated the effective reduction of CLDN8 expression.

These results, demonstrating successful knockdown of CLDN8 at both the transcriptional and translational levels, provide a solid foundation for investigating the role of CLDN8 in breast cancer treatment responses. The validation of CLDN8 knockdown sets the stage for subsequent drug

sensitivity experiments (Section 5.3.3), which will explore how CLDN8 expression influences breast cancer cells' responses to various therapeutic agents.

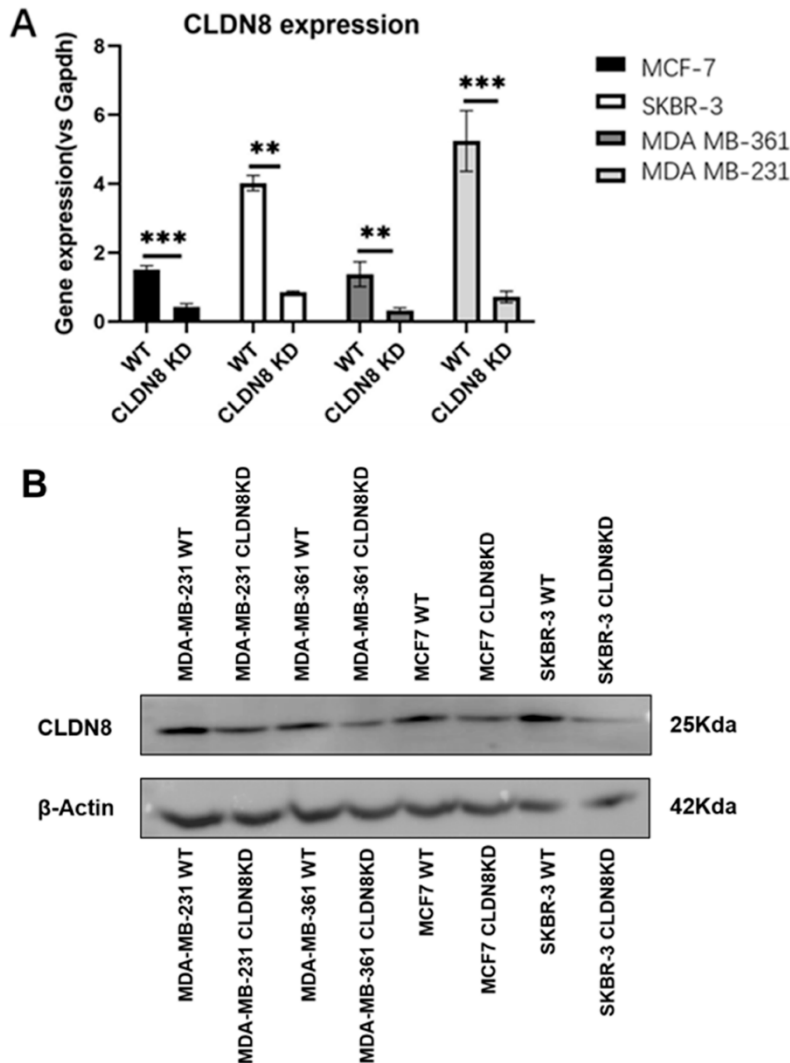


Figure 5.3.3: Expression of CLDN8 in breast cancer cell lines. (A) qPCR confirmation of KDs. Semi-quantitative analysis of the relative gene expression of CLDN8 in the four breast cancer cell lines, MDA-MB-231, MDA-MB-361, SKBR3, MCF-7. An unpaired t test was performed to statistically analyse the degree of KDs. *, $P < 0.05$, **, $P < 0.01$; ***, $P < 0.001$ (B) Western blot shows CLDN8 protein expression, respectively in WT (+) and KD (-) MDA-MB-231, MDA-MB-361 and SKBR3 cell lines. The corresponded protein expression of the housekeeping gene, β -Actin, in each cell model is also demonstrated. qPCR, quantitative real-time polymerase chain reaction; WT, wild type; KD, knockdown.

5.3.4 CLDN8 Expression and Endocrine Therapy Response in Breast Cancer

Subgroups

Upon evaluating the role of CLDN8 in the context of endocrine therapy for breast cancer, distinct differences were observed across subgroups defined by HER2 and ER status. Among HER2-negative patients, those who responded to endocrine therapy exhibited significantly higher levels of CLDN8 expression ($p = 0.015$), suggesting that CLDN8 could serve as a biomarker for treatment efficacy in this subgroup (Figure 5.3.4.1A).

Additionally, in the HER2-positive/ER-positive subgroup, a similar pattern was observed, with responders demonstrating a significant increase in CLDN8 expression levels ($p = 0.038$), further indicating the potential utility of CLDN8 as an indicator of a positive response to endocrine therapy within this patient population (Figure 5.3.4.1E)

For the luminal subtypes, specifically Luminal-A and Luminal-B, a trend of higher CLDN8 expression was observed among responders, although these findings did not reach statistical significance (Figures 5.3.4.1C and F). This trend, however, aligns with broader observations that higher CLDN8 expression may generally be associated with favourable responses to endocrine therapy.

To further validate the accuracy of clinical data, we established an *in vitro* model of breast cancer with CLDN8 knockdown and tested its response to endocrine therapies, including Tamoxifen, Fulvestrant, and Anastrozole. As shown in Figures 5.3.4.2(a), 5.3.4.3(a), and 5.3.4.4(a), no significant upward trend in IC50 values was observed for Fulvestrant in the MDA-MB-231 cell line. However, in other cell lines and with other therapeutic drugs, knocking down CLDN8 generally resulted in increased IC50 values, although some

increases were not significant. This suggests that knocking down CLDN8 may lead to increased resistance of breast cancer cells to endocrine therapy drugs, providing strong experimental evidence for further research on the role of CLDN8 in breast cancer treatment.

To further validate these findings, we conducted growth curve experiments. According to Figures 5.3.4.2(b), 5.3.4.3(b), and 5.3.4.4(b), significant differences were observed in the response of MDA-MB-361 cells to all endocrine therapy drugs before and after CLDN8 knockdown. On day five, the number of MDA-MB-361 CLDN8-knockdown cells was significantly lower than wild type (WT) ($p = 0.038$). Although other cell models did not show significant differences across all drugs, the number of CLDN8 knockdown cells still significantly increased on day five. Notably, as an ER+ breast cancer cell line, MCF7 did not show significant differences with Tamoxifen treatment, but it did show significant differences with Fulvestrant and Anastrozole, consistent with Figure 5.3.4.1D. It is also worth mentioning that SKBR3, as a HER2+ breast cancer cell line, showed significant differences only with Fulvestrant during endocrine therapy ($p = 0.098$).

These findings collectively underscore the potential of CLDN8 as a prognostic marker for responsiveness to endocrine therapy in breast cancer, particularly within HER2-positive/ER-positive cohorts. The consistent associations across multiple subgroups support the hypothesis that CLDN8 expression is indicative of treatment response and suggest that it could be leveraged to personalize therapeutic strategies for breast cancer patients.

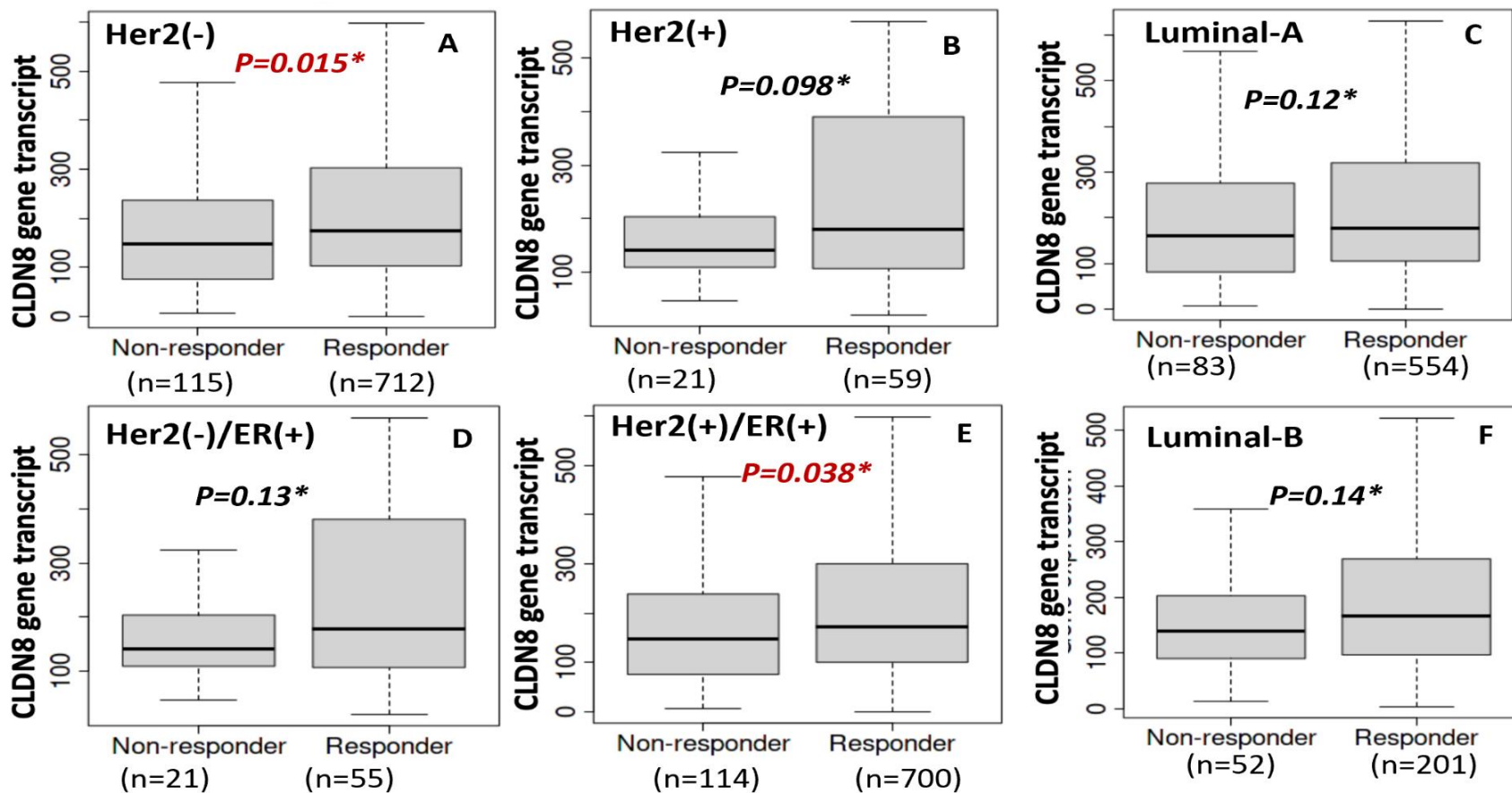


Figure 5.3.4.1: CLDN8 expression and endocrine therapy response across ER and HER2 subgroups (5-year RFS). CLDN8 expression in HER2(-) breast cancer patients (panel A), CLDN8 levels in HER2(+) patients (panel B), differential CLDN8 expression in the Luminal A subtype (panel C), CLDN8 expression in HER2(-)/ER(+) breast cancer (panel D), in HER2(+)/ER(+) breast cancer (panel E), and in Luminal B breast cancer (panel F). Data are presented as mean \pm SEM, and *p* values are indicated in each panel.

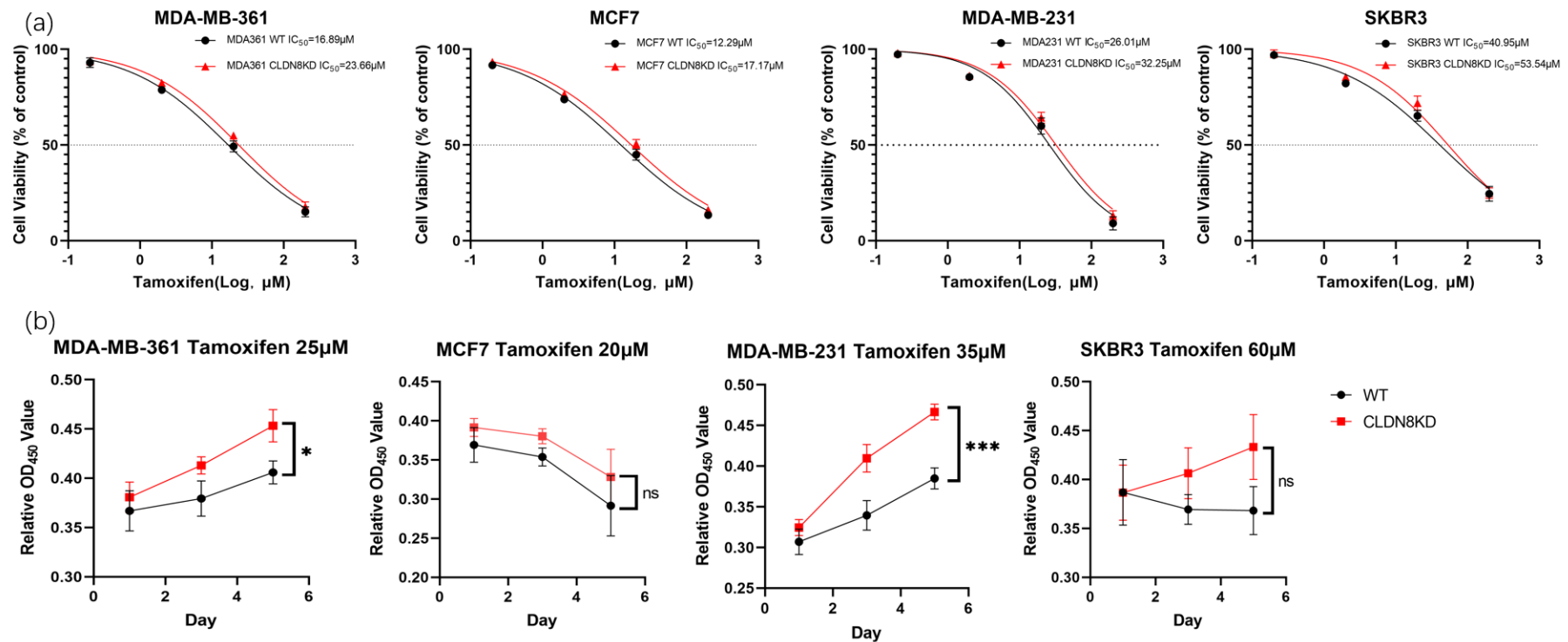


Figure 5.3.4.2: (a) Tamoxifen sensitivity tests. Both wild type (WT) and CLDN8 knockdown (CLDN8KD) cells were treated with increasing concentrations of Tamoxifen. The activity, measured as percentage viability compared to untreated controls, shows a similar dose-dependent inhibition in both WT and CLDN8KD cells across cell lines. CLDN8KD consistently shows higher IC_{50} values, indicating reduced drug sensitivity. (b) Growth assays of breast cancer cell lines treated with fixed concentrations of Tamoxifen (MDA-MB--361 at $25\mu M$, MCF7 at $20\mu M$, MDA-MB--231 at $35\mu M$, and SKBR-3 at $60\mu M$). Over a 5-day period, WT and CLDN8KD cells exhibit differential growth dynamics. In MCF7, both WT and CLDN8KD show comparable proliferative behaviour over time. Notably, in MDA-MB--231 and MDA-MB--361, a significant growth suppression is observed in WT compared to CLDN8KD cells by day 5 (***, $p < 0.001$), (*, $p < 0.05$). Data represent mean \pm SEM from $n = 3$ independent experiments/biological replicates.

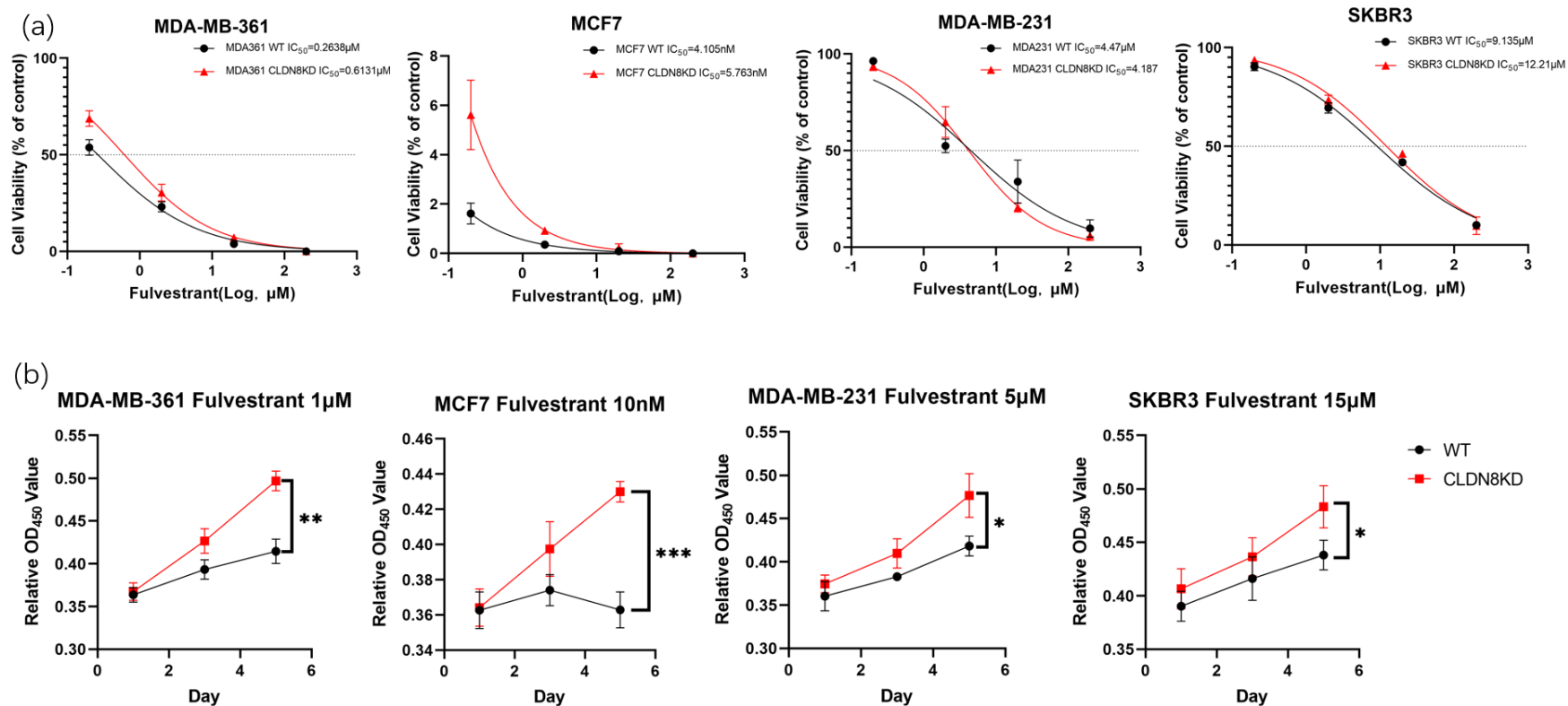


Figure 5.3.4.3: (a) Fulvestrant sensitivity tests and growth assays Dose-response curves for Fulvestrant are presented for MDA-MB-361, MCF7, MDA-MB-231, and SKBR3 cell lines. The assay compares WT and CLDN8KD variants, displaying their viability in response to escalating concentrations of Fulvestrant. Results demonstrate dose-dependent inhibition, with CLDN8KD cells exhibiting slight shifts in IC_{50} values compared to WT. (b) MDA-MB-361, MCF7, MDA-MB-231, and SKBR3 (WT and CLDN8KD) MDA-MB-361 at 1 μM , MCF7 at 10nM, MDA-MB-231 at 5 μM , and SKBR3 at 15 μM over 5 days reveal differential effects of CLDN8KD on cell proliferation. Data represent mean \pm SEM from $n = 3$ independent experiments/biological replicates.

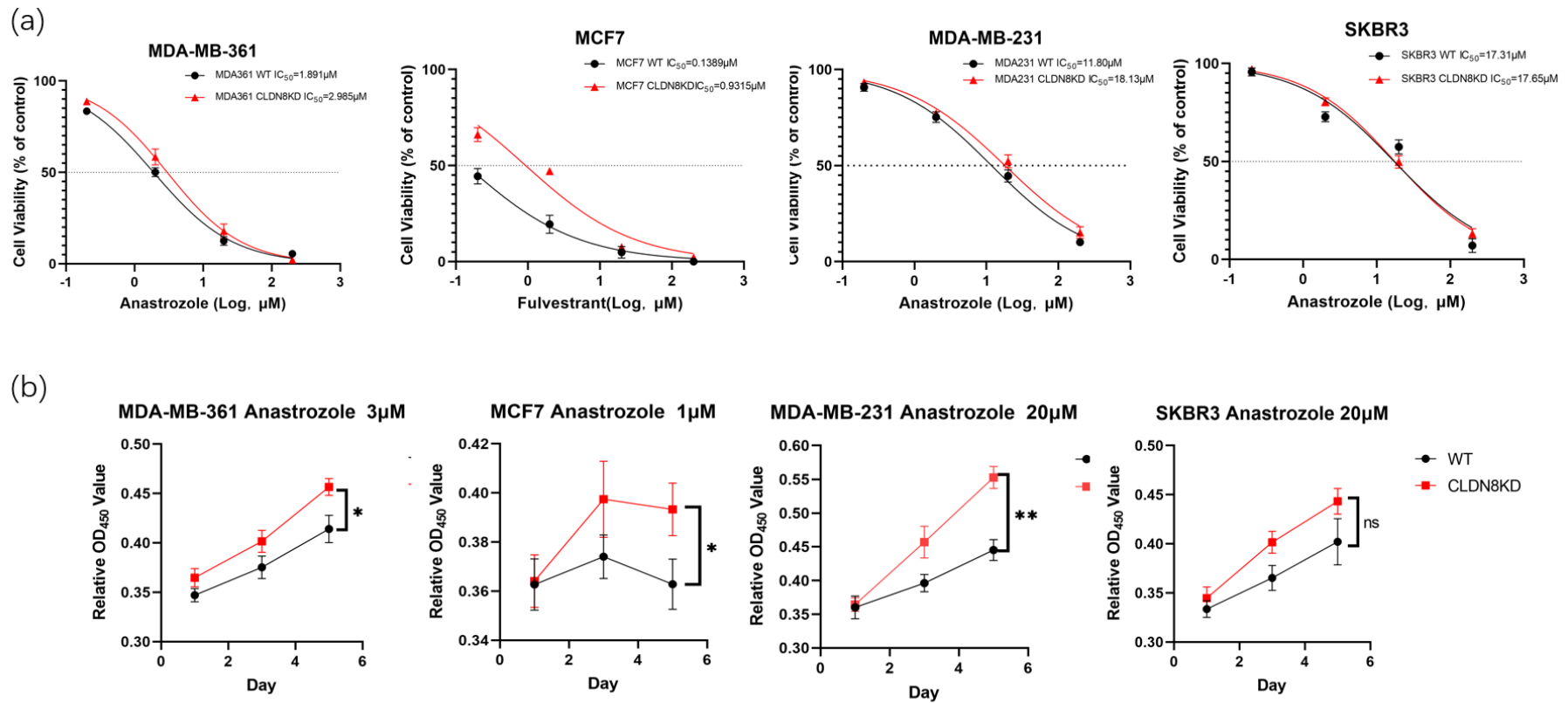


Figure 5.3.4.4: (a) Anastrozole sensitivity tests and growth assays. Anastrozole demonstrates increased efficacy compared to Fulvestrant across cell lines. Data points represent the mean \pm SEM of at least three biological replicates. CLDN8KD consistently shows higher IC₅₀ values, indicating reduced drug sensitivity. (b) MDA-MB-361, MCF7, MDA-MB-231, and SKBR3 (WT and CLDN8KD) CLDN8KD MDA-MB-361, MCF7 and MDA-MB-231 shows a significant increasing in proliferation at day 5 (*, $p < 0.05$, **, $p < 0.01$). SKBR3 cells show no significant difference between WT and CLDN8KD lines. Data represent mean \pm SEM from $n = 3$ independent experiments/biological replicates.

Table 5.3.4.1 Effect of CLDN8 Knockdown on IC50 Values of Hormone Therapy Drugs in Different Breast Cancer Cell Models

	Hormone therapy		
	Tamoxifen	Fulvestrant	Anastrozole
SKBR3 CELL MODELS			
SKBR3-WT	40.95±9.72µM	9.14±1.77µM	17.31±7.33µM
SKBR3-CLDN8KD	53.54±13.46µM	12.21±2.83µM	17.65±2.64µM
MDA-MB-361 CELL MODELS			
MDA-MB-361-WT	16.89±2.62µM	0.26±0.05µM	1.89±0.26µM
MDA-MB-361-CLDN8KD	23.66±3.35µM	0.61±0.10µM	2.99±0.42µM
MDA-MB-231 CEL MODELS			
MDA-MB-231-WT	26.01±6.12µM	4.47±2.03µM	11.80±2.42µM
MDA-MB-231-CLDN8KD	32.25±6.89µM	4.19±0.84µM	18.13±3.8µM
MCF7 CELL MODELS			
MCF7-WT	12.29±1.04µM	4.11±0.33nM	0.14±0.03µM
MCF7-CLDN8KD	17.17±2.16µM	5.76±1.26nM	0.93±0.12µM

5.3.5 CLDN8 Expression and Anti-HER2 Therapy Response in Breast Cancer

Subgroups

The analysis of Claudin-8 (CLDN8) expression across different breast cancer subtypes revealed a consistent relationship with therapeutic response to anti-HER2 therapy. Specifically, patients who responded favourably to treatment—irrespective of oestrogen receptor (ER) status—exhibited lower levels of CLDN8 expression, suggesting its potential role as a predictive biomarker for therapy efficacy.

For ER-negative patients, those who responded to anti-HER2 therapy showed significantly lower levels of CLDN8 expression ($p = 0.045$, Figure 5.3.5.1A). A

similar reduction in CLDN8 levels was also observed in ER-positive patients who responded to treatment ($p = 0.0072$, Figure 5.3.5.1B). Moreover, in ER-negative/HER2-positive patients, responders displayed a marked decrease in CLDN8 expression ($p = 0.026$, Figure 5.3.5.1C), reinforcing the link between reduced CLDN8 levels and favourable response to anti-HER2 therapy.

This trend was mirrored in ER-positive/HER2-positive patients ($p = 0.028$, Figure 5.3.5.1D) as well as in patients with Luminal-B breast cancer subtype ($p = 0.011$, Figure 5.3.5.1E). Across all these subgroups, the lower CLDN8 expression consistently correlated with better therapeutic outcomes, positioning CLDN8 as a potential biomarker for predicting responsiveness to anti-HER2 treatment.

To validate these clinical findings, we performed additional experiments involving drug sensitivity testing and growth assays using two anti-HER2 drugs, Neratinib and Lapatinib, on four breast cancer cell lines. The results confirmed the trends observed in clinical data: CLDN8 knockdown (CLDN8KD) led to a consistent reduction in IC₅₀ values for both anti-HER2 drugs across all tested breast cancer cell lines, as illustrated in Figures 5.3.5.2a and 5.3.5.2b. This indicated increased drug sensitivity following CLDN8 knockdown.

Growth assays further supported these results. Following CLDN8 knockdown, treatment with anti-HER2 drugs resulted in significantly reduced cell proliferation compared to wild-type (WT) conditions after five days of incubation (Figures 5.3.5.3a and 5.3.5.3b). The diminished cell count in CLDN8KD cells highlights the potential role of CLDN8 in mediating resistance to anti-HER2 therapies.

These findings collectively underscore the importance of CLDN8 as a predictive marker for anti-HER2 therapy response. The consistent association of lower CLDN8 expression with improved treatment outcomes suggests that targeting CLDN8 could be instrumental in tailoring personalized treatment strategies, ultimately enhancing the therapeutic efficacy of anti-HER2 therapies in breast cancer patients.

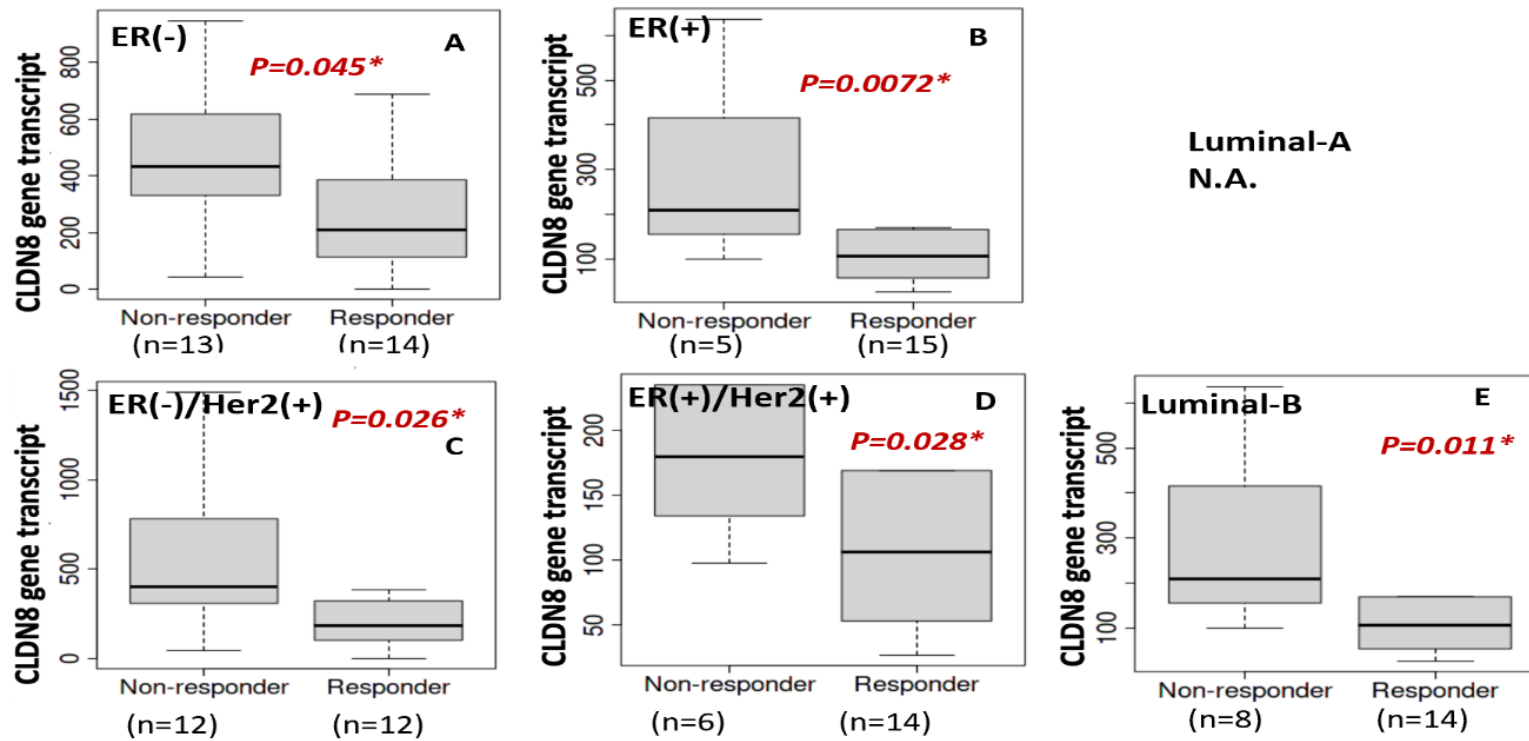


Figure 5.3.5.1: CLDN8 expression and anti-HER2 therapy response across ER and HER2 subgroups. CLDN8 expression in ER(-) breast cancer (panel A); in ER(+) patients (panel B); in ER(-)/HER2(+) breast cancer (panel C); in ER(+)/HER2(+) breast cancer (panel D); and in Luminal B breast cancer (panel E). Data are presented as mean \pm SEM, and *p* values are indicated in each panel.

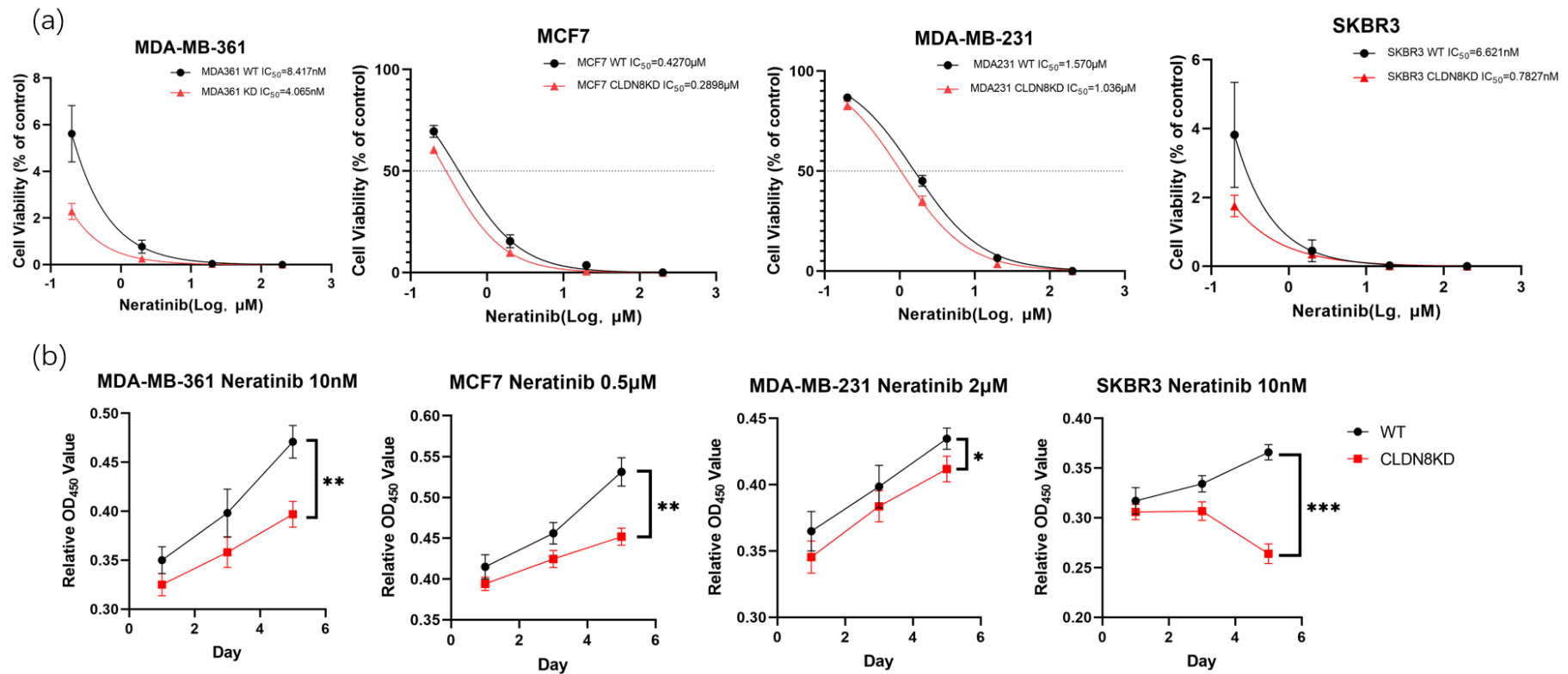


Figure 5.3.5.2: (a) Neratinib sensitivity tests and growth assays. Dose–response curves illustrate the activity percentage of breast cancer cell lines MDA-MB-361, MCF7, MDA-MB-231, and SKBR3 treated with increasing concentrations of Neratinib. In all cell lines, the IC_{50} for CLDN8KD is slightly lower than for WT. (b) Proliferation assays on MDA-MB-361, MCF7, MDA-MB-231, and SKBR3 (WT and CLDN8KD). CLDN8KD MDA-MB-361, MCF7, and MDA-MB-231 show a significant reduction in proliferation at day 5 ($p < 0.05$, * $p < 0.01$, ** $p < 0.001$). Data represent mean \pm SEM from $n = 3$ independent experiments (biological replicates).

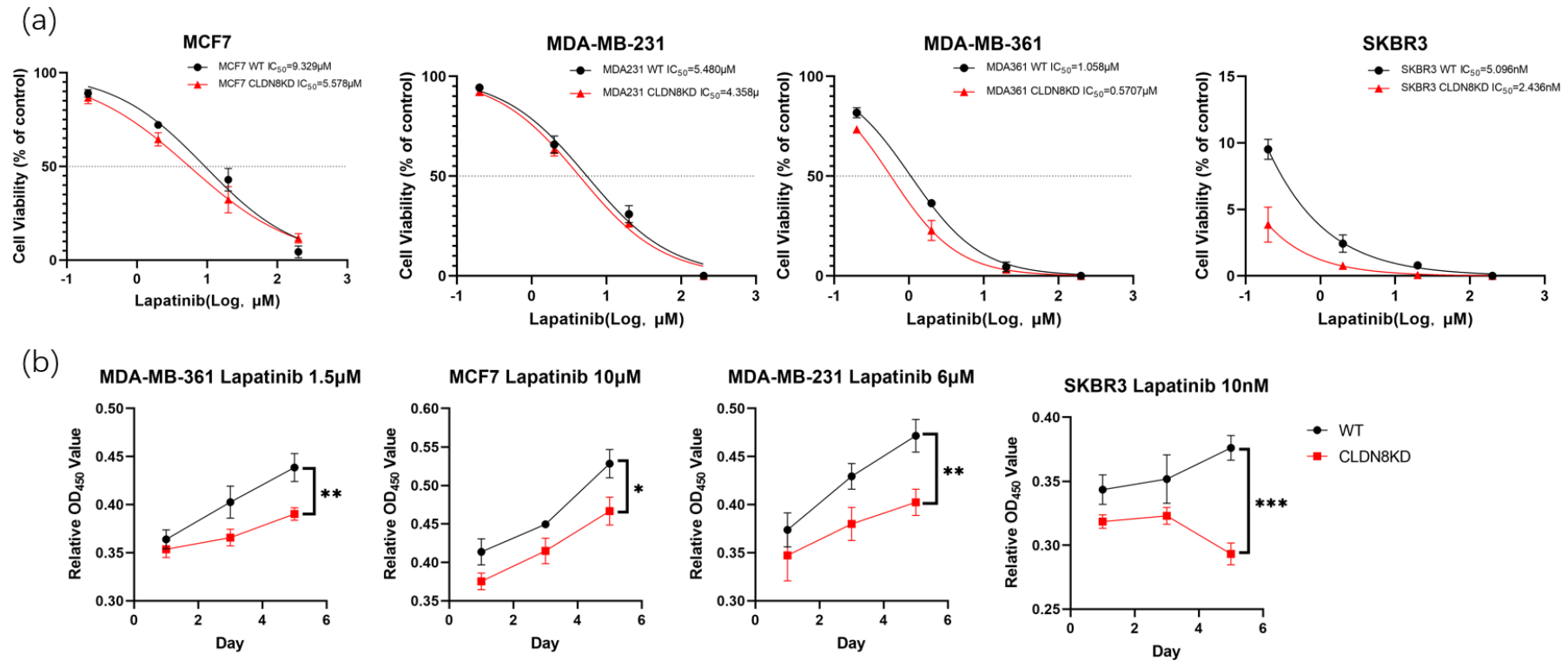


Figure 5.3.5.3: (a) Lapatinib sensitivity tests and growth assays. Dose–response curves illustrate the activity percentage of breast cancer cell lines MDA-MB-361, MCF7, MDA-MB-231, and SKBR3 treated with increasing concentrations of Lapatinib. In all cell lines, the IC_{50} for CLDN8KD is slightly lower than for WT. (b) Proliferation assays on MDA-MB-361, MCF7, MDA-MB-231, and SKBR3 (WT and CLDN8KD). CLDN8KD MDA-MB-361, MCF7, MDA-MB-231, and SKBR3 show a significant reduction in proliferation at day 5 ($p < 0.05$, $*p < 0.01$, $**p < 0.001$). Data represent mean \pm SEM from $n = 3$ independent experiments (biological replicates).

Table 5.3.5.1 Effect of CLDN8 Knockdown on IC50 Values of Anti-HER2+ Therapy Drugs in Different Breast Cancer Cell Models

	Anti-HER2+ therapy	
	Neratinib	Lapatinib
SKBR3 CELL MODELS		
SKBR3-WT	6.62±6.43nM	5.09±2.50nM
SKBR3-CLDN8KD	0.78±0.67nM	2.44±2.32nM
MDA-MB-361 CELL MODELS		
MDA-MB-361-WT	8.42±6.61nM	1.06±0.10µM
MDA-MB-361-CLDN8KD	4.07±3.05nM	0.58±0.06µM
MDA-MB-231 CELL MODELS		
MDA-MB-231-WT	1.57±0.14µM	5.48±1.34µM
MDA-MB-231-CLDN8KD	1.04±0.09µM	4.36±0.80µM
MCF7 CELL MODELS		
MCF7-WT	0.43±0.04µM	9.33±3.00µM
MCF7-CLDN8KD	0.29±0.01µM	5.58±1.26µM

5.3.6 CLDN8 Expression and Chemotherapy Response in Breast Cancer Subgroups

The analysis of CLDN8 expression in breast cancer subgroups highlights its potential as a biomarker for chemotherapy response. In HER2-negative patients (Figure 5.3.6.1A), CLDN8 expression did not significantly differ between responders and non-responders, indicating limited predictive value in this subgroup. In contrast, HER2-positive patients (Figure 5.3.6.1F) exhibited significantly lower CLDN8 levels in responders ($p = 0.01$), suggesting that higher CLDN8 expression may be associated with chemotherapy resistance.

In oestrogen receptor-negative (ER (-)) patients, non-responders demonstrated significantly higher CLDN8 levels ($p = 0.032$, Figure 5.3.6.1B), supporting an association between elevated CLDN8 expression and chemotherapy resistance. This pattern was also evident in the HER2-positive/ER-negative subgroup, where responders had significantly reduced CLDN8 levels ($p = 0.015$, Figure 5.3.6.1H).

Conversely, in oestrogen receptor-positive (ER (+)) subgroups, including HER2-negative/ER-positive (Figure 5.3.6.1C) and HER2-positive/ER-positive (Figure 5.3.6.1I) patients, no significant difference was observed in CLDN8 expression between responders and non-responders, suggesting an inconclusive role of CLDN8 in predicting chemotherapy response in these patients. Similarly, in triple-negative breast cancer (TNBC) patients (Figure 5.3.6.1D), CLDN8 levels did not significantly correlate with chemotherapy response ($p = 0.19$).

Further analysis of the luminal subtypes, Luminal-A (Figure 5.3.6.1E) and Luminal-B (Figure 5.3.6.1J), also showed no significant differences in CLDN8

expression between responders and non-responders, suggesting that CLDN8 may not be a reliable biomarker for chemotherapy response in these subtypes.

To validate these clinical findings, we established an *in vitro* model of breast cancer to assess the impact of CLDN8 on chemotherapy response. Four commonly used chemotherapy drugs—Docetaxel, Paclitaxel, Cisplatin, and Methotrexate (MTX)—were tested on CLDN8 knockdown (CLDN8KD) breast cancer cell lines. Figures 5.3.6.2a, 5.3.6.3a, 5.3.6.4a, and 5.3.6.5a show that knocking out CLDN8 led to decreased IC₅₀ values for all four chemotherapy drugs, indicating increased sensitivity of breast cancer cells to chemotherapy-induced inhibition or cell death.

Growth experiments further corroborated these findings. As illustrated in Figures 5.3.6.2b, 5.3.6.3b, 5.3.6.4b, and 5.3.6.5b, knocking out CLDN8 resulted in a significant response to MTX treatment specifically in MDA-MB-361 cells (HER2+/ER+ status), while no significant differences were observed for the other three chemotherapy drugs. This result aligns with the clinical data presented in Figure 5.3.6I ($p = 0.51$). Likewise, MCF7 cells (ER+ status) showed significant responses only to Docetaxel and Cisplatin, consistent with clinical data in Figure 5.3.6G ($p = 0.46$). Meanwhile, MDA-MB-231 cells (TNBC) showed significant responses only to Cisplatin, which aligned with clinical data from Figure 5.3.6D ($p = 0.19$). Encouragingly, SKBR3 cells (HER2+ status) exhibited significant differences in response to all four chemotherapy drugs. This consistency with clinical data (Figure 5.3.6H, $p = 0.015$) emphasizes the role of CLDN8 as a potential determinant of chemotherapy response in diverse breast cancer subtypes.

Overall, these findings reinforce the complexity of CLDN8's role in chemotherapy response across different breast cancer subtypes. The evidence suggests that lower CLDN8 expression may improve responsiveness to

chemotherapy, particularly in HER2-positive and ER-negative patients, while its predictive value appears to be less significant in other subgroups. As such, CLDN8 could serve as a valuable biomarker for informing personalized chemotherapy regimens in select breast cancer patients.

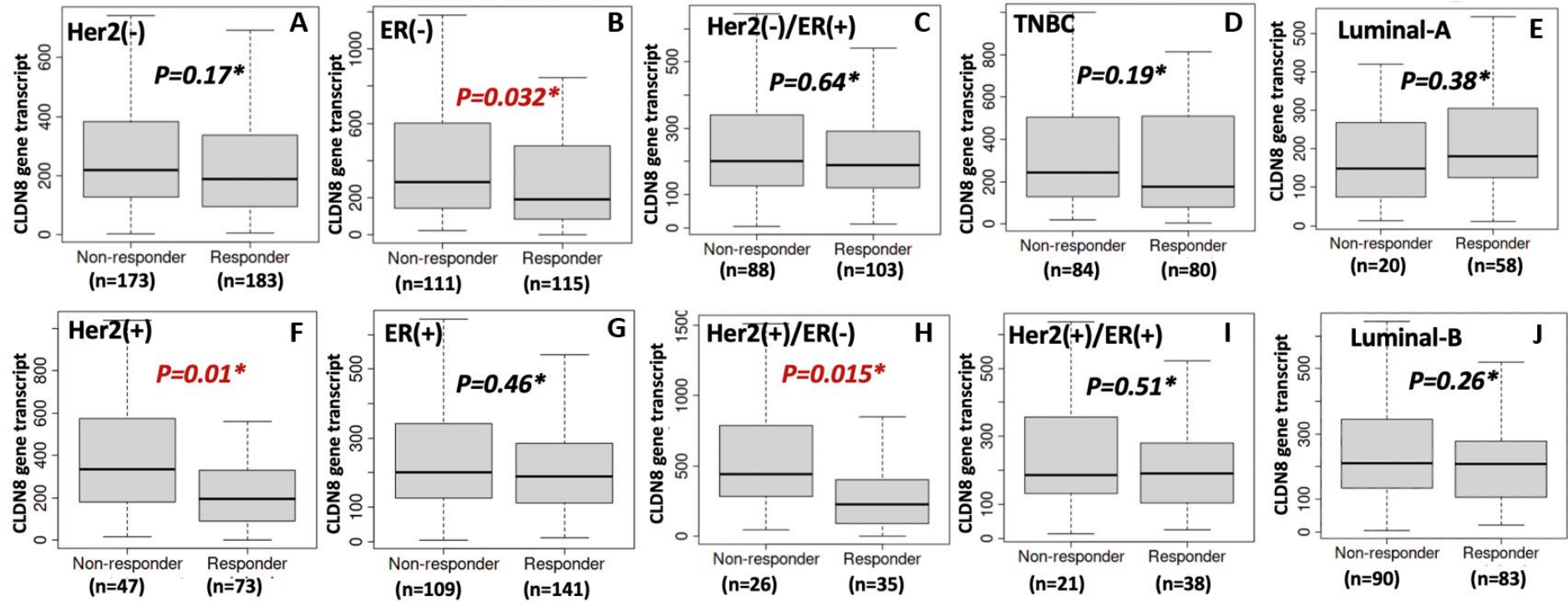


Figure 5.3.6.1 CLDN8 expression and anti-HER2 therapy response across ER and HER2 subgroups. CLDN8 expression in ER(-) breast cancer (panel A), in ER(+) patients (panel B), in ER(-)/HER2(+) breast cancer (panel C), in ER(+)/HER2(+) breast cancer (panel D), and in Luminal B breast cancer (panel E). Data are presented as mean \pm SEM, and p values are indicated in each panel.

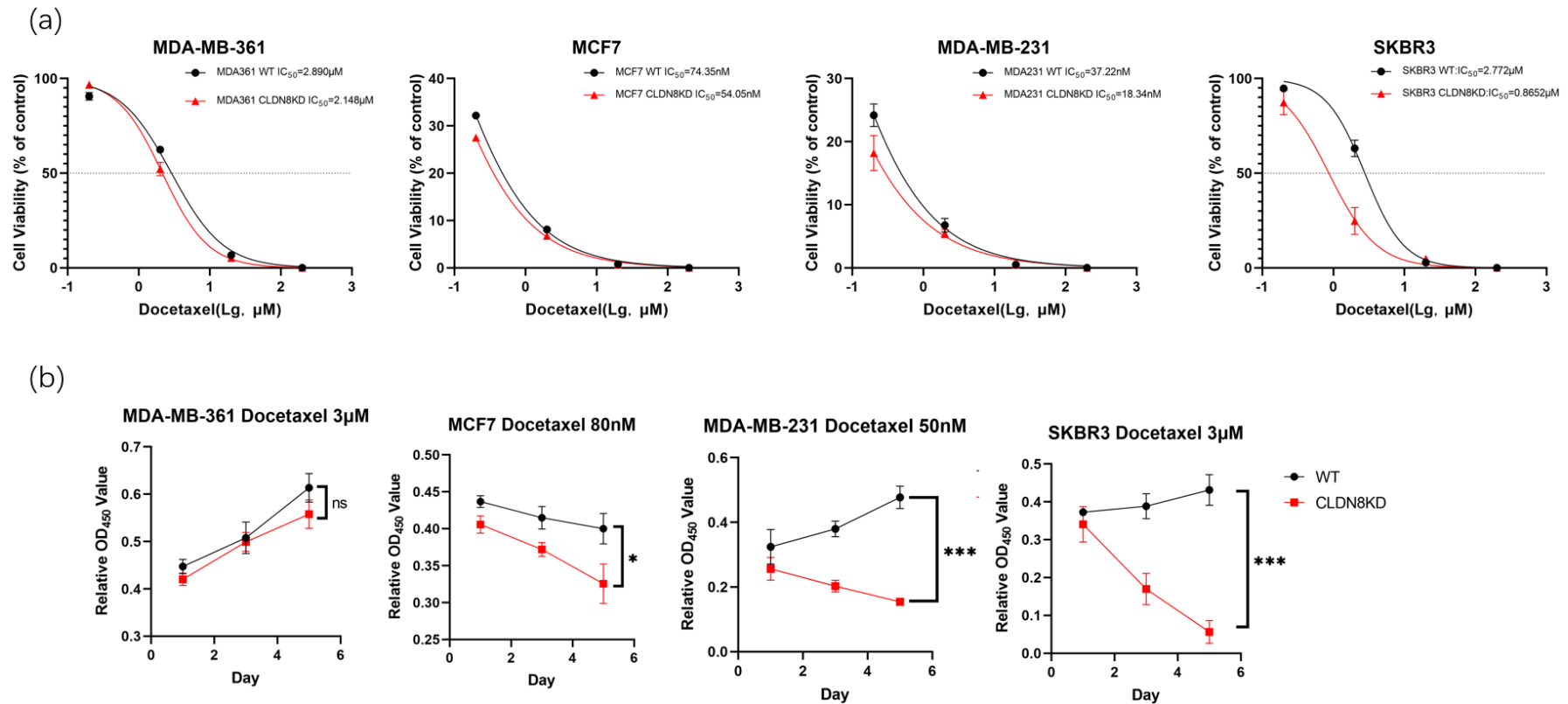


Figure 5.3.6.2 (a) Docetaxel sensitivity tests and growth assays. Dose-response curves illustrate the activity percentage of breast cancer cell lines MDA-MB-361, MCF7, MDA-MB-231, and SKBR3 treated with increasing concentrations of Docetaxel. In all cell lines, the IC_{50} for CLDN8KD is slightly lower than for WT. (b) on MDA-MB-361, MCF7, MDA-MB-231, and SKBR3 (WT and CLDN8KD) CLDN8KD MCF7, MDA-MB-231 and SKBR3 show a significant reduction in proliferation at day 5 (*, $p < 0.05$, ***, $p < 0.001$). Data are expressed as mean \pm SEM from triplicate experiments. Data represent mean \pm SEM from $n = 3$ independent experiments/biological replicates.

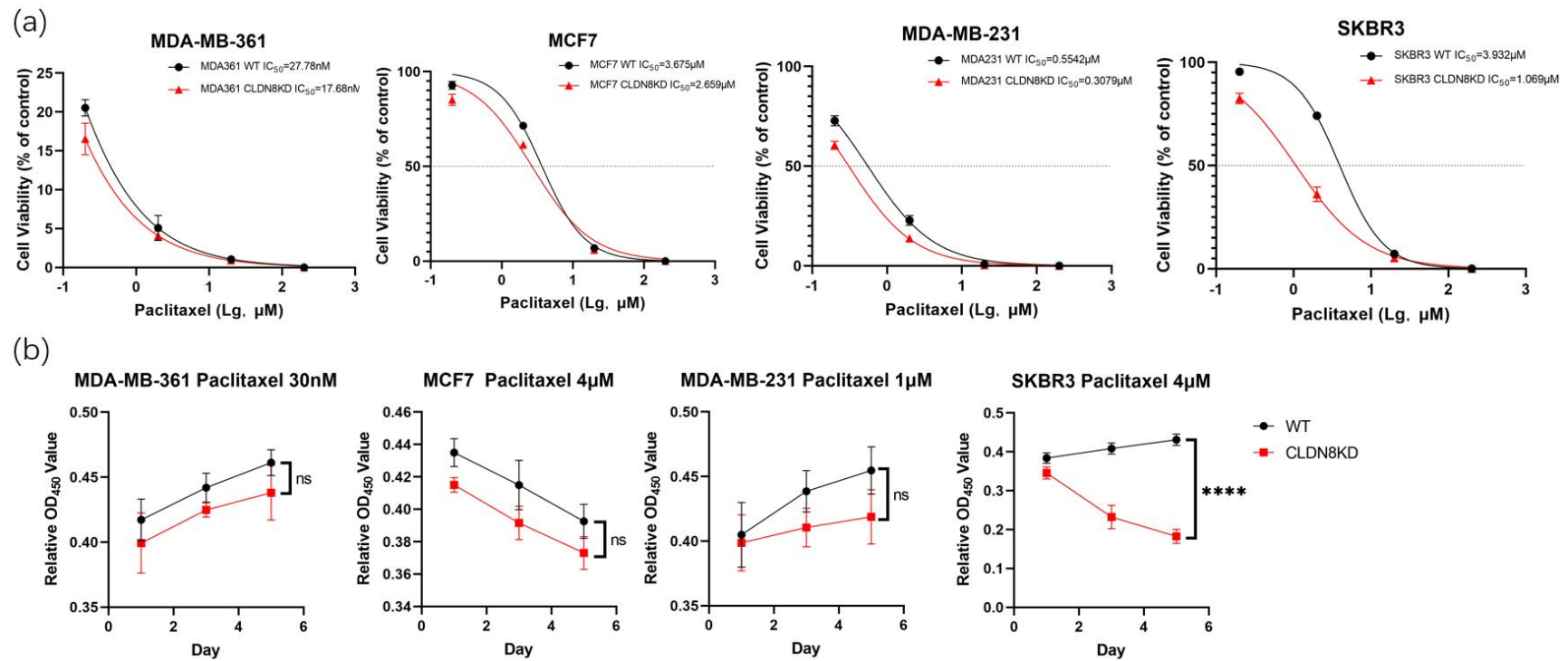


Figure 5.3.6.3: (a) Paclitaxel sensitivity tests and growth assays. Dose-response curves illustrate the activity percentage of breast cancer cell lines MDA-MB-361, MCF7, MDA-MB-231, and SKBR3 treated with increasing concentrations of Docetaxel. In all cell lines, the IC_{50} for CLDN8KD is slightly lower than for WT. (b) Proliferation assays on MDA-MB-361, MCF7, MDA-MB-231, and SKBR3 (WT and CLDN8KD). SKBR3 cells exhibit a stark contrast, with CLDN8KD cells showing significantly reduced proliferation compared to WT when treated with Paclitaxel, as indicated by the “****” ($p < 0.0001$) marker. Data represent mean \pm SEM from $n = 3$ independent experiments (biological replicates).

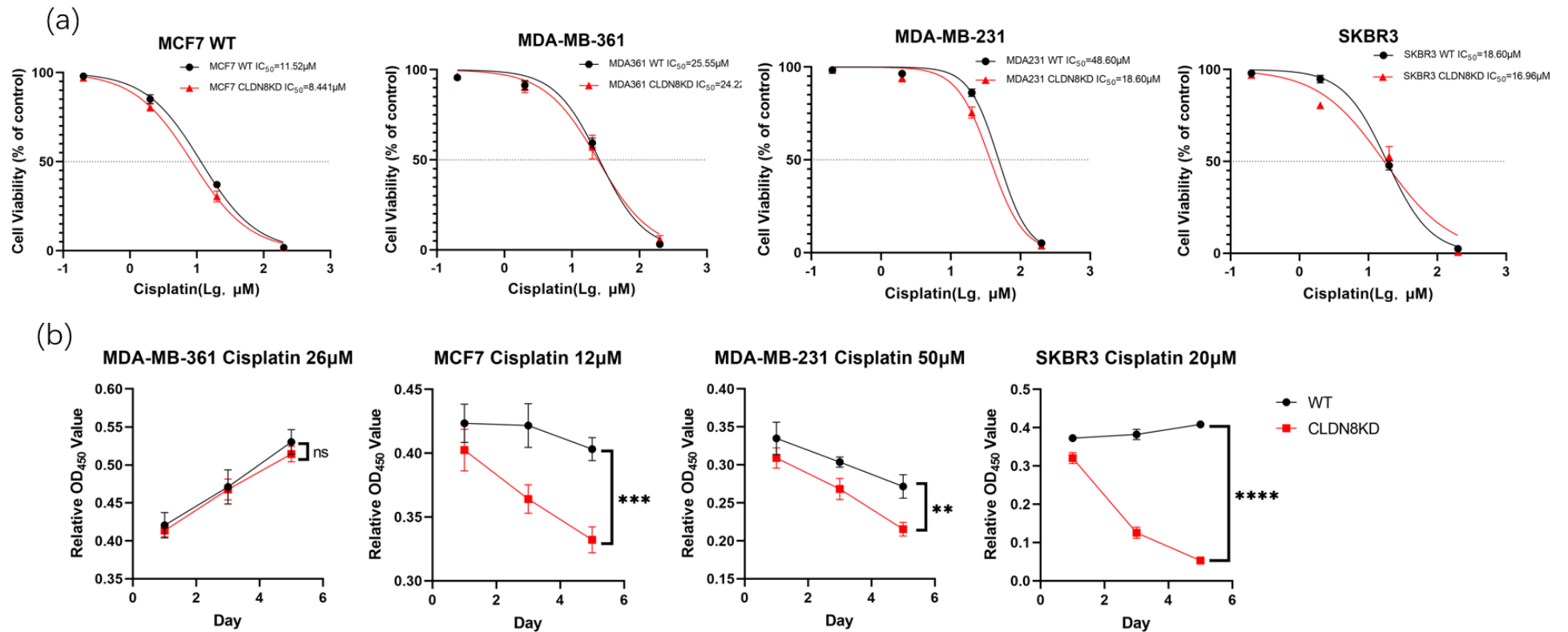


Figure 5.3.6.4 (a) Cisplatin sensitivity tests and growth assays. Dose-response curves illustrate the activity percentage of breast cancer cell lines MDA-MB-361, MCF7, MDA-MB-231, and SKBR3 treated with increasing concentrations of Cisplatin. In all cell lines, the IC_{50} for CLDN8KD is slightly lower than for WT. (b) on MDA-MB-361, MCF7, MDA-MB-231, and SKBR3 (WT and CLDN8KD). Proliferation assays following Cisplatin treatment at specific concentrations derived from IC_{50} values for each cell line over a 5-day period. SKBR3 cells show a marked decrease in proliferation in CLDN8KD compared to WT when treated with 20 μM Cisplatin (**** $p < 0.0001$). Data represent mean \pm SEM from $n = 3$ independent experiments/biological replicates.

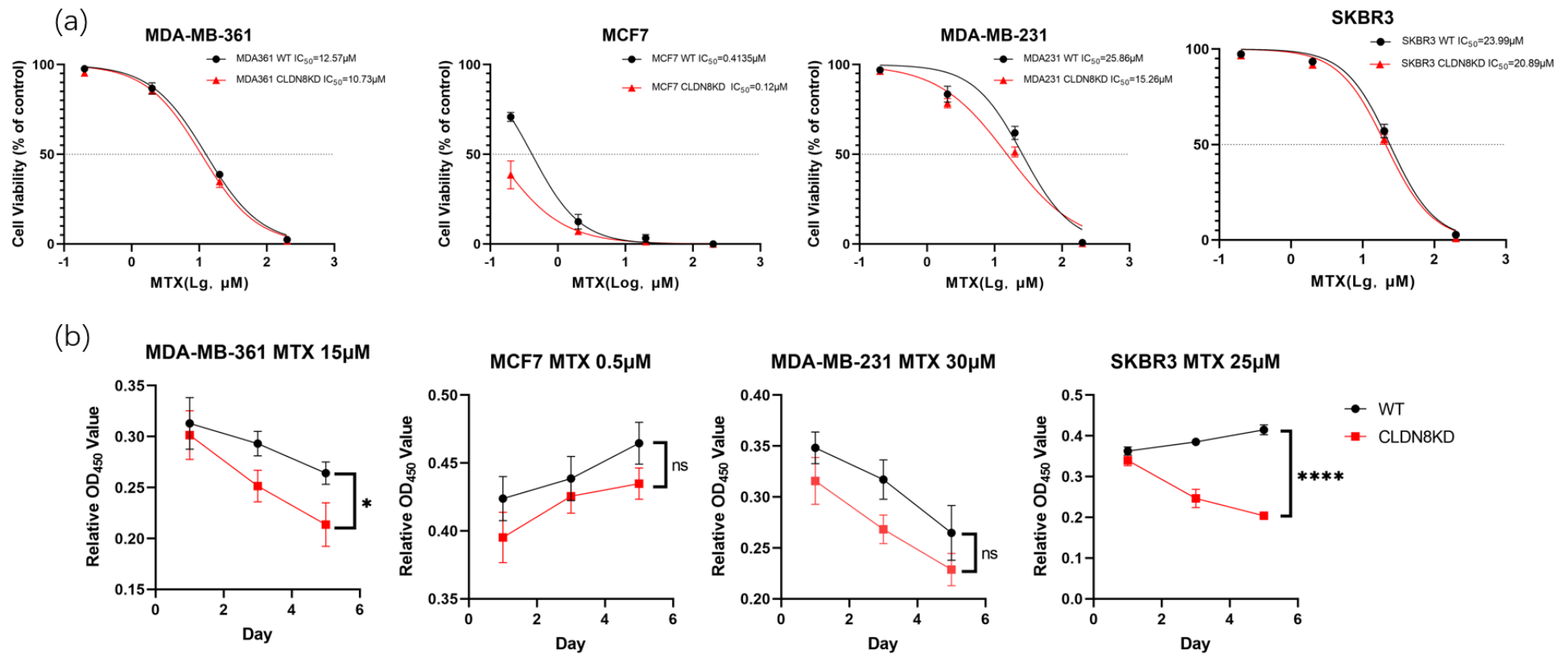


Figure 5.3.6.5 (a) MTX sensitivity tests and growth assays Dose-response curves illustrate the activity percentage of breast cancer cell lines MDA-MB-361, MCF7, MDA-MB-231, and SKBR3 treated with increasing concentrations of MTX. In all cell lines, the IC₅₀ for CLDN8KD is slightly lower than for WT. (b) MDA-MB-361, MCF7, MDA-MB-231, and SKBR3 (WT and CLDN8KD). Cell proliferation assays over six days post-Methotrexate treatment, with concentrations based on the calculated IC₅₀ for each cell line. Data represent mean ± SEM from n = 3 independent experiments/biological replicates.

Table 5.3.6.1 Effect of CLDN8 Knockdown on IC50 Values of Chemotherapy Drugs in Different Breast Cancer Cell Model

	Chemotherapy			
	Docetaxel	Paclitaxel	Cisplatin	MTX
SKBR3 CELL MODELS				
SKBR3-WT	2.77±0.34µM	3.93±0.38µM	18.60±1.41µM	23.99±2.67µM
SKBR3-CLDN8KD	0.86±0.17µM	1.07±0.10µM	16.96±5.75µM	20.89±2.92µM
MDA-MB-361 CELL MODELS				
MDA-MB-361-WT	2.89±0.40µM	27.78±8.05nM	25.55±4.04µM	12.57±1.34µM
MDA-MB-361-CLDN8KD	2.15±0.13µM	17.68±7.67nM	24.22±4.58µM	10.73±1.38µM
MDA-MB-231 CEL MODELS				
MDA-MB-231-WT	37.22±9.97nM	0.55±0.05µM	48.60±7.17µM	25.86±9.01µM
MDA-MB-231-CLDN8KD	18.34±9.31nM	0.31±0.02µM	36.82±7.03µM	15.26±5.28µM
MCF7 CELL MODELS				
MCF7-WT	74.35±6.53nM	3.68±0.51µM	11.52±1.27µM	0.41±0.05µM
MCF7-CLDN8KD	54.05±5.37nM	2.66±0.68µM	8.44±0.88µM	0.12±0.04µM

5.4 Discussion

In our study, we systematically explored the role of Claudin-8 (CLDN8) in the development, prognosis, and therapeutic response of breast cancer.

Comparative analysis between normal breast tissue and tumour tissue revealed significant differences in CLDN8 expression levels, with normal tissue exhibiting significantly higher levels of CLDN8 compared to tumour tissue. This suggests a potential key role for CLDN8 in maintaining the normal physiological function of the breast and may be downregulated in the process of tumour formation.

Further analysis revealed that high CLDN8 expression was associated with improved disease-free survival (DFS) and overall survival (OS), particularly in patients who did not undergo systemic treatment or received hormonal therapy, highlighting the potential of CLDN8 as a favourable prognostic marker. However, in patients undergoing chemotherapy, high CLDN8 expression was associated with poorer OS, suggesting its potential limitations in predicting chemotherapy response.

To further understand the mechanism of action of CLDN8, we conducted a series of drug sensitivity tests and growth experiments covering representative cell lines of different breast cancer subtypes: MDA-MB-231 (triple-negative breast cancer, TNBC), MDA-MB-361 (HER2+/ER+ breast cancer), MCF7 (ER+ breast cancer), and SKBR3 (HER2+ breast cancer). The results showed that in hormonal therapy, knockdown of CLDN8 increased the sensitivity of most cell lines to TAMOXIFEN, FULVESTRANT, and ANASTROZOLE, especially in the MDA-MB-361 cell line, consistent with clinical data indicating a favourable response to hormonal therapy with high CLDN8 expression. Conversely, loss of CLDN8 universally enhanced sensitivity to chemotherapy-induced cell death, particularly in HER2-positive

and ER-negative subtypes, providing experimental support for the potential role of CLDN8 in chemotherapy resistance.

Research on anti-HER2 therapy further emphasizes the importance of CLDN8 in the treatment response of breast cancer. Patients responsive to anti-HER2 therapy, regardless of ER status, exhibited lower levels of CLDN8, especially in ER-negative/HER2-positive and ER-positive/HER2-positive patients. This finding highlights the value of CLDN8 as a potential biomarker for predicting response to anti-HER2 therapy. Sensitivity testing and growth experiments with Neratinib and Lapatinib on the four cell lines further confirmed this, demonstrating that CLDN8 knockout significantly increased sensitivity to anti-HER2 drugs and reduced cell counts, consistent with clinical observations of positive treatment responses with lower CLDN8 expression. Regarding hormonal therapy drug sensitivity, CLDN8 knockout led to an increase in IC₅₀ values for TAMOXIFEN, FULVESTRANT, and ANASTROZOLE in most cell lines, indicating an increasing trend in resistance. Particularly, this change was significant in the MDA-MB-361 cell line, consistent with the observed association between high CLDN8 expression and favourable response to hormonal therapy in clinical data. This emphasizes the potential role of CLDN8 as a predictive marker for hormonal therapy sensitivity in ER+ breast cancer.

We observed an apparent “response” to endocrine agents in TNBC (e.g., MDA-MB-231). This does not imply classical ER-dependent sensitivity. Rather, converging evidence supports a composite explanation: (1) Micromolar tamoxifen elicits ER-independent suppression—via mitochondrial/oxidative stress and NO pathways, with cytotoxicity documented even in ER-negative cells (174-176). (2) Non-genomic estrogen signaling (GPER)—TNBC can express GPER (GPR30); tamoxifen and

estrogens can act as non-selective GPER ligands, producing context-dependent responses not strictly aligned with ER status (177, 178). (3) Anastrozole off-target cytotoxicity — at higher in-vitro concentrations, anastrozole shows ER/aromatase-independent cytotoxic effects, potentially exaggerating an apparent “response” (179). (4) Culture conditions — conventional serum contains residual steroids; charcoal-stripped serum (CSS/CS-FBS) can markedly alter endocrine phenotypes, and lot-to-lot variability impacts reproducibility (180). (5) TNBC claudin-low context — the claudin-low program common in TNBC reflects junctional/membrane remodeling, shaping receptor signaling and drug uptake (a contextual rather than direct causal factor) (181).

Taken together, the TNBC “response” here most likely reflects high-dose ER-independent pharmacology + GPER-mediated non-genomic signaling + culture/model context, rather than bona fide ER-axis sensitivity. To align with clinical biology, we recommend repeating under CSS, using nanomolar dosing, confirming lack of ER activity with ERE/ESR1 assays, and testing GPER involvement (antagonists/knockdown) (178, 180).

In summary, our study reveals the multifaceted role of CLDN8 in breast cancer treatment, serving as a biomarker for predicting response to hormonal therapy and potentially modulating chemotherapy resistance.

Chapter VI: Functional Analysis of CLDN8 in a Breast Cancer Brain Metastasis Model

6.1 Introduction

Breast cancer brain metastasis is a serious complication that significantly impacts patient prognosis, often leading to reduced survival time and diminished quality of life. One of the major challenges in treating brain metastasis is the difficulty of effective drug penetration across the BBB to reach the metastatic sites in the brain. The BBB, composed of endothelial cells and their tight junctions (TJs), serves as a natural defence barrier of the brain against harmful substances, but it also restricts therapeutic agents from entering the central nervous system. Finding ways to effectively modulate or partially increase the permeability of the BBB to enhance drug concentrations in the brain has long been a difficult issue in treating patients with brain metastasis.

Artemisinin, a natural compound extracted from the plant *Artemisia annua*, has gained attention for its potential therapeutic effects against various cancers, especially for its ability to enhance drug penetration into brain metastasis. In Chapter 3, we studied the regulatory effect of Artemisinin on TJ proteins, particularly Claudin-8 (CLDN8), in breast cancer and endothelial cells. RNA sequencing data showed that Artemisinin treatment significantly altered the expression of genes related to tight junctions, including a marked downregulation of CLDN8, suggesting that Artemisinin may increase drug permeability to the brain by modulating the BBB.

In Chapter 4, we further analysed the expression of CLDN8 in different breast cancer subtypes using data from the TCGA database and samples from the Cardiff clinical cohort. The results indicated that CLDN8 expression was significantly downregulated in high-grade tumours and advanced TNM stages, which could be associated with increased metastatic potential and poorer prognosis.

Chapter 5 explored the role of CLDN8 expression in breast cancer treatment, particularly noting that high CLDN8 expression was associated with better disease-free survival (DFS) in patients receiving endocrine therapy. The downregulation of CLDN8 induced by Artemisinin may be linked to increased BBB permeability, aiding in the delivery of therapeutic agents to brain metastases.

In this chapter, we focus on the dual role of Artemisinin in breast cancer cells and endothelial cells to understand its potential in treating breast cancer brain metastasis. We aim to investigate whether Artemisinin, while modulating BBB permeability, also influences the proliferation and invasiveness of breast cancer cells. By exploring the regulatory effects of Artemisinin on both endothelial and breast cancer cells, we hope to shed light on how Artemisinin could act on both the BBB and cancer cells, providing new insights into the treatment of breast cancer brain metastasis.

However, this also raises a potential risk: Could using Artemisinin to assist chemotherapeutic drugs in penetrating the BBB during brain metastasis treatment increase the risk of further metastasis of breast cancer cells?

Existing research suggests that the downregulation of tight junction proteins (such as CLDN8) may be linked to increased tumour invasiveness. Thus, by downregulating CLDN8, Artemisinin may enhance drug penetration into the brain but may also make cancer cells more prone to cross the BBB. Therefore, a comprehensive assessment of Artemisinin's dual effects on endothelial cells and breast cancer cells is crucial—not only focusing on its potential to increase drug permeability but also evaluating whether it might contribute to an increased risk of tumour spread.

Through this study, we aim to elucidate the dual role of Artemisinin in regulating the BBB and breast cancer cell behaviour and provide a scientific basis for its potential clinical use in treating breast cancer brain metastasis.

6.2 Materials and Methods

6.2.1 Cell Lines and Culture Conditions

In this study, four human breast cancer cell lines were used, including SKBR3, MDA-MB-231, MCF-7, and MDA-MB-361. These cell lines represent various breast cancer subtypes: SKBR3 is HER2-positive, MDA-MB-231 is triple-negative breast cancer (TNBC), MCF-7 is oestrogen receptor-positive (ER+), and MDA-MB-361 is HER2-positive/ER-positive (HER2+/ER+). Additionally, human brain microvascular endothelial cells hCMEC/D3 and TY10 were used to model the BBB.

MDA-MB-231 and MCF-7 cells were cultured in Dulbecco's Modified Eagle Medium (DMEM), while MDA-MB-361 and SKBR3 cells were cultured in RPMI-1640 medium. All culture media were supplemented with 10% foetal bovine serum (FBS) and 1× penicillin/streptomycin (Sigma-Aldrich). The hCMEC/D3 and TY10 endothelial cells were cultured in endothelial growth medium (EGM-2, Lonza) supplemented with 5% FBS, endothelial cell growth factors, and antibiotics. All cells were maintained at 37°C in a humidified atmosphere with 5% CO₂.

6.2.2 Knockdown of CLDN8

To investigate the impact of Artemisinin on CLDN8, we performed CLDN8 knockdown in breast cancer cell lines (SKBR3, MDA-MB-231, and MCF-7) and endothelial cell lines (hCMEC/D3 and TY10). CLDN8 knockdown was carried

out using small interfering RNA (siRNA) and transfected with Lipofectamine RNAiMAX (Invitrogen). A total of 70,000 cells per well were used for transfection. After 48 hours of incubation, knockdown efficiency was confirmed through quantitative PCR (qPCR) and Western blotting.

6.2.3 Artemisinin Treatment Protocol

Artemisinin was purchased from Sigma-Aldrich and dissolved in dimethyl sulfoxide (DMSO) to prepare a 100 mM stock solution. For all experiments, cells were treated with Artemisinin at a final concentration of 50 μ M for 24 hours, and control cells were treated with an equivalent concentration of DMSO.

6.2.4 Cell Adhesion Assay

To assess the impact of Artemisinin on breast cancer cell adhesion, SKBR3, MDA-MB-231, and MCF-7 cells were pre-treated with Artemisinin or DMSO control. Then, 30,000 cells were seeded per well onto Matrigel-coated 96-well plates. Adhesion potential was quantified by measuring absorbance after staining, as detailed in previous protocols.

6.2.5 Cell Invasion Assay

The invasive ability of breast cancer cells in the presence or absence of Artemisinin was evaluated using a transwell invasion assay. A total of 3,000 SKBR3 and MDA-MB-231 cells and 7,000 MCF-7 cells were seeded into transwell inserts with an 8 μ m pore size, which were then placed above the monolayers of hCMEC/D3 and TY10 cells to mimic the BBB. Artemisinin was added to simulate treatment effects, and cell invasion was quantified after 24 hours using an EVOS imaging system.

6.2.6 Cell Migration Assay (Scratch Assay)

To assess the effect of Artemisinin on the migratory ability of breast cancer cells, we used a scratch assay. SKBR3, MDA-MB-231, and MCF-7 cells were cultured in 6-well plates until they formed a confluent monolayer. A scratch was made using a sterile pipette tip, and 70,000 cells were used per well for the experiment. Cells were treated with Artemisinin (10 μ M) or DMSO, and images were captured at 0, 24, and 48 hours using a microscope to monitor the healing process. The migration rate was assessed by measuring the closure of the scratch area.

6.2.7 Permeability Coefficient (PCP) Assay

The permeability of endothelial cells was assessed to evaluate the effect of Artemisinin on BBB integrity. A total of 70,000 hCMEC/D3 or TY10 cells were seeded into transwell inserts with a 0.4 μ m pore size and allowed to form a tight monolayer. FITC-dextran was added to the upper compartment, and samples were collected from the lower compartment to assess permeability, with Artemisinin treatment administered to evaluate its effect on the BBB.

6.2.8 Transendothelial Electrical Resistance (TEER) Assay

The TEER assay was used to assess the integrity of the endothelial cell monolayer under Artemisinin treatment. A total of 70,000 hCMEC/D3 or TY10 cells were seeded into transwell inserts. After the cells reached confluency, TEER values were measured. Artemisinin was added, and TEER was monitored periodically to observe changes in barrier function.

6.3 Results

6.3.1 CLDN8 Knockdown Efficiency and Validation

To evaluate the role of Artemisinin in breast cancer cells, Claudin-8 (CLDN8) knockdown was first performed across four breast cancer cell lines: SKBR3,

MDA-MB-231, MCF-7, and MDA-MB-361. Knockdown was achieved using small interfering RNA (siRNA) specific to CLDN8, and its efficiency was validated by both quantitative PCR (qPCR) and Western blotting.

The effectiveness of CLDN8 knockdown was quantified through qPCR, which measured the relative expression levels of CLDN8 mRNA in the four breast cancer cell lines post-transfection. Results indicated significant reductions in CLDN8 expression across all cell lines. (Figure 6.3.1a).

To further validate knockdown at the protein level, Western blotting was conducted using specific antibodies against CLDN8 and GAPDH (used as a loading control). Results showed a marked decrease in CLDN8 protein expression in all cell lines post-siRNA transfection.

The consistent reduction in both mRNA and protein levels highlighted the robustness of the knockdown, establishing a solid foundation for further functional assays.

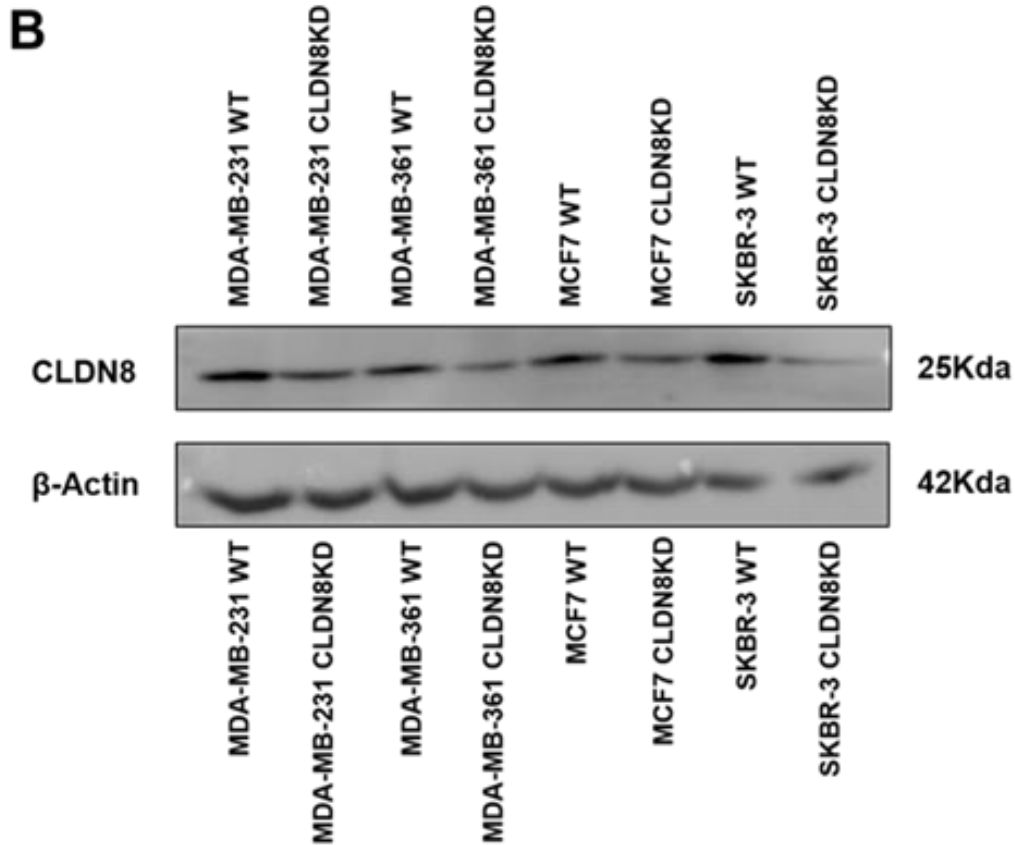
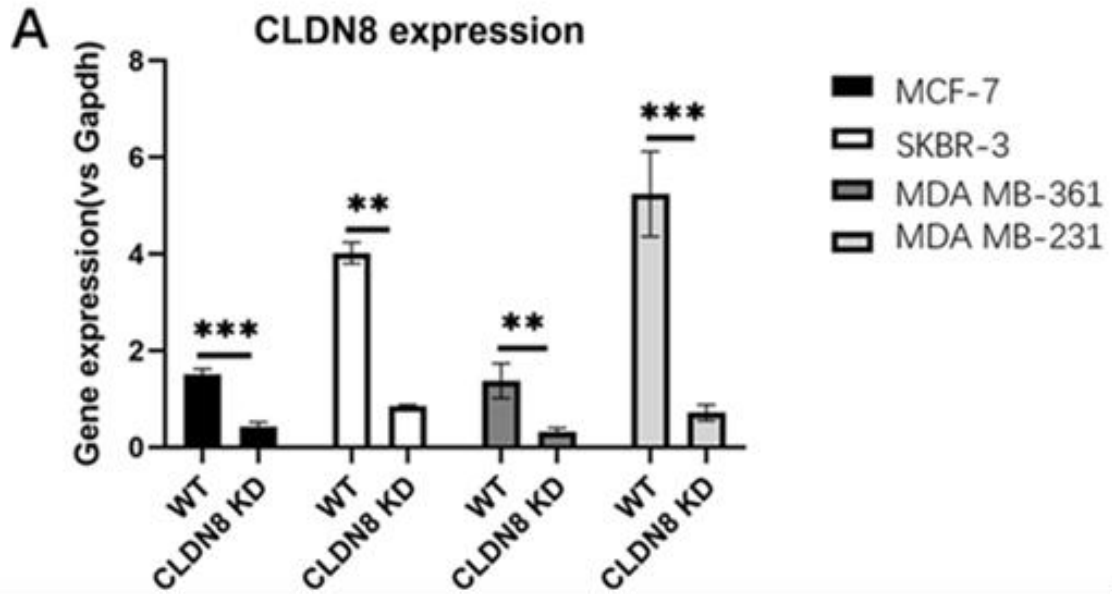


Figure 6.3.1: Expression of CLDN8 in breast cancer cell lines. (A) qPCR analysis confirming knockdown efficiency in MDA-MB-231, MDA-MB-361, SKBR3, and MCF-7 cells. Fold changes calculated using the $2^{-\Delta\Delta Ct}$ method; statistical significance by unpaired t-test (* $P < 0.05$, ** $P < 0.01$, *** $P < 0.001$). (B) Western blot of CLDN8 protein levels in WT and KD cells; β -actin served as loading control. WT, wild type; KD, knockdown.

6.3.2 Impact of CLDN8 Knockdown and Artemisinin on Breast Cancer Cell Adhesion

In this study, we assessed the impact of CLDN8 knockdown and Artemisinin (Artemisinin) treatment on the adhesion capacity of breast cancer cells. The experiment was conducted across four breast cancer cell lines (MCF7, MDA-MB-231, SKBR3, and MDA-MB-361), analysing the effects on both WT cells and CLDN8KD cells, as well as the influence of Artemisinin treatment. The results are illustrated in Figures 6.3.2a and 6.3.2b.

As shown in Figure 6.3.2a, we first evaluated the impact of CLDN8 knockdown on breast cancer cell adhesion. Without Artemisinin treatment, CLDN8 knockdown significantly reduced the adhesion ability of MDA-MB-231 and SKBR3 cells. Compared to the respective wild-type cells, the number of adherent cells was significantly lower ($p < 0.01$). However, for MCF7 and MDA-MB-361 cells, no significant difference was observed between CLDN8 knockdown and wild-type cells (labelled as "ns"), suggesting that CLDN8 may have a stronger role in promoting adhesion in some breast cancer subtypes, while its role in other subtypes is less evident.

As shown in Figure 6.3.2b, we further examined the effects of Artemisinin treatment on breast cancer cell adhesion. The results indicated that Artemisinin significantly reduced cell adhesion in both wild-type and CLDN8 knockdown cells. Specifically, in CLDN8 knockdown MDA-MB-231 and SKBR3 cells, the number of adherent cells was further reduced following Artemisinin treatment ($p < 0.001$). However, in MCF7 and MDA-MB-361 cells, Artemisinin also reduced adhesion capacity, with similar effects observed regardless of CLDN8 knockdown ($p < 0.001$).

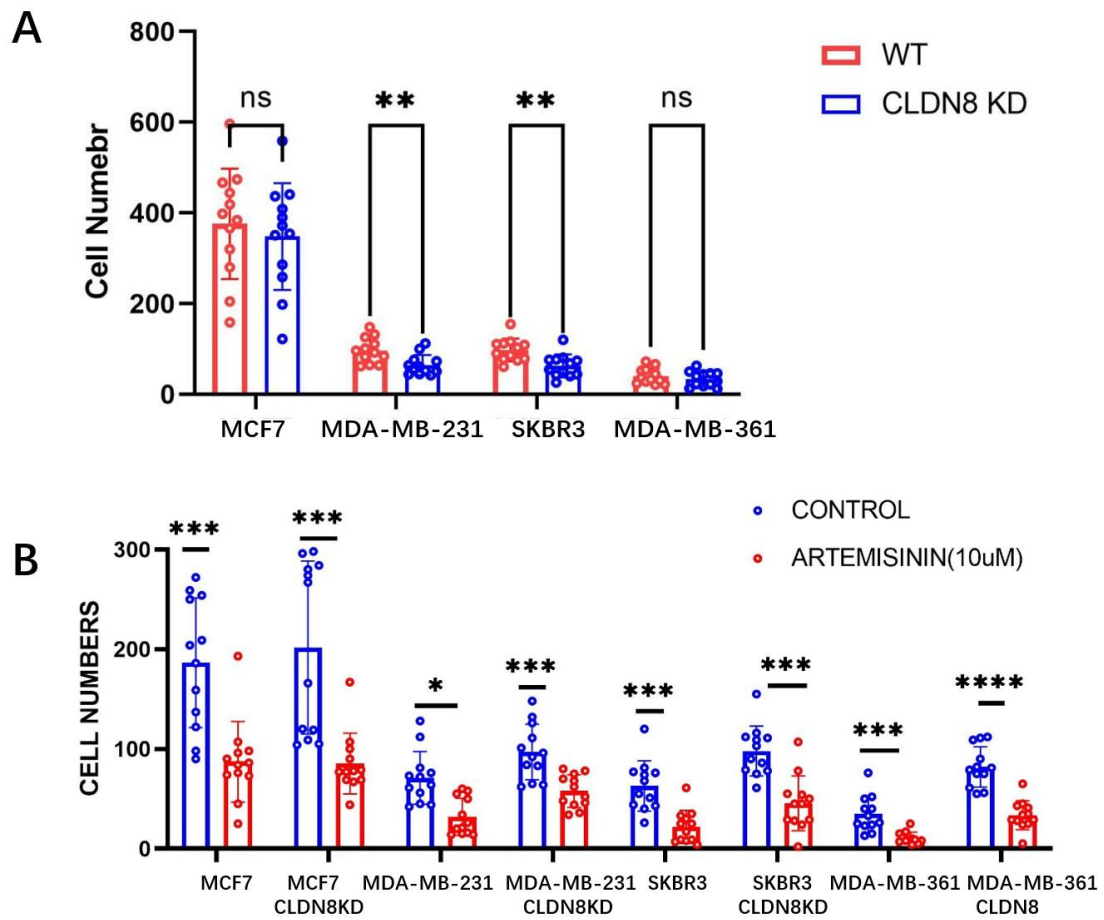


Figure 6.3.2 (A) Impact of CLDN8 Knockdown on Breast Cancer Cell Adhesion. Cell adhesion assay displaying the number of adherent cells in wild-type (WT) and CLDN8 knockdown (CLDN8KD) conditions for four breast cancer cell lines (MCF7, MDA-MB-231, SKBR3, and MDA-MB-361). (B) Effect of Artemisinin on Breast Cancer Cell Adhesion.

6.3.3 Scratch Wound Healing Assay Results for Breast Cancer Cell Lines

To evaluate the impact of CLDN8 knockdown and Artemisinin treatment on breast cancer cell migration, scratch wound healing assays were conducted on four breast cancer cell lines: MCF7, MDA-MB-231, SKBR3, and MDA-MB-361. The rate of cell migration was assessed both with and without CLDN8 knockdown, as well as with Artemisinin treatment, to understand whether Artemisinin enhances or inhibits breast cancer cell motility.

The first figure (Figure 6.3.3a) depicts the effect of CLDN8 knockdown on the rate of migration in MCF7, MDA-MB-231, SKBR3, and MDA-MB-361 breast cancer cell lines. The results indicated a significant reduction in migration rates in CLDN8 knockdown MCF7 cells compared to wild-type MCF7 ($p < 0.01$), suggesting that CLDN8 is crucial for the migratory ability of MCF7 cells. In contrast, no significant changes in migration rates were observed in MDA-MB-231, SKBR3, and MDA-MB-361 cells after CLDN8 knockdown. This suggests that the dependency of migration on CLDN8 may be cell-type specific, with MCF7 being particularly reliant on CLDN8 for migration.

The second figure (Figure 6.3.3b) shows the effect of Artemisinin (10 μM) on cell migration rates across MCF7, MDA-MB-231, and their corresponding CLDN8 knockdown variants. The results demonstrate that treatment with Artemisinin significantly reduced the migration rates of MCF7, MDA-MB-231, and their CLDN8 knockdown counterparts ($p < 0.05$). The migration inhibition effect was consistently observed across both wild-type and CLDN8 knockdown cells, suggesting that Artemisinin's anti-migratory effects may operate through mechanisms that are independent of CLDN8. This highlights the potential of Artemisinin to inhibit breast cancer cell migration, regardless of CLDN8 expression levels.

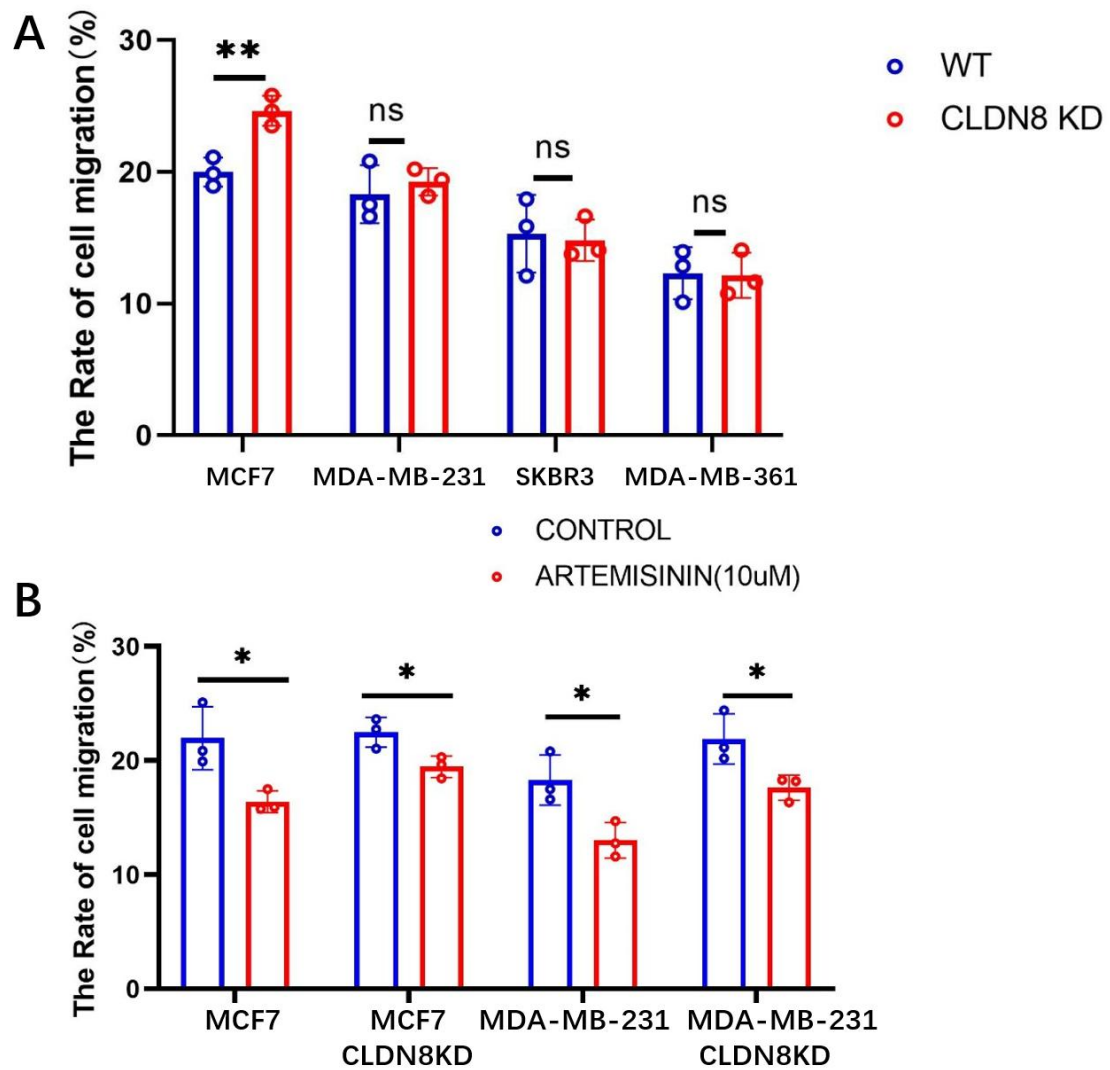


Figure 6.3.3 (A) Migration rates of breast cancer cell lines with CLDN8 knockdown compared to wild type. Significant reduction in migration rate is observed in MCF7 with CLDN8 knockdown ($p < 0.01$). (B) Migration rates of breast cancer cell lines with or without Artemisinin (10 μ M) treatment.

6.3.4 Invasion Assay Results for Breast Cancer Cells Across the Blood-Brain Barrier (BBB)

To evaluate the effect of Claudin-8 (CLDN8) knockdown and Artemisinin treatment on the invasive abilities of breast cancer cell lines, transwell invasion assays were conducted using hCMEC/D3 cells to model the BBB. The experiment aimed to investigate whether CLDN8 influences the invasive

capacity of breast cancer cells and whether Artemisinin treatment impacts their potential to cross the endothelial barrier.

The first figure (Figure 6.3.4a) illustrates the invasive potential of four breast cancer cell lines—MCF7, MDA-MB-231, SKBR3, and MDA-MB-361—with and without CLDN8 knockdown. The results demonstrate that CLDN8 knockdown significantly enhances the invasion ability of MCF7 ($p < 0.05$), MDA-MB-231 ($p < 0.01$), SKBR3 ($p < 0.0001$), and MDA-MB-361 ($p < 0.05$) cell lines. In particular, MDA-MB-231 and SKBR3 cells exhibited pronounced increases in their invasive potential following CLDN8 knockdown.

The second figure (Figure 6.3.4B) presents the effect of Artemisinin (10 μ M) treatment on the invasion capabilities of MCF7, SKBR3, MDA-MB-231, MDA-MB-361, and their respective CLDN8 knockdown variants. Artemisinin treatment significantly decreased the number of invasive cells in MCF7 and MCF7 CLDN8KD cells ($p < 0.0001$ and $p < 0.001$, respectively), as well as in SKBR3 and SKBR3 CLDN8KD cells ($p < 0.001$). Interestingly, in MDA-MB-231 cells, Artemisinin showed a significant reduction in invasion only in CLDN8KD cells ($p < 0.001$), while no significant effect was observed in MDA-MB-231 wild-type cells.

This suggests that Artemisinin may have a more pronounced inhibitory effect on cell invasion in the absence of CLDN8 expression, indicating that its anti-invasive action might be partially independent of CLDN8 pathways. Furthermore, for MDA-MB-361 cells and their CLDN8KD variants, Artemisinin also led to a decrease in invasion ($p < 0.001$ and $p < 0.05$, respectively).

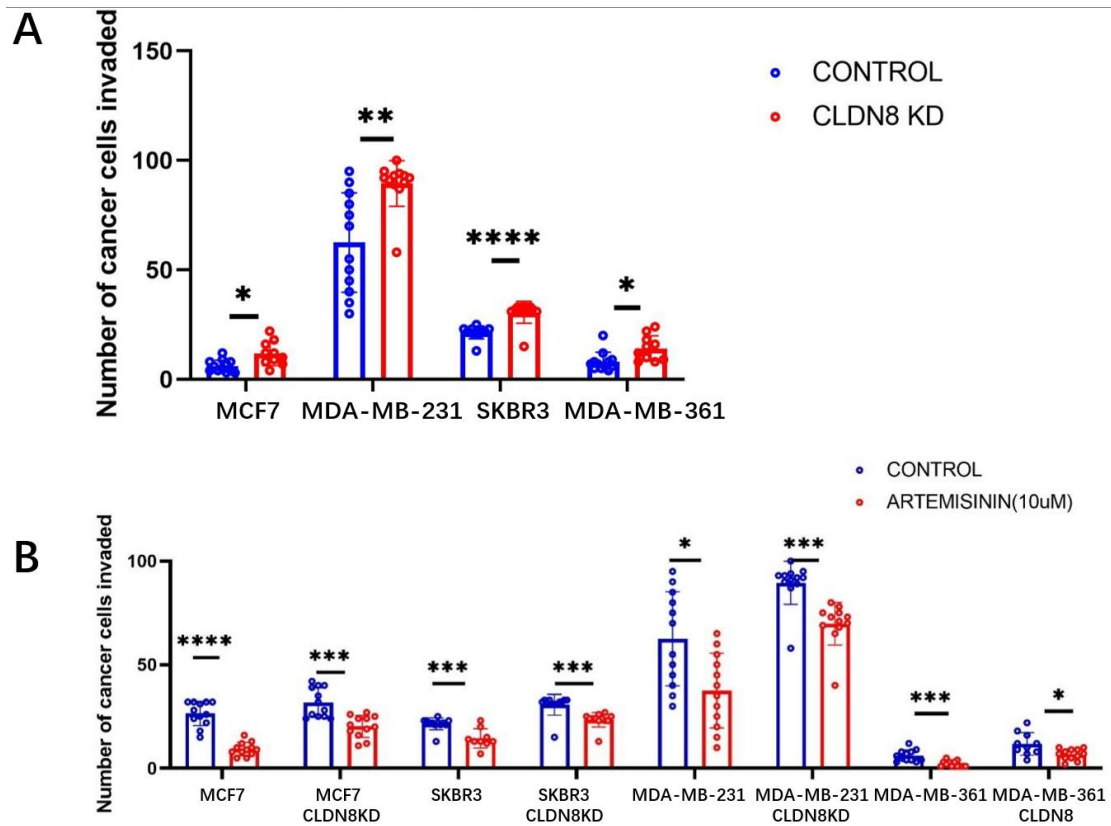


Figure 6.3.4 (A) Number of invasive breast cancer cells with or without CLDN8 knockdown. Significant enhancement in invasion observed across MCF7, MDA-MB-231, SKBR3, and MDA-MB-361 cell lines upon CLDN8 knockdown. (B) Number of invasive breast cancer cells after treatment with Artemisinin (10 μ M). Artemisinin significantly reduced invasion in all tested cell lines, regardless of CLDN8 status.

6.3.5 Impact of Artemisinin Treatment on TEER and Paracellular Permeability of Breast Cancer Cell Lines

This section evaluates the effect of Artemisinin on the integrity of breast cancer cell monolayers by measuring transendothelial electrical resistance (TEER) and paracellular permeability (PCP). TEER represents the barrier integrity, with higher values indicating better tight junctions, whereas PCP measures the permeability across the cell layer, indicating the barrier's permeability strength. In this study, both TEER and PCP were assessed in SKBR3 and MDA-MB-231 breast cancer cell lines, with and without Claudin-8 (CLDN8) knockdown, in response to Artemisinin treatment.

The results presented in Figures 6.3.5A to 6.3.5H collectively demonstrate the impact of Artemisinin on the barrier integrity of SKBR3 and MDA-MB-231 breast cancer cell lines, as well as their CLDN8 knockdown variants, as assessed through TEER and PCP measurements over a 150-minute timeframe.

For TEER measurements (Figures 6.3.5A-D), Artemisinin treatment significantly reduced TEER values in both SKBR3 and MDA-MB-231 wild-type cells ($p < 0.0001$), indicating a compromise in tight junction integrity. TEER values decreased as early as 15 minutes after treatment, suggesting a rapid effect of Artemisinin on disrupting cellular tight junctions. In SKBR3 CLDN8 knockdown cells (Figure 6.3.5B), Artemisinin did not result in a significant TEER change, highlighting the potential dependence on CLDN8 for the observed effects on tight junctions. Conversely, MDA-MB-231 CLDN8 knockdown cells (Figure 6.3.5D) experienced a moderate reduction in TEER compared to their wild-type counterparts, indicating that although CLDN8 contributes to barrier integrity, other factors may also be involved in Artemisinin's effects.

For PCP analysis (Figures 6.3.5E-H), Artemisinin treatment significantly increased paracellular permeability in both SKBR3 and MDA-MB-231 wild-type cells ($p < 0.0001$), consistent with the observed reduction in TEER values. This demonstrates a reduction in tight junction functionality and an increase in cell monolayer permeability due to Artemisinin. In SKBR3 CLDN8 knockdown cells (Figure 6.3.5F), the permeability increase was less pronounced compared to the wild type, reinforcing the role of CLDN8 in maintaining barrier integrity. Similarly, in MDA-MB-231 CLDN8 knockdown cells (Figure 6.3.5H), a slight increase in permeability was observed at 15 minutes ($p < 0.05$), indicating that the effect of Artemisinin on PCP is partially dependent on CLDN8 in these cells.

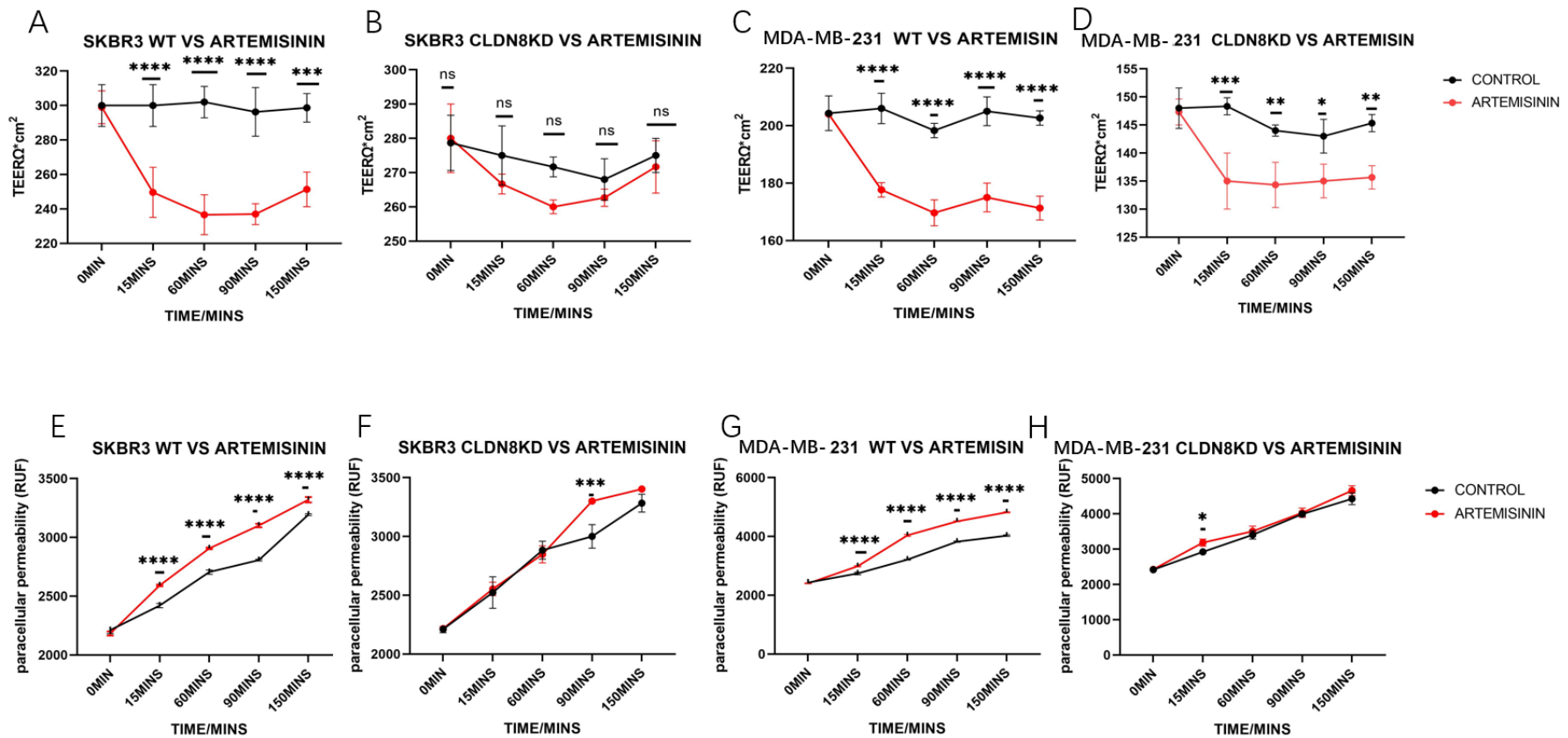


Figure 6.3.5 TEER Analysis (Figure 6.3.5A-D) Figures 6.3.5A to 6.3.5D show TEER measurements over a period of 150 minutes. TEER values were assessed for both SKBR3 and MDA-MB-231 cell lines, including their CLDN8 knockdown variants, in the presence or absence of Artemisinin treatment. Paracellular Permeability (PCP) Analysis (Figure 6.3.5E-H). The PCP was assessed by measuring the permeability of FITC-dextran across the cell monolayer. TEER ($\Omega\text{-cm}^2$) and PCP changes after treatment. Data are presented as mean \pm SEM from $n = 3$ independent experiments.

6.3.6 CLDN8 Knockdown Efficiency in TY10 and hCMEC/D3 Endothelial Cells

To assess the efficiency of CLDN8 knockdown in endothelial cells, we performed qPCR and Western blot analysis on two endothelial cell lines: TY10 and hCMEC/D3. The knockdown efficiency was quantified both at the mRNA level and the protein level, allowing for a comprehensive understanding of the impact of CLDN8 silencing.

Figure 6.3.6A shows the results of the qPCR analysis of CLDN8 expression in TY10 cells. The relative mRNA expression of CLDN8 in CLDN8 knockdown cells (CLDN8 KD) was significantly reduced compared to wild-type (WT) TY10 cells, with an approximate 70% reduction (** $p < 0.01$). GAPDH was used as an internal control for normalization.

Figure 6.3.6B depicts the Western blot results of CLDN8 expression in hCMEC/D3 cells. Protein extracts from WT and CLDN8 KD hCMEC/D3 cells were analysed, with GAPDH as a loading control. The blot clearly shows a substantial reduction in CLDN8 protein levels in the CLDN8 KD cells compared to the WT cells.

Figure 6.3.6C provides the quantification of the Western blot results, illustrating a significant decrease in CLDN8 protein expression in hCMEC/D3 CLDN8 KD cells (** $p < 0.001$), normalized to GAPDH.

These results confirm the successful knockdown of CLDN8 in both TY10 and hCMEC/D3 endothelial cell lines, with marked reductions observed in both gene and protein expression levels, which is essential for the subsequent functional analyses involving these cell lines.

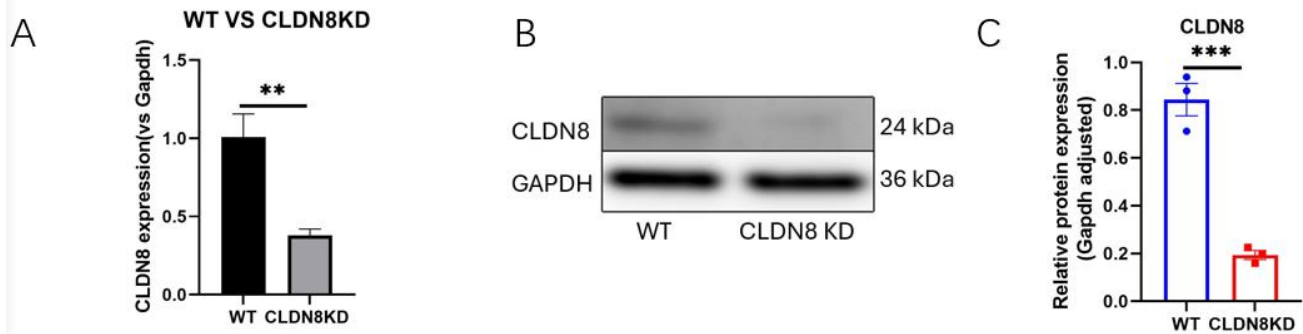


Figure 6.3.6 illustrates the knockdown efficiency of the CLDN8 gene in TY10 and hCMEC/D3 endothelial cells. Panel A shows the relative expression of CLDN8 mRNA in TY10 cells analysed by qPCR, indicating a significant reduction in CLDN8 expression in the CLDN8 knockdown group (CLDN8 KD) compared to the wild type ($p < 0.01$). Panels B and C depict the Western blot results for CLDN8 protein expression in hCMEC/D3 cells.

6.3.7 Adhesion of Endothelial Cells

To evaluate the impact of Claudin-8 (CLDN8) knockdown and Artemisinin treatment on endothelial cell adhesion, we used human brain microvascular endothelial cells (hCMEC/D3) and TY10 cells to perform adhesion assays. The goal was to understand how these factors influence the adhesion behaviour of endothelial cells that form the BBB.

The first figure (Figure 6.3.7a) shows the adhesion capacity of hCMEC/D3 and TY10 endothelial cells in control groups and after CLDN8 knockdown. The results demonstrated that CLDN8 knockdown significantly reduced the adhesion capacity in both endothelial cell lines. Specifically, compared to control, the number of adherent cells in the CLDN8 knockdown group for hCMEC/D3 was significantly reduced ($p < 0.0001$), and TY10 cells also exhibited a similar significant reduction ($p < 0.001$).

The second figure (Figure 6.3.7b) illustrates the effect of Artemisinin (10 μ M) on the adhesion of hCMEC/D3 and TY10 endothelial cells, as well as their CLDN8 knockdown variants. The results indicate that Artemisinin treatment significantly reduced cell adhesion regardless of CLDN8 knockdown status. Specifically, the number of adherent hCMEC/D3 and TY10 cells significantly decreased following Artemisinin treatment ($p < 0.001$ and $p < 0.01$, respectively). Similarly, Artemisinin effectively reduced adhesion in CLDN8 knockdown cells ($p < 0.05$).

6.3.8 Scratch Wound Healing Assay Results for Endothelial Cells

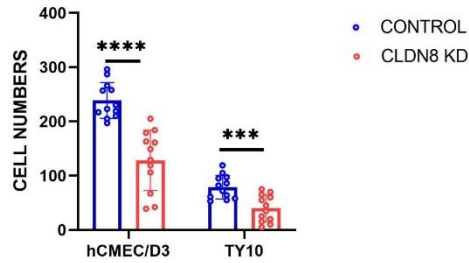
To evaluate the impact of CLDN8 knockdown and Artemisinin treatment on endothelial cell migration, scratch wound healing assays were performed on two endothelial cell lines: hCMEC/D3 and TY10. The rate of cell migration was compared between wild-type and CLDN8 knockdown endothelial cells, as well as in the presence or absence of Artemisinin treatment, to assess whether Artemisinin influences endothelial cell migration and how CLDN8 plays a role in this process.

The first figure (Figure 6.3.8a) depicts the effect of CLDN8 knockdown on the migration rate of hCMEC/D3 and TY10 cells. The results show that the migration rate was significantly reduced in both CLDN8 knockdown hCMEC/D3 and TY10 cells compared to the wild-type cells ($p < 0.05$). This suggests that CLDN8 may play an important role in promoting endothelial cell migration, and its knockdown impairs the migration potential of both cell types.

The second figure (Figure 6.3.8b) shows the effect of Artemisinin (10 μ M) on the migration rates of both endothelial cell lines (hCMEC/D3 and TY10) and their corresponding CLDN8 knockdown variants. Interestingly, no significant

differences in migration rates were observed in any of the cells after Artemisinin treatment, regardless of CLDN8 expression. These results suggest that Artemisinin may not have a notable effect on endothelial cell migration, and the presence or absence of CLDN8 does not appear to modulate this response.

A



B

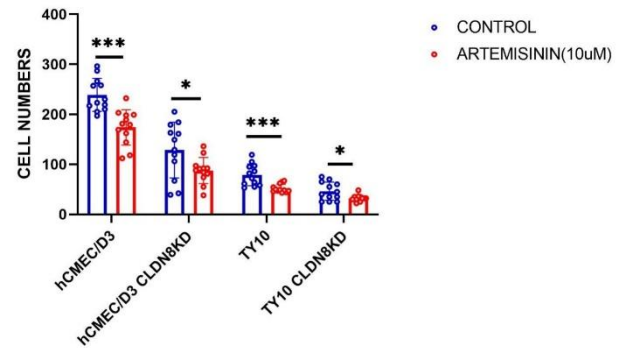
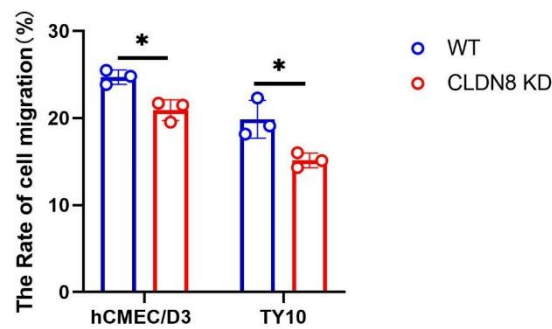


Figure 6.3.7 (A) Number of adherent hCMEC/D3 and TY10 endothelial cells in control and CLDN8 knockdown groups. Results show that CLDN8 knockdown significantly reduces adhesion capacity (hCMEC/D3: $p < 0.0001$; TY10: $p < 0.001$). (B) Effect of Artemisinin (10 μM) on the number of adherent hCMEC/D3 and TY10 endothelial cells and their CLDN8 knockdown variants (hCMEC/D3: $p < 0.001$; TY10: $p < 0.01$).

A



B

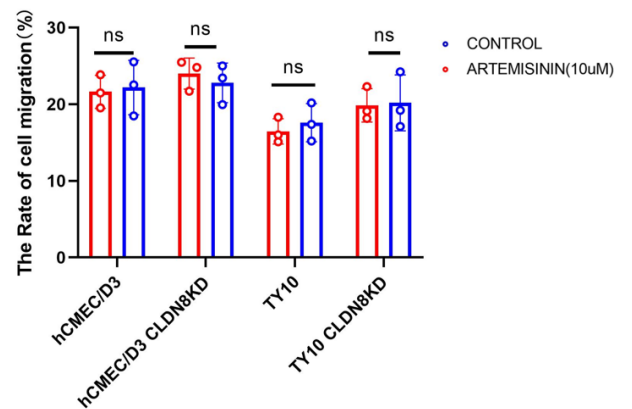


Figure 6.3.8 (A) Migration rate of hCMEC/D3 and TY10 cells with CLDN8 knockdown compared to wild-type. Significant reduction in migration rate is observed in both CLDN8 knockdown cell lines ($p < 0.05$). (B) Migration rate of hCMEC/D3 and TY10 cells with or without Artemisinin (10 μM) treatment. No significant differences were observed after Artemisinin treatment across all tested cells.

6.3.9 TNBC Cell Invasion Assay Across Endothelial Cell Monolayers

To study the invasion capability of triple-negative breast cancer (TNBC) cells through endothelial cell monolayers, we used 3000 MDA-MB-231 TNBC cells under different conditions over a period of 72 hours. Through the two figures (Figure 6.3.9a and Figure 6.3.8b), we analysed the effects of CLDN8 knockdown and Artemisinin treatment on TNBC cell penetration through endothelial cell monolayers.

Figure 6.3.9 (A) shows the changes in TNBC cell invasion numbers after knocking down CLDN8 in hCMEC/D3 and TY10 endothelial cells. Compared to the control group, CLDN8 knockdown significantly increased the number of TNBC cells penetrating the hCMEC/D3 and TY10 endothelial cells. In hCMEC/D3 cells, CLDN8 knockdown increased the number of invading cells approximately threefold ($p < 0.0001$). In TY10 cells, CLDN8 knockdown also significantly enhanced TNBC cell invasion ($p < 0.05$). These results indicate that CLDN8 in endothelial cells may play a role in maintaining barrier function, and knocking down CLDN8 weakens the barrier, thereby promoting cancer cell invasion.

Figure 6.3.8 (B) shows the effect of Artemisinin (10 μ M) treatment on hCMEC/D3 and TY10 endothelial cells, as well as their CLDN8 knockdown variants. Although the presence of CLDN8 greatly affects the permeability of endothelial cells, Artemisinin treatment significantly reduced the ability of TNBC cells to penetrate the BBB. Under Artemisinin treatment, the number of TNBC cells invading hCMEC/D3 and TY10 cells, as well as their CLDN8 knockdown variants, was significantly reduced ($p < 0.0001$ to $p < 0.01$). This indicates that although CLDN8 knockdown weakens the barrier function of endothelial cells, Artemisinin, through its unique mechanism of action, can effectively reduce the number of cancer cells penetrating the BBB.

In summary, although the absence of CLDN8 leads to reduced barrier function in endothelial cells, simultaneous Artemisinin treatment of breast cancer cells and endothelial cells still significantly decreases the number of TNBC cells crossing the BBB. Therefore, Artemisinin treatment does not increase the risk of breast cancer metastasis; instead, it may reduce the likelihood of cancer cells invading brain tissue through its inhibitory mechanism.

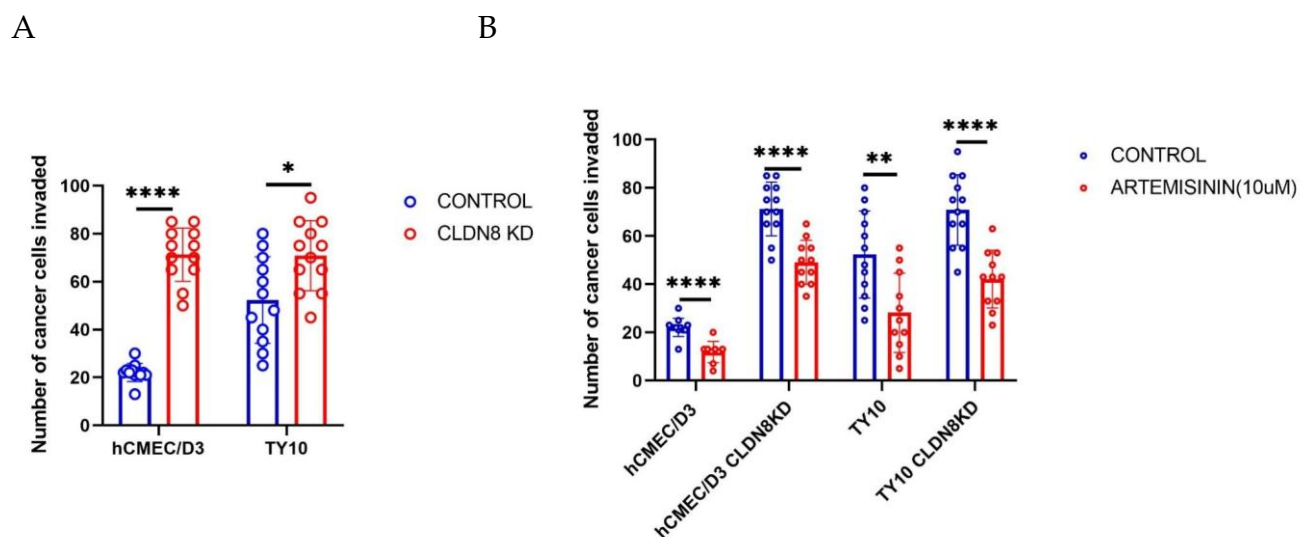


Figure 6.3.9 (A) The impact of CLDN8 on the invasion of TNBC (MDA-MB-231) cells through endothelial cell monolayers formed by hCMEC/D3 and TY10. (B) The effect of Artemisinin (10 μM) treatment on TNBC (MDA-MB-231) cell invasion through endothelial cell monolayers formed by hCMEC/D3 and TY10. (**p < 0.01, ****p < 0.0001)

6.3.10 Impact of Artemisinin Treatment on TEER and Paracellular Permeability of Endothelial Cells

Figures 6.3.10A to 6.3.10D show TEER measurements over a period of 150 minutes. TEER values were used to assess the barrier integrity of hCMEC/D3 and TY10 endothelial cells, as well as their CLDN8 knockdown variants, in the presence or absence of Artemisinin treatment. Figure 6.3.10A shows the effect of Artemisinin on hCMEC/D3 wild-type cells, where TEER values significantly decreased ($p < 0.0001$). The TEER values began to decline as early as 15 minutes post-treatment and continued to decrease throughout the experimental timeframe, indicating that Artemisinin compromises the tight junction integrity in hCMEC/D3 wild-type cells. Figure 6.3.10B shows the effect of Artemisinin on hCMEC/D3 CLDN8 knockdown cells, where no significant changes were observed. This suggests that Artemisinin's ability to reduce TEER may depend on the presence of CLDN8. Figure 6.3.10C shows a significant reduction in TEER for TY10 wild-type cells treated with Artemisinin ($p < 0.0001$), consistent with the observations in hCMEC/D3 wild-type cells, indicating that Artemisinin similarly weakens tight junction integrity. Figure 6.3.10D shows that TY10 CLDN8 knockdown cells also experienced a reduction in TEER; however, it was less pronounced compared to the wild-type cells, suggesting that CLDN8 plays a role in maintaining barrier integrity, though other factors may also influence Artemisinin's effect.

Figures 6.3.10E to 6.3.10H illustrate the effect of Artemisinin on the paracellular permeability (PCP) of hCMEC/D3 and TY10 cells. PCP was assessed by measuring the permeability of FITC-dextran across the cell monolayer. Figure 6.3.10E shows that paracellular permeability significantly increased in hCMEC/D3 wild-type cells treated with Artemisinin ($p < 0.0001$), with the trend continuing throughout the experiment, indicating that Artemisinin effectively disrupts tight junctions, resulting in increased permeability. Figure 6.3.10F shows that hCMEC/D3 CLDN8 knockdown cells exhibited a less pronounced increase in permeability following Artemisinin

treatment, further supporting the idea that CLDN8 is a critical determinant of barrier function in hCMEC/D3 cells. Figure 6.3.10G shows a similar increase in PCP for TY10 wild-type cells, consistent with the TEER findings, suggesting that Artemisinin significantly impacts cell monolayer integrity ($p < 0.0001$). Figure 6.3.10H presents PCP data for TY10 CLDN8 knockdown cells, where a slight increase in permeability was observed at 15 minutes ($p < 0.05$). This suggests that Artemisinin-induced increases in permeability are partially dependent on CLDN8 expression in TY10 cells.

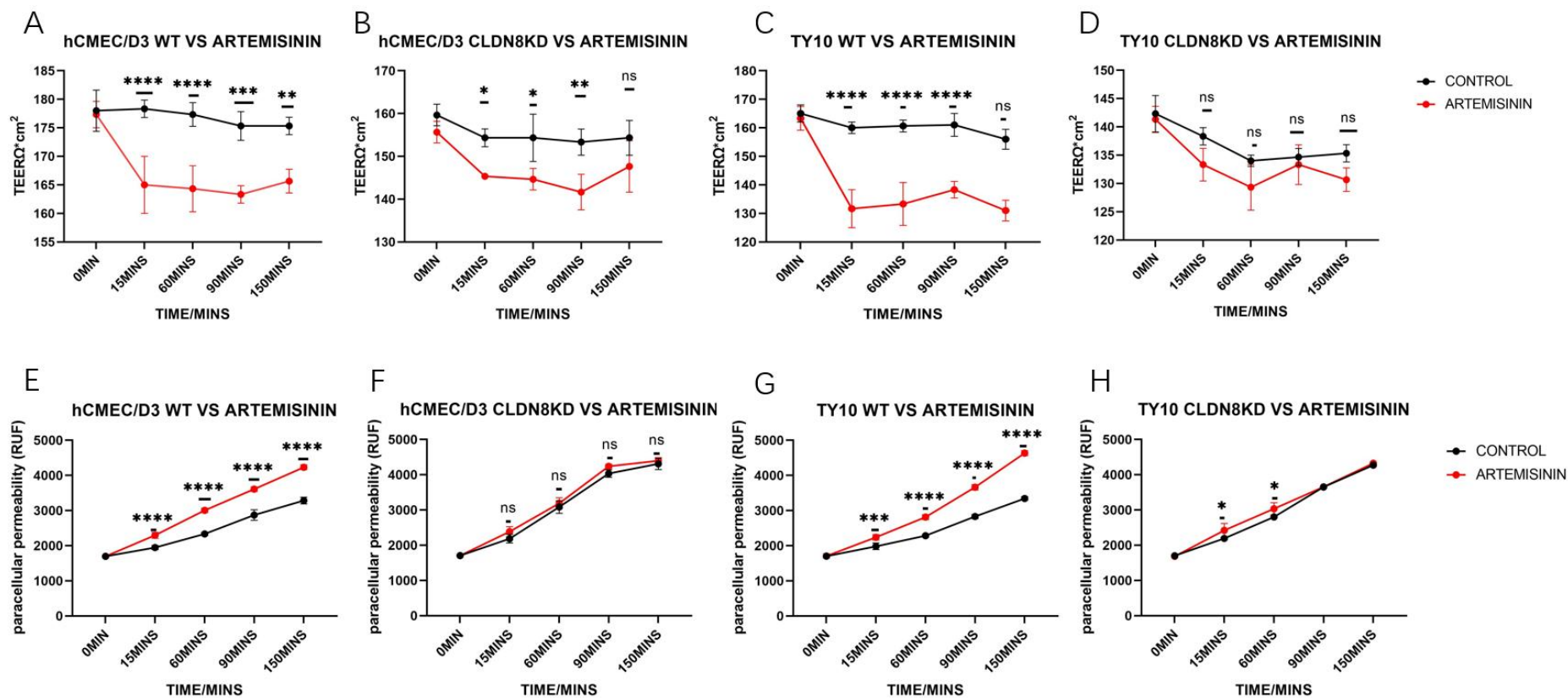


Figure 6.3.10: Effects of Artemisinin on TEER and Paracellular Permeability (PCP) of hCMEC/D3 and TY10 Endothelial Cells. Figures A-D show the changes in TEER values of hCMEC/D3 and TY10 cells under Artemisinin treatment, assessing cell barrier integrity. Figures E-H demonstrate the effect of Artemisinin on the paracellular permeability of hCMEC/D3 and TY10 cells. TEER ($\Omega \cdot \text{cm}^2$) and PCP changes after treatment. Data are presented as mean \pm SEM from $n = 3$ independent experiments.

6.3.11 Combined Treatment of Brain Metastatic Breast Cancer with Artemisinin

This experiment aims to explore whether Artemisinin can enhance the permeability of the BBB and evaluate its potential in the combined treatment of brain metastatic breast cancer.

A Transwell experiment using an 8 μm pore diameter Transwell chamber to simulate the BBB environment was used, allowing us to better observe the effect of Artemisinin on the tight junctions of brain endothelial cells. The 8 μm chamber was specifically chosen because a smaller pore size of 0.4 μm would physically limit passage, making it difficult to accurately assess the effect of Artemisinin on endothelial tight junctions.

In the experiment, 60,000 hCMEC/D3 human brain endothelial cells were seeded in the upper chamber and cultured overnight to form a dense monolayer, mimicking the BBB environment. In the lower chamber, 5,000 breast cancer cells were added to evaluate their ability to penetrate the endothelial monolayer.

To investigate the synergistic therapeutic effect of Artemisinin, we added Artemisinin (10 μM) along with different drug combinations in the upper chamber, including paclitaxel (2 μM) and cisplatin (10 μM) for triple-negative breast cancer cells (MDA-MB-231), and neratinib (10 nM) and lapatinib (10 nM) for HER2-positive breast cancer cells (SKBR3). After three days of exposure to both Artemisinin and the drugs, cell viability was assessed using the MTT assay to determine the anticancer effects of the drugs and the potential synergistic effect of Artemisinin.

The results showed that, in the case of MDA-MB-231 triple-negative breast cancer cells, the combination of Artemisinin with either paclitaxel or cisplatin

significantly reduced cell viability, demonstrating a pronounced synergistic anticancer effect. Similarly, for HER2-positive breast cancer cells (SKBR3), the combination of Artemisinin with either neratinib or lapatinib also significantly reduced cell viability, indicating an enhancement of the anti-HER2 therapeutic effect.

These findings suggest that Artemisinin can influence the structure of tight junctions in brain endothelial cells, thereby increasing the permeability of the BBB. This effect not only helps drugs pass through the BBB to more effectively reach brain metastases but also exhibits synergistic anticancer effects without increasing the risk of cancer metastasis. This provides new insights and potential feasibility for the application of Artemisinin as an adjuvant in the treatment of brain metastatic breast cancer. Further research will focus on elucidating the specific mechanisms through which Artemisinin enhances drug delivery to brain tumours and its clinical application value.

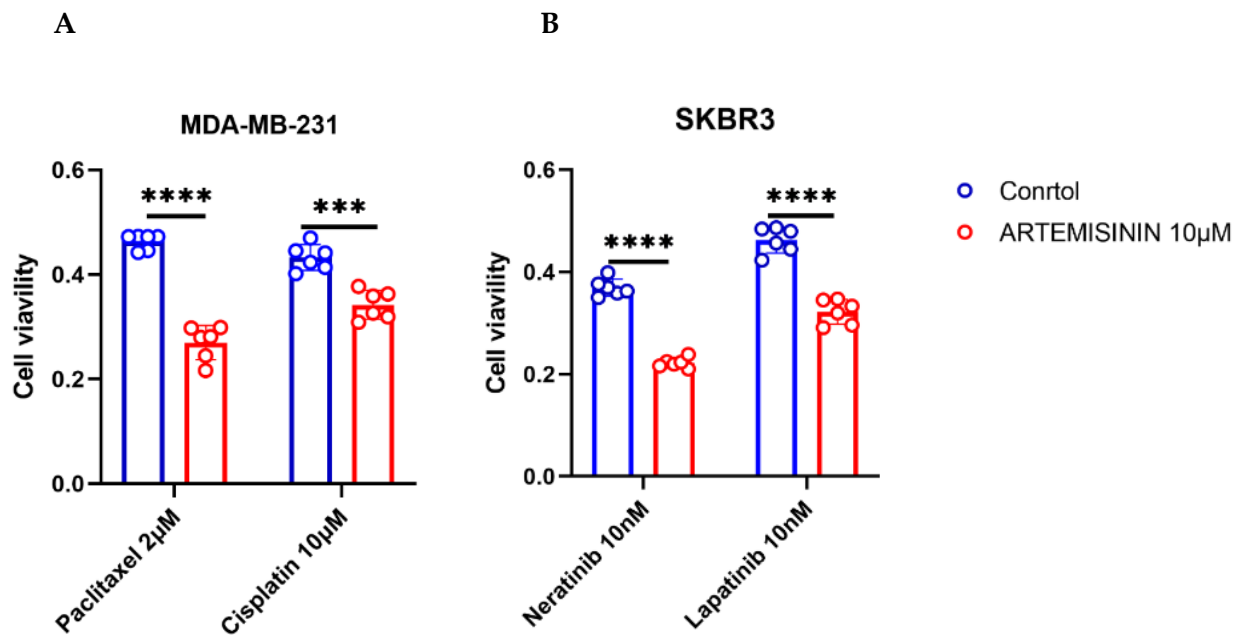


Figure 6.3.11 In the triple-negative breast cancer cell line MDA-MB-231, Artemisinin (10µM) was combined with the chemotherapy drugs paclitaxel (2µM) and cisplatin (10µM), respectively (A). In HER2-positive breast cancer cells SKBR3, Artemisinin (10µM) was combined with the anti-HER2 drugs neratinib (10nM) and lapatinib (10nM), respectively (Figure 6.3.11B). Compared to the control group, the combination with Artemisinin significantly reduced cell viability ($p < 0.0001$).

6.4 Discussion

This chapter aimed to elucidate the dual role of Artemisinin in breast cancer brain metastasis treatment, focusing on its impact on both breast cancer cells and the BBB formed by endothelial cells. The study reveals that while Artemisinin shows promise in facilitating drug delivery through the BBB by altering endothelial cell tight junction integrity, it also affects breast cancer cell behaviour in a complex manner.

Artemisinin's ability to downregulate Claudin-8 (CLDN8) was a critical finding, given CLDN8's significant role in maintaining BBB integrity. TEER and PCP analyses indicated that Artemisinin treatment led to reduced

transendothelial electrical resistance and increased permeability across both hCMEC/D3 and TY10 endothelial cells. This reduction in barrier function was more pronounced in wild-type cells, suggesting a key involvement of CLDN8 in maintaining endothelial integrity. Importantly, Artemisinin's influence on permeability was substantially diminished in CLDN8 knockdown variants, underscoring the dependency of Artemisinin's effect on CLDN8 presence.

In breast cancer cells, CLDN8 knockdown experiments demonstrated that CLDN8 contributes differently to cell adhesion, migration, and invasion capabilities depending on the cancer subtype. Specifically, breast cancer cell lines such as SKBR3 and MDA-MB-231 showed significant reductions in adhesion ability when CLDN8 was knocked down, whereas others like MCF-7 and MDA-MB-361 did not exhibit the same effect. This indicates a subtype-specific role for CLDN8 in mediating adhesion, which could have implications for the aggressiveness and metastatic potential of these cells.

Migration and invasion assays also revealed important insights into Artemisinin's effects on breast cancer cells. The scratch wound healing assay indicated that Artemisinin treatment significantly inhibited cell migration, an effect that was observed irrespective of CLDN8 expression levels. This suggests that the anti-migratory effect of Artemisinin operates through mechanisms independent of CLDN8, positioning Artemisinin as a potential anti-metastatic agent.

Furthermore, the transwell invasion assay showed that CLDN8 knockdown enhanced the invasive capabilities of breast cancer cells, likely due to a loss of barrier integrity that facilitates tumour cell migration. However, Artemisinin treatment reduced invasion across both wild-type and CLDN8 knockdown variants, implying that Artemisinin could counteract some of the adverse effects associated with reduced CLDN8 expression. This finding is

particularly promising, as it indicates that Artemisinin may mitigate the risk of further metastasis even when tight junctions are compromised.

Endothelial cell experiments mirrored these findings in terms of adhesion and migration, emphasizing the importance of CLDN8 in maintaining endothelial barrier properties. CLDN8 knockdown in endothelial cells reduced cell adhesion and migration, highlighting the role of CLDN8 in maintaining cellular cohesion and motility. Interestingly, while Artemisinin treatment significantly reduced the adhesive capacity of endothelial cells, it did not notably affect migration, suggesting a selective effect on cellular functions related to the BBB.

The invasion experiments using TNBC cells penetrating the BBB model provided critical insights into the safety of using Artemisinin for patients with breast cancer brain metastasis. Despite a compromised endothelial barrier due to CLDN8 knockdown, Artemisinin still effectively reduced the number of cancer cells crossing the barrier. This strongly indicates that while Artemisinin enhances BBB permeability for drug delivery, it does not necessarily increase the risk of metastasis, providing a dual benefit in terms of improving drug access to the brain while limiting cancer cell invasion.

To further explore the potential of Artemisinin in combination therapy, an additional experiment was conducted to evaluate its effect on breast cancer cell viability when combined with various drugs. The experiment selected two breast cancer cell lines prone to brain metastasis: triple-negative breast cancer cells MDA-MB-231 and HER2-positive breast cancer cells SKBR3. We investigated the anticancer effects of Artemisinin combined with different drugs on these two cell lines. In the triple-negative breast cancer cell line MDA-MB-231, Artemisinin (10 μ M) was combined with the chemotherapy drugs paclitaxel (2 μ M) and cisplatin (10 μ M), respectively (Figure 6.3.11A).

The results showed that, compared to the control group, the combination with Artemisinin significantly reduced cell viability ($p < 0.0001$), indicating that Artemisinin enhances the cytotoxic effect of chemotherapy drugs on MDA-MB-231 cells. In HER2-positive breast cancer cells SKBR3, Artemisinin (10 μM) was combined with the anti-HER2 drugs neratinib (10 nM) and lapatinib (10 nM), respectively (Figure 6.3.11B). Compared to the control group, the combination with Artemisinin significantly reduced cell viability ($p < 0.0001$), suggesting that Artemisinin also significantly enhances the efficacy of anti-HER2 drugs. Overall, the results indicate that Artemisinin, when combined with different types of chemotherapy and targeted drugs, significantly enhances their anticancer effects, demonstrating potential for treating breast cancer brain metastasis.

In summary, this chapter highlights the potential of Artemisinin as a therapeutic agent for breast cancer brain metastasis through its dual effect on both endothelial and cancer cells. Artemisinin effectively enhances BBB permeability, potentially improving drug delivery to metastatic sites while also exhibiting anti-adhesive, anti-migratory, and anti-invasive effects on breast cancer cells. However, the downregulation of tight junction proteins like CLDN8 requires careful consideration, as it could inadvertently enhance cancer cell invasiveness. The balance between these effects must be carefully managed, and further studies are required to optimize Artemisinin's use in clinical settings, ensuring both effective drug delivery and minimal risk of metastasis.

**Chapter VII: Protein-Level Effects of
Artemisinin on Tight Junctions and the Wnt/ β -
Catenin Pathway: Potential Role in Breast Cancer
Metastasis**

7.1 Introduction

Tight junctions are a crucial form of intercellular connection, playing a key role in regulating cell polarity, maintaining tissue integrity, and preventing the free passage of extracellular factors across the cell layer. Claudin-8 (CLDN8) is one of the primary proteins constituting tight junctions and is essential for maintaining these biological barriers. Recent studies have shown that CLDN8 plays a critical role in the progression of various diseases, particularly in the invasiveness and metastasis of tumours.

Artemisinin has gained widespread attention for its broad biological activities, particularly its potential in antimalarial and anticancer treatments. While its mechanisms of action in cell death and survival pathways have been extensively studied, the specific mechanisms by which Artemisinin affects cell junctions and communication remain unclear. Brain metastasis of breast cancer is a serious clinical issue, and understanding the molecular mechanisms influencing this process is crucial for developing new therapeutic strategies.

In our previous chapters, we discovered through QPCR that Artemisinin treatment significantly reduced the expression of CLDN8 in CMEC/D3 cells. Additionally, the decrease in CLDN8 was associated with a marked impairment in tight junction function. Specifically, Artemisinin-induced reduction of CLDN8 expression directly affected the integrity of tight junctions, increasing cell permeability. Clinical data further support these findings. In Chapter 5, we analysed clinical samples from breast cancer patients and found that those with low CLDN8 expression were more likely to develop lymph node metastasis and had significantly shorter survival times. These data suggest that CLDN8 not only plays an essential role in

maintaining cell structure but is also closely related to tumour invasiveness and prognosis.

This study aims to explore how Artemisinin modulates tight junction functions in brain endothelial cells and breast cancer cells by affecting CLDN8 and related proteins such as β -catenin (CTNNB1) and glycogen synthase kinase 3 beta (GSK3 β). Using Western blot and protein array technologies, we analysed the impact of Artemisinin treatment on the expression levels of CLDN8, β -catenin, and GSK3 β in CMEC/D3 brain endothelial cells and breast cancer cell lines (, MCF7, MDA-MB-361, SKBR3, MDA-MB-231). We employed subcellular fractionation analysis and co-immunoprecipitation to determine the precise localization of these proteins within cells and their potential interactions. Additionally, functional assays such as permeability tests were used to assess the impact of Artemisinin on cell barrier function. Through these studies, we aim to elucidate the mechanisms by which Artemisinin regulates tight junction proteins and affects the behaviour of related cancer cells, thereby providing new insights and strategies for breast cancer treatment.

To further clarify the relationship between CLDN8 and β -catenin, we examined their subcellular localization and found that both proteins were expressed at the cell membrane. This suggests that they may physically interact or work in coordination to maintain membrane stability and the integrity of tight junctions. Our recent findings also indicate that Artemisinin treatment of D3 endothelial cells led to a significant reduction in the phosphorylation of GSK3 β at Ser9, a site known to inhibit its activity. The reduction in Ser9 phosphorylation suggests activation of GSK3 β , which is crucial for the degradation of β -catenin. Specifically, when GSK3 β is active, it phosphorylates β -catenin at Thr41/Ser45, tagging it for proteasomal

degradation. This mechanism aligns with our observation that Artemisinin treatment not only increases the phosphorylation of β -catenin at these sites but also leads to its subsequent degradation. The data suggest that the regulation of β -catenin degradation by GSK3 β is a key downstream effect of CLDN8 reduction, as CLDN8 likely plays a role in maintaining β -catenin stability at the cell membrane. When CLDN8 expression is reduced, β -catenin may dissociate from the membrane and become more susceptible to cytoplasmic degradation.

These findings suggest that the Artemisinin-induced reduction in CLDN8 expression affects the localization and stability of β -catenin, potentially leading to its translocation from the cell membrane to the cytoplasm, where it is targeted for degradation by GSK3 β . This regulation of β -catenin through the GSK3 β pathway highlights a complex interplay between tight junction integrity and intracellular signalling pathways involved in cancer progression.

The Wnt/ β -catenin signalling pathway is also implicated in this process, as GSK3 β is a well-known regulator within this pathway. In the absence of Wnt signalling, GSK3 β remains active and promotes the phosphorylation and degradation of β -catenin, preventing it from accumulating in the nucleus and activating transcriptional programs associated with cell proliferation and survival. Our data suggest that Artemisinin may enhance GSK3 β activity by reducing its inhibitory phosphorylation at Ser9, thereby promoting β -catenin degradation and potentially attenuating Wnt signalling. This attenuation of Wnt signalling could contribute to the observed reduction in cell migration and invasion, making Artemisinin a promising candidate for reducing metastatic potential in breast cancer.

Overall, this chapter aims to provide a deeper understanding of how Artemisinin affects CLDN8, β -catenin, and GSK3 β , and the subsequent impact on cell behavior and signaling pathways. By elucidating these mechanisms, we hope to provide a scientific basis for the potential clinical use of Artemisinin in targeting both breast cancer cells and the endothelial barriers they encounter during metastasis.

7.2 Materials and Methods

7.2.1 Cell Culture

Cell Lines: The study involved CMEC/D3 brain endothelial cells and several breast cancer cell lines: MCF7, MDA-MB-361, SKBR3, and MBA231, representing different breast cancer subtypes.

Culture Conditions: All cells were cultured in Dulbecco's Modified Eagle Medium (DMEM), supplemented with 10% *foetal* bovine serum (FBS), 1% penicillin-streptomycin, and 1% L-glutamine. The cells were maintained at 37°C in a humidified atmosphere with 5% CO₂.

7.2.2 Treatments

Artemisinin Treatment: Cells were treated with Artemisinin at a final concentration of 1 μ M for 24 hours to investigate its effect on CLDN8, β -catenin, and other related proteins.

CLDN8 Knockdown: Knockdown of CLDN8 was performed using small interfering RNA (siRNA, Sc:44865) transfected into cells with Lipofectamine 2000 according to the manufacturer's protocol.

7.2.3 Western Blot (WB) Analysis

Protein Extraction: Total proteins were extracted by lysing cells in RIPA buffer supplemented with protease and phosphatase inhibitors to ensure protein stability and accurate downstream analysis.

Protein Quantification: The protein concentrations of the lysates were quantified using the BCA protein assay.

SDS-PAGE and Transfer: Equal amounts of proteins were separated by SDS-PAGE and transferred to PVDF membranes for further analysis.

Blocking and Incubation: Membranes were blocked with 5% non-fat milk and then incubated overnight at 4°C with primary antibodies, including:

Anti-CLDN8 (1:1000, Abcam, Cambridge, UK)

Anti- β -catenin (1:1000, Merck, formerly Sigma-Aldrich, Darmstadt, Germany)

Anti-GSK3 β (1:1000, Cell Signalling, Danvers, MA, USA)

Anti-ZO1 (1:1000, Merck, formerly Sigma-Aldrich, Darmstadt, Germany)

Anti-GAPDH (1:1000, Merck, formerly Sigma-Aldrich, Darmstadt, Germany)

Secondary Antibodies: The blots were incubated with HRP-conjugated secondary antibodies for 1 hour at room temperature.

Detection: Protein bands were visualized using an enhanced chemiluminescence (ECL) detection reagent, with signals quantified to assess the relative expression levels.

7.2.4 Protein Array

Sample Preparation: Protein samples from untreated cells (WT), Artemisinin-treated cells, and CLDN8 knockdown CMEC/D3 cells were collected and analysed.

Data Analysis: Differential expression of proteins, including phosphorylation sites, was analysed, providing insights into Artemisinin's effect on protein interactions and modifications.

7.2.5 Subcellular Fractionation

Fractionation Protocol: Cells were fractionated into cytoplasmic, membrane, cytoskeletal, soluble nuclear, and nuclear components using a subcellular protein fractionation kit (Thermo Fisher).

Western Blot: Each fraction was analysed using Western blot to detect β -catenin, ZO1, and other relevant markers, allowing for the determination of protein localization changes.

7.2.6 Immunofluorescence (IFC)

Cell Fixation: Cells were fixed using 4% paraformaldehyde for 15 minutes to preserve cellular structures.

Permeabilization and Blocking: Cells were permeabilized with 0.1% Triton X-100 and blocked using 5% bovine serum albumin (BSA) to prevent nonspecific binding.

Primary and Secondary Antibodies: Cells were incubated overnight at 4°C with primary antibodies against CLDN8, β -catenin, and ZO1. Fluorescently labelled secondary antibodies were used for visualization, followed by mounting with DAPI-containing medium.

Imaging: Cells were imaged using a fluorescence microscope to analyse the localization and expression of targeted proteins.

7.2.7 Co-Immunoprecipitation (Co-IP)

Preparation: Cells were lysed in IP lysis buffer to extract total proteins.

Antibody Incubation: Lysates were incubated overnight at 4°C with an anti- β -catenin antibody or IgG control to precipitate β -catenin and associated complexes.

Protein A/G Beads: Protein A/G beads were used to pull down antibody-protein complexes, followed by washing and elution for further analysis via Western blot.

7.2.8 Kinexus Phosphoprotein Array

Phosphorylation Profiling: To assess changes in the phosphorylation of proteins, including β -catenin and GSK3 β , we used Kinexus phosphoprotein arrays.

Sample Preparation: Protein concentrations were measured, and equal amounts (100 μ g) from each sample were labelled with a proprietary fluorescent dye.

Hybridization and Detection: Labelled protein samples were hybridized to the phosphoprotein arrays, and changes in fluorescence intensities were measured to identify significant changes in phosphorylation.

Data Interpretation: Changes in phosphorylation levels were reported as percentage changes compared to controls, and significance was assessed using the Z-score.

7.3 Results

7.3.1 Artemisinin Reduces CLDN8 Expression in CMEC/D3 Cells

In this section, we explored the effect of Artemisinin treatment and CLDN8 knockdown on Claudin-8 (CLDN8) protein expression in CMEC/D3 cells. The Western blot analysis was conducted to determine whether Artemisinin modulates CLDN8 levels, either independently or synergistically with CLDN8 knockdown. We analysed CLDN8 expression under four distinct conditions: untreated CMEC/D3 cells (WT), Artemisinin-treated CMEC/D3 cells (WT + Artemisinin), CLDN8 knockdown cells (CLDN8 KD), and CLDN8 knockdown cells treated with Artemisinin (CLDN8 KD + Artemisinin). Results revealed a substantial reduction in CLDN8 protein levels following Artemisinin treatment, with an even more pronounced effect observed in the CLDN8 knockdown groups. Western blot images demonstrated that CLDN8 protein, typically present at approximately 27 kDa, was significantly diminished after treatment with Artemisinin alone and almost completely absent when Artemisinin was combined with CLDN8 knockdown. GAPDH, used as a loading control and appearing at 36 kDa, confirmed consistent protein loading across all samples. The corresponding bar graph quantitatively illustrated these effects, showing that both Artemisinin treatment and CLDN8 knockdown significantly reduced CLDN8 expression relative to the untreated control. The group treated with both Artemisinin and CLDN8 knockdown displayed the lowest CLDN8 levels, indicating a possible additive or synergistic effect. Statistical analysis revealed highly significant differences in CLDN8 protein expression among the various treatment groups (**P<0.001, ****P<0.0001). These findings suggest that Artemisinin plays a

strong role in reducing CLDN8 levels, potentially contributing to the modulation of tight junction integrity in CMEC/D3 cells.

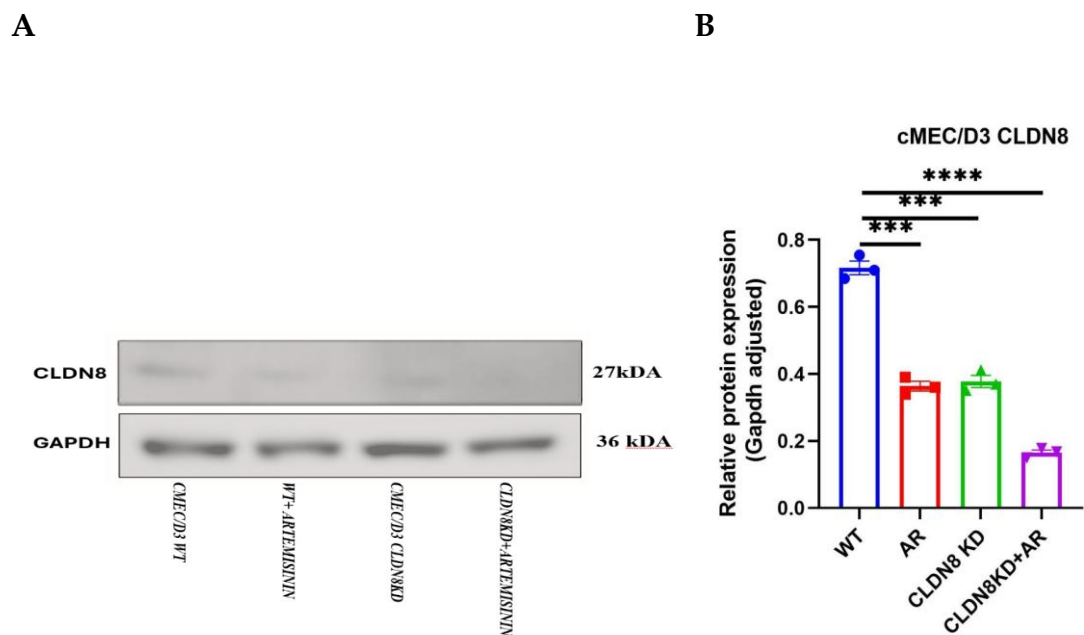


Figure 7.31 A) Effects of Artemisinin and CLDN8 Knockdown on CLDN8 Expression in hCMEC/D3 Cells. Western blot shows CLDN8 (~27 kDa) and GAPDH (~36 kDa, loading control) under four conditions: WT, WT + Artemisinin, CLDN8 KD, and CLDN8 KD + Artemisinin. CLDN8 expression decreases after Artemisinin treatment and is almost absent in the CLDN8 KD + Artemisinin group. B) Quantification of CLDN8 Expression. Bar graph (normalized to GAPDH) confirms significant CLDN8 reduction in all treatment groups compared to WT, with the lowest expression in the CLDN8 KD + Artemisinin group (**P<0.001, ****P<0.0001).

7.3.2 Artemisinin and CLDN8 Knockdown Affect β -catenin Expression

In this section, we aimed to identify downstream pathways impacted by CLDN8 knockdown (CLDN8KD) and Artemisinin treatment in CMEC/D3 cells. Initially, our goal was to broadly explore potential downstream targets, using Kinexus phosphoprotein arrays to compare the phosphorylation profiles between CLDN8KD or Artemisinin-treated CMEC/D3 cells and untreated wild-type (WT) cells. Interestingly, we identified β -catenin (CTNNB1) as a significant target, showing considerable changes in its phosphorylation status under both conditions (Table 7.3.1).

Table 7.3.2 illustrates the changes in multiple phosphorylation sites of β -catenin following CLDN8KD and Artemisinin treatment. In CLDN8KD cells, the phosphorylation levels of β -catenin at S552, S33+S37+T41+S45, Y654, and Y489 decreased by 15.17%, 20.59%, 38.58%, and 90.50%, respectively, with the most significant reduction occurring at the Y489 site (Z-Score: -4.30).

Similarly, Artemisinin treatment led to a reduction in β -catenin phosphorylation at S675, S33+S37+T41+S45, Y489, and Y654 by 14.64%, 19.92%, 17.31%, and 45.73%, respectively, with the Y654 site showing the most notable reduction (Z-Score: -1.08). These results indicate that both CLDN8KD and Artemisinin significantly affect the phosphorylation status of β -catenin, with particular emphasis on the Y489 site, which seems to play a crucial role in regulating β -catenin activity and related pathways.

The interaction between CLDN8 and β -catenin was further explored through enrichment analysis, which indicated that these proteins form part of a complex tight junction network involving occludens (TJP3). As depicted in Figure 7.3.2, β -catenin acts as a core node in this network, bridging CLDN8 and other members of the Claudin family via TJP3. This complex interaction supports the stability and integrity of tight junctions while also modulating dynamic changes in cell connections through phosphorylation events.

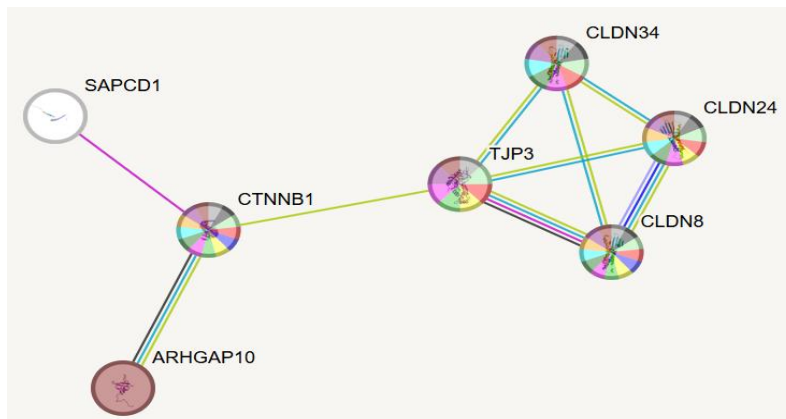
Our findings underscore the pivotal role of β -catenin in the context of tight junction stability and signalling. The reduced phosphorylation at critical sites, particularly Y489, suggests a regulatory mechanism that may influence both cell adhesion and signal transduction. The biological processes and pathways involving these interactions are significantly enriched in cell junction organization, tight junction assembly, and cell adhesion—highlighting the

importance of β -catenin and CLDN8 in maintaining cellular integrity and potentially modulating disease progression.

Table7.3.2: Phospho- β -catenin Profiling in hCMEC/D3 Cells Following Artemisinin Treatment

cMEC/D3 WT VS CLDN8KD								
No.	Target Name	Antibody P-Site	Cat No.	Average Normalized (531, control)	Average Normalized(532, CLDN8kd)	%CFC	Z-Score	Ratio
438	CTNNB1	S552	PN945	3224.557403	2735.267879	-15.17385063	-0.25918795	
435	CTNNB1	S33+S37+T41+S45	PN578	2361.148641	1874.957891	-20.59128094	-0.373748835	
439	CTNNB1	Y654	PN579	8119.202734	4986.975858	-38.57801041	-0.868695103	
437	CTNNB1	Y489	PN745	14813.53073	1407.170189	-90.50077788	-4.297684466	

cMEC/D3 WT VS ARTEMISININ								
No.	Target Name	Antibody P-Site	Cat No.	Average Normalized (531, control)	Average Normalized(532, CLDN8kd)	%CFC	Z-Score	Ratio
440	CTNNB1	S675	PN946	8818.959368	7528.056083	-14.63781872	-0.31372128	
435	CTNNB1	S33+S37+T41+S45	PN578	2361.148641	1890.690601	-19.92496498	-0.346344389	
437	CTNNB1	Y489	PN745	14813.53073	12249.57571	-17.30819658	-0.397488361	
439	CTNNB1	Y654	PN579	8119.202734	4406.058021	-45.73287346	-1.077413449	



Functional enrichments in your network

Note: some enrichments may be expected here (why?)

[explain columns](#)

Biological Process (Gene Ontology)				
GO-term	description	count in network	strength	false discovery rate
GO:0045216	Cell-cell junction organization	5 of 174	1.91	1.90e-05
GO:0007043	Cell-cell junction assembly	4 of 124	1.96	0.00046
GO:0070830	Bicellular tight junction assembly	3 of 49	2.24	0.0024
GO:0007155	Cell adhesion	5 of 965	1.16	0.0096

Cellular Component (Gene Ontology)				
GO-term	description	count in network	strength	false discovery rate
GO:0005923	Bicellular tight junction	5 of 127	2.04	5.31e-07
GO:0016327	Apicolateral plasma membrane	2 of 22	2.41	0.0107

Reference publications (PubMed)				
publication	(year) title	count in network	strength	false discovery rate
PMID:32668412	(2020) Analysis of the expression and genetic alteration of ...	4 of 25	2.65	0.00065
PMID:24009024	(2013) Emerging roles of claudins in human cancer.	4 of 79	2.15	0.0249
PMID:34482810	(2021) Cleavage of E-cadherin by porcine respiratory bacteri...	3 of 16	2.72	0.0435

Local network cluster (STRING)				
cluster	description	count in network	strength	false discovery rate
CL:21722	Claudin, and Positive regulation of blood-brain barrier perme...	4 of 29	2.59	1.04e-06
CL:21715	Mixed, incl. Cell-cell junction organization, and Bicellular tigh...	5 of 125	2.05	1.04e-06
CL:21757	Claudin	2 of 6	2.97	0.0020
CL:21724	Positive regulation of blood-brain barrier permeability, and C...	2 of 14	2.6	0.0066

KEGG Pathways				
pathway	description	count in network	strength	false discovery rate
hsa04670	Leukocyte transendothelial migration	4 of 111	2.01	1.28e-05
hsa04530	Tight junction	4 of 157	1.86	2.48e-05
hsa05160	Hepatitis C	4 of 157	1.86	2.48e-05
hsa04514	Cell adhesion molecules	3 of 138	1.79	0.0010
hsa05130	Pathogenic Escherichia coli infection	3 of 187	1.65	0.0020

(more ...)

WikiPathways				
pathway	description	count in network	strength	false discovery rate
WP4239	Epithelial to mesenchymal transition in colorectal cancer	3 of 160	1.72	0.0148
WP4905	1q21.1 copy number variation syndrome	2 of 27	2.32	0.0171

Annotated Keywords (UniProt)				
keyword	description	count in network	strength	false discovery rate
KW-0796	Tight junction	4 of 98	2.06	1.57e-05
KW-0965	Cell junction	5 of 809	1.24	0.00078
KW-1003	Cell membrane	6 of 3277	0.71	0.0286

(MEDIUM CONFIDENCE 0.400)

Figure 7.3.2 CLDN8 and β -catenin interact via TJP3 within the tight junction network, where β -catenin acts as a central node linking CLDN8 and other Claudin proteins. This interaction helps maintain junction integrity and modulates cell adhesion dynamics through β -catenin phosphorylation. Enrichment analysis highlights their involvement in key processes such as tight junction assembly and cell adhesion, underscoring the roles of CLDN8 and β -catenin in junction regulation and disease progression. β -catenin β -catenin β -catenin β -catenin

7.3.3 Artemisinin and CLDN8 Knockdown Differentially Regulate β -catenin Expression in Brain Endothelial and Breast Cancer Cells

In this section, we conducted Western blot analysis to validate the findings regarding β -catenin expression in CMEC/D3 and MCF7 cells under four different treatment conditions: Wild Type (WT), WT treated with Artemisinin (WT + Artemisinin), CLDN8 Knockdown (CLDN8KD), and CLDN8KD treated with Artemisinin (CLDN8KD + Artemisinin). The results demonstrated that in CMEC/D3 cells, β -catenin expression decreased significantly in both the WT + Artemisinin and CLDN8KD groups compared to the WT, but no further reduction was observed in the CLDN8KD + Artemisinin group. In contrast, in MCF7 cells, β -catenin expression decreased in the WT + Artemisinin and CLDN8KD groups compared to WT, and continued to decrease significantly in the CLDN8KD + Artemisinin group (Figure 7.3.3). These observations suggest that the regulation of β -catenin by Artemisinin in brain endothelial cells is dependent on the presence of CLDN8, whereas in breast cancer cells, Artemisinin's effect is independent of CLDN8.

Figure 7.3.3A shows the Western blot results for β -catenin expression in CMEC/D3 and MCF7 cells across the four treatment conditions. The quantitative analysis, presented in Figure 7.3.3B, reveals that in CMEC/D3 cells, β -catenin expression significantly decreased in both the WT + Artemisinin and CLDN8KD groups compared to WT ($***P < 0.001$), but there was no further decrease in the CLDN8KD + Artemisinin group (not significant). In MCF7 cells, β -catenin expression also significantly decreased in the WT + Artemisinin and CLDN8KD groups compared to WT ($***P < 0.001$) and continued to decrease in the CLDN8KD + Artemisinin group ($***P < 0.001$). These results indicate that although both Artemisinin and CLDN8 knockdown independently reduce β -catenin expression in CMEC/D3 and

MCF7 cells, their combined effect further reduces β -catenin expression only in MCF7 cells.

To extend these observations, we also analysed β -catenin expression in three additional breast cancer cell lines—MDA-MB-361, SKBR3, and MBA231—under two treatment conditions: CLDN8 Knockdown (CLDN8KD) and CLDN8KD treated with Artemisinin (CLDN8KD + Artemisinin). The results, shown in Figure 7.3.3A, indicate that in all tested breast cancer cell lines, the knockdown of CLDN8 followed by Artemisinin treatment resulted in a further reduction in β -catenin expression. The corresponding bar graph (Figure 7.3.3B) quantitatively shows the relative protein expression levels of β -catenin, normalized to GAPDH. Statistical analysis revealed that compared to CLDN8KD alone, the combination of Artemisinin treatment with CLDN8 knockdown significantly reduced β -catenin expression across all breast cancer cell lines (* $P < 0.005$, *** $P < 0.001$, **** $P < 0.0001$).

These findings support the hypothesis that CLDN8 modulates the response of β -catenin to Artemisinin in breast cancer cells. In brain endothelial cells, Artemisinin's effect on β -catenin seems to be contingent on CLDN8, whereas in breast cancer cells, Artemisinin continues to reduce β -catenin levels even in the absence of CLDN8.

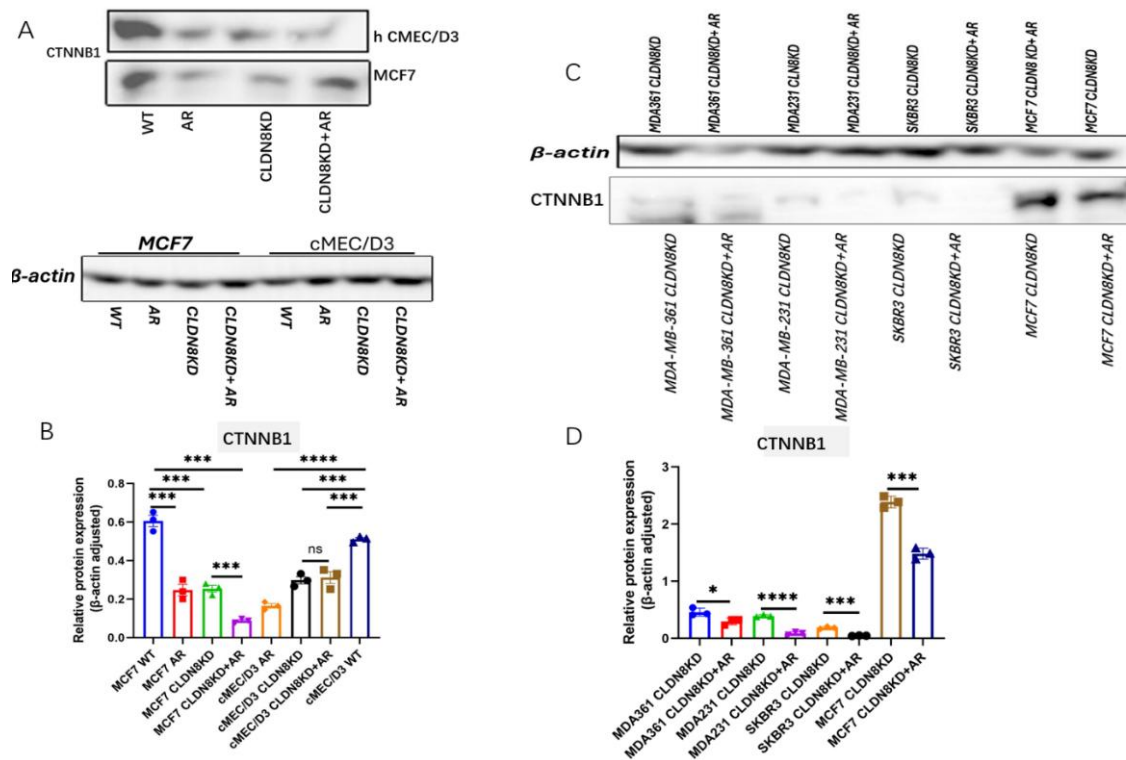


Figure 7.3.3 (A) Western blot analysis of β -catenin expression in CMEC/D3 and MCF7 cells under four conditions: WT, WT + Artemisinin (AR), CLDN8 knockdown (CLDN8KD), and CLDN8KD + AR. In CMEC/D3 cells, β -catenin expression decreased in both WT + AR and CLDN8KD groups, with no further reduction in the combined treatment. In MCF7 cells, β -catenin continued to decline in the CLDN8KD + AR group. (B) Quantification of β -catenin levels normalized to β -actin in CMEC/D3 and MCF7 cells. Significant differences are indicated (* $P < 0.05$, *** $P < 0.001$, **** $P < 0.0001$). (C) β -catenin expression in MDA-MB-361, SKBR3, and MBA231 cells under CLDN8KD and CLDN8KD + AR conditions. (D) Corresponding quantification showing that artemisinin further reduced β -catenin levels after CLDN8 knockdown in all three lines. (* $P < 0.05$, *** $P < 0.001$, **** $P < 0.0001$).

7.3.4 Subcellular Localisation of β -catenin in CMEC/D3 and MDA-231 Cells

To further understand the subcellular dynamics of β -catenin, we performed subcellular fractionation followed by Western blot analysis to determine its localization in CMEC/D3 and MDA-231 cells. The results showed that in both cell types, β -catenin was predominantly found in the membrane fraction, suggesting its crucial role in cell junctions.

In CMEC/D3 cells, β -catenin presented a strong signal in the membrane fraction, while weaker signals were detected in the cytoplasmic and cytoskeletal fractions, with minimal detection in the soluble nuclear fraction. This localization suggests that β -catenin's stable association with the endothelial cell membrane may be essential for maintaining tight junction integrity.

In contrast, β -catenin exhibited a broader distribution in MDA-231 cells, being present in multiple cellular fractions. Although β -catenin still predominantly localized to the membrane, it was also significantly found in the cytoplasmic and cytoskeletal fractions, indicating a more dynamic role for β -catenin in these breast cancer cells. The increased cytoplasmic presence in MDA-231 cells may reflect greater mobility of β -catenin, potentially affecting processes such as migration and invasion.

Notably, β -catenin was minimally detected in the soluble nuclear fraction in both cell types, suggesting limited nuclear activity under these conditions. These differences in subcellular localization between CMEC/D3 and MDA-231 cells highlight the specific functional roles of β -catenin in different contexts: maintaining tight membrane association in CMEC/D3 cells, while exhibiting broader functional distribution in MDA-231 cells.

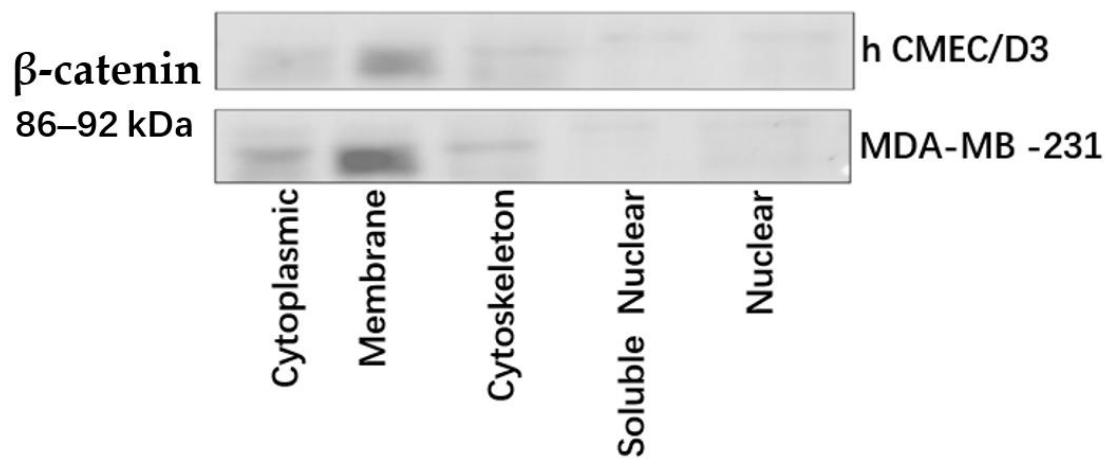


Figure 7.3.4 β -catenin (~92 kDa) was predominantly localized in the membrane fraction of both CMEC/D3 and MDA-231 cells, with much weaker signals in the cytoplasmic and cytoskeletal fractions and minimal nuclear presence. This indicates that β -catenin is mainly membrane-associated in both cell types.

7.3.5 Localization and Colocalization of ZO1 and CLDN8

In this section, we aimed to verify the membrane localization of CLDN8 in CMEC/D3 cells. However, direct detection of CLDN8 in membrane protein extracts was challenging, potentially due to the low expression levels of CLDN8 or the sensitivity limitations of the antibody used. As a result, we initially focused on confirming the localization of ZO1, a well-established marker of tight junctions, to the cell membrane using Western blot analysis.

The Western blot results showed that ZO1 was predominantly expressed in the membrane fraction, with minimal detection in the cytoplasmic, soluble nuclear, or nuclear fractions (Figure 7.3.5A). ZO1, which was detected at approximately 192 kDa, displayed a membrane-specific localization, supporting its role in maintaining tight junction integrity in endothelial cells.

To further investigate the localization of CLDN8, we used immunofluorescence (IFC) analysis, which revealed that CLDN8 colocalized with ZO1 on the cell membrane of CMEC/D3 cells (Figure 7.3.5B). The colocalization of CLDN8 and ZO1 suggests that these proteins are expressed at the same cellular site, indicating a potential interaction between them. This finding reinforces the concept that CLDN8 is an integral part of tight junctions and may interact with ZO1 to regulate tight junction function and cellular barrier integrity.

A

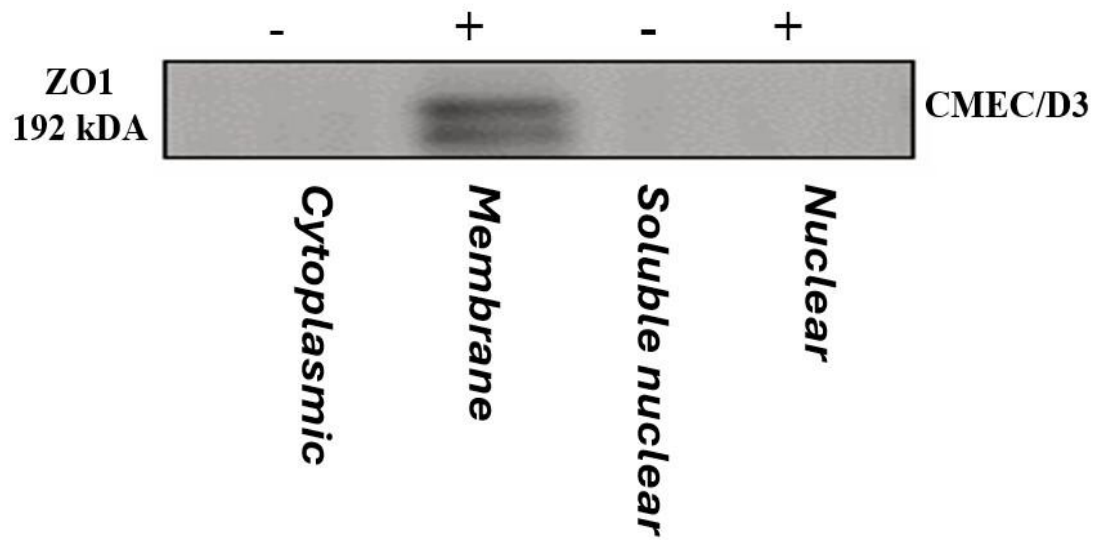


Figure 7.3.5A: Western blot analysis depicting the localization of ZO1 protein across different cellular fractions in CMEC/D3 cells. The lanes represent cytoplasmic, membrane, soluble nuclear, and nuclear fractions, respectively. ZO1 was detected primarily in the membrane fraction (+), with no significant presence in the cytoplasmic, soluble nuclear, or nuclear fractions (-). This pattern underscores the membrane-specific localization of ZO1 in CMEC/D3 cells.

B

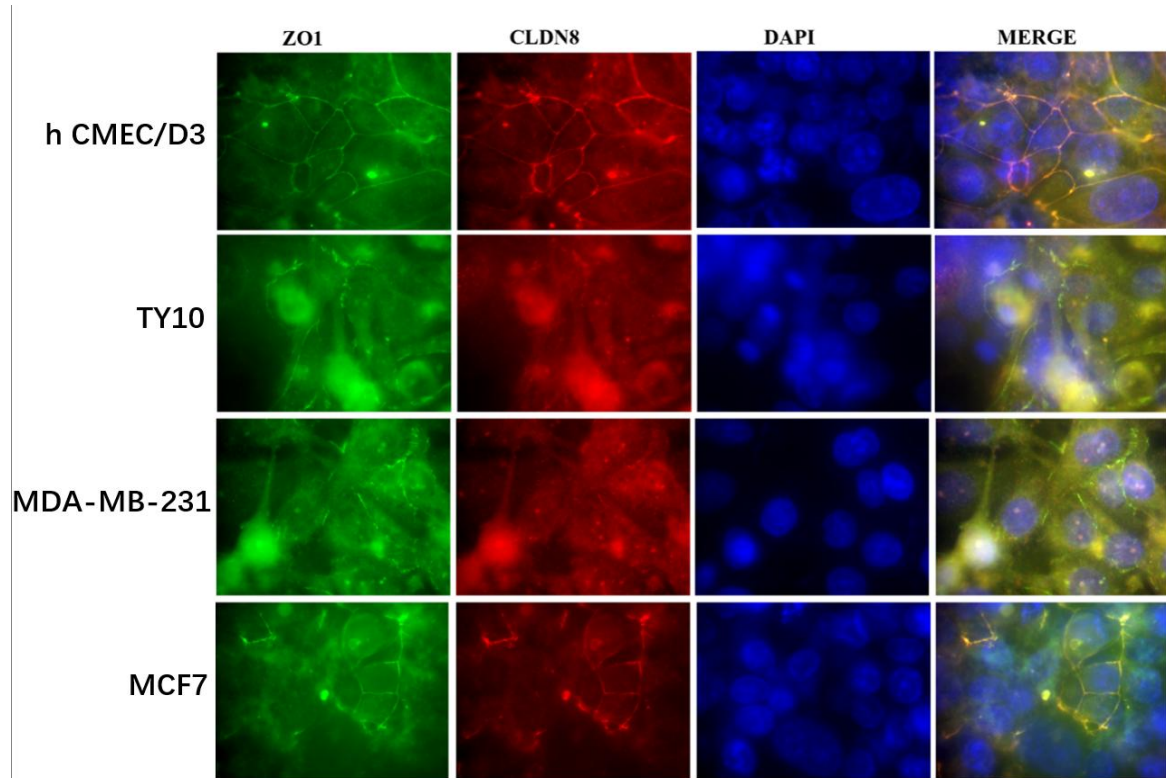


Figure 7.3.5 B) Immunofluorescence analysis further confirmed the colocalization of CLDN8 and ZO-1 on the cell membrane, indicating their expression at the same location. This colocalization suggests a potential interaction between these proteins, which may play an important role in maintaining tight junction structure and function in endothelial cells.

7.3.6 Co-Immunoprecipitation (Co-IP) of CLDN8 and β -catenin

To verify the interaction between CLDN8 and β -Catenin, we conducted a Co-Immunoprecipitation (Co-IP) experiment. Co-IP is a crucial technique used to detect interactions between proteins, helping to determine whether different proteins form a complex. In this study, we used an antibody against β -catenin for the Co-IP assay to ascertain whether CLDN8 binds to β -catenin either directly or indirectly.

The results demonstrated that specific bands for CLDN8 were clearly detected in the samples precipitated with the β -catenin antibody, while no significant bands were observed in the IgG control group (Figure 7.3.5A). This difference indicates a specific binding between CLDN8 and β -catenin, which may play an important role in maintaining tight junctions and in signal transduction.

By confirming the physical interaction between CLDN8 and β -catenin, we gained further insight into the potential collaborative mechanisms of these proteins in cellular functions. Together with the previous immunofluorescence co-localization results, it can be inferred that CLDN8 and β -catenin interacts at the cell membrane, and this interaction might be crucial for maintaining intercellular tight junctions and regulating cellular behaviours. Additionally, the presence of this protein complex suggests that CLDN8 and β -catenin may play an important role in tumour invasion and metastasis.

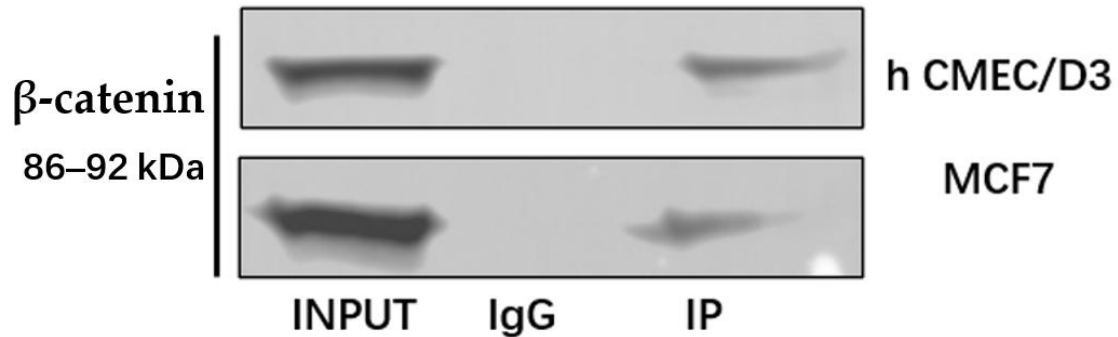


Figure 7.3.6 the results of the Co-Immunoprecipitation (Co-IP) analysis to determine the interaction between CLDN8 and β -catenin in hCMEC/D3 and MCF7 cells. The top panel represents the results from hCMEC/D3 cells, while the bottom panel represents the results from MCF7 cells. Three lanes are shown for each cell line: "INPUT" represents the whole-cell lysate, "IgG" is the negative control where a non-specific IgG antibody was used, and "IP" represents the sample immunoprecipitated with the β -catenin antibody.

7.3.7 Structural Changes of CLDN8 and β -catenin Following Artemisinin Treatment

In this section, we examined the impact of Artemisinin on the structural arrangement of Claudin-8 (CLDN8) and β -catenin (β -catenin) in both CMEC/D3 brain endothelial cells and breast cancer cells.

Immunofluorescence analysis was utilized to observe changes in the localization and distribution patterns of these proteins following Artemisinin treatment.

Under normal conditions, CLDN8 and β -catenin fluorescence signals appeared as continuous, linear patterns along the cell membrane, indicating their localization and tight association with the cell junctions. However, after treatment with Artemisinin, we observed a marked shift in the fluorescence distribution of both CLDN8 and β -catenin from a linear to a punctate pattern.

This transformation in the signal distribution suggests that Artemisinin treatment induces significant structural changes in the localization of CLDN8 and β -catenin on the cell membrane (Figure 7.3.7).

The observed change from a linear to punctate distribution indicates a potential disassembly or reorganization of the protein complexes that form tight junctions. For CLDN8, the punctate signal may reflect a disruption in the tight junction integrity, leading to a reduced ability of endothelial cells to maintain the barrier function of the BBB. Similarly, for β -catenin, this change suggests alterations in its association with the cytoskeleton and junctional complexes, which could impact cell adhesion and intracellular signalling.

Further examination of colocalization patterns between CLDN8 and β -catenin revealed that these proteins, which initially exhibited strong colocalization on the cell membrane, showed a reduced overlap following Artemisinin treatment. This suggests that the integrity of their interaction was compromised, potentially contributing to the destabilization of tight junctions. The breakdown in their colocalization may also indicate an increased likelihood of β -catenin translocating to the cytoplasm, where it could be targeted for degradation.

These findings are consistent with the Western blot data presented earlier, which demonstrated a reduction in CLDN8 and β -catenin expression following Artemisinin treatment. Together, these results highlight the effect of Artemisinin on disrupting the structural organization of key tight junction proteins, thereby potentially weakening the barrier function of endothelial cells and altering the behaviour of cancer cells. Understanding these structural changes is essential for deciphering the mechanisms by which Artemisinin modulates cell junctions, providing insights into its potential therapeutic effects in treating breast cancer brain metastasis.

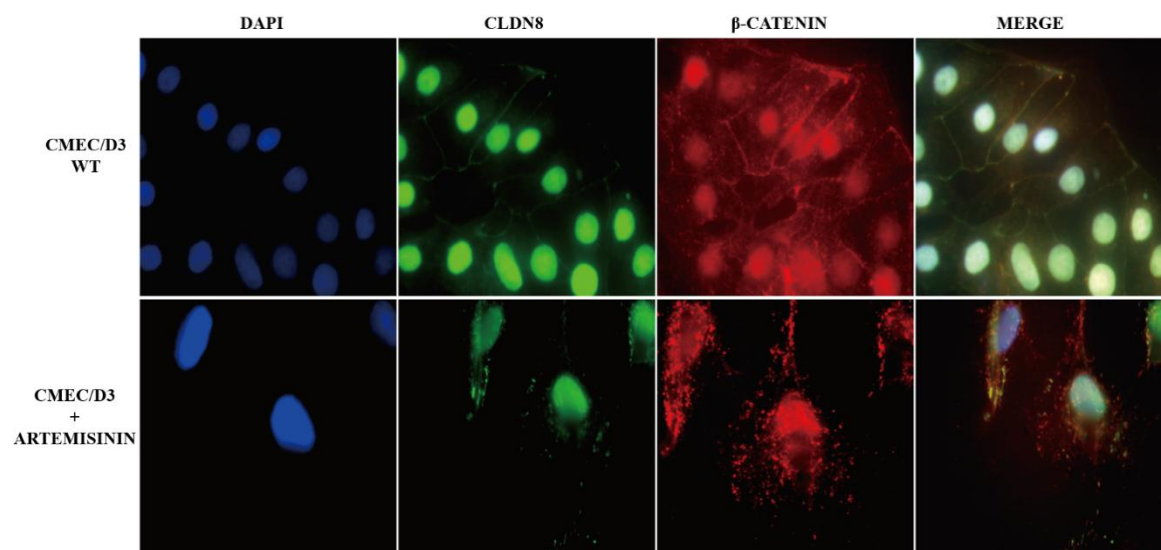


Figure 7.3.7 After Artemisinin treatment, the fluorescence signals of CLDN8 and β -catenin changed from linear to punctate distribution, suggesting structural changes in their localization on the cell membrane.

7.3.8 Impact of Artemisinin on AKT, GSK3 β , and β -catenin Phosphorylation in hCMEC/D3 Cells

In this section, we conducted a detailed analysis of the phosphorylation status of different protein sites following Artemisinin treatment to reveal the role of Artemisinin in regulating cellular signalling and the relationship between tight junction proteins, such as CLDN8. The experiment focused primarily on the phosphorylation changes of β -catenin (CTNNB1) at the Thr41/Ser45 sites and GSK3 β (glycogen synthase kinase 3 β) at the Tyr216 and Ser9 sites.

The results showed that the phosphorylation level of β -catenin at Thr41 and Ser45 was highest when Artemisinin was at a concentration of 10 μ M (Figure 7.3.8 B). These phosphorylation sites are usually mediated by GSK3 β , marking β -catenin for degradation, an important process in regulating its stability. That is, after phosphorylation, β -catenin is typically ubiquitinated

and degraded through the proteasomal pathway. Therefore, the degradation trend of β -catenin was most evident at 10 μ M Artemisinin treatment.

Combined with other experimental results, we hypothesize that the loss of the anchoring effect of CLDN8 on the cell membrane may lead to the release of β -catenin from the membrane into the cytoplasm, making it more susceptible to phosphorylation and subsequent degradation. This suggests that the loss of CLDN8 may promote β -catenin degradation by reducing its membrane anchorage.

Additionally, the phosphorylation of GSK3 β at Tyr216 also peaked at a concentration of 10 μ M (Figure 7.3.8 C). Phosphorylation at the Tyr216 site is generally considered a marker of GSK3 β activation, which means that GSK3 β activity is most significantly enhanced at this concentration. Activated GSK3 β can effectively phosphorylate β -catenin, tagging it for degradation.

Meanwhile, phosphorylation at Ser9, which is an inhibitory site for GSK3 β , was significantly reduced at 10 μ M Artemisinin (Figure 7.3.8 D), further supporting the hypothesis that GSK3 β is most active under these conditions.

Based on these findings, we propose a mechanism: under Artemisinin treatment, the decrease in CLDN8 expression leads to a loss of anchoring of β -catenin in the cell membrane, making β -catenin more accessible in the cytoplasm. With enhanced GSK3 β activity, β -catenin is then phosphorylated and tagged for degradation. The activation of GSK3 β at the Tyr216 site and dephosphorylation at the Ser9 site are critical steps in this process. This proposed mechanism explains the significant decrease in β -catenin levels in cells treated with a specific concentration of Artemisinin.

These findings not only reveal the process by which Artemisinin regulates β -catenin degradation through GSK3 β but also highlight the importance of CLDN8 in maintaining β -catenin stability. This indicates that the loss of

CLDN8's anchoring effect may significantly alter intracellular signalling dynamics, thereby impacting cell proliferation and migration. These insights provide new perspectives for further exploration of the potential applications of Artemisinin in cancer therapy, particularly in regulating tumour cell signalling pathways and cell junctions.

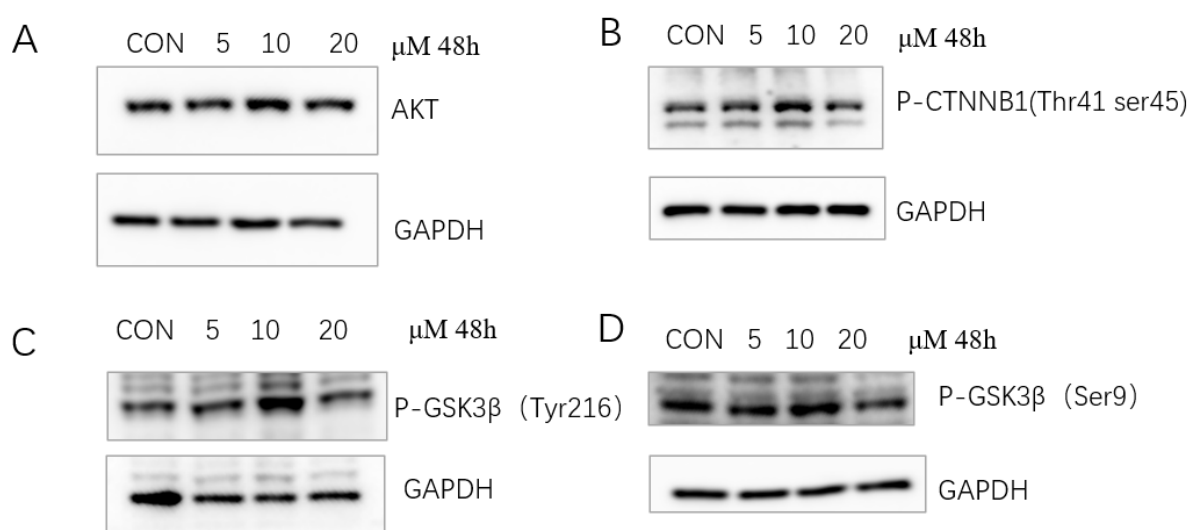


Figure 7.3.8: The effect of different concentrations of Artemisinin on AKT, P- β -catenin, and GSK3 β in hCMEC/D3 cells after 48 hours of treatment. (A) Total AKT expression remained unchanged under Artemisinin treatment (5, 10, and 20 μ M, 48 h). (B) Phosphorylation of β -catenin (Thr41/Ser45) peaked at 10 μ M, indicating enhanced β -catenin degradation via the proteasomal pathway. (C) Phosphorylation of GSK3 β at Tyr216 (activation site) was also highest at 10 μ M, suggesting increased GSK3 β activity. (D) Phosphorylation of GSK3 β at Ser9 (inhibitory site) decreased at 10 μ M, further confirming GSK3 β activation. GAPDH served as the loading control.

7.4 Discussion

This chapter focused on elucidating the role of Artemisinin in the modulation of tight junction proteins and signalling pathways in both brain endothelial

cells and breast cancer cells. Specifically, we investigated how Artemisinin influences the expression and phosphorylation of key proteins such as Claudin-8 (CLDN8), β -catenin (β -catenin), and glycogen synthase kinase 3 beta (GSK3 β). The findings provide new insights into the complex interplay between these proteins and their implications for cellular behaviour, particularly in the context of breast cancer metastasis.

First, the Western blot analysis presented in Section 7.3.1 demonstrated that Artemisinin significantly reduced CLDN8 expression in CMEC/D3 cells, particularly when combined with CLDN8 knockdown. These results suggest that Artemisinin could weaken tight junction integrity by diminishing CLDN8 levels, thus increasing cell permeability. This decrease in barrier function is highly relevant in the context of cancer metastasis, where a compromised BBB could facilitate the migration of cancer cells into the brain. Importantly, the data indicate that Artemisinin's impact on CLDN8 is pronounced and could potentially synergize with other molecular events to further compromise tight junction stability.

The subsequent findings on β -catenin phosphorylation and expression (Sections 7.3.2 and 7.3.3) provided deeper insights into the downstream effects of CLDN8 reduction. Our results from Kinexus phosphoprotein arrays revealed that both Artemisinin treatment and CLDN8 knockdown reduced the phosphorylation of β -catenin at multiple sites, including S33+S37+T41+S45, Y654, and Y489. The most significant reduction was observed at the Y489 site, highlighting its potential role as a regulatory node in the interaction between CLDN8 and β -catenin. The reduced phosphorylation at these sites suggests that β -catenin is being targeted for degradation, which aligns with the role of GSK3 β as a mediator of β -catenin stability.

We also demonstrated in Sections 7.3.4 and 7.3.5 that β -catenin and CLDN8 both predominantly localize to the cell membrane in CMEC/D3 cells, suggesting a coordinated role in maintaining cell junction integrity. The loss of CLDN8 following Artemisinin treatment may result in β -catenin becoming more susceptible to phosphorylation and subsequent cytoplasmic degradation. The subcellular fractionation analysis further supported this notion, showing that β -catenin was primarily localized to the membrane but exhibited a broader distribution, including the cytoplasmic fraction, in MDA-231 breast cancer cells. This redistribution could indicate a loss of anchorage, making β -catenin more vulnerable to degradation by GSK3 β .

The immunofluorescence results in Section 7.3.7 showed that Artemisinin treatment changed the distribution of both CLDN8 and β -catenin from a linear to a punctate pattern along the cell membrane. This observation suggests that Artemisinin disrupts the structural integrity of tight junctions, potentially by causing disassembly or reorganization of the junctional proteins. Such structural changes are crucial, as they can weaken cell-cell adhesion, making endothelial and cancer cells more prone to separation and increasing the potential for metastasis.

The Western blot data on phosphorylation presented in Section 7.3.8 further clarify the signalling pathways involved. Artemisinin treatment led to increased phosphorylation of β -catenin at Thr41/Ser45 and GSK3 β at Tyr216, which are key indicators of β -catenin targeting for degradation. Concurrently, there was a decrease in phosphorylation of GSK3 β at Ser9, an inhibitory site. This suggests that Artemisinin activates GSK3 β , enhancing its ability to phosphorylate β -catenin, thereby promoting its degradation. We hypothesize that this mechanism is closely tied to the loss of CLDN8-mediated membrane

anchoring of β -catenin, making it more accessible to active GSK3 β in the cytoplasm.

Overall, the results presented in this chapter provide compelling evidence that Artemisinin modulates both CLDN8 and β -catenin in a manner that impacts tight junction integrity and intracellular signalling dynamics. The reduction in CLDN8 expression appears to weaken cell junctions, while the subsequent activation of GSK3 β and increased phosphorylation of β -catenin promote its degradation, further compromising the structural stability of the junctions. These findings suggest a dual effect of Artemisinin: it enhances BBB permeability, which could be beneficial for drug delivery, while simultaneously reducing the metastatic potential of breast cancer cells by downregulating β -catenin.

The involvement of the Wnt/ β -catenin signalling pathway adds another layer of complexity to our findings. By activating GSK3 β , Artemisinin effectively attenuates Wnt signalling, which is critical for cell proliferation and survival. The attenuation of Wnt signalling may contribute to the observed reduction in cell migration and invasion, thus positioning Artemisinin as a promising candidate for anti-metastatic therapy. Notably, the degradation of β -catenin in endothelial cells may exert an indirect inhibitory effect on tumour cell migration. Previous studies have shown that endothelial β -catenin activation is often associated with increased expression of pro-angiogenic factors, such as VEGF, IL-6, and MMPs, which remodel the tumour microenvironment and provide a more “migration-friendly” condition for tumour cells(182-184). Therefore, Artemisinin-induced degradation of endothelial β -catenin may reduce the secretion of these pro-migratory factors, thereby limiting tumour cell transendothelial invasion and distant metastasis. Meanwhile, in breast cancer cells, Artemisinin further suppresses cell migration and invasion by

inhibiting the Wnt/ β -catenin signaling pathway. These two mechanisms may work synergistically to exert anti-metastatic effects.

In conclusion, this chapter highlights the significant impact of Artemisinin on the regulation of tight junction proteins and intracellular signalling pathways in both endothelial and cancer cells. The modulation of CLDN8, β -catenin, and GSK3 β provides valuable insights into how Artemisinin affects cell junction stability and metastatic behaviour. Future studies should focus on further elucidating the precise molecular interactions between CLDN8 and β -catenin, as well as exploring the therapeutic potential of Artemisinin in preventing breast cancer metastasis to the brain, particularly in combination with other targeted therapies.

Chapter VIII: General Discussion

8.1 Key findings from the current study

In this thesis, we set out to investigate the role of Claudin-8 (CLDN8) in breast cancer and its brain metastases, and to evaluate the therapeutic potential of Artemisinin in this context. Through seven preceding chapters, we combined bioinformatic analyses, clinical sample studies, *in vitro* functional assays, and molecular experiments to build a coherent story linking tight junction integrity (via CLDN8), the Wnt/ β -catenin signalling pathway, and metastatic progression. Here we summarize the key findings from those chapters:

8.1.1 CLDN8 Downregulation in Breast Cancer

Initial transcriptomic screening (Chapter 3) highlighted tight junction genes as Artemisinin-responsive, pinpointing CLDN8 as a candidate mediator of BBB regulation. We confirmed in Chapter 4 that CLDN8 mRNA and protein are significantly downregulated in breast carcinomas compared to normal tissue. Low CLDN8 expression was especially associated with aggressive tumour features – including higher grade, lymph node metastasis, and negative hormone receptor status. Notably, CLDN8 levels were highest in luminal-subtype tumours and lowest in HER2-enriched and triple-negative breast cancers (TNBC), mirroring the known poor-prognosis “claudin-low” phenotype of breast cancer(173). These data suggest that loss of CLDN8 is a common event in aggressive breast cancers and may contribute to their metastatic propensity.

8.1.2 CLDN8 as a Prognostic Biomarker

Our clinical cohort analyses further indicated that CLDN8 has potential prognostic value. Patients with higher CLDN8 expression tended to have better outcomes, consistent with external reports that CLDN8-positive tumours (often AR-positive and luminal) correlate with longer overall

survival. Conversely, CLDN8-low tumours align with the claudin-low subtype and worse prognosis. Chapter 4 showed that CLDN8 immunohistochemical expression varied across subtypes (, reduced in basal/TNBC tumours) and may predict treatment response. In Chapter 5, we explored CLDN8 in the context of therapy: interestingly, CLDN8 expression appeared to be modulated by endocrine therapy and HER2-targeted treatments. For instance, analysis suggested CLDN8 levels were higher in ER-positive/AR-positive tumours (which often respond to hormonal therapy), raising the possibility that CLDN8 expression is maintained by hormonal signalling. While detailed mechanisms were beyond our scope, these observations reinforce CLDN8 as both a marker of a less invasive phenotype and potentially a mediator of therapeutic sensitivity.

8.1.3 Functional Role of CLDN8 in Cell Adhesion and Invasiveness

In Chapters 6 and 7, we used cell-based assays to define what loss or gain of CLDN8 means for cell behaviour. Consistently, CLDN8 proved to be a crucial component of cell–cell junctions that restrain cancer cell motility and invasion. Knocking down CLDN8 in breast cancer cells led to a significant loss of cell adhesion in certain lines (notably in SKBR3 and MDA-MB-231, which showed >50% decrease in adherent cells). This indicates CLDN8 contributes to cell–matrix or cell–cell adhesion in those contexts. CLDN8 knockdown also had cell-line-specific effects on migration: for example, MCF7 cells (luminal) showed a sharp drop in scratch-wound healing migration when CLDN8 was silenced, whereas more mesenchymal MDA-MB-231 cells were unaffected by CLDN8 loss. These differences suggest that well-differentiated epithelial cells rely on CLDN8 to maintain cohesive movement, while highly invasive cells (which already have low CLDN8) migrate independently of it. Crucially, across all tested breast cancer lines,

CLDN8 knockdown enhanced invasiveness through a brain endothelial barrier: Transwell assays showed significantly increased TNBC cell invasion when CLDN8 was silenced in the cancer cells (3–4 fold in MDA-MB-231 and SKBR3, for example). Likewise, silencing CLDN8 in brain endothelial cells (hCMEC/D3 and TY10) disrupted tight junctions and greatly facilitated transmigration of cancer cells. These functional experiments underscore a key point: CLDN8 helps maintain barrier integrity and suppress metastatic invasion, both at the level of tumour cell clusters and the brain microvasculature. Its downregulation removes a physical and biochemical constraint on metastasis, allowing cancer cells to detach, migrate, and eventually penetrate the BBB more readily.

8.1.4 Artemisinin's Impact on Cancer and Endothelial Cells

A major thrust of this work was evaluating Artemisinin (Artemisinin) – a natural sesquiterpene lactone – as a therapeutic that might counteract the pro-metastatic effects of CLDN8 loss. In vitro, Artemisinin treatment produced several beneficial effects on cancer cell behaviour. Migration assays showed that 10 μ M Artemisinin significantly slowed wound closure in both MCF7 and MDA-MB-231 cells (reducing migration rates by ~20–30% vs. control). Importantly, this anti-migratory effect was observed even in CLDN8-knockdown cells, suggesting Artemisinin can inhibit cell motility through mechanisms independent of CLDN8. Invasion assays demonstrated a similar trend: Artemisinin treatment (10 μ M) led to markedly fewer cancer cells invading across an endothelial monolayer in multiple cell lines. For instance, Artemisinin reduced MCF7 cell invasion by >80% (even when CLDN8 was knocked down). In MDA-MB-231 (TNBC) cells, Artemisinin also curtailed invasion, an effect most pronounced when CLDN8 was absent. Additionally, Artemisinin decreased cancer cell adhesion in all tested lines – both CLDN8-

intact and CLDN8-silenced – indicating it makes cancer cells less prone to stick to a substrate or endothelium. Taken together, these results suggest that Artemisinin phenocopies some effects of high CLDN8 (reducing motility and invasiveness) even in cells where CLDN8 is low, pointing to a distinct mode of action.

8.1.5 Effects of Artemisinin on Tight Junction Integrity

While Artemisinin clearly suppresses cancer cell aggressiveness, our experiments also revealed a seemingly paradoxical effect on tight junction proteins. In Chapter 3, RNA-seq and qPCR validation showed that Artemisinin down-regulated CLDN8 expression in brain endothelial cells. Consistently, real-time barrier assays (Chapter 6) found that treating monolayers with Artemisinin reduced TEER (transendothelial electrical resistance) and increased paracellular permeability in both SKBR3 and MDA-MB-231 cell monolayers. For example, within 15 minutes of Artemisinin exposure, TEER dropped significantly (~15–20% decrease) in wild-type cells. This drop was less pronounced or null in CLDN8-knockdown monolayers, implying that the integrity loss was largely due to CLDN8 and related TJs being targeted by Artemisinin. Similarly, in brain endothelial cells, Artemisinin lowered barrier function to a degree (mimicking CLDN8 knockdown). This dual effect of Artemisinin – weakening tight junctions yet reducing cancer cell invasiveness – is a critical point of discussion. Intuitively, disrupting TJs could facilitate metastasis, but our co-culture experiments suggest that the net effect of Artemisinin is protective. In a simulated BBB model (Chapter 6), simultaneous Artemisinin treatment of both endothelial and cancer cells led to a *significant decrease* in transmigrating TNBC cells, even when CLDN8 was knocked out. It is important to recognise that CLDN8 acts at two distinct biological interfaces. In BBB endothelium, CLDN8 primarily

serves as a sealing component of tight junctions; its reduction manifests first as lower TEER and increased paracellular permeability, a state that can be harnessed transiently and in a controlled window to improve drug penetration—but which, if unchecked, may also facilitate tumour cell extravasation. By contrast, in tumour epithelium, reduced CLDN8 weakens cell–cell adhesion and epithelial polarity, aligning across cohorts with greater migratory/ invasive capacity and worse prognosis. In other words, although Artemisinin transiently compromises the endothelial barrier, it so profoundly dampens the invasive capability of the cancer cells that overall fewer cells cross the barrier. This finding alleviates concerns that Artemisinin might “open the gates” to metastasis; instead, it points to Artemisinin’s ability to counteract metastatic spread via tumour-intrinsic mechanisms.

8.1.6 Relationship between CLDN8 expression and breast cancer treatment sensitivity and implications for Artemisinin therapy

To investigate the influence of CLDN8 expression on breast cancer treatment responses, we conducted MTT cell proliferation assays on multiple breast cancer cell lines (Chapter 5). Results clearly demonstrated that cell lines with higher CLDN8 expression showed increased sensitivity to endocrine therapies such as tamoxifen, whereas cell lines with lower CLDN8 expression were more sensitive to chemotherapy drugs (, paclitaxel) and anti-HER2 drugs (, trastuzumab). These findings suggest that CLDN8 expression status could serve as a critical predictive biomarker for personalized breast cancer treatment.

Artemisinin markedly reduced CLDN8 expression in brain microvascular endothelial cells, transiently increasing BBB permeability and thereby facilitating drug delivery to brain metastases. Simultaneously, Artemisinin exhibited significant anti-invasive and anti-migratory effects on breast cancer

cells, substantially reducing their invasive capacity and BBB penetration, even under conditions of low CLDN8 expression. These findings highlight Artemisinin's dual therapeutic advantages in treating breast cancer brain metastasis. Combinations of Artemisinin with paclitaxel or cisplatin markedly reduced viability of triple-negative MDA-MB-231 cells, and similar synergistic enhancement was observed in HER2-positive SKBR3 cells treated with Artemisinin combined with neratinib or lapatinib. These findings indicate that Artemisinin-induced transient disruption of endothelial tight junctions increases BBB permeability, facilitating improved chemotherapeutic drug delivery to brain metastatic lesions. Importantly, Artemisinin demonstrated synergistic anticancer efficacy without increasing metastatic risk.

8.1.7 Artemisinin-Induced Changes in Protein Localization and Interaction between CLDN8 and β -catenin

Immunofluorescence confocal microscopy (IFC) experiments visually confirmed the colocalization of CLDN8 with the tight junction-associated protein ZO1 at the cell membrane of brain microvascular endothelial cells (CMEC/D3), directly verifying the structural and functional importance of CLDN8 in maintaining tight junction integrity. Furthermore, significant morphological changes of CLDN8 and β -catenin proteins were directly observed following Artemisinin treatment. Initially, CLDN8 and β -catenin exhibited linear and continuous localization patterns along the cell membrane, indicative of stable tight junction structures. However, Artemisinin exposure altered these linear distributions to punctate patterns, suggesting significant disruptions or reorganization in the tight junction complexes. This punctate localization may represent the disassembly or internalization of tight junction proteins, indicate compromised barrier integrity and altered cell-cell adhesion dynamics.

Additionally, co-immunoprecipitation (Co-IP) assays conclusively demonstrated direct physical interactions between CLDN8 and β -catenin proteins. The observed structural reorganization following Artemisinin treatment further supports the hypothesis that Artemisinin disrupts CLDN8– β -catenin interactions, potentially causing β -catenin release from the membrane-bound complexes into the cytoplasm, where it becomes susceptible to phosphorylation and degradation. These findings underscore a crucial interplay between tight junction integrity and intracellular signalling pathways in the context of Artemisinin's anticancer mechanism.

8.1.8 Molecular Mechanisms – CLDN8, β -Catenin, and Artemisinin

Understanding how CLDN8 and Artemisinin intersect with the Wnt/ β -catenin pathway provides a unifying explanation for our observations. Figure 8.1.8 (conceptual diagrams) illustrate the proposed model in three scenarios: (A) normal physiological state, (B) the tumour microenvironment during metastasis, and (C) the effect of Artemisinin treatment. Below, we discuss each in turn, integrating our findings with known biology.

(A) Normal Physiological State – Intact CLDN8 and Regulated β -Catenin:

Under healthy conditions (in non-tumour breast epithelium and brain endothelium), CLDN8 is abundantly expressed and incorporated into tight junctions. Together with other junctional proteins, CLDN8 helps form a stable intercellular seal that maintains tissue polarity and barrier function. In epithelial cells, adherens junctions (anchored by E-cadherin/ β -catenin complexes) lie just beneath the tight junctions, and there is a dynamic interplay between these structures. β -Catenin in normal cells primarily resides in two pools: a large fraction at the cell membrane (bound to E-cadherin and perhaps indirectly influenced by tight junction scaffolds), and a cytosolic pool that is kept under strict control by the destruction complex

(Axin, APC, GSK3 β , CK1)(185). In the absence of Wnt signals, GSK3 β is active and continuously phosphorylates any free β -catenin, targeting it for proteasomal degradation. This means that β -catenin does not accumulate in the nucleus to drive gene transcription. CLDN8 contributes to this homeostasis by promoting robust cell–cell contacts; effectively, it helps “corral” β -catenin at the membrane (in complex with cadherins and actin via catenin) and preserves the quiescent, adhesive phenotype of cells. The outcome is that epithelial and endothelial layers remain cohesive and non-migratory, and the BBB remains intact. In this normal state, β -catenin’s transcriptional activity is minimal – cell proliferation and migration programs are largely off. We can liken CLDN8 to a gatekeeper: it fortifies the gate (tight junction) and indirectly ensures that the “gatekeeper” signalling molecule β -catenin remains in check. Thus, under physiological conditions, high CLDN8 = strong junctional integrity and low Wnt/ β -catenin signalling.

(B) Tumour Microenvironment – CLDN8 Loss Leading to β -Catenin

Activation: In the context of an evolving breast tumour and especially during brain metastasis, the normal balance is disrupted. Breast cancer cells often undergo epithelial–mesenchymal transition (EMT) as they acquire invasive capabilities; a well-known feature of EMT is the loss of junctional proteins (both tight junction components and E-cadherin). Indeed, our clinical data showed CLDN8 is frequently downregulated in breast tumours, particularly in basal-like and TNBC subtypes that are prone to metastasis. As illustrated in Figure B, when CLDN8 expression is lost or greatly reduced, tight junctions weaken or disassemble. This has two major consequences: (1) the physical barrier to cell dissociation and migration is lowered (cells become less adhesive and more migratory), and (2) junctional complexes that sequester signalling molecules are destabilized. With CLDN8 (and often E-cadherin) gone, a larger fraction of β -catenin is released from the cell membrane.

Concurrently, the tumour microenvironment provides Wnt signals and other growth factors that hijack the β -catenin destruction pathway. Many breast tumours secrete Wnt ligands or activate pathways like PI3K/Akt that converge on GSK3 β inhibition. In metastasis models, Wnt/ β -catenin signalling is strongly implicated in promoting invasion and colonisation(186). In our scenario, CLDN8 loss and Wnt activation act synergistically: Wnt ligands bind Frizzled/LRP receptors on the cancer cell surface (and possibly on endothelial cells), which triggers the disassembly or inhibition of the Axin–APC destruction complex GSK3 β becomes inhibited (, via phosphorylation at Ser9 by upstream Akt or dishevelled signalling), and thus β -catenin is no longer phosphorylated and degraded. Any β -catenin released into the cytoplasm is now stabilized and can accumulate in the nucleus. Figure B depicts this state: nuclear β -catenin (in complex with TCF/LEF transcription factors) drives the expression of genes that confer invasive, stem-like properties. Examples of β -catenin target genes relevant to metastasis include Slug and Snail (EMT transcription factors that repress E-cadherin), VEGF (to promote angiogenesis), MMPs like MMP-2/-9 (which degrade extracellular matrix), and stem cell regulators like Oct4 and Nanog. The outcome is a positive feedback loop: loss of junctions leads to more β -catenin signalling, which further suppresses junctional proteins and enhances EMT. Phenotypically, the tumour cells become less adherent and more invasive, matching our observations that CLDN8 knockdown increased migration and invasion. In the brain metastasis context, circulating tumour cells arriving in the brain can more easily transmigrate if both the tumour cell has high β -catenin (increasing its motility) and the endothelial tight junctions are weakened (from inflammatory or tumour-secreted factors). It is likely that metastatic breast cancer cells induce downregulation of CLDN8 in the BBB endothelium they interact with (for instance, via secreted cytokines or exosomes), compounding the problem. In sum, Figure B represents a

“metastatic cascade” state: CLDN8 is low, β -catenin is constitutively active, tight junctions are compromised, and tumour cells aggressively invade and intravasate/extravasate. This scenario aligns with the poor clinical outcomes associated with low-CLDN8 tumours and explains why CLDN8 loss is a driver of brain metastatic progression.

(C) Artemisinin Treatment – Restoration of β -Catenin Control via GSK3 β

Activation: Figure 8.1.8 C illustrates how Artemisinin intervenes in the above malignant process. Our data show that Artemisinin effectively re-engages the β -catenin degradation machinery even in the presence of Wnt signals.

Artemisinin’s exact molecular targets are still being elucidated, but our results and other studies suggest it acts at multiple levels of the Wnt/ β -catenin pathway. In our model, Artemisinin enters the cells (it is a small, lipophilic molecule that readily crosses cell membranes and even the BBB(186) and leads to activation of GSK3 β . Biochemically, we observed Artemisinin-treated endothelial cells had lowered phospho-Ser9-GSK3 β , which corresponds to an active GSK3 β capable of phosphorylating β -catenin. Artemisinin thereby counteracts Wnt effect: even if Wnt ligands are present, Artemisinin pushes the equilibrium back towards β -catenin destruction (Figure C, right side). In treated cells, β -catenin is phosphorylated (we saw increases in phospho-Thr41/Ser45- β -catenin) and marked for degradation. Instead of accumulating in the nucleus, β -catenin gets ubiquitinated and degraded in the cytoplasm. Functionally, this means Wnt target genes are no longer transcriptionally upregulated – the “grow and invade” program is halted. Our invasion and migration assays confirm that Artemisinin diminishes the downstream effects of β -catenin activation: cells show lower expression of mesenchymal markers and MMPs (as noted in Chapter 7 protein analyses) and correspondingly reduced invasive capacity. An external study in lung cancer similarly found that Artemisinin and its derivatives suppress tumour metastasis by inhibiting

Wnt/ β -catenin signalling, leading to decreased EMT and stemness markers (187). Moreover, Artemisinin may have an upstream effect by interfering with Wnt ligand/receptor interactions. There is evidence that Artemisinin can bind or modulate cell-surface Frizzled receptors or co-receptors (like LRP5/6), effectively mimicking secreted Wnt inhibitors (187). In Figure 8.1.8 C, we indicate this by showing Artemisinin blocking Wnt–receptor binding (red “X” at the receptor), although the primary proven action is downstream at GSK3 β . The net impact of Artemisinin is to stabilize the cellular junctions and phenotype despite low CLDN8. By promoting β -catenin degradation, Artemisinin indirectly allows cells to maintain or re-express junctional proteins (since β -catenin-driven EMT transcription factors are suppressed). In our co-culture experiments, we saw that even though Artemisinin reduced CLDN8 acutely, it did not lead to increased cancer cell invasion – in fact, invasion dropped, suggesting that any junction-weakening is outweighed by the loss of pro-invasion signalling. One might imagine that in a treated tumour, cells remain more epithelial-like (less EMT), and any tumour cells that reach the brain find a microenvironment less permissive for colonization because Artemisinin also strengthens the hand of the endothelium. (Interestingly, Artemisinin has been reported to upregulate certain Wnt antagonists like Axin2 and NKD2 in tumours(187), and it can even induce differentiation in cancer stem cells.) From a BBB perspective, Artemisinin’s ability to activate GSK3 β may help restore endothelial stability after an initial drop in CLDN8. GSK3 β also has other substrates in junctional regulation, and by inhibiting β -catenin, Artemisinin might prevent the downregulation of other TJ proteins that β -catenin/TCF could cause during inflammation or cancer. Thus, Figure C depicts a treated scenario where β -catenin is kept out of the nucleus, tumour cells regain some adhesion (or at least lose their extreme invasiveness), and the vicious cycle of metastasis is broken. In essence, Artemisinin pharmacologically recreates a condition analogous to the

normal state (A) – high GSK3 β activity and low Wnt signalling – thereby impeding the progression depicted in (B).

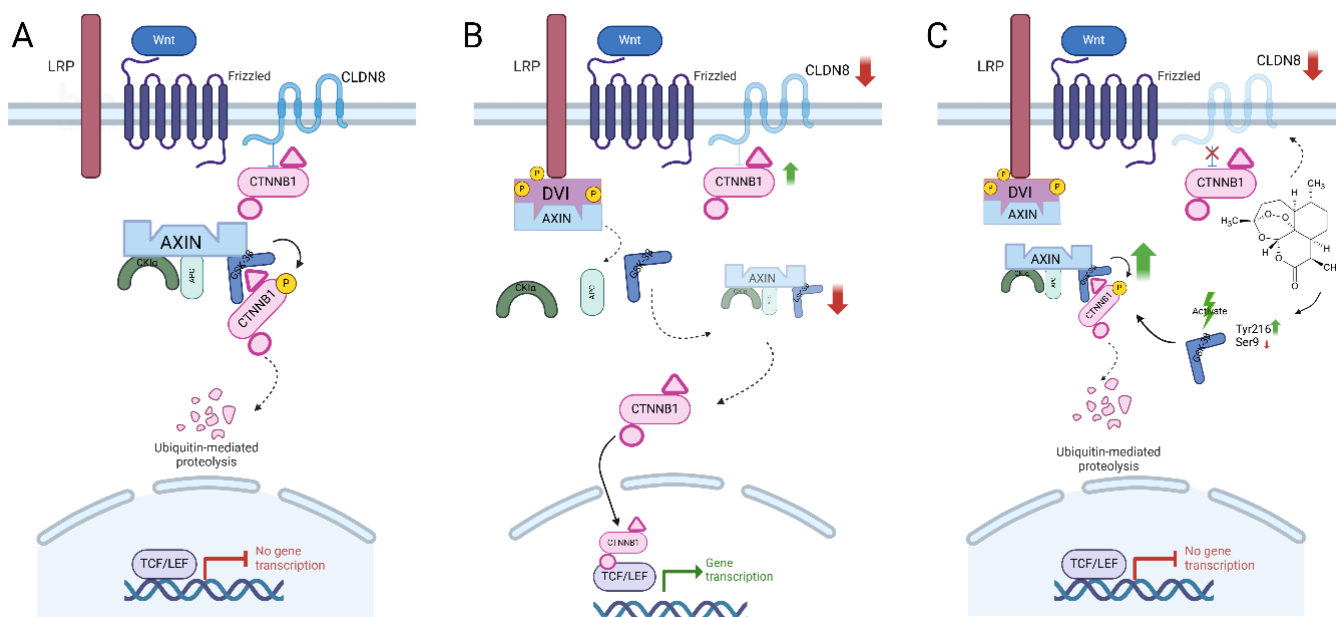


Figure 8.1.8. Schematic illustration of the regulatory role of CLDN8 and Artemisinin in modulating the Wnt/ β -catenin signalling pathway in breast cancer brain metastasis

8.2 Clinical Relevance and Therapeutic Implications

Our findings have several important implications for breast cancer patients, especially those at risk of or suffering from brain metastases. Firstly, CLDN8 emerges as a potential biomarker for tumour aggressiveness and metastatic propensity. Given the strong association of low CLDN8 with TNBC and other aggressive subtypes, CLDN8 expression in a primary tumour could be used to stratify patients: tumours with absent or low CLDN8 might warrant closer surveillance for metastasis (particularly to the brain) or more aggressive upfront therapy. This is analogous to the way claudin-low status

(characterized by loss of multiple claudin including CLDN3,4,7) is recognized as a poor-prognosis subtype (173). In practical terms, immunohistochemical staining for CLDN8 on breast tumour biopsies could be incorporated into pathology workups. If validated in larger cohorts, a “CLDN8-low” result could alert clinicians to a higher likelihood of BBB transmigration by tumour cells. There is also indication that CLDN8 might predict responsiveness to certain therapies – for example, since CLDN8 correlates with androgen receptor (AR) and ER positivity(173). CLDN8-high tumours may respond better to hormonal therapies. Conversely, CLDN8-low/claudin-low tumours, which often overlap with triple-negative disease, currently lack targeted therapies – these are precisely the patients who might benefit from a novel approach like Wnt/ β -catenin inhibition.

Secondly, our work suggests a new therapeutic strategy targeting the Wnt/ β -catenin pathway in metastatic breast cancer, with Artemisinin as a promising lead compound. Wnt/ β -catenin signalling has long been recognized as a driver of metastasis and treatment resistance, but it has been challenging to target clinically. Artemisinin offers several advantages in this regard. It is an FDA-approved anti-malarial with an excellent safety profile over decades of use, and importantly, it can penetrate the BBB (188). This means Artemisinin (and its derivatives like artesunate) could reach micro metastases in the brain and the brain endothelium – a critical requirement for any therapy aimed at brain metastasis. Our data provide proof-of-concept that Artemisinin *in vitro* reduces cancer cell invasion through an endothelial barrier, which is a surrogate for preventing brain metastatic colonization. Clinically, this raises the exciting possibility of using Artemisinin or derivatives as metastasis-suppressing agents in breast cancer. For instance, patients with CLDN8-low or Wnt-activated tumours could receive Artemisinin adjunctively to curb the likelihood of brain metastases. There is precedent for this approach in other

cancers: a recent study showed that blocking Wnt/ β -catenin can suppress breast cancer cells' ability to metastasize to the lung and brain (189). Our results align with those findings and extend them by identifying a readily available drug that can achieve such Wnt blockade. Another clinically relevant observation is that Artemisinin's effects were apparent at micromolar concentrations (5–10 μ M in our cell assays). These concentrations are attainable in patients; artesunate, for example, has been given at high doses in clinical trials for cancer with manageable toxicity. This suggests that repurposing Artemisinin is feasible.

It is also worth noting that Artemisinin might be especially useful in the context of triple-negative breast cancer, where standard hormonal or HER2-targeted therapies are ineffective. TNBCs frequently have hyperactive Wnt/ β -catenin signalling and are prone to brain metastasis (190). Our study showed that even highly invasive TNBC cells (MDA-MB-231) had their invasion significantly curtailed by Artemisinin, particularly when CLDN8 was absent (mimicking the claudin-low state). This suggests that TNBC patients, who urgently need new treatment options, could derive benefit from Artemisinin-based therapy. Moreover, Artemisinin could potentially be combined with existing treatments. For example, combining Artemisinin with chemotherapy or immune checkpoint inhibitors might have synergistic effects – Artemisinin could normalize tumour cells to a more epithelial (and chemo sensitive or immunogenic) state by inhibiting EMT and stemness. There is emerging evidence that Wnt pathway activation contributes to immune evasion, so Artemisinin might even improve immune response against tumours.

From a translational perspective, another avenue is developing Artemisinin derivatives or analogues optimized for anti-cancer activity.

Dihydroartemisinin (DHA) and artesunate (ARS) were mentioned in our

discussion of mechanism (Figure C). These derivatives have been reported to have similar or stronger anti-tumour effects (187). Artesunate in particular has entered clinical trials for cancer. Our mechanistic insights – that these drugs act on GSK3 β / β -catenin – provide a clear biomarker to track in trials (nuclear β -catenin levels, or expression of β -catenin target genes in patient tumours). It also opens the possibility of personalizing therapy: patients could be selected for Artemisinin-based therapy if their tumours show evidence of Wnt/ β -catenin activation (, nuclear β -catenin on IHC or a gene signature of Wnt activation). In the context of brain metastases, since surgical biopsies are rare, one could use the primary tumour features (like CLDN8-low, high Axin2 or other Wnt targets) as a surrogate to decide on therapy.

Finally, our results highlight the clinical significance of the tumour microenvironment and BBB integrity. Therapies that strengthen the BBB or restore its selective permeability could be a novel approach to preventing metastasis. While Artemisinin does not *directly* raise CLDN8 levels (it lowered them short-term), its net effect was to protect the BBB function by reducing the onslaught of invading cells. Another strategy could be to upregulate CLDN8 or other junction proteins in patients. Though not straightforward, there are drugs (like histone deacetylase inhibitors or differentiation agents) that can induce claudin expression. Moreover, hormonal therapies (ER/AR agonists) might incidentally raise CLDN8 as suggested by AR's regulation of CLDN8 (173). If a link between AR signalling and CLDN8 holds, AR-positive breast cancers might maintain higher CLDN8 and have fewer brain metastases – this is speculative, but future clinical data mining could explore it. In summary, the clinical message is two-fold: (1) CLDN8 could serve as a useful marker for identifying high-risk patients and as a readout of tight junction status in tumours; (2) Targeting the Wnt/ β -catenin pathway with a

brain-penetrant agent like Artemisinin represents a promising therapeutic strategy to reduce brain metastatic burden in breast cancer.

8.3 Limitations of the Study and Future Directions

While this study provides important insights, it also has limitations that must be acknowledged. These limitations point toward directions for future research to validate and build upon our findings:

8.3.1 Sample Size and Cohort Composition

Our clinical analyses (Chapter 4) were based on a limited patient cohort, especially regarding brain metastases. Only a small number of brain metastatic samples were available for CLDN8 analysis, and cerebellar metastases were particularly underrepresented. Metastases to different brain regions (cerebrum vs. cerebellum) might have distinct biology; for example, the cerebellum's microenvironment could respond differently to CLDN8 loss or Wnt signals. Our data hinted at trends but were not powered to draw definitive conclusions on site-specific effects. A future direction is to examine a larger, multi-institutional cohort of breast cancer brain metastases, including enough cerebellar cases, to confirm that CLDN8 downregulation is a general feature and to correlate it with patient outcomes (, survival after brain metastasis, response to therapies). Additionally, our TCGA-based findings for CLDN8 in primary tumours need external validation. We relied on transcript data; it would be valuable to use tissue microarrays from hundreds of patients to robustly link CLDN8 protein levels with rates of brain metastasis development.

8.3.2 In Vitro Model Limitations

Our functional assays were conducted in simplified two-dimensional or Transwell systems. While the hCMEC/D3 cell monolayer is a well-established BBB model, it does not recapitulate all aspects of the true BBB (such as astrocyte and pericyte interactions, or blood flow shear stress). Similarly, our co-culture invasion assay, though informative, is not a full simulation of metastasis which involves circulation and extravasation steps. Therefore, one limitation is that we did not demonstrate in an *in vivo* model that Artemisinin can prevent or reduce brain metastases. As a future direction, animal models of breast cancer brain metastasis should be employed. For instance, an orthotopic breast tumour model with spontaneous brain metastasis, or an intracardiac injection model of metastasis, could be used to test Artemisinin treatment. Endpoints would include number of brain metastatic foci with and without Artemisinin treatment, as well as any effects on BBB permeability *in vivo*. Such studies would provide crucial validation in a physiological setting and address whether the timing of Artemisinin (preventative vs. after metastasis seeding) matters.

8.3.3 Mechanistic Depth

While we identified GSK3 β and β -catenin as key mediators of Artemisinin's effect, the precise molecular target of Artemisinin in the Wnt pathway remains unclear. Artemisinin is known to generate reactive oxygen species (ROS) in iron-rich cells, and it has many reported effects. It is possible that Artemisinin's activation of GSK3 β is indirect – for example, via inhibiting Akt (since Akt can inhibit GSK3 β). We did observe hints that Artemisinin lowered p-Akt in our phospho-protein arrays (data not shown in detail). A limitation is that we did not fully trace the upstream signalling cascade from Artemisinin to GSK3 β . Future research could use chemical proteomics to identify Artemisinin-binding proteins in breast cancer cells. One hypothesis is

that Artemisinin might stabilize the Axin complex or promote degradation of dishevelled (DVL) proteins, thereby enhancing the destruction complex function. Another mechanism to explore is Artemisinin's effect on calcium signalling or other pathways that intersect with Wnt. Understanding this could allow the design of even more potent analogues that specifically target that node. Additionally, our co-immunoprecipitation experiments hinted at a CLDN8- β -catenin interaction; however, the nature of this interaction (direct or via scaffolding proteins like ZO-1 or E-cadherin) wasn't fully resolved. It would be illuminating to map the protein-protein interactions of CLDN8 in cells (using proteomics) to see if catenin appears in the complex. This could uncover novel links between tight junctions and signalling pathways beyond Wnt (for instance, tight junctions also modulate Hippo signalling, etc., which we did not explore).

8.3.4 Artemisinin Pharmacology

We should note that the concentrations of Artemisinin used *in vitro* (5–50 μ M) are higher than what is achieved with standard anti-malarial dosing. High doses of Artemisinin or its derivatives can have off-target effects and potential neurotoxicity (188). While Artemisinin is relatively safe, prolonged use at high doses in cancer patients is not well studied. A future direction is to conduct preclinical trials to assess the safety of chronic Artemisinin administration in models, especially in combination with other treatments. Moreover, since Artemisinin disrupts tight junctions acutely (as we saw with TEER reduction), one must be cautious: could this lead to unwanted effects like enabling other cells or drugs to cross the BBB? There is an intriguing duality here – a transient BBB “loosening” might actually help deliver chemotherapeutic drugs to the brain (if given together, Artemisinin could increase chemo permeability to brain tumours), but it could also risk normal brain exposure

to toxins. Careful pharmacokinetic and pharmacodynamic studies are needed to find a therapeutic window where cancer inhibition is maximized and BBB integrity is not pathologically compromised. Derivatives like artesunate (water-soluble) might have different effects on tight junctions that are worth comparing.

8.3.5 Breadth of Efficacy

Our focus was on breast cancer brain metastasis, but it remains to be tested if the CLDN8– β -catenin–Artemisinin paradigm holds true for other metastatic sites or cancers. For example, do low-CLDN8 breast tumours also metastasize more to the lung or liver? (Basal claudin-low tumours do tend to metastasize viscera.) Does Artemisinin reduce metastasis in general or is there something special about the brain microenvironment? Future studies could examine metastasis to other organs in the presence of Artemisinin. Similarly, CLDN8 is expressed in other tissues (like kidney and colon); it would be interesting to see if Artemisinin's mechanism has relevance in other cancers where Wnt signalling is active. These explorations can broaden the impact of our findings beyond breast cancer.

In summary, addressing these limitations involves scaling up and translating our research: larger patient studies to solidify CLDN8 as a biomarker, animal and eventually clinical trials to test Artemisinin as a metastasis-preventive therapy, and deeper molecular dissection of how CLDN8 and Artemisinin exert their effects. Despite the gaps, the consistency of our data with the proposed model encourages further investment in this line of investigation.

8.4 Conclusion

Metastasis to the brain is one of the most devastating developments in breast cancer, and overcoming the barriers to treat it requires thinking beyond

conventional paradigms. This thesis contributes to that effort by illuminating the role of a tight junction protein (Claudin-8) and a repurposed drug (Artemisinin) in the context of breast cancer brain metastasis. We have demonstrated that CLDN8 is more than just a structural component of tight junctions – it is intricately tied to signalling pathways that govern cancer cell behaviour. Its downregulation in breast cancer correlates with a switch to a more invasive, migratory phenotype, largely via the deregulation of the Wnt/ β -catenin pathway. β -Catenin emerges as a critical lynchpin: when sequestered at cell membranes (high CLDN8, intact junctions), cells remain in a differentiated, non-metastatic state; when released into the nucleus (low CLDN8, active Wnt signalling), it drives the programs necessary for metastasis. Our work underscores the importance of the tumour–stroma interface (in this case, tumour cells and the BBB endothelium) in mediating metastasis. Tight junction integrity in the endothelium can be a last line of defence against circulating tumour cells – and proteins like CLDN8 help reinforce that line.

Crucially, we have identified Artemisinin as a therapeutic that can reinforce anti-metastatic control even when the natural barriers are lost. Artemisinin's ability to promote β -catenin degradation through GSK3 β essentially substitutes for the lost CLDN8 function in keeping oncogenic signalling in check. It is remarkable that a drug derived from ancient herbal medicine (Artemisinin, used for malaria) could find a new purpose in modern cancer therapy. Our data, together with corroborating studies, suggest that Artemisinin and its derivatives could form the basis of a targeted metastasis intervention, one that is urgently needed for conditions like TNBC brain metastases which lack effective treatments. Furthermore, the therapeutic promise of Artemisinin is bolstered by its low cost and wide availability, raising hope for accessible treatment options.

In conclusion, this research highlights a novel interplay between cell junction architecture and metastatic signalling pathways in breast cancer. CLDN8 and the Wnt/ β -catenin pathway act in opposition in regulating metastasis: when CLDN8 is lost, Wnt/ β -catenin is unleashed to drive tumour spread; when Wnt/ β -catenin is blocked (by Artemisinin), the metastatic process is impeded even if junctions are compromised. These findings pave the way for new strategies to predict, prevent, and treat brain metastases. By integrating molecular insights with clinical relevance, we move a step closer to translating these discoveries into improved outcomes – for example, through biomarkers that flag high-risk patients and repurposed therapies that can be rapidly deployed. The broader implication is that targeting the “soil” (the microenvironment and signalling context) of metastasis can be as important as targeting the “seed” (the cancer cell itself). Strengthening tight junctions or pharmacologically mimicking their anti-metastatic signals offers a complementary approach to traditional cytotoxic therapies.

Ultimately, the hope is that with approaches inspired by this work, patients with breast cancer might face a lower risk of their disease reaching the brain, and those already affected by brain metastases could have new avenues for treatment. The convergence of a biomarker (CLDN8) and a readily available drug (Artemisinin) is a promising tandem that warrants further clinical exploration. If successful, it could exemplify how understanding the mechanistic underpinnings of metastasis leads to tangible improvements in patient care – the central goal of translational cancer research.

REFERENCE

1. Ji W, Lou Y, Jiang WG, Ruge F, Martin TA. Knockdown of Claudin-8 (CLDN8) Indicates a Link Between Breast Cancer Cell Sensitivity to Chemotherapeutics and Reveals a Potential Use of CLDN8 as a Molecular Diagnostic and Target for Therapy. *Int J Mol Sci.* 2025;26(11).
2. Ji W, Zhuang X, Jiang WG, Martin TA. Tight junctional protein family, Claudins in cancer and cancer metastasis. *Front Oncol.* 2025;15:1596460.
3. Zhuang X, Ji W, Fang Z, Yang Y, Ruge F, Dou QP, et al. Claudin-10 in the Blood-Brain Barrier Function of Cerebral Endothelial Cells and Transendothelial Invasion of Breast Cancer Cells. *Anticancer Res.* 2023;43(9):3923-34.
4. Lambert AW, Pattabiraman DR, Weinberg RA. Emerging Biological Principles of Metastasis. *Cell.* 2017;168(4):670-91.
5. Boire A, Brastianos PK, Garzia L, Valiente M. Brain metastasis. *Nat Rev Cancer.* 2020;20(1):4-11.
6. Huang WT, Lu NM, Hsu WY, Chang SE, Atkins A, Mei R, et al. CSF-ctDNA SMSEQ Analysis to Tailor the Treatment of a Patient with Brain Metastases: A Case Report. *Case Rep Oncol.* 2018;11(1):68-74.
7. Weidle UH, Niewöhner J, Tiefenthaler G. The Blood-Brain Barrier Challenge for the Treatment of Brain Cancer, Secondary Brain Metastases, and Neurological Diseases. *Cancer Genomics Proteomics.* 2015;12(4):167-77.
8. Hardesty DA, Nakaji P. The Current and Future Treatment of Brain Metastases. *Front Surg.* 2016;3:30.
9. Lin X, DeAngelis LM. Treatment of Brain Metastases. *J Clin Oncol.* 2015;33(30):3475-84.
10. Lowery FJ, Yu D. Brain metastasis: Unique challenges and open opportunities. *Biochimica et Biophysica Acta (BBA)-Reviews on Cancer.* 2017;1867(1):49-57.
11. Suki D, Khoury Abdulla R, Ding M, Khatua S, Sawaya R. Brain metastases in patients diagnosed with a solid primary cancer during childhood: experience from a single referral cancer center. *J Neurosurg Pediatr.* 2014;14(4):372-85.
12. Villano JL, Durbin EB, Normandeau C, Thakkar JP, Moirangthem V, Davis FG. Incidence of brain metastasis at initial presentation of lung cancer. *Neuro Oncol.* 2015;17(1):122-8.
13. Nayak L, Lee EQ, Wen PY. Epidemiology of brain metastases. *Curr Oncol Rep.* 2012;14(1):48-54.
14. Goldhirsch A, Wood WC, Coates AS, Gelber RD, Thürlimann B, Senn HJ. Strategies for subtypes--dealing with the diversity of breast cancer: highlights of the St. Gallen International Expert Consensus on the Primary Therapy of Early Breast Cancer 2011. *Ann Oncol.* 2011;22(8):1736-47.
15. Rippaus N, Taggart D, Williams J, Andreou T, Wurdak H, Wronski K, et al. Metastatic site-specific polarization of macrophages in intracranial breast cancer metastases. *Oncotarget.* 2016;7(27):41473-87.
16. Lyle LT, Lockman PR, Adkins CE, Mohammad AS, Sechrest E, Hua E, et al. Alterations in Pericyte Subpopulations Are Associated with Elevated Blood-Tumor Barrier Permeability in Experimental Brain Metastasis of Breast Cancer. *Clin Cancer Res.* 2016;22(21):5287-99.
17. Medress Z, Hayden Gephart M. Molecular and Genetic Predictors of Breast-to-Brain Metastasis: Review and Case Presentation. *Cureus.* 2015;7(1):e246.
18. Corti C, Antonarelli G, Criscitiello C, Lin NU, Carey LA, Cortés J, et al. Targeting brain metastases in breast cancer. *Cancer Treat Rev.* 2022;103:102324.

19. Shima H, Yamada A, Ishikawa T, Endo I. Are breast cancer stem cells the key to resolving clinical issues in breast cancer therapy? *Gland Surg.* 2017;6(1):82-8.
20. Nam DH, Jeon HM, Kim S, Kim MH, Lee YJ, Lee MS, et al. Activation of notch signaling in a xenograft model of brain metastasis. *Clin Cancer Res.* 2008;14(13):4059-66.
21. Prasad VV, Gopalan RO. Continued use of MDA-MB-435, a melanoma cell line, as a model for human breast cancer, even in year, 2014. *NPJ Breast Cancer.* 2015;1:15002.
22. Altundag K. Tumor types, breast tumor subtypes and extension of systemic disease may influence outcome in cancer patients with brain metastases. *Journal of Neuro-Oncology.* 2017;132(3):523-.
23. Lee HT, Xue J, Chou PC, Zhou A, Yang P, Conrad CA, et al. Stat3 orchestrates interaction between endothelial and tumor cells and inhibition of Stat3 suppresses brain metastasis of breast cancer cells. *Oncotarget.* 2015;6(12):10016-29.
24. Renner W, Langsenlehner U, Krenn-Pilko S, Eder P, Langsenlehner T. BCL2 genotypes and prostate cancer survival. *Strahlentherapie und Onkologie.* 2017;193(6):466-71.
25. Kanojia D, Morshed RA, Zhang L, Miska JM, Qiao J, Kim JW, et al. β III-Tubulin Regulates Breast Cancer Metastases to the Brain. *Mol Cancer Ther.* 2015;14(5):1152-61.
26. Pangen RP, Channathodiyil P, Huen DS, Eagles LW, Johal BK, Pasha D, et al. The GALNT9, BNC1 and CCDC8 genes are frequently epigenetically dysregulated in breast tumours that metastasise to the brain. *Clin Epigenetics.* 2015;7(1):57.
27. Wu K, Fukuda K, Xing F, Zhang Y, Sharma S, Liu Y, et al. Roles of the cyclooxygenase 2 matrix metalloproteinase 1 pathway in brain metastasis of breast cancer. *J Biol Chem.* 2015;290(15):9842-54.
28. Liu J, Jin X, Liu KJ, Liu W. Matrix metalloproteinase-2-mediated occludin degradation and caveolin-1-mediated claudin-5 redistribution contribute to blood-brain barrier damage in early ischemic stroke stage. *J Neurosci.* 2012;32(9):3044-57.
29. Khan AP, Rajendiran TM, Ateeq B, Asangani IA, Athanikar JN, Yocum AK, et al. The role of sarcosine metabolism in prostate cancer progression. *Neoplasia.* 2013;15(5):491-501.
30. Lucarelli G, Ditunno P, Bettocchi C, Spilotros M, Rutigliano M, Vavallo A, et al. Serum sarcosine is a risk factor for progression and survival in patients with metastatic castration-resistant prostate cancer. *Future Oncol.* 2013;9(6):899-907.
31. Khan AP, Rajendiran TM, Ateeq B, Asangani IA, Athanikar JN, Yocum AK, et al. The role of sarcosine metabolism in prostate cancer progression. *Neoplasia (New York, NY).* 2013;15(5):491-501.
32. Baum CE, Price DK, Figg WD. Sarcosine as a potential prostate cancer biomarker and therapeutic target. *Cancer Biol Ther.* 2010;9(5):341-2.
33. Locasale JW, Cantley LC. Metabolic flux and the regulation of mammalian cell growth. *Cell Metab.* 2011;14(4):443-51.
34. Ward PS, Thompson CB. Metabolic reprogramming: a cancer hallmark even warburg did not anticipate. *Cancer Cell.* 2012;21(3):297-308.
35. Chen J, Lee HJ, Wu X, Huo L, Kim SJ, Xu L, et al. Gain of glucose-independent growth upon metastasis of breast cancer cells to the brain. *Cancer Res.* 2015;75(3):554-65.
36. Woolston CM, Deen S, Al-Attar A, Shehata M, Chan SY, Martin SG. Redox protein expression predicts progression-free and overall survival in ovarian cancer patients treated with platinum-based chemotherapy. *Free Radic Biol Med.* 2010;49(8):1263-72.
37. Yang W, Zou L, Huang C, Lei Y. Redox regulation of cancer metastasis: molecular signaling and therapeutic opportunities. *Drug Dev Res.* 2014;75(5):331-41.

38. Kim HM, Jung WH, Koo JS. Expression of reactive oxygen species-related proteins in metastatic breast cancer is dependent on the metastatic site. *Int J Clin Exp Pathol* [Internet]. 2014 2014; 7(12):[8802-12 pp.].
39. Williams BJ, Suki D, Fox BD, Pelloski CE, Maldaun MV, Sawaya RE, et al. Stereotactic radiosurgery for metastatic brain tumors: a comprehensive review of complications. *J Neurosurg*. 2009;111(3):439-48.
40. Rostami R, Mittal S, Rostami P, Tavassoli F, Jabbari B. Brain metastasis in breast cancer: a comprehensive literature review. *J Neurooncol*. 2016;127(3):407-14.
41. Tsukada Y, Fouad A, Pickren JW, Lane WW. Central nervous system metastasis from breast carcinoma. Autopsy study. *Cancer*. 1983;52(12):2349-54.
42. Niwińska A, Tacikowska M, Murawska M. The effect of early detection of occult brain metastases in HER2-positive breast cancer patients on survival and cause of death. *Int J Radiat Oncol Biol Phys*. 2010;77(4):1134-9.
43. Guérin A, Sasane M, Dea K, Zhang J, Culver K, Nitulescu R, et al. The economic burden of brain metastasis among lung cancer patients in the United States. *J Med Econ*. 2016;19(5):526-36.
44. Ramakrishna N, Temin S, Chandarlapaty S, Crews JR, Davidson NE, Esteva FJ, et al. Recommendations on Disease Management for Patients With Advanced Human Epidermal Growth Factor Receptor 2-Positive Breast Cancer and Brain Metastases: ASCO Clinical Practice Guideline Update. *J Clin Oncol*. 2018;36(27):2804-7.
45. Romond EH, Perez EA, Bryant J, Suman VJ, Geyer CE, Jr., Davidson NE, et al. Trastuzumab plus adjuvant chemotherapy for operable HER2-positive breast cancer. *N Engl J Med*. 2005;353(16):1673-84.
46. Leyland-Jones B. Human epidermal growth factor receptor 2-positive breast cancer and central nervous system metastases. *J Clin Oncol*. 2009;27(31):5278-86.
47. Palmieri D, Bronder JL, Herring JM, Yoneda T, Weil RJ, Stark AM, et al. Her-2 overexpression increases the metastatic outgrowth of breast cancer cells in the brain. *Cancer Res*. 2007;67(9):4190-8.
48. Senda N, Yamaguchi A, Nishimura H, Shiozaki T, Tsuyuki S. Pertuzumab, trastuzumab and docetaxel reduced the recurrence of brain metastasis from breast cancer: a case report. *Breast Cancer*. 2016;23(2):323-8.
49. Yonemori K, Tsuta K, Ono M, Shimizu C, Hirakawa A, Hasegawa T, et al. Disruption of the Blood-Brain Barrier by brain metastases of triple-negative and basal-type breast cancer but not HER2/neu-positive breast cancer. *Cancer*. 2010;116(2):302-8.
50. Witzel I, Oliveira-Ferrer L, Pantel K, Müller V, Wikman H. Breast cancer brain metastases: biology and new clinical perspectives. *Breast Cancer Research*. 2016;18(1):8.
51. Swain SM, Baselga J, Kim SB, Ro J, Semiglazov V, Campone M, et al. Pertuzumab, trastuzumab, and docetaxel in HER2-positive metastatic breast cancer. *N Engl J Med*. 2015;372(8):724-34.
52. Swain SM, Baselga J, Miles D, Im YH, Quah C, Lee LF, et al. Incidence of central nervous system metastases in patients with HER2-positive metastatic breast cancer treated with pertuzumab, trastuzumab, and docetaxel: results from the randomized phase III study CLEOPATRA. *Ann Oncol*. 2014;25(6):1116-21.
53. Verma S, Miles D, Gianni L, Krop IE, Welslau M, Baselga J, et al. Trastuzumab emtansine for HER2-positive advanced breast cancer. *N Engl J Med*. 2012;367(19):1783-91.
54. Martin M, López-Tarruella S. Emerging Therapeutic Options for HER2-Positive Breast Cancer. *Am Soc Clin Oncol Educ Book*. 2016;35:e64-70.

55. Liu H, Wu Q, Gong X, He X, Wu H, Sheng Z, et al. [Analysis of prognostic factors in NSCLC patients with brain metastases diagnosed by contrast-enhanced MRI after whole brain radiotherapy]. *Zhongguo Fei Ai Za Zhi*. 2011;14(9):719-22.
56. Stumpf PK, Cittelly DM, Robin TP, Carlson JA, Stuhr KA, Contreras-Zarate MJ, et al. Combination of Trastuzumab Emtansine and Stereotactic Radiosurgery Results in High Rates of Clinically Significant Radionecrosis and Dysregulation of Aquaporin-4. *Clin Cancer Res*. 2019;25(13):3946-53.
57. Banerji U, van Herpen CML, Saura C, Thistlethwaite F, Lord S, Moreno V, et al. Trastuzumab duocarmazine in locally advanced and metastatic solid tumours and HER2-expressing breast cancer: a phase 1 dose-escalation and dose-expansion study. *Lancet Oncol*. 2019;20(8):1124-35.
58. Ung M, Lacaze JL, Maio Ed, Dalenc F. Breast Cancer Treatment and Antibody Drug Conjugates: Beyond T-DM1. *Medical Research Archives*. 2021;9(8).
59. Krop IE, Lin NU, Blackwell K, Guardino E, Huober J, Lu M, et al. Trastuzumab emtansine (T-DM1) versus lapatinib plus capecitabine in patients with HER2-positive metastatic breast cancer and central nervous system metastases: a retrospective, exploratory analysis in EMILIA. *Ann Oncol*. 2015;26(1):113-9.
60. Bartsch R, Berghoff AS, Vogl U, Rudas M, Bergen E, Dubsy P, et al. Activity of T-DM1 in Her2-positive breast cancer brain metastases. *Clin Exp Metastasis*. 2015;32(7):729-37.
61. Murthy R, Borges VF, Conlin A, Chaves J, Chamberlain M, Gray T, et al. Tucatinib with capecitabine and trastuzumab in advanced HER2-positive metastatic breast cancer with and without brain metastases: a non-randomised, open-label, phase 1b study. *Lancet Oncol*. 2018;19(7):880-8.
62. Freedman RA, Gelman RS, Wefel JS, Melisko ME, Hess KR, Connolly RM, et al. Translational Breast Cancer Research Consortium (TBCRC) 022: A Phase II Trial of Neratinib for Patients With Human Epidermal Growth Factor Receptor 2-Positive Breast Cancer and Brain Metastases. *J Clin Oncol*. 2016;34(9):945-52.
63. Lin NU, Borges V, Anders C, Murthy RK, Paplomata E, Hamilton E, et al. Intracranial Efficacy and Survival With Tucatinib Plus Trastuzumab and Capecitabine for Previously Treated HER2-Positive Breast Cancer With Brain Metastases in the HER2CLIMB Trial. *J Clin Oncol*. 2020;38(23):2610-9.
64. Choi YJ, Anders L. Signaling through cyclin D-dependent kinases. *Oncogene*. 2014;33(15):1890-903.
65. Hamilton E, Infante JR. Targeting CDK4/6 in patients with cancer. *Cancer Treat Rev*. 2016;45:129-38.
66. Vijayaraghavan S, Moulder S, Keyomarsi K, Layman RM. Inhibiting CDK in Cancer Therapy: Current Evidence and Future Directions. *Target Oncol*. 2018;13(1):21-38.
67. Tolaney SM, Sahebjam S, Le Rhun E, Bachelot T, Kabos P, Awada A, et al. A Phase II Study of Abemaciclib in Patients with Brain Metastases Secondary to Hormone Receptor-Positive Breast Cancer. *Clin Cancer Res*. 2020;26(20):5310-9.
68. Razavi P, Anjos CHd, Brown DN, Qing L, Ping C, Herbert J, et al. Molecular profiling of ER+ metastatic breast cancers to reveal association of genomic alterations with acquired resistance to CDK4/6 inhibitors. *Journal of Clinical Oncology*. 2019;37(15_suppl):1009-.
69. Samuels Y, Ericson K. Oncogenic PI3K and its role in cancer. *Curr Opin Oncol*. 2006;18(1):77-82.
70. Song MS, Salmena L, Pandolfi PP. The functions and regulation of the PTEN tumour suppressor. *Nat Rev Mol Cell Biol*. 2012;13(5):283-96.
71. Lee JJ, Loh K, Yap YS. PI3K/Akt/mTOR inhibitors in breast cancer. *Cancer Biol Med*. 2015;12(4):342-54.

72. Cancer Genome Atlas N. Comprehensive molecular portraits of human breast tumours. *Nature*. 2012;490(7418):61-70.
73. Boogerd W, Dalesio O, Bais EM, van der Sande JJ. Response of brain metastases from breast cancer to systemic chemotherapy. *Cancer*. 1992;69(4):972-80.
74. Franciosi V, Cocconi G, Michiara M, Di Costanzo F, Fosser V, Tonato M, et al. Front-line chemotherapy with cisplatin and etoposide for patients with brain metastases from breast carcinoma, nonsmall cell lung carcinoma, or malignant melanoma: a prospective study. *Cancer*. 1999;85(7):1599-605.
75. Peer D, Karp JM, Hong S, Farokhzad OC, Margalit R, Langer R. Nanocarriers as an emerging platform for cancer therapy. *Nat Nanotechnol*. 2007;2(12):751-60.
76. Chong C, Marino F, Pak H, Racle J, Daniel RT, Müller M, et al. High-throughput and Sensitive Immunopeptidomics Platform Reveals Profound Interferon-Mediated Remodeling of the Human Leukocyte Antigen (HLA) Ligandome. *Mol Cell Proteomics*. 2018;17(3):533-48.
77. Cortés J, Rugo HS, Awada A, Twelves C, Perez EA, Im SA, et al. Prolonged survival in patients with breast cancer and a history of brain metastases: results of a preplanned subgroup analysis from the randomized phase III BEACON trial. *Breast Cancer Res Treat*. 2017;165(2):329-41.
78. Carnevale J, Ko AH. MM-398 (nanoliposomal irinotecan): emergence of a novel therapy for the treatment of advanced pancreatic cancer. *Future Oncol*. 2016;12(4):453-64.
79. Freedman RA, Gelman RS, Wefel JS, Melisko ME, Hess KR, Connolly RM, et al. Translational Breast Cancer Research Consortium (TBCRC) 022: A Phase II Trial of Neratinib for Patients With Human Epidermal Growth Factor Receptor 2-Positive Breast Cancer and Brain Metastases. *Journal of clinical oncology : official journal of the American Society of Clinical Oncology*. 2016;34(9):945-52.
80. Hu T, Liu C, Li Q, Xiong J, Ma Y, Wu G, et al. Apatinib + CPT-11 + S-1 for treatment of refractory brain metastases in patient with triple-negative breast cancer: Case report and literature review. *Medicine (Baltimore)*. 2018;97(15):e0349.
81. Schmid P, Adams S, Rugo HS, Schneeweiss A, Barrios CH, Iwata H, et al. Atezolizumab and Nab-Paclitaxel in Advanced Triple-Negative Breast Cancer. *N Engl J Med*. 2018;379(22):2108-21.
82. Goldberg SB, Schalper KA, Gettinger SN, Mahajan A, Herbst RS, Chiang AC, et al. Pembrolizumab for management of patients with NSCLC and brain metastases: long-term results and biomarker analysis from a non-randomised, open-label, phase 2 trial. *Lancet Oncol*. 2020;21(5):655-63.
83. Kluger HM, Chiang V, Mahajan A, Zito CR, Sznol M, Tran T, et al. Long-Term Survival of Patients With Melanoma With Active Brain Metastases Treated With Pembrolizumab on a Phase II Trial. *J Clin Oncol*. 2019;37(1):52-60.
84. Schmid P, Rugo HS, Adams S, Schneeweiss A, Barrios CH, Iwata H, et al. Atezolizumab plus nab-paclitaxel as first-line treatment for unresectable, locally advanced or metastatic triple-negative breast cancer (IMpassion130): updated efficacy results from a randomised, double-blind, placebo-controlled, phase 3 trial. *Lancet Oncol*. 2020;21(1):44-59.
85. Litton JK, Rugo HS, Ettl J, Hurvitz SA, Gonçalves A, Lee KH, et al. Talazoparib in Patients with Advanced Breast Cancer and a Germline BRCA Mutation. *N Engl J Med*. 2018;379(8):753-63.
86. Kumthekar P, Tang SC, Brenner AJ, Kesari S, Piccioni DE, Anders C, et al. ANG1005, a Brain-Penetrating Peptide-Drug Conjugate, Shows Activity in Patients with Breast Cancer with Leptomeningeal Carcinomatosis and Recurrent Brain Metastases. *Clin Cancer Res*. 2020;26(12):2789-99.

87. Minniti G, Scaringi C, Paolini S, Clarke E, Cicone F, Esposito V, et al. Repeated stereotactic radiosurgery for patients with progressive brain metastases. *J Neurooncol.* 2016;126(1):91-7.
88. Miller JA, Kotecha R, Ahluwalia MS, Mohammadi AM, Chao ST, Barnett GH, et al. Overall survival and the response to radiotherapy among molecular subtypes of breast cancer brain metastases treated with targeted therapies. *Cancer.* 2017;123(12):2283-93.
89. Lien EA, Wester K, Lønning PE, Solheim E, Ueland PM. Distribution of tamoxifen and metabolites into brain tissue and brain metastases in breast cancer patients. *Br J Cancer.* 1991;63(4):641-5.
90. Brown PD, Ballman KV, Cerhan JH, Anderson SK, Carrero XW, Whitton AC, et al. Postoperative stereotactic radiosurgery compared with whole brain radiotherapy for resected metastatic brain disease (NCCTG N107C/CEC-3): a multicentre, randomised, controlled, phase 3 trial. *Lancet Oncol.* 2017;18(8):1049-60.
91. <https://www.ptcog.ch/> PTC-OGaoJao.
92. Atkins KM, Pashtan IM, Bussi re MR, Kang KH, Niemierko A, Daly JE, et al. Proton Stereotactic Radiosurgery for Brain Metastases: A Single-Institution Analysis of 370 Patients. *Int J Radiat Oncol Biol Phys.* 2018;101(4):820-9.
93. Shen L, Weber CR, Raleigh DR, Yu D, Turner JR. Tight junction pore and leak pathways: a dynamic duo. *Annu Rev Physiol.* 2011;73:283-309.
94. Fanning AS, Mitic LL, Anderson JM. Transmembrane proteins in the tight junction barrier. *J Am Soc Nephrol.* 1999;10(6):1337-45.
95. Shin K, Fogg VC, Margolis B. Tight junctions and cell polarity. *Annu Rev Cell Dev Biol.* 2006;22:207-35.
96. Kuvacheva NV, Morgun AV, Malinovskaya NA, Gorina YV, Khilazheva ED, Pozhilenkova EA, et al. TIGHT JUNCTIONS PROTEINS IN CEREBRAL ENDOTHELIAL CELLS DURING EARLY POSTNATAL DEVELOPMENT. *Tsitologiya.* 2016;58(5):364-9.
97. Martin TA, Mason MD, Jiang WG. Tight junctions in cancer metastasis. *Front Biosci (Landmark Ed).* 2011;16(3):898-936.
98. Escudero-Esparza A, Jiang WG, Martin TA. The Claudin family and its role in cancer and metastasis. *Front Biosci (Landmark Ed).* 2011;16(3):1069-83.
99. Martin TA, Jiang WG. Loss of tight junction barrier function and its role in cancer metastasis. *Biochim Biophys Acta.* 2009;1788(4):872-91.
100. Furuse M, Hirase T, Itoh M, Nagafuchi A, Yonemura S, Tsukita S, et al. Occludin: a novel integral membrane protein localizing at tight junctions. *J Cell Biol.* 1993;123(6 Pt 2):1777-88.
101. McCarthy KM, Skare IB, Stankewich MC, Furuse M, Tsukita S, Rogers RA, et al. Occludin is a functional component of the tight junction. *J Cell Sci.* 1996;109 (Pt 9):2287-98.
102. Saitou M, Fujimoto K, Doi Y, Itoh M, Fujimoto T, Furuse M, et al. Occludin-deficient embryonic stem cells can differentiate into polarized epithelial cells bearing tight junctions. *The Journal of cell biology.* 1998;141(2):397-408.
103. Saitou M, Furuse M, Sasaki H, Schulzke JD, Fromm M, Takano H, et al. Complex phenotype of mice lacking occludin, a component of tight junction strands. *Mol Biol Cell.* 2000;11(12):4131-42.
104. Krug SM, Schulzke JD, Fromm M. Tight junction, selective permeability, and related diseases. *Semin Cell Dev Biol.* 2014;36:166-76.
105. Osanai M, Takasawa A, Murata M, Sawada N. Claudins in cancer: bench to bedside. *Pflugers Arch.* 2017;469(1):55-67.

106. Bazzoni G. The JAM family of junctional adhesion molecules. *Curr Opin Cell Biol.* 2003;15(5):525-30.
107. Iwatsuki M, Mimori K, Yokobori T, Ishi H, Beppu T, Nakamori S, et al. Epithelial-mesenchymal transition in cancer development and its clinical significance. *Cancer Sci.* 2010;101(2):293-9.
108. Guarino M. Epithelial-mesenchymal transition and tumour invasion. *Int J Biochem Cell Biol.* 2007;39(12):2153-60.
109. Sánchez-Tilló E, de Barrios O, Siles L, Cuatrecasas M, Castells A, Postigo A. β -catenin/TCF4 complex induces the epithelial-to-mesenchymal transition (EMT)-activator ZEB1 to regulate tumor invasiveness. *Proc Natl Acad Sci U S A.* 2011;108(48):19204-9.
110. Hou J, Wang Z, Xu H, Yang L, Yu X, Yang Z, et al. Stanniocalcin 2 suppresses breast cancer cell migration and invasion via the PKC/claudin-1-mediated signaling. *PLoS One.* 2015;10(4):e0122179.
111. Ma F, Ding X, Fan Y, Ying J, Zheng S, Lu N, et al. A CLDN1-negative phenotype predicts poor prognosis in triple-negative breast cancer. *PLoS One.* 2014;9(11):e112765.
112. Tabariès S, Dupuy F, Dong Z, Monast A, Annis MG, Spicer J, et al. Claudin-2 promotes breast cancer liver metastasis by facilitating tumor cell interactions with hepatocytes. *Mol Cell Biol.* 2012;32(15):2979-91.
113. Tabariès S, Annis MG, Hsu BE, Tam CE, Savage P, Park M, et al. Lyn modulates Claudin-2 expression and is a therapeutic target for breast cancer liver metastasis. *Oncotarget.* 2015;6(11):9476-87.
114. Todd MC, Petty HM, King JM, Piana Marshall BN, Sheller RA, Cuevas ME. Overexpression and delocalization of claudin-3 protein in MCF-7 and MDA-MB-415 breast cancer cell lines. *Oncol Lett.* 2015;10(1):156-62.
115. Kim TH, Huh JH, Lee S, Kang H, Kim GI, An HJ. Down-regulation of claudin-2 in breast carcinomas is associated with advanced disease. *Histopathology.* 2008;53(1):48-55.
116. Osanai M, Murata M, Chiba H, Kojima T, Sawada N. Epigenetic silencing of claudin-6 promotes anchorage-independent growth of breast carcinoma cells. *Cancer Sci.* 2007;98(10):1557-62.
117. Wu Q, Liu X, Liu YF, Lu Y, Wang LP, Zhang XW, et al. Inhibition of p38 activity reverses claudin-6 induced cell apoptosis, invasion, and migration. *Chin Med J (Engl).* 2013;126(18):3539-44.
118. Song P, Li Y, Dong Y, Liang Y, Qu H, Qi D, et al. Estrogen receptor β inhibits breast cancer cells migration and invasion through CLDN6-mediated autophagy. *J Exp Clin Cancer Res.* 2019;38(1):354.
119. Jia Y, Guo Y, Jin Q, Qu H, Qi D, Song P, et al. A SUMOylation-dependent HIF-1 α /CLDN6 negative feedback mitigates hypoxia-induced breast cancer metastasis. *J Exp Clin Cancer Res.* 2020;39(1):42.
120. Zhang Y, Zheng A, Lu H, Jin Z, Peng Z, Jin F. The Expression and Prognostic Significance of Claudin-8 and Androgen Receptor in Breast Cancer. *Onco Targets Ther.* 2020;13:3437-48.
121. Martin TA, Lane J, Ozupek H, Jiang WG. Claudin-20 promotes an aggressive phenotype in human breast cancer cells. *Tissue Barriers.* 2013;1(3):e26518.
122. Hintermann E, Bayer M, Ehser J, Aurrand-Lions M, Pfeilschifter JM, Imhof BA, et al. Murine junctional adhesion molecules JAM-B and JAM-C mediate endothelial and stellate cell interactions during hepatic fibrosis. *Cell Adh Migr.* 2016;10(4):419-33.
123. Ebnet K, Aurrand-Lions M, Kuhn A, Kiefer F, Butz S, Zander K, et al. The junctional adhesion molecule (JAM) family members JAM-2 and JAM-3 associate with the cell polarity protein PAR-3: a possible role for JAMs in endothelial cell polarity. *J Cell Sci.* 2003;116(Pt 19):3879-91.
124. Mayer BJ. SH3 domains: complexity in moderation. *J Cell Sci.* 2001;114(Pt 7):1253-63.

125. Nomme J, Fanning AS, Caffrey M, Lye MF, Anderson JM, Lavie A. The Src homology 3 domain is required for junctional adhesion molecule binding to the third PDZ domain of the scaffolding protein ZO-1. *J Biol Chem.* 2011;286(50):43352-60.
126. Tavares GA, Panepucci EH, Brunger AT. Structural characterization of the intramolecular interaction between the SH3 and guanylate kinase domains of PSD-95. *Mol Cell.* 2001;8(6):1313-25.
127. Guillemot L, Schneider Y, Brun P, Castagliuolo I, Pizzuti D, Martines D, et al. Cingulin is dispensable for epithelial barrier function and tight junction structure, and plays a role in the control of claudin-2 expression and response to duodenal mucosa injury. *J Cell Sci.* 2012;125(Pt 21):5005-14.
128. Hou J, Renigunta A, Yang J, Waldegger S. Claudin-4 forms paracellular chloride channel in the kidney and requires claudin-8 for tight junction localization. *Proc Natl Acad Sci U S A.* 2010;107(42):18010-5.
129. Amasheh S, Milatz S, Krug SM, Bergs M, Amasheh M, Schulzke JD, et al. Na⁺ absorption defends from paracellular back-leakage by claudin-8 upregulation. *Biochem Biophys Res Commun.* 2009;378(1):45-50.
130. Gong Y, Wang J, Yang J, Gonzales E, Perez R, Hou J. KLHL3 regulates paracellular chloride transport in the kidney by ubiquitination of claudin-8. *Proc Natl Acad Sci U S A.* 2015;112(14):4340-5.
131. Arreola-Mendoza L, Del Razo LM, Mendoza-Garrido ME, Martin D, Namorado MC, Calderon-Salinas JV, et al. The protective effect of alpha-tocopherol against dichromate-induced renal tight junction damage is mediated via ERK1/2. *Toxicol Lett.* 2009;191(2-3):279-88.
132. Guan M, Ma J, Keaton JM, Dimitrov L, Mudgal P, Stromberg M, et al. Association of kidney structure-related gene variants with type 2 diabetes-attributed end-stage kidney disease in African Americans. *Hum Genet.* 2016;135(11):1251-62.
133. Ashikari D, Takayama K-I, Obinata D, Takahashi S, Inoue S. CLDN8, an androgen-regulated gene, promotes prostate cancer cell proliferation and migration. *Cancer Sci.* 2017;108(7):1386-93.
134. Gokulan K, Cerniglia CE, Thomas C, Pineiro SA, Khare S. Effects of residual levels of tetracycline on the barrier functions of human intestinal epithelial cells. *Food Chem Toxicol.* 2017;109(Pt 1):253-63.
135. Clark PM, Dawany N, Dampier W, Byers SW, Pestell RG, Tozeren A. Bioinformatics analysis reveals transcriptome and microRNA signatures and drug repositioning targets for IBD and other autoimmune diseases. *Inflamm Bowel Dis.* 2012;18(12):2315-33.
136. Wang H, Chao K, Ng SC, Bai AH, Yu Q, Yu J, et al. Pro-inflammatory miR-223 mediates the cross-talk between the IL23 pathway and the intestinal barrier in inflammatory bowel disease. *Genome Biol* [Internet]. 2016 2016/03//; 17:[58 p.].
137. Shangkuan WC, Lin HC, Chang YT, Jian CE, Fan HC, Chen KH, et al. Risk analysis of colorectal cancer incidence by gene expression analysis. *PeerJ.* 2017;5:e3003.
138. Ouban A, Ahmed AA. Claudins in human cancer: a review. *Histol Histopathol.* 2010;25(1):83-90.
139. Zhang X, Wang H, Li Q, Liu Y, Zhao P, Li T. Differences in the expression profiles of claudin proteins in human nasopharyngeal carcinoma compared with non-neoplastic mucosa. *Diagn Pathol.* 2018;13(1):11-.
140. Zhao X, Sun S, Zeng X, Cui L. Expression profiles analysis identifies a novel three-mRNA signature to predict overall survival in oral squamous cell carcinoma. *American journal of cancer research.* 2018;8(3):450-61.
141. Lu S, Singh K, Mangray S, Tavares R, Noble L, Resnick MB, et al. Claudin expression in high-grade invasive ductal carcinoma of the breast: correlation with the molecular subtype. *Mod Pathol.* 2013;26(4):485-95.

142. Xu J, Yang Y, Hao P, Ding X. Claudin 8 Contributes to Malignant Proliferation in Human Osteosarcoma U2OS Cells. *Cancer Biother Radiopharm*. 2015;30(9):400-4.
143. Kielgast F, Schmidt H, Braubach P, Winkelmann VE, Thompson KE, Frick M, et al. Glucocorticoids Regulate Tight Junction Permeability of Lung Epithelia by Modulating Claudin 8. *Am J Respir Cell Mol Biol*. 2016;54(5):707-17.
144. Woodrow CJ, Haynes RK, Krishna S. Artemisinins. *Postgrad Med J*. 2005;81(952):71-8.
145. J. Craig Venter Institute. Women's History Month: Tu Youyou. Published March 19 JCVI.
146. Li J, Zhou B. Biological actions of artemisinin: insights from medicinal chemistry studies. *Molecules*. 2010;15(3):1378-97.
147. Zaman S SRSaotcabaoaarah-.
148. Jansen FH. The pharmaceutical death-ride of dihydroartemisinin. *Malaria Journal*. 2010;9(1):212.
149. Addissouky T. Artemisinin and its derivatives throughout the therapeutic mechanisms and clinical potential. *Discover Chemistry*. 2025;2:2-10.
150. N N, C GPD, Chakraborty C, V K, D TK, V B, et al. Mechanism of artemisinin resistance for malaria PfATP6 L263 mutations and discovering potential antimalarials: An integrated computational approach. *Scientific Reports*. 2016;6(1):30106.
151. Onchieku NM, Kumari S, Pandey R, Sharma V, Kumar M, Deshmukh A, et al. Artemisinin Binds and Inhibits the Activity of Plasmodium falciparum Ddi1, a Retroviral Aspartyl Protease. *Pathogens*. 2021;10(11).
152. Luo Q, Yang J, Yang M, Wang Y, Liu Y, Liu J, et al. Utilization of nanotechnology to surmount the blood-brain barrier in disorders of the central nervous system. *Materials Today Bio*. 2025;31:101457.
153. ChemicalBook CAC--CPPCicOaf.
154. Jiang W, Appadurai E, Ruge F, Sanders A, Martin T. Controlling tight junctions in the Blood-Brain Barrier (BBB) with artemisinin as a potential adjuvant in the treatment of metastatic disease. *Cancer Research*. 2020;80:P2-20.
155. Liu F, Liu J, Xiang H, Sun Z, Li Y, Li X, et al. Dihydroartemisinin protects blood-brain barrier permeability during sepsis by inhibiting the transcription factor SNAI1. *Clin Exp Pharmacol Physiol*. 2022;49(9):979-87.
156. Zhang T, Zhang X, Lin C, Wu S, Wang F, Wang H, et al. Artemisinin inhibits TLR4 signaling by targeting co-receptor MD2 in microglial BV-2 cells and prevents lipopolysaccharide-induced blood-brain barrier leakage in mice. *J Neurochem*. 2021;157(3):611-23.
157. Chen L, Zhao X, Sheng R, Lazarovici P, Zheng W. Artemisinin alleviates astrocyte overactivation and neuroinflammation by modulating the IRE1/NF- κ B signaling pathway in in vitro and in vivo Alzheimer's disease models. *Free Radical Biology and Medicine*. 2025;229:96-110.
158. Guan X, Guan Y. Artemisinin induces selective and potent anticancer effects in drug resistant breast cancer cells by inducing cellular apoptosis and autophagy and G2/M cell cycle arrest. *J buon*. 2020;25(3):1330-6.
159. Jamalzadeh L, Ghafoori H, Aghamaali M, Sariri R. Induction of Apoptosis in Human Breast Cancer MCF-7 Cells by a Semi-Synthetic Derivative of Artemisinin: A Caspase-Related Mechanism. *Iran J Biotechnol*. 2017;15(3):157-65.
160. Yao Y, Guo Q, Cao Y, Qiu Y, Tan R, Yu Z, et al. Artemisinin derivatives inactivate cancer-associated fibroblasts through suppressing TGF- β signaling in breast cancer. *J Exp Clin Cancer Res*. 2018;37(1):282.
161. Wen L, Chan BC, Qiu MH, Leung PC, Wong CK. Artemisinin and Its Derivatives as Potential Anticancer Agents. *Molecules*. 2024;29(16).

162. Heron-Milhavet L DAMJSLI-CJA, Actin Cytoskeleton Dynamics, and Signaling Pathways. *J Cell Signal*. 2022;3(3):141-147.
163. Komarova YA, Kruse K, Mehta D, Malik AB. Protein Interactions at Endothelial Junctions and Signaling Mechanisms Regulating Endothelial Permeability. *Circ Res*. 2017;120(1):179-206.
164. Yamana S, Tokiyama A, Mizutani K, Hirata K, Takai Y, Rikitake Y. The Cell Adhesion Molecule Necl-4/CADM4 Serves as a Novel Regulator for Contact Inhibition of Cell Movement and Proliferation. *PLoS One*. 2015;10(4):e0124259.
165. Hamill KJ, Hiroyasu S, Colburn ZT, Ventrella RV, Hopkinson SB, Skalli O, et al. Alpha actinin-1 regulates cell-matrix adhesion organization in keratinocytes: consequences for skin cell motility. *J Invest Dermatol*. 2015;135(4):1043-52.
166. Zhu X, Zhang X, Ye Z, Chen Y, Lv L, Zhang X, et al. Silencing of semaphorin 3C suppresses cell proliferation and migration in MCF-7 breast cancer cells. *Oncol Lett*. 2017;14(5):5913-7.
167. Pardo-Pastor C, Rubio-Moscardo F, Vogel-González M, Serra SA, Afthinos A, Mrkonjic S, et al. Piezo2 channel regulates RhoA and actin cytoskeleton to promote cell mechanobiological responses. *Proceedings of the National Academy of Sciences*. 2018;115(8):1925-30.
168. Günzel D, Yu AS. Claudins and the modulation of tight junction permeability. *Physiol Rev*. 2013;93(2):525-69.
169. MerckMillipore. MKndBBBh-DCL.
170. Yang L, Sun X, Meng X. Differences in the expression profiles of claudin proteins in human gastric carcinoma compared with non-neoplastic mucosa. *Mol Med Rep*. 2018;18(2):1271-8.
171. Zhao X, Sun S, Zeng X, Cui L. Expression profiles analysis identifies a novel three-mRNA signature to predict overall survival in oral squamous cell carcinoma. *Am J Cancer Res*. 2018;8(3):450-61.
172. Li AX, Zeng JJ, Martin TA, Ye L, Ruge F, Sanders AJ, et al. Striatins and STRIPAK complex partners in clinical outcomes of patients with breast cancer and responses to drug treatment. *Chin J Cancer Res*. 2023;35(4):365-85.
173. Zhang Y, Zheng A, Lu H, Jin Z, Peng Z, Jin F. The Expression and Prognostic Significance of Claudin-8 and Androgen Receptor in Breast Cancer. *Onco Targets Ther*. 2020;13:3437-48.
174. Nazarewicz RR, Zenebe WJ, Parihar A, Larson SK, Alidema E, Choi J, et al. Tamoxifen induces oxidative stress and mitochondrial apoptosis via stimulating mitochondrial nitric oxide synthase. *Cancer Res*. 2007;67(3):1282-90.
175. Bekele RT, Venkatraman G, Liu R-Z, Tang X, Mi S, Benesch MGK, et al. Oxidative stress contributes to the tamoxifen-induced killing of breast cancer cells: implications for tamoxifen therapy and resistance. *Scientific Reports*. 2016;6(1):21164.
176. Li Z, Wang N, Fang J, Huang J, Tian F, Li C, et al. Role of PKC-ERK signaling in tamoxifen-induced apoptosis and tamoxifen resistance in human breast cancer cells. *Oncol Rep*. 2012;27(6):1879-86.
177. Lappano R, Pisano A, Maggiolini M. GPER Function in Breast Cancer: An Overview. *Frontiers in Endocrinology*. 2014;Volume 5 - 2014.
178. Wei W, Chen ZJ, Zhang KS, Yang XL, Wu YM, Chen XH, et al. The activation of G protein-coupled receptor 30 (GPR30) inhibits proliferation of estrogen receptor-negative breast cancer cells in vitro and in vivo. *Cell Death & Disease*. 2014;5(10):e1428-e.
179. Hassan F, El-Hiti GA, Abd-Allateef M, Yousif E. Cytotoxicity anticancer activities of anastrozole against breast, liver hepatocellular, and prostate cancer cells. *Saudi Med J*. 2017;38(4):359-65.
180. Sikora MJ, Johnson MD, Lee AV, Oesterreich S. Endocrine Response Phenotypes Are Altered by Charcoal-Stripped Serum Variability. *Endocrinology*. 2016;157(10):3760-6.

181. Prat A, Parker JS, Karginova O, Fan C, Livasy C, Herschkowitz JI, et al. Phenotypic and molecular characterization of the claudin-low intrinsic subtype of breast cancer. *Breast Cancer Research*. 2010;12(5):R68.
182. Wang K, Qiu X, Zhao Y, Wang H, Chen L. The Wnt/ β -catenin signaling pathway in the tumor microenvironment of hepatocellular carcinoma. *Cancer Biol Med*. 2021;19(3):305-18.
183. Jiang X, Wang J, Deng X, Xiong F, Zhang S, Gong Z, et al. The role of microenvironment in tumor angiogenesis. *J Exp Clin Cancer Res*. 2020;39(1):204.
184. Chen A, Cuevas I, Kenny PA, Miyake H, Mace K, Ghajar C, et al. Endothelial Cell Migration and Vascular Endothelial Growth Factor Expression Are the Result of Loss of Breast Tissue Polarity. *Cancer Research*. 2009;69(16):6721-9.
185. van der Wal T, van Amerongen R. Walking the tight wire between cell adhesion and WNT signalling: a balancing act for β -catenin. *Open Biol*. 2020;10(12):200267.
186. De P, Carlson JH, Wu H, Marcus A, Leyland-Jones B, Dey N. Wnt-beta-catenin pathway signals metastasis-associated tumor cell phenotypes in triple negative breast cancers. *Oncotarget*. 2016;7(28):43124-49.
187. Tong Y, Liu Y, Zheng H, Zheng L, Liu W, Wu J, et al. Artemisinin and its derivatives can significantly inhibit lung tumorigenesis and tumor metastasis through Wnt/ β -catenin signaling. *Oncotarget*. 2016;7(21):31413-28.
188. Pacios-Michelena A, Kasaragod VB, Schindelin H. Artemisinins and their impact on inhibitory neurotransmission. *Current Opinion in Pharmacology*. 2021;59:19-25.
189. Jang G-B, Kim J-Y, Cho S-D, Park K-S, Jung J-Y, Lee H-Y, et al. Blockade of Wnt/ β -catenin signaling suppresses breast cancer metastasis by inhibiting CSC-like phenotype. *Scientific Reports*. 2015;5(1):12465.
190. Klemm F, Bleckmann A, Siam L, Chuang HN, Rietkötter E, Behme D, et al. β -catenin-independent WNT signaling in basal-like breast cancer and brain metastasis. *Carcinogenesis*. 2011;32(3):434-42.